

**FOSSIL FUEL
MAGAZINE**

DOE/MC/10865-13

CO₂ FORMATION DAMAGE STUDY
Final Report

Work Performed for the Department of Energy
Under Contract No. DE-AC21-79MC10865

Date Published—July 1983

New Mexico State University
Las Cruces, New Mexico



National Petroleum Technology Office
U.S. DEPARTMENT OF ENERGY
Tulsa, Oklahoma

DISCLAIMER

This report was prepared as an account of work sponsored by an agency of the United States Government. Neither the United States Government nor any agency thereof, nor any of their employees, makes any warranty, expressed or implied, or assumes any legal liability or responsibility for the accuracy, completeness, or usefulness of any information, apparatus, product, or process disclosed, or represents that its use would not infringe privately owned rights. Reference herein to any specific commercial product, process, or service by trade name, trademark, manufacturer, or otherwise does not necessarily constitute or imply its endorsement, recommendation, or favoring by the United States Government or any agency thereof. The views and opinions of authors expressed herein do not necessarily state or reflect those of the United States Government.

This report has been reproduced directly from the best available copy.

CO₂ FORMATION DAMAGE STUDY
Final Report

Contributors:

Patrick F. Phelan
Gerald Smith
J. Donald Chavez

John T. Patton, *Principal Investigator*
Department of Chemical Engineering
New Mexico State University
Las Cruces, New Mexico 88003

Royal Watts, *Technical Project Officer*
Morgantown Energy Technology Center
P.O. Box 880
Morgantown, West Virginia 26505

Work Performed for the Department of Energy
Under Contract No. DE-AC21-79MC10865

Date Published—July 1983

TABLE OF CONTENTS

	<u>Page</u>
<u>ABSTRACT.</u>	x
<u>SECTION ONE. INTRODUCTION.</u>	1
1.1 Carbon Dioxide Flooding	1
1.2 Concern about Possible Reservoir Damage	1
1.3 One Known Instance of CO ₂ Damage.	2
1.4 Literature Search	3
1.5 Approach to Studying the Problem.	4
1.6 Proposed Mechanisms of Reservoir Damage	4
<u>SECTION TWO. CONTACT WITH PETROLEUM INDUSTRY</u>	6
2.1 Conference with Industry Experts.	6
2.2 Contacts with Other Consultants	7
2.3 Annual Conference with Consultants.	8
2.4 SPE/DOE Joint Symposia.	8
<u>SECTION THREE. PRECIPITATION OF SOLIDS FROM CRUDE OIL.</u>	9
3.1 Introduction.	9
3.2 Apparatus for Filter Tests.	11
3.3 Experimental Procedure.	13
3.4 Experimental Results.	14
3.4.1 Wilmington Crude	14
3.4.2 Maljamar Crude	16
3.4.3 Hilly Upland Crude	21
3.5 Oil Displacement Tests.	25
3.5.1 Introduction	25
3.5.2 Description of Model	25
3.5.3 Preparation of Sand Pack	27
3.5.4 Conventional Waterflood.	27
3.5.5 Secondary CO ₂ -Enhanced Waterflood.	27
3.5.6 Tertiary Waterflood.	29
3.6 Conclusions	30
<u>SECTION FOUR. DEPOSITION OF CALCIUM CARBONATE.</u>	31
4.1 Introduction	31
4.1.1 Results.	31
4.1.2 Proposed Damage Mechanism.	31

Table of Contents (Continued)

	<u>Page</u>
4.2 Nature of CaCO ₃ Precipitate.	33
4.2.1 Introduction.	33
4.2.2 Apparatus	33
4.2.3 Procedure	35
4.2.4 Results	36
4.3 Effect of Concentration on Precipitation Rate.	37
4.3.1 Introduction.	37
4.3.2 Results	37
4.4 Effect of Residence Time on CaCO ₃ Precipitation.	38
4.4.1 Introduction.	38
4.4.2 Results	38
4.4.3 Importance of Concentration Changes	39
4.4.4 Equation Accounts for Concentration Changes	41
4.4.5 Applicability to a CO ₂ Flood.	41
4.4.6 Conclusions	43
4.5 Dependence Upon Nature of Surface.	43
4.5.1 Introduction.	43
4.5.2 Procedure	44
4.5.3 Results	44
4.5.4 Rate of Scale Growth.	47
4.5.5 Math Model for Precipitation on Various Surfaces.	51
4.5.6 Character of CaCO ₃ Scale.	55
4.6 Effect of CaCO ₃ Deposition on Permeability	55
4.6.1 Introduction.	55
4.6.2 Permeability and Darcy's Law.	55
4.6.3 Apparatus	58
4.6.4 Procedure	60
4.6.5 Results	61
4.6.6 Mathematical Model.	63
4.6.7 Physical Explanation.	68
4.6.8 Other Mathematical Models	69
4.6.9 Porosity Changes.	71

Table of Contents (Continued)

	<u>Page</u>
4.7 Reservoir Damage During a CO ₂ Flood.	71
4.7.1 Introduction.	71
4.7.2 Results	72
4.7.3 Physical Interpretation	75
4.7.4 Applicability to a Real CO ₂ Flood	75
<u>SECTION FIVE. DEPOSITION OF FERRIC HYDROXIDE.</u>	78
5.1 Introduction	78
5.2 Apparatus.	78
5.3 Procedure.	80
5.3.1 Dissolution in Carbonic Acid.	80
5.3.2 Treatment With Strong Acids	80
5.3.3 Sodium Carbonate Fusion	80
5.3.4 Analyses.	81
5.4 Experimental Results	81
5.4.1 Iron Extracted With Carbonated Brine.	81
5.4.2 Acid-soluble Iron	81
5.4.3 Sodium Carbonate Fusion	81
5.5 Conclusions.	82
5.5.1 Extraction of Iron.	82
5.5.2 Applicability to CO ₂ Flood.	82
5.5.3 Remedy for Damage	82
<u>SECTION SIX. ACCEPTABLE LEVELS OF FORMATION DAMAGE.</u>	83
6.1 Introduction	83
6.2 Miscible Floods.	83
6.3 Immiscible Floods.	84
6.4 Frequency of Stimulation	85
<u>SECTION SEVEN. SUMMARY AND CONCLUSIONS.</u>	86
<u>REFERENCES</u>	89

APPENDICES

	<u>Page</u>
A. Literature Relating to Plausible Mechanisms of CO ₂ -Caused Reservoir Damage	91
B. Computerized Data Bases	158
C. Descriptors for Computerized Literature Search	161
D. Persons Attending First Conference on CO ₂ Formation Damage at New Mexico State University	162
E. Properties of Crude Oils	163
F. Apparatus for Filtration Experiments	171
G. Filtration Tests Using Various Crude Oils	173
H. Reservoirs from Which the Crude Oils of This Study Were Obtained . . .	178
I. Gas Chromatographic Analyses of Crudes	182
J. Apparatus for Flow Tests	184
K. Experimental Results from Oil Displacement Tests Using an Unconsolidated Sand Pack	185
L. Experimental Results from CaCO ₃ Precipitation Tests Using Static Bed of Limestone	189
M. Derivation of the Equations Presented in Section 4.4	191
N. Materials Used in Fluid Beds	194
O. Derivation of Math Model for Scale Growth on Glass or Resin-Coated Surfaces	195
P. Computer Simulation for Predicting the Production History of an Oil Well During a CO ₂ Flood	200
Q. Mineralogical Assays of Core Samples from Pennzoil's CO ₂ Pilot Test .	225

LIST OF FIGURES

<u>Figure</u>	<u>Page</u>
3.1 Filtration Apparatus	12
3.2 Filtration Characteristics of Wilmington Crude Show No Evidence of Organic Precipitates at 50.5±1°C.	15
3.3 Organic Precipitates Retard Filtration of Maljamar Crude at 50.5°C	17
3.4 Filtration Behavior of Maljamar Crude at 37±1°C Suggests Organic Solids Become Less Soluble as Temperature is Lowered	19
3.5 Filtration Behavior of Maljamar Crude Shows Anomalous Dependence Upon CO ₂ Pressure at 26±2°C.	20
3.6 Filtration Rate of Maljamar Crude Depends Upon Temperature	22
3.7 Filtration Behavior of Hilly Upland Crude Shows Precipitation Increases with CO ₂ Pressure.	24
3.8 Schematic Diagram of Experimental Apparatus.	26
3.9 Results of Oil-Displacement Tests Using Maljamar Crude in Unconsolidated Sand Pack	28
4.1 Fluidized Bed for Determining Nature of CaCO ₃ Precipitate.	34
4.2 Precipitation of CaCO ₃ on Limestone Shows Non-Linear Dependence Upon Residence Time.	40
4.3 Experimental Results Confirm Mathematical Model, Eq. 4.6	42
4.4 Growth of CaCO ₃ Scale on Glass Surface Controls Rate of Calcium Precipitation at 25°C.	49
4.5 Growth of CaCO ₃ Scale on Silicone-Coated Surface Controls Rate of Calcium Precipitation at 25°C.	50
4.6 Comparison of Math Model (Eq. 4.10) with Experimental Results (glass beads, 70-80 US Std. mesh; 25°C).	52
4.7 Comparison of Math Model (Eq. 4.10) with Experimental Results (silicone-coated Beads, 35-45 US Std. mesh; 25°C	52
4.8 Silicone-Coated Glass Beads 35-45 US. Std. Mesh.	56
4.9 Silicone-Coated Beads after CaCO ₃ Scale has Covered Them	56
4.10 Silicone-Coated Beads Showing Crystal Growth Upon CaCO ₃ Scale. . . .	57
4.11 Apparatus for Permeability Experiments	59
4.12 Permeability Profile of Unconsolidated Pack of Limestone Chips . .	62
4.13 Permeability Decreases as CaCO ₃ Precipitates within Limestone Bed.	64
4.14 Parallel Capillaries Provide Simple Model.	65

List of Figures (Continued)

<u>Figure</u>	<u>Page</u>
4.15 A More Realistic Model of a Porous Medium.	65
4.16 Experimental Results Plotted to Test Equation 4.18	67
4.17 Experimental Results Plotted to Test Equation 4.21	70
4.18 Computer Simulation Predicts Damage Abrupt Decline in Production After CaCO ₃ Precipitation Begins	73
4.19 Porosity Decreases Rapidly Near Wellbore According to Model.	74
4.20 Model Shows Permeability Decreases Rapidly Near Wellbore	76
5.1 Lined Vessel for Carbonated Brine.	79
M.1 Plot of Experimental Results to Test Equation M.6	193
P.1 Conversion of Molarity to Molality for Ca(HCO ₃) ₂ Solutions at 60°C	211
P.2 Fortran Computer Program	219

LIST OF TABLES

<u>Table</u>	<u>Title</u>	<u>Page</u>
3.1	Precipitate from Maljamar Crude Depends Upon Pressure. . .	18
3.2	Precipitate from Hilly Upland Crude Increases with CO ₂ Pressure at 77°F	21
4.1	Calcium Remaining in Limestone Bed	36
4.2	Precipitation on Limestone Increases with Concentrations of Ca ⁺⁺ and CO ₃ ⁼	38
4.3	Scale Formation on Limestone Favored by Increased Residence Time	39
4.4	Experimental Results for Precipitation of CaCO ₃ on Three Different Surfaces	45
4.5	Surface Areas of the Materials Used in the Experiments Described in Table 4.4	45
4.6	Calcium Remaining in Fluid Bed of Silicone-Coated Beads. .	46
4.7	Calcium Remaining on Glass Beads	46
4.8	Comparison of Soluble and Insoluble Calcium in Effluents from Fluidized Beds	47
4.9	Limiting Concentrations Observed During Scale - Formation Experiments	48
4.10	Rate Constants for CaCO ₃ Precipitation (based on model given by Eq. 4.10)	54
4.11	Rate Constants for Growth of CaCO ₃ Scale Over Glass and Silicone-Coated Surfaces	54
A.1	References by Subject	91
E.1	Comparison of Crude Oils Used in this Study	164
E.2	Hempel and Vacuum Distillation Analysis of Wilmington Crude	166
E.3	Properties of Distillate Fractions from Wilmington Crude .	167
E.4	Distillation Characteristics of Maljamar Crude	168
E.5	Distillation Characteristics of Hilly Upland Crude	169
E.6	Viscosity of Hilly Upland Crude Saturated with Carbon Dioxide at 78°F	170
G.1	Results of Filtration Tests Using Wilmington Crude Saturated with CO ₂ at 50.5±2°C	173

List of Tables (Continued)

<u>Table</u>	<u>Page</u>	
G.2	Results of Filtration Tests Using Maljamar Crude Saturated with CO ₂ at 27+2°C	174
G.3	Results of Filtration Tests Using Maljamar Crude Saturated with CO ₂ at 37+1°C	175
G.4	Results of Filtration Tests Using Maljamar Crude Saturated with CO ₂ at 50.5+1°C	176
G.5	Results of Filtration Tests Using Hilly Upland Crude Saturated with CO ₂ at 28+0.5°C	177
H.1	Tar Zone Reservoir Data Wilmington Oil Field	179
H.2	Reservoir Data Maljamar Oil Field	180
H.3	Reservoir Data for the Hilly Upland Oilfield and Pilot Area	181
I.1	Analysis of Wilmington Crude Oil	182
I.2	Analysis of Maljamar Crude Oil	183
I.3	Analysis of Hilly Upland Crude Oil	183
K.1	Injection of Maljamar Crude During Preparation of Sand Pack	185
K.2	Conventional Waterflood with Brine No CO ₂ Present	186
K.3	Resaturation with Maljamar Crude before the CO ₂ -Enhanced Secondary Waterflood	187
K.4	Secondary CO ₂ -Enhanced Waterflood	188
L.1	Porosity Changes and Amounts of CaCO ₃ Deposited	189
L.2	Permeability Changes and Porosity	189
L.3	Calculated Volumes of CaCO ₃ Precipitate	190
P.1	Vapor Pressure of Water Above Solutions of NaCl and Na ₂ CO ₃ at 54°C	206
P.2	Calcium Concentration Profile Before CaCO ₃ Deposition Begins	213
Q.1	X-Ray Diffraction Results	225
Q.2	Thin Section Point Count Data	226

ABSTRACT

Occasional reports from industry suggested that the use of carbon dioxide to enhance the recovery of tertiary oil might be causing formation damage. This project was undertaken to define the mechanisms responsible for such occurrences. A proposal, outlining the research, was prepared in response to a U.S. Department of Energy RFP issued in 1979 soliciting laboratory research on CO₂ formation damage.

The contract objectives were threefold;

- (1) Provide a comprehensive literature survey to elicit all that is currently known or suspected, relative to formation damage that might occur during the injection of carbon dioxide into an oil reservoir.
- (2) Under simulated reservoir conditions, demonstrate in the laboratory each of the damage mechanisms and quantify the degree to which each mechanism could cause damage.
- (3) For those damage mechanisms identified to be significant, develop a feasible remedy, easily applied in actual field operations.

The literature search was initiated with a manual review of four prominent abstracts and indices thought to include most of the pertinent literature. The manual search included both the International Petroleum Abstracts and indices of all Society of Petroleum Engineering publications. In addition, electronic data search systems were employed to search six extensive data bases, two of which were the Geological Reference file and the University of Tulsa Petroleum Abstract Service.

In all, 112 references that might pertain to CO₂ formation damage mechanisms were uncovered and abstracted for inclusion in this report. Surprisingly, the extensive literature survey produced no documented cases of CO₂ damage

during field tests of the CO₂ flooding process. Several industrial companies did volunteer information concerning specific instances when CO₂ damage was thought to occur; however, in almost every instance an alternate explanation seemed to be equally plausible.

The literature did provide insight into four possible damage mechanisms, namely;

- (1) Precipitation of reservoir mineral in the vicinity around the producing well as carbon dioxide escapes from the water phase due to pressure draw down.
- (2) Plugging of reservoir interstices by insoluble organic solids precipitated as the carbon dioxide dissolves in crude oil.
- (3) Formation of an immobile gas phase, predominately CO₂, which would drastically lower the effective permeability to oil and, especially water.
- (4) Dissolution of cementation, especially carbonates or feldspars, that could allow fines to migrate in the reservoir and plug tiny flow passages.

Each of these mechanisms was investigated in depth during the laboratory experiments. The precipitation of reservoir minerals is a possible mechanism, but will occur only in those reservoirs where sufficient water is injected to displace carbonic acid from the center of the pattern to the low pressure region around the producing wells. This circumstance will likely exist only in immiscible floods designed to enhance the production of viscous oils. It should be of only minor significance in the miscible displacement of light oils.

The second mechanism, involving the deposition of organic particulates, was found to be an unlikely source of reservoir damage. The maximum damage

that was observed in experiments designed to overemphasize this possible mechanism, was only a 20 percent permeability reduction. Damage that might occur during normal field operations should be much less than 20 percent.

The third mechanism, related to the presence of an immobile gas phase, is a real problem but not unique to the injection of carbon dioxide. It should be observed in the injection of rich gas, nitrogen or any other gas which is not totally soluble in the reservoir oil or water phases. In the case of carbon dioxide, the damage should be self-correcting, as the solubility of carbon dioxide in water will eventually allow the water to dissolve away the gas and, hence, the blocking effect.

The damage due to dissolution of cementation material also presents a real hazard to oil recovery operations. This damage will exist primarily in the area of the injection well. It is believed that any such damage can be cured by appropriate well stimulation techniques such as fracturing or acidizing.

Over and above the possible solutions to the damage problems mentioned above, one additional technique is available. Researchers on the project were privileged to witness four CO₂ injection tests conducted by Champlin Petroleum Company in the Wilmington field in California. These tests showed dramatically that liquid carbon dioxide can be injected at a more rapid rate and at a lower well-head pressure than that required for the injection of gas or supercritical carbon dioxide. The increased injectivity of liquid CO₂ would tend to offset a good portion of any damage induced by CO₂ in the reservoir.

SECTION ONE
INTRODUCTION

1.1 Carbon Dioxide Flooding

For more than 30 years, oil recovery experts have known that carbon dioxide, (CO_2) possesses a unique ability to displace crude oil from reservoir rock. Although many other gases have been tested for their efficacy in displacing crude oil, only carbon dioxide has the ability to both reduce residual oil saturations to near zero and produce significant quantities of tertiary oil from porous media that had previously been water flooded to the economic limit. Early studies provided the fundamental understanding required to explain the high efficiency of carbon dioxide, but the depressed price of crude, until the late 1970's, made most field applications of CO_2 appear unprofitable.

Oil displacement by gas can occur under both miscible and immiscible phase conditions. Carbon dioxide is unique in that it can effectively displace oil under both conditions; the determining factor is usually the depth of the reservoir, because the depth controls the pressure at which the flood is conducted. All other factors being equal, it is more desirable to conduct the flood under miscible conditions than under immiscible conditions.

1.2 Concern about Possible Reservoir Damage

Some pilot scale field tests in the 1970's were so promising that commercial CO_2 floods seemed economically feasible. However, the magnitude and complexity of possible chemical interactions made some experts, including those in the U.S. Department of Energy, ask whether the process might damage the

oil-bearing formations. They were especially concerned that injectivity might be adversely affected, or that reservoir permeability might be lowered. Either might occur if the pores in the reservoir rock became plugged. As a result of this concern, the U.S. Department of Energy awarded, in late 1979, a research contract to the Chemical Engineering Department at New Mexico State University, Las Cruces, to investigate the question.

The study had four objectives:

1. Determine what formation damage problems have been encountered in past or ongoing CO₂ projects in carbonate reservoirs.
2. Define possible physical or chemical mechanisms which could cause formation damage.
3. Conduct laboratory experiments to investigate plausible mechanisms of damage. Study and evaluate experimental results.
4. Establish unacceptable levels of formation damage and develop methods or processes which will assure acceptable levels based on existing data and laboratory results.

1.3 One Known Instance of CO₂ Damage

As soon as this project was initiated, experts from the oil industry were polled concerning documented cases of CO₂ formation damage. Five oil companies having CO₂ flood projects sent representatives to serve as an advisory committee. When asked about any reservoir damage associated with their floods, they stated that there were no known instances. Although there had been operating problems (such as unexpected pressure changes), there was a reluctance to define these as CO₂ damage. For most of the problems, alternative explanations were more plausible.

Nor were any instances of CO₂ damage found in the literature when a literature search (described later) was performed. However, in 1981,

Pennzoil reported (private communication) damage at their production wells in their Rock Creek experimental CO₂ flood. Precipitation was damaging the reservoir rock around the production wells, causing oil rates to decline. When the production wells were acidized, production was stimulated, but then it declined again. The source of the precipitate was believed to be the reservoir itself, which, from analyses of core samples was found to contain acid-soluble iron minerals. Presumably, carbonic acid was forming in the reservoir as CO₂ dissolved in connate water and the acid was attacking the reservoir rock, bringing ferric ions into solution. As the CO₂ was released in the low pressure region near the producing wells, iron was precipitating as ferric hydroxide. This was one of the possible damage mechanisms proposed at the outset of the project (see Section Two) and subsequently tested in the laboratory. (The experimental results and conclusions are described in Section Five).

1.4 Literature Search

Six computer-accessible data bases were searched for references related to reservoir damage. No documented cases of CO₂ damage during field tests were found. Some laboratory studies were found which pertained indirectly to plausible mechanisms of damage, but none described CO₂ damage explicitly.

Of the articles collected, those relating to the dissolution of carbonate and sulfate rocks and to the reprecipitation of carbonate and sulfate compounds were the most plentiful. For example, reports of scale formation in oil field water-handling equipment were numerous, because countless studies concerning this problem have been made. Only two articles mentioning asphaltene deposition in CO₂-crude mixtures were found (1, 2,), however.

Abstracts of the articles are presented in serial order in Appendix A with full citation information. An alphabetical author index is also presented in Appendix A, as is a listing of the references by subject.

The keywords used for the search, and the data bases are described in Appendices B and C, respectively.

1.5 Approach to Studying the Problem

The initial conference among industry experts provided the necessary guidance for an effective literature search. (The conference is described below). Several hypothetical damage mechanisms were also proposed at this time, and topics relating to these mechanisms were included in the literature search. Experiments were then designed and performed to confirm three of these mechanisms. (See Sections Three, Four and Five).

1.6 Proposed Mechanisms of Reservoir Damage

The mechanisms are described more fully in subsequent sections of this report where the corresponding experiments are also described. Briefly, however, they are of four types:

1. Dissolution of reservoir rock in the vicinity of the injection well, followed by precipitation of the dissolved material at remote locations in the reservoir. The precipitation might plug the pores in the reservoir. Carbonates, sulfates or hydroxides were assumed to be the minerals involved in this kind of mechanism.
 - a. Limestone or dolomite could dissolve in carbonic acid, then calcium carbonate or magnesium carbonate might precipitate in regions where CO_2 pressure (and, hence, carbonate solubility) is less.

- b. Calcium sulfate or barium sulfate could dissolve near the injection well where the pressure is highest, then they might precipitate in the lower pressure regions of the reservoir.
 - c. Ferric ions from, perhaps, the dissolution of Siderite (ferric carbonate) could reprecipitate in low-pressure regions as the CO_2 bubbled out of solution. The loss of CO_2 would raise the pH and the iron would precipitate as gelatinous ferric hydroxide.
2. Formation of insoluble asphaltene-like solids when CO_2 dissolves in crude oil. Such insoluble materials might be swept along by the CO_2 flood until they became lodged at constrictions in the pores.
 3. Formation of an immobile phase(s) at the CO_2 -oil interface where CO_2 , oil and water would be present simultaneously.
 4. Attack by carbonic acid on feldspar or carbonate minerals which cement sandstones together, thereby releasing tiny grains which might clog pores. Alternately, the feldspars might be converted to clay minerals which could swell and clog pores.

As described in Section Two, it was decided, on the advice of the industry advisory committee, to study the first two mechanisms before considering the last two. It was felt that field solutions for the latter problems would require more time and complex apparatus than were available to this project.

SECTION TWO
CONTACT WITH PETROLEUM INDUSTRY

2.1 Conference with Industry Experts

At the inception of the project, a consulting group composed of experts from industry and universities met at New Mexico State University to discuss their experiences and suggest possible mechanisms of CO₂ damage.*

As mentioned earlier, some of the representatives of the five oil companies which had CO₂ flood projects at the time said that production problems had been encountered, such as unexpected rises in injection pressure. But none of the problems could be conclusively attributed to CO₂ damage; most could be attributed to other, more plausible, causes.

Although no definite instances of CO₂ damage were known at the time, numerous hypothetical kinds of damage were discussed. It was concluded that plugging of the reservoir rock was the most likely type of damage, and it might occur in either of three ways. The first would involve dissolution of calcium carbonate rock in carbonic acid, followed by reprecipitation of calcium carbonate in the vicinity of the producing well. The second would involve deposition of asphalt-like solids from the oil, as the carbon dioxide dissolved in it. The third would arise from the formation of an immobile phase(s) at the CO₂-oil interface where CO₂, oil and water would be simultaneously present under high pressure.

*A list of those attending the conference, and their affiliations, is presented in Appendix D.

On further discussion of the asphaltene problem, the group concluded that it would be best to perform experiments using a simple apparatus employing CO₂ at temperatures and pressures which simulate reservoir conditions. It was agreed that the simplest system would be one containing a high pressure, thermostated reservoir for solutions of CO₂ and crude oil, followed by a filter section to measure the flowability of the solutions. Synthetic filters containing both round and angular micron-size pores should be utilized.

The third mechanism, that involving phase effects, was more difficult to describe. As CO₂ replaces oil, multiple liquid phases can occur under all but immiscible conditions. Even under immiscible conditions, at least three phases (water, crude oil and gas) compete for the flow channels in the reservoir matrix. Since the permeability of any phase and, hence its mobility, is a function of saturation, it is obvious that high gas saturation would lower the injectivity of water and vice versa. After much discussion it was agreed that experimental confirmation of the exact degree of mobility impairment and, more importantly, development of a field solution would require more time and complex apparatus than was available to this project. Accordingly, work relating to the third mechanism was given a low level of priority and was not to be attempted until the first two mechanisms had been fully defined.

2.2 Contacts with Other Consultants

The goals of the project were also discussed with several geologists. One, Dr. Lokesh Chaturvedi of New Mexico State University, suggested a fourth plausible mechanism. He proposed that carbonic acid might attack feldspars among the reservoir minerals, and convert them to clays which would imbibe water and swell. This mechanism, and others involving acid attack on the

cementing materials in sandstone reservoirs, were added to the list, but they were given lowest priority. The principal reason was that field experience generally indicates that acidizing a well has beneficial effects on production, not adverse ones.

2.3 Annual Conference with Consultants

As the project progressed, the consultants were contacted as needed. To ensure timely review of the experimental work, the group also met annually at New Mexico State University. After a thorough briefing on the past year's work, the consultants toured the laboratories, scrutinized the procedures, and examined the results. Their comments helped guide and speed the work.

2.4 SPE/DOE* Joint Symposia

Key members of the research team kept abreast of developments in enhanced recovery technology by attending the annual symposia on enhanced oil recovery, held in Tulsa, Oklahoma every April. These meetings also provided an opportunity to meet and talk informally with more experts in the oil industry.

*SPE/DOE stands by Society of Petroleum Engineers/Department of Energy.

SECTION THREE

PRECIPITATION OF SOLIDS FROM CRUDE OIL

3.1 Introduction

While a mechanistic understanding of oil displacement by CO_2 is basic to establishing the CO_2 requirements of, and predicting performance for CO_2 reservoir floods, its accomplishment may fall short if one fails to consider the asphaltic deposition behavior that is often associated with a particular crude. The introduction of CO_2 under reservoir conditions might lead to asphaltic deposition, and that could possibly damage the reservoir by either reducing the reservoir permeability or even plugging the reservoir pores.

It is well-known that finely-divided black solids can be precipitated from many crude oils if pentane or hexane is poured into them (3). In view of this, it was suggested that CO_2 might have a similar effect on crudes. Interest in this mechanism was given impetus by reports (1,2,4) that traces of black solids formed in mixtures of CO_2 and crude when CO_2 exceeded 70 mole percent. These black solids were observed during phase-equilibrium studies involving CO_2 and crude. However, the solids or semisolids seemed to be different from those which precipitate when hydrocarbons like pentane or hexane are poured into the crude oils (4).

During a CO_2 -flood of a reservoir, the solids could form in either (or both) of two ways: The first would resemble "salting out". That is, the high concentration of dissolved carbon dioxide might change the polarity or solubility characteristics of the crude oil enough that high-molecular-weight components of the crude would precipitate. The second way would involve extraction of solubilizing hydrocarbons (those in the range C_6 to C_{30}) from the crude as CO_2 swept the reservoir. Thus, the relatively insoluble compounds (i.e., those having high molecular weights) would be left

behind. Although the two ways are conceptually different, the results would be the same: organic particles would be left behind in the reservoir. Moreover, as explained later, our experiments could not distinguish between the two precipitation mechanisms.

A third, but related, kind of damage might occur in the vicinity of the producing well during a CO₂ flood. The mechanism is analogous to liquid chromatography, and it may be important for certain crudes, although we did not study it experimentally. According to this mechanism, the mobilized oil, saturated with CO₂ and containing the high-molecular-weight components, would migrate without incident until it neared the producing well. There, the mixture of CO₂ and oil would partially vaporize (or "flash") because of the reduced reservoir pressure. As this happened, the compounds of high molecular weight that had come with the crude would be left behind as an asphaltic residue. This residue could accumulate at the producing well and plug the flow channels.

To test the possibility that CO₂ might cause solids to form in crude oils, three crude oils were saturated with CO₂ and subjected to filtration tests at temperatures and pressures which were typical of those in the reservoirs from which the oils were obtained. The crudes we used had been obtained during pilot CO₂ tests, and included: a Wilmington crude (California), a Maljamar crude (New Mexico) and a Hilly Upland crude (West Virginia). Prior to the filtration tests, the crudes were compared as to asphaltic content by inducing precipitation with either pentane or hexane. Other properties of these crudes are presented in Appendix E.

After the filtration tests, the Maljamar crude was subjected to a series of displacement tests. These determined whether CO₂ adversely affected that oil's ability to be displaced from a porous medium.

3.2 Apparatus for Filter Tests

A schematic diagram of the apparatus is presented in Fig. 3.1.

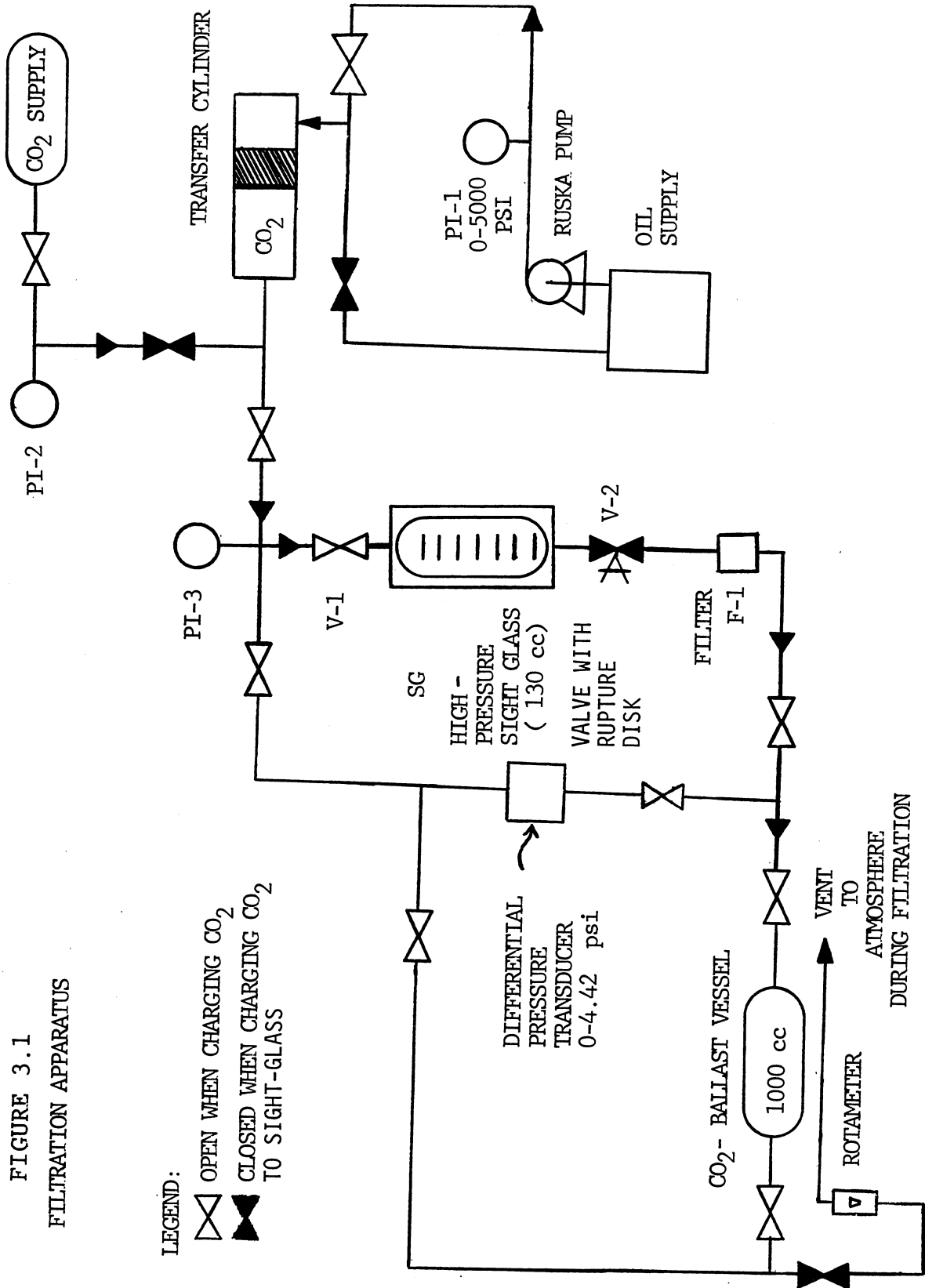
The most important elements of the system are the high-pressure Jerguson sight-glass (SG) and the Millipore filter (F-1). The sight glass serves as a reaction vessel in which crude oil is mixed with CO₂ under high pressure. When valve V-2 is opened, the mixture passes through the filter, and the rate of filtration is measured by visually observing the oil level as it falls past the graduations on the sight-glass window. (Specifications for the sight glass and filter are presented in Appendix F).

The sight glass, filter, CO₂-ballast vessel, pressure transducer and attendant valves and tubing are mounted on a single board, and this system is operated as an integrated unit which can be separated from the CO₂ supply (cylinder).

Liquid CO₂ from the inverted cylinder is transferred into the sightglass via a transfer cylinder whose piston is driven by oil pumped by a Ruska positive displacement proportioning pump. (Specifications for the pump are given in Appendix F). The pump allows the test apparatus and the sight glass with its crude oil to be pressurized with CO₂ above the cylinder pressure of 950 psig. For CO₂ pressures less than 950 psig, the apparatus is filled directly from the inverted CO₂ cylinder. For safety, a 2800-psig rupture disk is an integral part of valve V-2 below the sight glass.

The test apparatus is equipped with a Bourns differential pressure transducer (Appendix F). This transducer is calibrated to measure a pressure difference of 0 to 5 psi across the filter element. A Hewlett Packard, model 3476A, multimeter records the pressure-drop by measuring the calibrated electrical output from the pressure transducer.

FIGURE 3.1
FILTRATION APPARATUS



3.3 Experimental Procedure

In order for the filtration rate to be a measure of the solids content of the CO₂-crude mixture, the pressure-drop across the filter must be constant; and it must be the same for each experiment, regardless of the system pressure, (the pressure under which the CO₂-crude mixture is prepared). To keep the pressure-drop constant, the 1000-cc ballast vessel is used. It is filled with CO₂ to the same pressure as the CO₂ in the sight glass. Then, with the sight glass isolated from the ballast vessel, some CO₂ is bled from the vessel, until its pressure is 4.4 psi lower than that in the sight glass, as indicated by the pressure transducer. After valve V-2 is opened and crude oil begins flowing through the filter, the pressure-drop across the filter is kept at 4.4 psi by venting more CO₂ from the ballast vessel. As filtration proceeds, the venting rate is gradually reduced manually to maintain the 4.4 psi differential pressure.

For each experiment, four steps are involved. First, the entire test apparatus is purged of air with CO₂. This is done to eliminate the possibility of forming precipitates by reactions between the crude oil and oxygen. Second, the sight glass is filled with approximately 30 ml of previously filtered (2 micron, absolute) crude oil. The crude oil must be filtered to remove any dirt which may have contaminated it when it was being obtained in the field. Any particles smaller than 2 microns will not interfere with the test, because they readily pass through the 8-micron filter, F1. Third, the apparatus is pressurized with CO₂ to the desired operating pressure and is held at constant temperature for 24 hours in an air bath (not shown). Fourth, any particles precipitated by the CO₂ are collected on the filter (F1) while the volumetric flow rate is simultaneously measured.

3.4 Experimental Results

3.4.1 Wilmington Crude--This crude came from a reservoir that was previously waterflooded. Analysis by gas chromatography showed that 70% of the Wilmington crude is C_{36} -hydrocarbons or higher molecular weight species (12). This crude also contains a significant amount of asphaltenes. When either hexane or pentane was added to the Wilmington crude, tiny black particles formed, and these were quantitatively collected on an 8-micron filter. (Additional information about this crude oil, its gas chromatographic analysis, and the reservoir from which it came are presented in Appendices E, H and I.) However, upon conducting a similar experiment with CO_2 using the previously-described apparatus, no particulates were observed, either in the sight glass or on the 8-micron filter.

The absence of particulates was also demonstrated by the three filtration experiments whose results are depicted in Fig. 3.2. That graph shows the volume of filtrate as a function of time for CO_2 -crude mixtures prepared at $50.5^\circ C$ ($122.9^\circ F$) under CO_2 pressures of 500, 1000 and 1500 psig. (The experimental data from which Fig. 3.2 was derived are presented in Appendix G.) It is significant that the curve corresponding to 1500 psig is uppermost, because this indicates that the filtration rate increases with increasing CO_2 pressure.* This, in turn, demonstrates that no particles were produced by the CO_2 . If particulates had been produced by the CO_2 , more of them would be formed as the CO_2 pressure (and, hence, mole fraction of CO_2) increased, and the resistance to filtration would increase, too. In fact, just the reverse was observed; the resistance to filtration decreased with increasing amounts of CO_2 .

*As described in Section 3.3, the pressure-drop across the filter was only 4.4 psig in each experiment. The pressure of 1500 psi refers to the partial pressure of CO_2 in the oil as it was filtered.

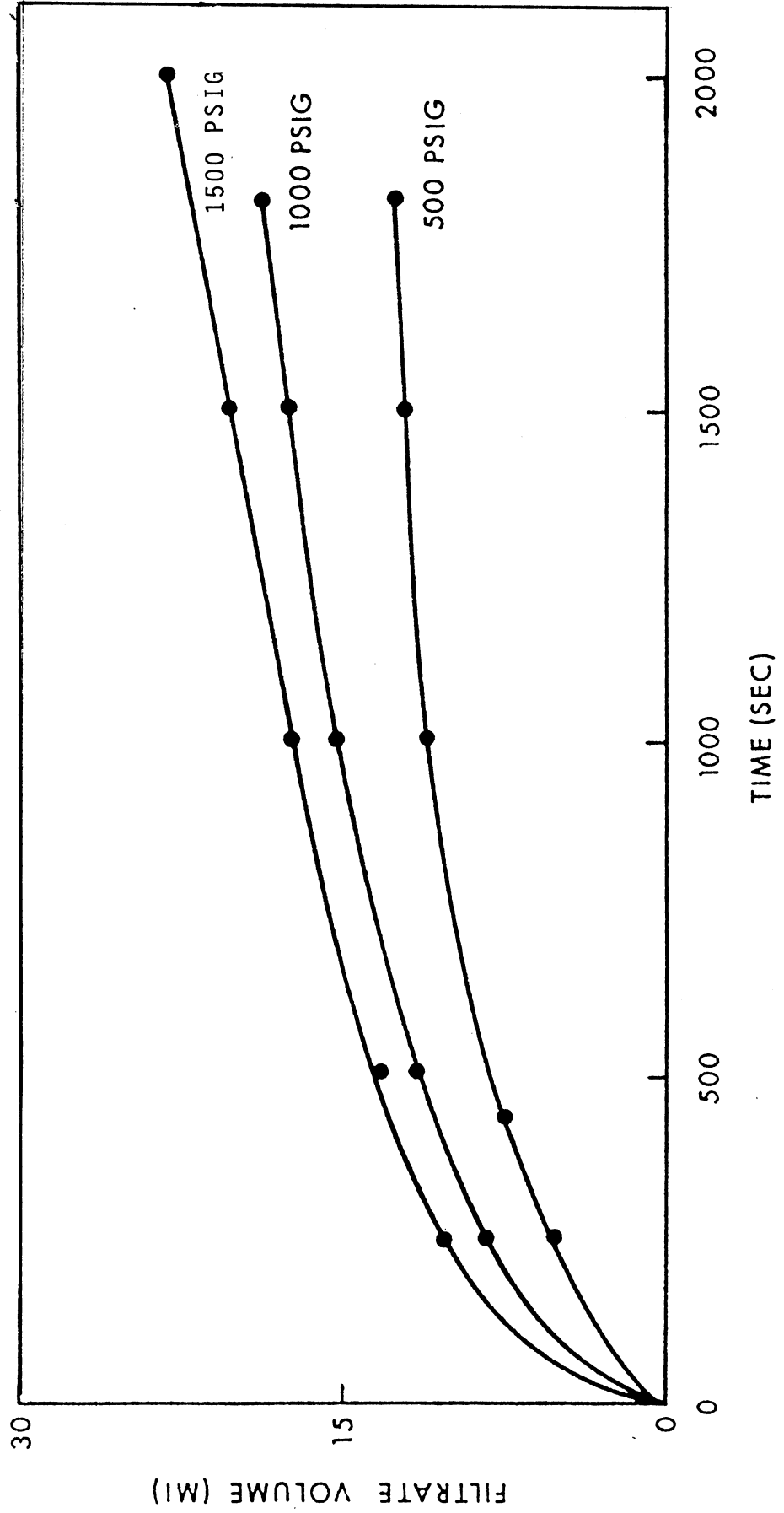


Figure 3.2 Filtration Characteristics of Wilmington Crude Show No Evidence of Organic Precipitates at $50.5 \pm 1^\circ\text{C}$ (Pressures are those of CO_2)

It is to be expected that, if particulates are absent from the oil, it will filter more rapidly when the mole fraction of CO_2 is increased. This is because CO_2 readily dissolves in the Wilmington crude, causing it to swell and reducing its apparent viscosity in proportion to the amount of CO_2 which dissolves. As viscosity is reduced, the ease of filtration increases.

3.4.2 Maljamar Crude--Gas chromatography showed that 70% of the hydrocarbons in the Maljamar crude are in the C_5 - C_{36} range (12). Thus, this oil is much lighter than the Wilmington crude.

The Maljamar crude also differs from the Wilmington crude in that no asphaltene particles precipitated when hexane or pentane was poured into it. However, when mixed with CO_2 , the crude yielded a fine gray precipitate, which was easily recovered on the 8-micron filter.

Not surprisingly, the results of the filtration experiments with Maljamar crude differed from those obtained using the Wilmington crude. Fig. 3.3 illustrates how the CO_2 pressure affected the filtration rate. The relative order of the curves is just the reverse of that obtained with Wilmington crude. This suggests that the amount of precipitate increased as the ratio of CO_2 to oil increased. As discussed in Section 3.1, the dissolved CO_2 might change the properties of the oil enough that previously-soluble asphaltic compounds are forced to precipitate. Alternately, the CO_2 may extract enough of the light hydrocarbons from the oil phase into the CO_2 -rich phase above it that the asphaltics must precipitate. Either explanation is consistent with our observations.

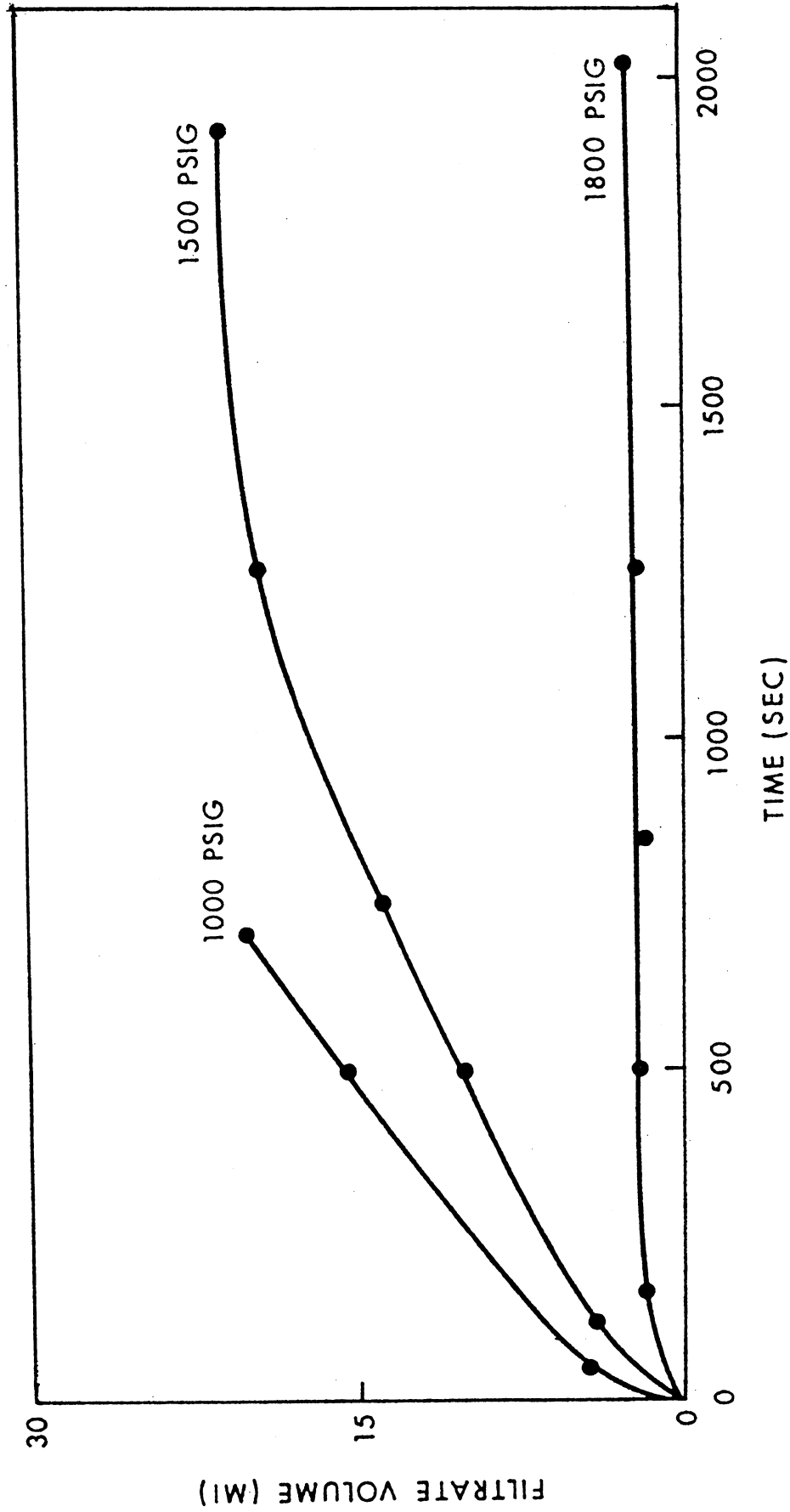


Figure 3.3. Organic Precipitates Retard Filtration of MaJjamar Crude at 50.5°C (Pressures are those of CO₂.)

Precipitation of asphaltics from the Maljamar crude was found to increase with temperature as well as with CO₂ pressure (See Table 3.1). Comparing the

Table 3.1
Precipitate from Maljamar Crude Depends Upon Pressure

Temperature °F	Pressure psig	Volume of Crude Oil Filtered, ml	Mass of Precipitate Collected g	Wt.%*
77	1000	30.0	none	0
	1500	25.9	0.031	0.12
	1800	22.5	0.054	0.19
100	1000	28.5	none	0
	1500	25.8	0.061	0.24
	1800	30.3	0.091	0.36

*Based on the weight of oil put into sight glass before CO₂ was added.

results shown in Figure 3.3 with those presented in Figs. 3.4 and 3.5 (for 37° and 26°C, respectively) also shows that the asphaltics become less soluble as the temperature is lowered. When the CO₂ pressure is only 1000 psig, little or no precipitate is formed, apparently; the filtration rate is appreciable throughout the entire experiment, as indicated by the positive slope of the upper curve (1000 psig) on each graph. By contrast, when the CO₂ pressure is 1500 or 1800 psig and the temperature is 37°C or less, the filter quickly becomes clogged with solids and the filtration rate drops to zero, as indicated by the plateaus on the two lower curves of both Figs. 3.4 and 3.5. The lower curves in Fig. 3.4 are essentially the same, given the limits of experimental error, but those in Fig. 3.5 are anomalous and seem to indicate that less precipitate is formed under 1800 psig CO₂ than under 1500 psig CO₂.

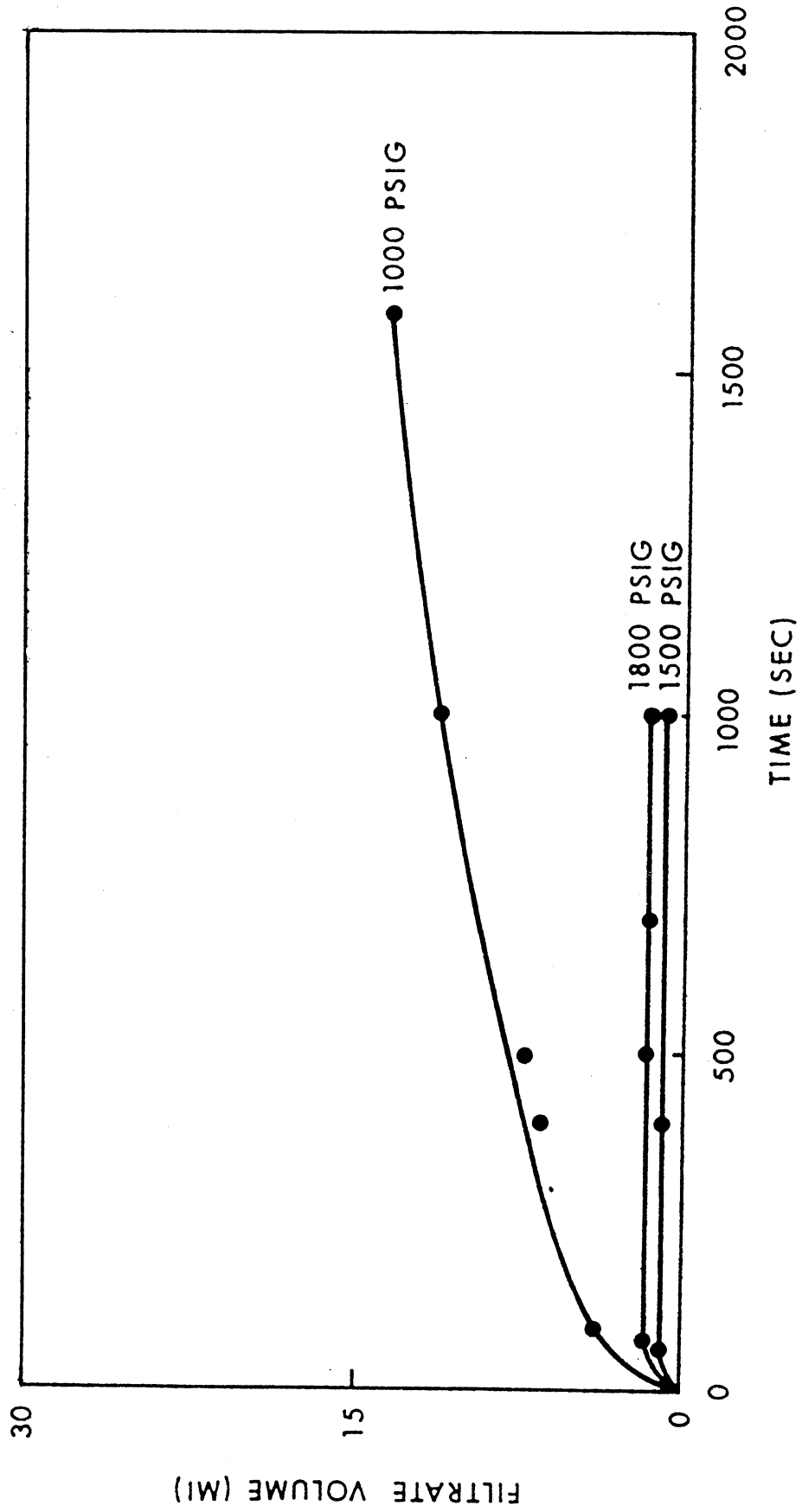


Figure 3.4 Filtration Behavior of Maljamar Crude at $37 \pm 1^\circ\text{C}$ Suggests Organic Solids Become Less Soluble as Temperature is Lowered. (Pressures are those of CO_2 .)

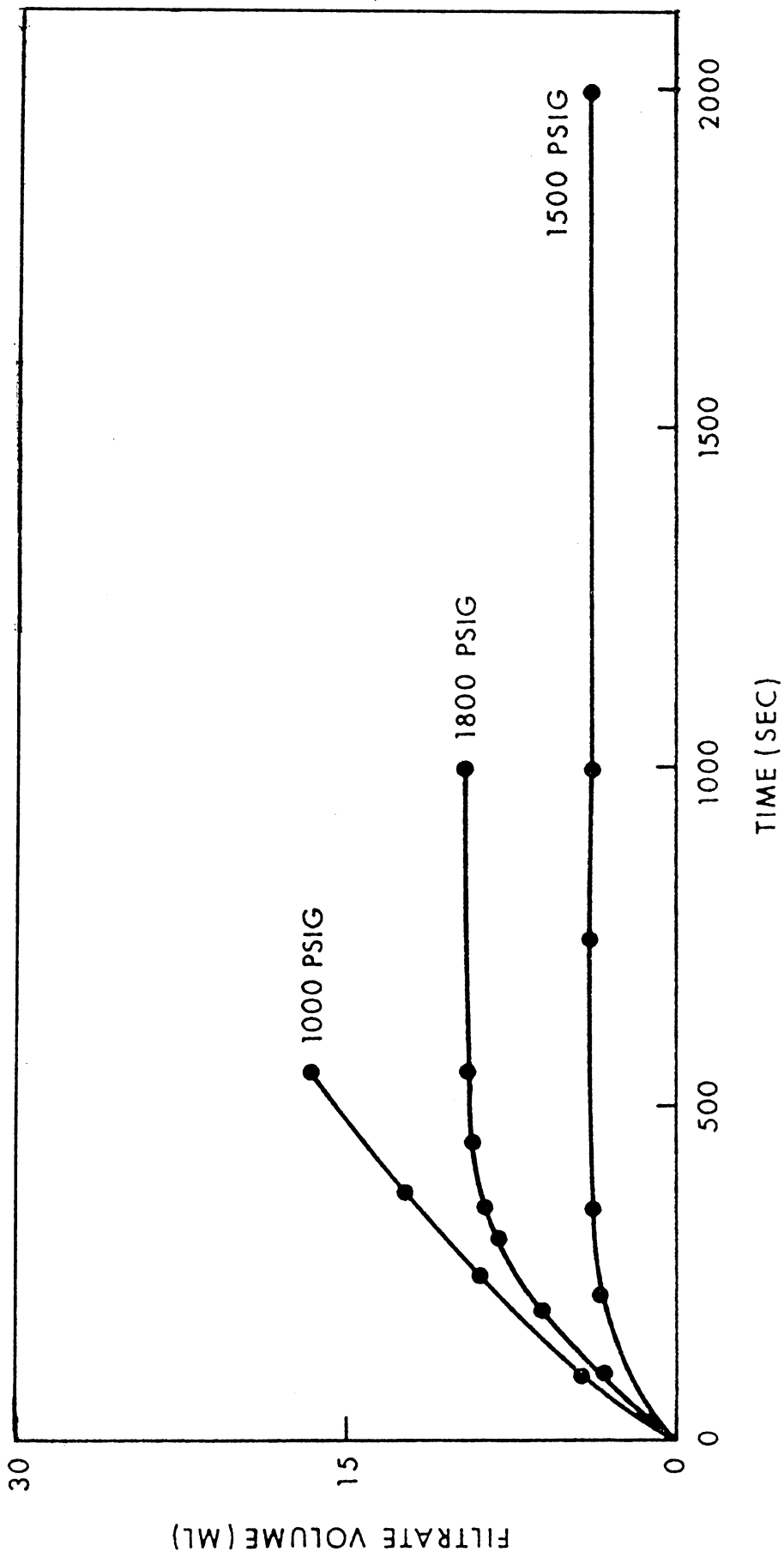


Figure 3.5 Filtration Behavior of Maljamar Crude Shows Anomalous Dependence Upon CO₂ Pressure at 26±2°C.

An anomaly is also observed if one compares the filtration rates, measured at 26, 37 and 50°C, but at constant pressure (1000 psig). (This comparison is presented graphically in Figure 3.6.) Because no precipitate is present in the crude under these conditions, the filtration rate might be expected to increase as the temperature increases, because the viscosity would be reduced. However, the results at 37°C show an exception to this trend; the flow rate is only 60% as great as it is at 27°C. This decrease may be attributed to the fact that CO₂ is a liquid at 27°C, but at 37°C it is a supercritical fluid (critical temperature is 31°C). As a supercritical fluid, it is much less soluble in the crude than when it is a liquid, so it reduces the apparent viscosity less at 37°C than at 27°C. Accordingly, the filtration rate is less at 37°C than at 27°C.

3.4.3 Hilly Upland Crude--As with Maljamar crude, the Hilly Upland crude yielded no asphaltenes when it was mixed with hexane or pentane; but when it was mixed with CO₂, it produced measurable quantities of precipitate. (See Table 3.2) Unlike the Maljamar crude, however, the precipitate formed at

Table 3.2

Precipitate from Hilly Upland Crude
Increases with CO₂ Pressure at 77°F

Volume of Crude Oil Filtered, ml	CO ₂ Pressure psig	Mass of Precipitate g	Wt. % Collected
31.77	300	0.062	0.25
31.77	500	0.065	0.27
41.21	800	0.076	0.28
40.44	950	0.080	0.32

*Based on weight of oil in sight glass

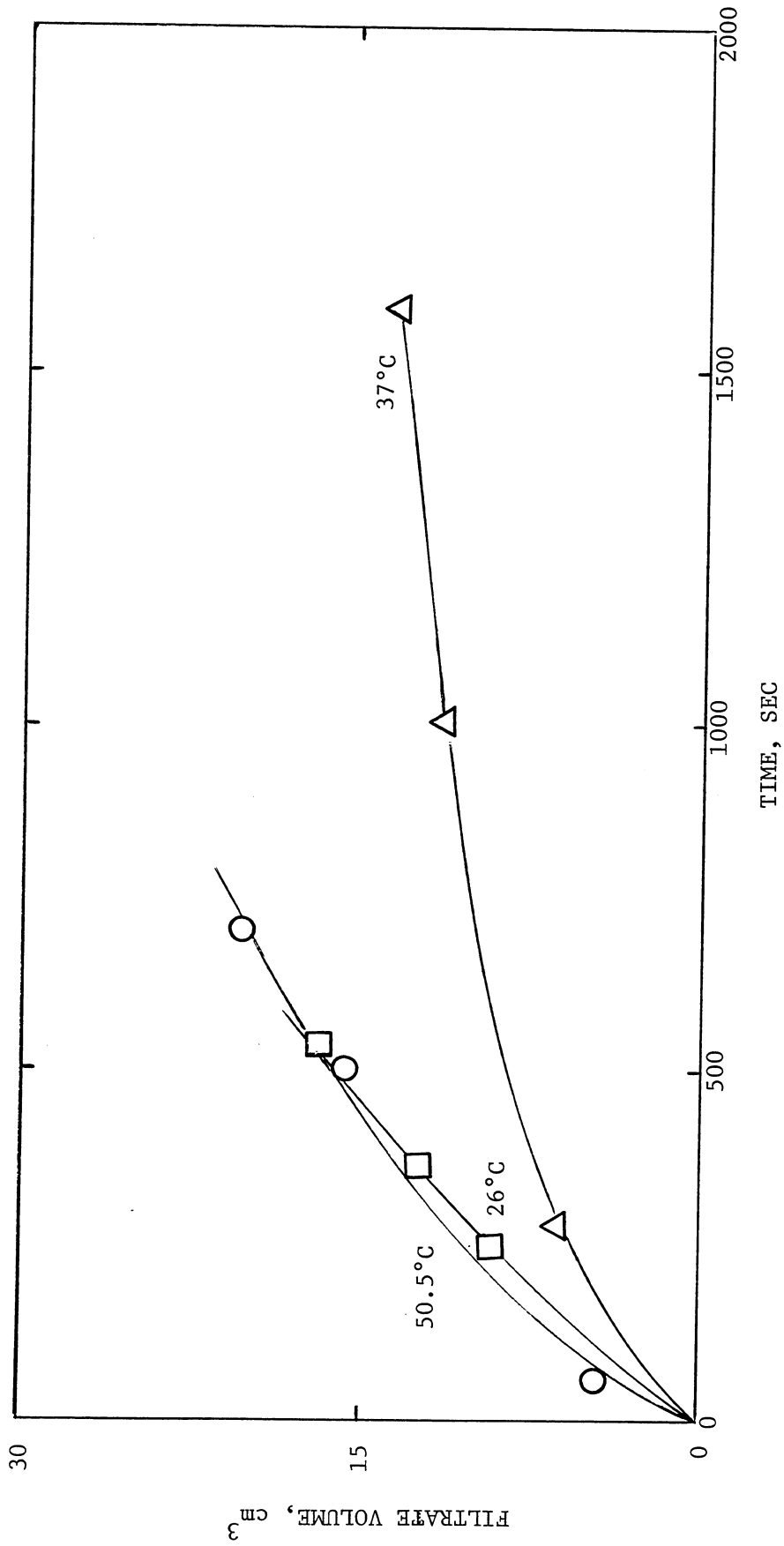


Fig. 3.6 Filtration Rate of Maljamar Crude Depends Upon Temperature
(CO₂ Pressure Constant at 1000 psig)

pressures below 1000 psig, and the precipitate was yellow instead of gray. The precipitate dissolved readily in carbon disulfide (CS_2), but no other attempts were made to identify it.

As with the Maljamar crude, the amount of precipitate from the Hilly Upland oil increased with increasing CO_2 pressure. This is also reflected in the results from the filtration experiments, which are depicted in Fig. 3.7. The filtration rate was constant for a given CO_2 pressure, as indicated by the straight lines in Fig. 3.7. But as the pressure and, hence, the proportion of CO_2 increased, the filtration rate decreased. The filtration rates are indicated by the slopes of the lines, and the slopes vary inversely with the CO_2 pressure.

The change in filtration rate with CO_2 pressure is not due to changes in viscosity. The viscosity of this crude is known to decrease with increasing CO_2 pressure (6). Consequently, increases in CO_2 pressure would cause the filtration rate to increase if nothing else were happening.

That the filtration rates never fell to zero shows that the precipitate from the Hilly Upland crude is more permeable than the precipitate from the Maljamar crude, and that it clogs filter pores less. This suggests that it would be less damaging to an oil reservoir than the precipitate from the Maljamar oil.

As with the Maljamar crude, the precipitation of solids from the Hilly Upland oil can be attributed to the CO_2 reducing the solubility of asphaltics. Alternately, it can be explained by solvent extraction of light hydrocarbons from the oil into the CO_2 -phase above the oil. This would make the asphaltics more concentrated and reduce the amount of solubilizing hydrocarbons in the oil, thereby causing precipitation.

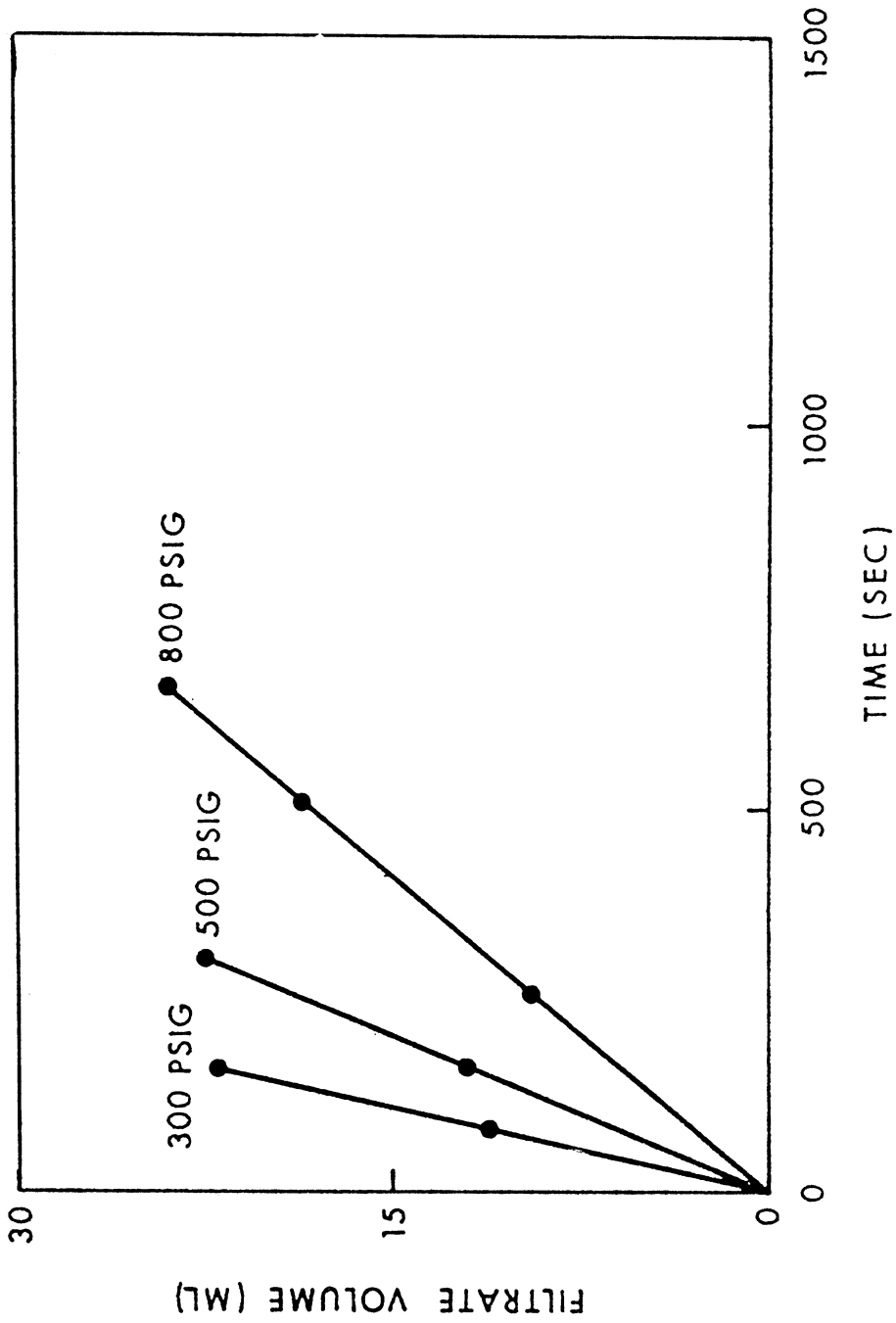


Figure 3.7 Filtration Behavior of Hilly Upland Crude Shows Precipitation Increases with CO₂ Pressure. (Temperature: 26±2°C.)

3.5 Oil Displacement Tests

3.5.1 Introduction--The filtration tests (described previously) only provided qualitative estimates of potential formation damage. To demonstrate actual damage and measure it quantitatively, the Maljamar crude was tested under conditions which simulated CO₂-floods. An unconsolidated sand-pack served as a model of an oil-bearing formation. Under tertiary recovery conditions, a permeability reduction of 25% was observed even after 29% of the residual oil had been displaced. Under conditions simulating CO₂ secondary recovery (no previous waterflood) some permeability reduction was observed. The relative permeability to water at residual oil saturation was 34% lower using CO₂ as a secondary recovery phase as compared to a conventional waterflood.

3.5.2 Description of Model--The sand pack was contained within a 1.5-in diam. (nominal) schedule 80 stainless steel (316S) tube 61 cm long. The tube was flanged at both ends, and inlet and outlet ports were installed in the flanges. The sand was compacted, and its porosity was gravimetrically determined by a mass balance on water.

The injection system is diagrammed in Fig. 3.8. The volumes of the transfer cylinders and the properties of the sand pack are listed in Appendix J. The piping system had valves on both ends of each transfer cylinder. Tees were located in the downstream lines to facilitate refilling the cylinders and to serve as air bleed-off ports. The pressure on each side of the model was measured using bourdon gauges. The gauges had been standardized against each other and against a known pressure.

The entire system was contained within a constant-temperature box (not shown) to keep it at 25±1°C. The positive displacement pump (Ruska) was equipped with an electronic pulse generator to maintain a constant rate of injection. Variations in injection rate were less than ±0.1 percent of the average flow rate.

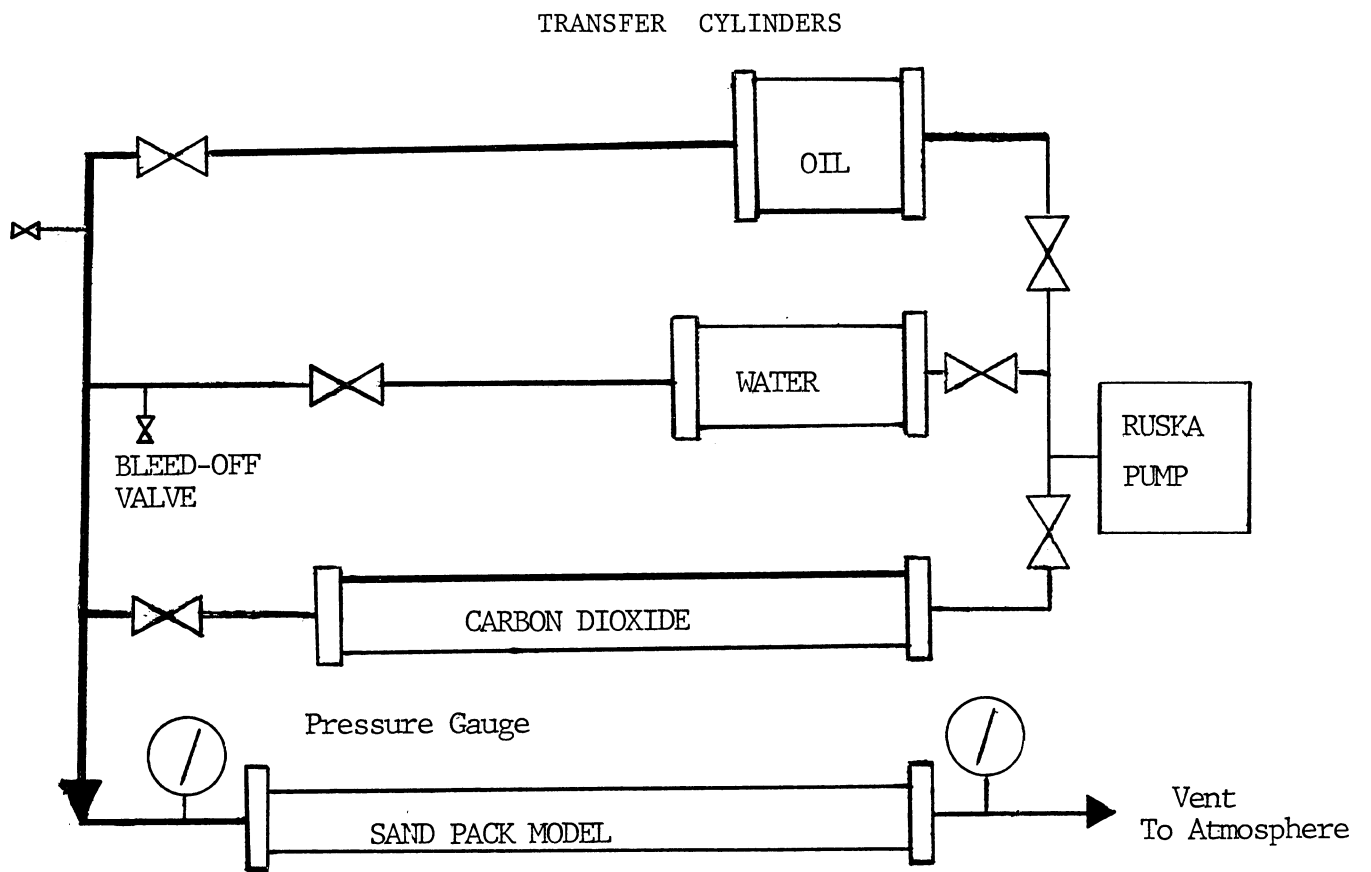


FIGURE 3.8
 SCHEMATIC DIAGRAM OF
 EXPERIMENTAL APPARATUS

3.5.3 Preparation of Sand Pack--After the apparatus was assembled, the tubing and sand pack were purged of all trapped air by injecting gaseous CO_2 . The CO_2 was then removed by injecting a sodium hydroxide solution (pH 10.5) which absorbed the CO_2 . The injection of de-ionized water, followed by 4.0 pore volumes (PV) of a standard brine solution, left the sand pack 100% saturated with brine at pH 7.0. The absolute permeability of this formation model to the brine at 100% brine saturation was determined to be 274 md. Pore volume of the model was 316 cc.

The formation model was next flooded with Maljamar crude oil, selected because the filtration experiments suggested it would be the most likely crude to cause formation damage during a CO_2 flood. After the injection of 3.0 PV of crude oil, the permeability to oil at the irreducible water saturation, S_{iwr} , was determined to be 133 md. The residual water saturation was determined to be 32.0%. (See Appendix K for raw data).

3.5.4 Conventional Waterflood--The model was then waterflooded with brine. The injection rate ranged from 0.05 cc/sec to 0.09 cc/sec at S_{or} . Figure 3.9 shows the oil production which resulted. (Raw data are presented in Appendix K.)

After 4.8 PV of the brine was injected, the permeability to brine at residual oil saturation, S_{or} , was determined to be 118 md. The residual oil saturation was determined to be 10.4%.

3.5.5. Secondary CO_2 -Enhanced Waterflood--Following the waterflood, the model was resaturated with Maljamar crude oil. The permeability to oil at S_{iwr} was determined to be 131 md, compared to 133 md when the pack was first saturated. The connate water saturation (S_{cw}) was 32%, duplicating that obtained after the first saturation.

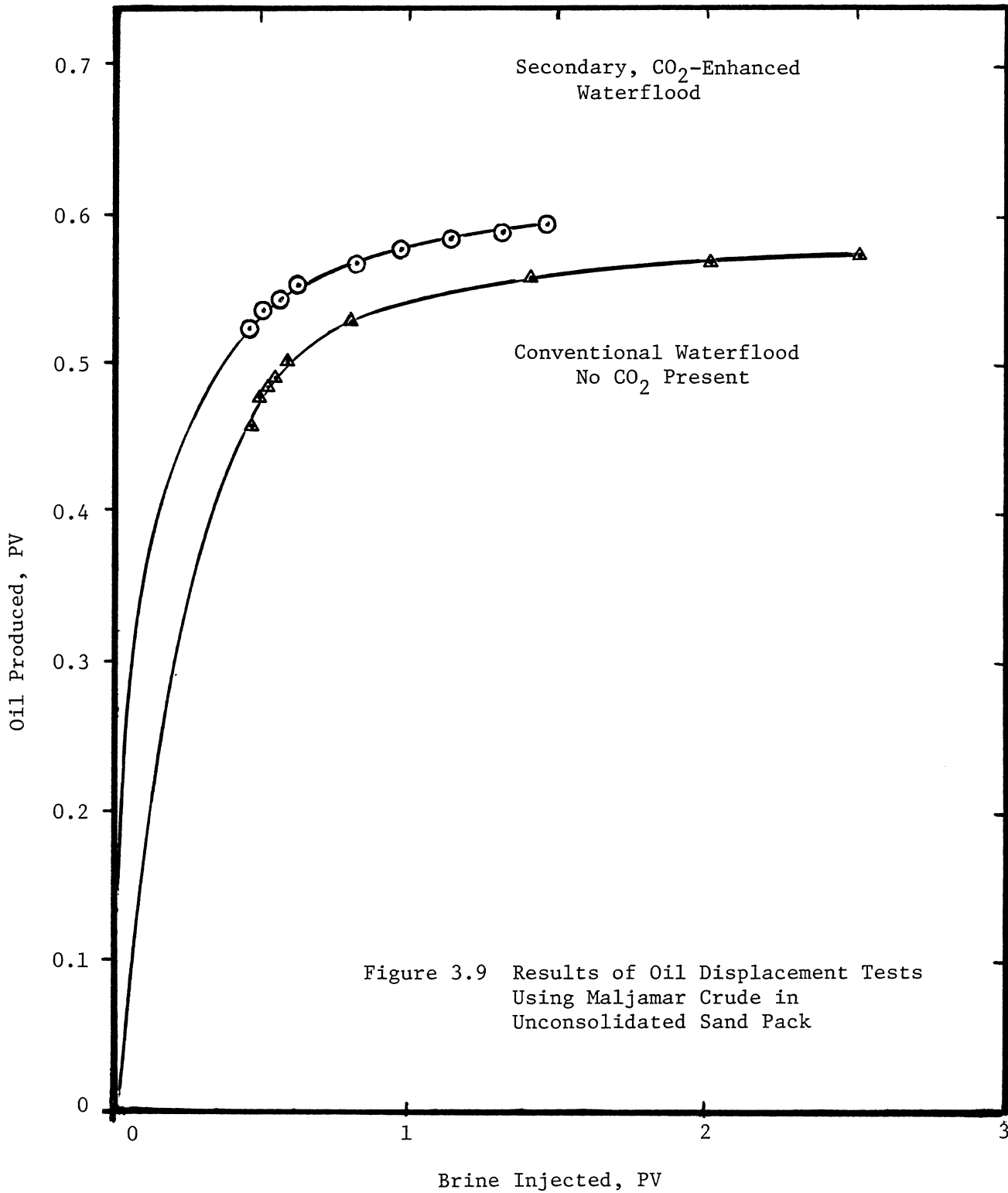


Figure 3.9 Results of Oil Displacement Tests Using Maljamar Crude in Unconsolidated Sand Pack

The formation model was then flooded with approximately 1 PV of CO₂ at a pressure of 1650 psig, resulting in the production of 61.5 cc of oil at gas breakthrough. The model was shut in for 72 hours to allow the CO₂ to completely saturate the oil.

The model containing CO₂-saturated crude was flooded with brine at a frontal advance rate of about 22 ft/day. Oil production essentially ceased after 4.8 PV of brine had been injected. The permeability to brine at residual oil saturation was determined to be 78 md, 34% lower than the 118 md obtained during the conventional waterflood. The residual oil saturation was determined to be 9.4%, slightly below the 10.4% saturation obtained in the conventional waterflood. These results, plotted in Fig. 3.9, show the small improvement over conventional waterflooding obtained by immiscible CO₂ flooding of a high-gravity oil.

It is well-known that immiscible displacement of Maljamar oil by CO₂ will not recover the substantial quantity of tertiary oil obtained by miscible flooding. The flood with Maljamar crude was designed solely to provide data on formation damage.

3.5.6 Tertiary Waterflood--The model was resaturated with Maljamar crude and waterflooded to a residual oil saturation of 12.92%. Then 0.8 PV of CO₂ was injected at a pressure of 1650 psig. Only 2 cc of oil was produced. The model was shut in for 24 hours to allow the CO₂ and crude oil to come to equilibrium. The model was then flooded with brine to a residual oil saturation of 9.2%. The permeability to brine at the new residual oil saturation was determined to be 88 md. The additional oil recovery of 10.0 cc represented 28.8% of the oil remaining in place after the waterflood.

3.6 Conclusions

Our results provide clear evidence that moderate amounts of dissolved CO_2 only modestly affect the flow characteristics of crude oils. For certain crudes, such as Maljamar, contact with CO_2 can precipitate organic materials which might result in some degree of plugging of the reservoir.

- (a) Precipitate formation cannot be reliably predicted from the crude's asphaltene content as determined by the standard light hydrocarbon dilution test. The nature of the precipitate differs in appearance from one crude to another and, in general, differs from the asphaltenes precipitated when pentane is poured into the crude.
- (b) The amount of organic precipitate generated is proportional to the CO_2 pressure. At constant temperature, the amount of organic precipitate increases with CO_2 pressure. By contrast, at constant pressure, no consistent trend is apparent when temperature increases. For certain crudes, such as Maljamar, it appears that a threshold temperature may exist above which organic precipitates no longer occur. Elevation of the temperature decreases particulate formation. This would suggest a CO_2 -enhanced thermal flood might have commercial possibilities.
- (c) Only one of the three crudes we tested (Maljamar) gave a precipitate that potentially could cause formation damage.

When this crude was saturated with CO_2 in a sand pack model, the resulting permeability to brine was reduced only 34%. This amount of permeability damage is not severe. The decrease in permeability might even be beneficial by lowering gas and water mobilities in the region behind the oil bank.

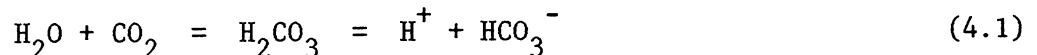
SECTION FOUR
DEPOSITION OF CALCIUM CARBONATE

4.1 Introduction

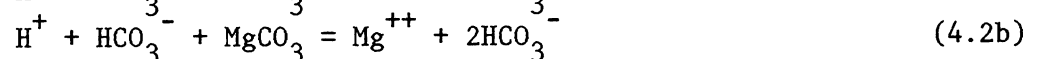
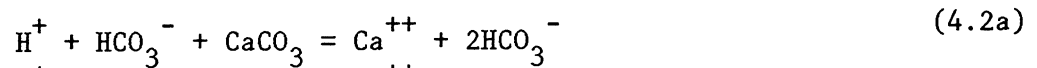
4.1.1. Results--Experiments showed that formation damage could result from precipitation of calcium carbonate within the reservoir, thereby plugging the flow channels. Using an unconsolidated pack of crushed limestone, we found that when CaCO_3 precipitated in it, both porosity and permeability decreased gradually and in a predictable fashion. In other tests, we found that the CaCO_3 forms as scale on the mineral surfaces rather than as tiny particles in the bulk liquid. CaCO_3 also precipitates readily on other surfaces besides limestone, notably glass and silicone resin. The latter observation suggests that CaCO_3 would precipitate as readily in oil-wet reservoirs as in water-wet ones.

4.1.2 Proposed Damage Mechanism--In limestone or dolomite reservoirs, carbonic acid would form near the CO_2 -injection well as CO_2 dissolved in the connate water. The carbonic acid would dissolve the carbonate rock and become saturated with CaCO_3 or MgCO_3 . These substances might precipitate as the CO_2 flood approached the producing well and, thereby, plug the pores in the reservoir.

When CO_2 dissolves in water, it forms carbonic acid in accord with the well-known reaction depicted by Eq. 4.1. The carbonic acid reacts



rapidly with carbonate compounds such as CaCO_3 to form soluble bicarbonate salts, as depicted by Eq. 4.2. As CO_2 is injected under high pressure, the



equilibrium of Eq. 4.1 would be forced to the right, and the acid concentration (H^+) would increase. As the concentration of carbonic acid increased, Equilibria 2a and 2b would similarly be forced to the right and the calcium or magnesium carbonate would dissolve. (Methods to predict whether $CaCO_3$ will precipitate from brine at high temperatures and pressures have been described by Oddo and Tomson (15, 25).)

Reservoir damage might occur as the calcium or magnesium carbonate, which dissolved in the high-pressure region of the reservoir, migrated to remote, low-pressure regions of the reservoir. As the pressure became lower, carbon dioxide would bubble out of solution causing Equilibrium 4.1 to shift to the left which, in turn, would cause Equilibria 4.2a and 4.2b to shift to the left. That is, calcium bicarbonate and magnesium bicarbonate would decompose into CO_2 , water, and the solids calcium carbonate and magnesium carbonate.

It is important to know the character of the precipitate. Specifically would it be tiny particles in the bulk liquid, or a scale on the walls of the pores in the reservoir rock? The reservoir's permeability might be drastically reduced if tiny particles formed, because they might be swept along until they lodged in a pore throat and thereby blocked the pore completely. On the other hand, if the $CaCO_3$ formed as a scale, it would be distributed along the length of the pores; and, although the cross-sectional area of each pore would be reduced, the pores would not be completely blocked. Indeed, if the scale deposited preferentially in pores of large diameter or in the large-diameter sections of non-uniform pores, the reduction in permeability might be negligible.

Experiments to determine the character of the precipitate and the factors governing the rate of precipitation are discussed in the following sections.

4.2 Nature of CaCO₃ Precipitate

4.2.1 Introduction--One would expect that, during a CO₂ flood where frontal advance rates are about 1 ft/day, the pressure would decrease very gradually. And because the solubility of CaCO₃ depends on pressure, the concentration of CaCO₃ would change only gradually. The concentrations of Ca⁺⁺ and CO₃⁼ would be approximately those corresponding to saturation, because of the slow advance rate and because the surface area for scale formation would be large relative to the volume of Ca⁺⁺ solution. These conditions are unfavorable for nucleation and crystal growth in the bulk liquid, but favor scale formation.

Unfortunately, the above conditions are not easy to simulate in the laboratory. If experiments are to be performed in a reasonable period of time, and if sufficient amounts of CaCO₃ are to be precipitated so that analytical accuracy can be maintained, then the precipitation rate must be high. To achieve this, the concentrations of Ca⁺⁺ and CO₃⁼ must be considerably above the saturation concentrations. Moreover, large volumes of solution must be employed. These conditions favor nucleation in the bulk liquid at the expense of scale formation. To resolve this dilemma, the approach we used was to perform a series of experiments, each under conditions closer to reservoir conditions than the one before, then extrapolate the results to the reservoir conditions. One further simplification was made. Instead of forming Ca⁺⁺ and CO₃⁼ by dissolving limestone in carbonic acid, we prepared separate solutions of CaCl₂ and Na₂CO₃ in 3% (wt) NaCl brine, then we mixed these to give supersaturated solutions of CaCO₃.

4.2.2 Apparatus--Experiments were performed using a 3/4-in. i.d. vertical tube made of methyl methacrylate, equipped with two inlet ports at the bottom. (See Fig. 4.1) The tube was filled to the desired height with crushed limestone, sieved to 60-70 mesh (U.S.A. standard). The particles of limestone were supported by a screen.

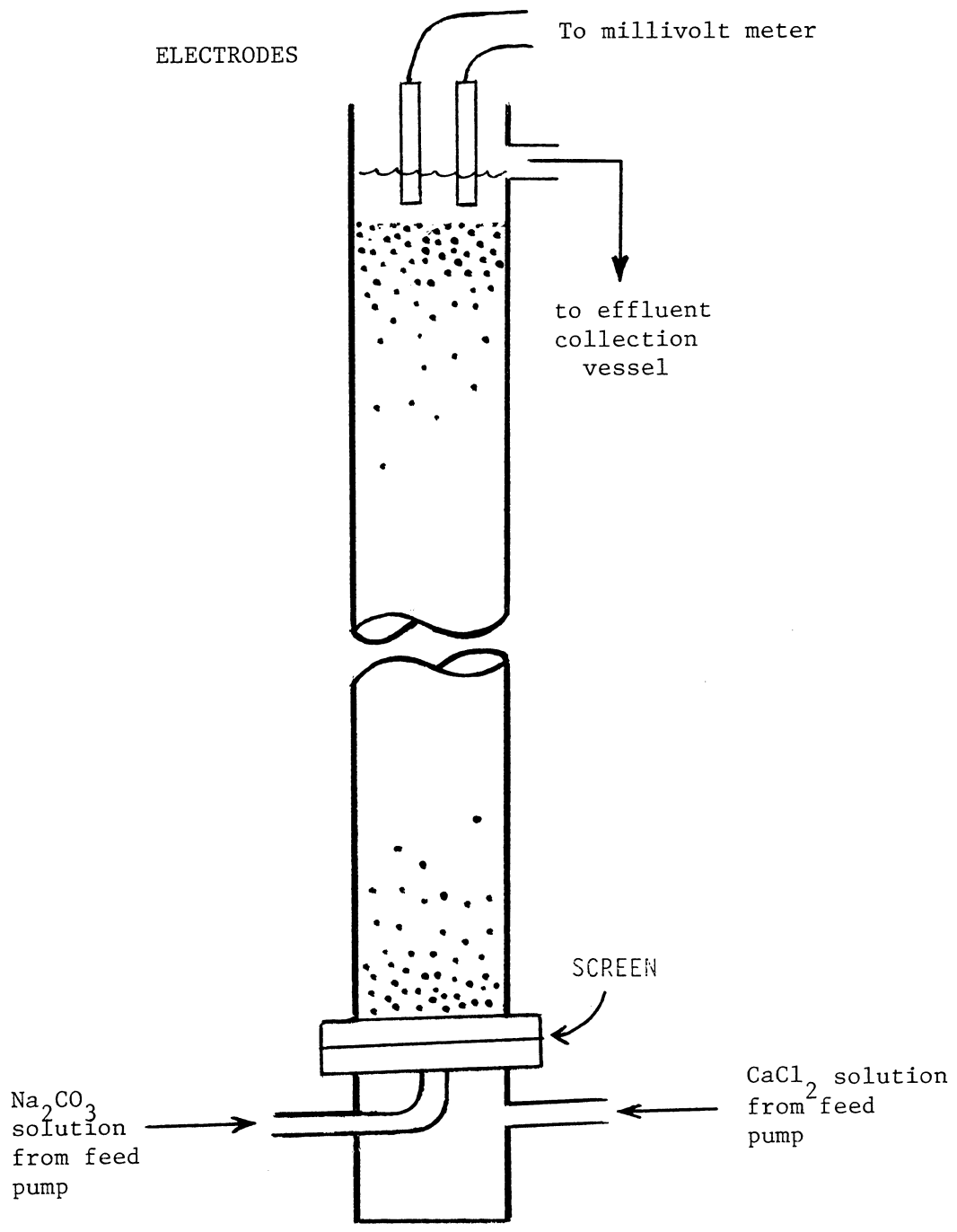


Fig. 4.1 FLUIDIZED BED FOR DETERMINING NATURE OF CaCO₃ PRECIPITATE

Standard solutions of CaCl_2 and Na_2CO_3 were pumped into the tube and upward through the limestone using calibrated metering pumps (Fluid Metering, Inc., model RP-D). The flow rate (4 ml/sec) was always sufficient to fluidize the bed of limestone, but not sweep any limestone particles out the top.

The effluent Ca^{++} concentration was measured continuously by a specific-ion electrode (Orion, model 93-20) in conjunction with a calomel reference electrode (Fisher, model E-6A) using a millivolt meter (Orion, model 811). The Ca^{++} electrode was calibrated using standard Ca^{++} solutions containing 3% wt. NaCl. Readings were automatically corrected for temperature changes using a temperature compensator probe (Orion, model 91-70-02) (not shown).

4.2.3 Procedure--When the Ca^{++} and $\text{CO}_3^{=}$ solutions mixed just above the support screen, CaCO_3 began to precipitate, either as scale on the surfaces of the limestone or as fine particles in the liquid. The fine particles remained with the upward flowing solution and were swept out as a milky suspension. The residence time of the tiny particles was too short for them to grow large enough to stay in the fluidized bed.

The soluble Ca^{++} in the effluent was measured continuously with the specific-ion electrode located just above the fluidized bed. The total calcium concentration (soluble Ca^{++} and particles of CaCO_3) was measured by a 4-step procedure: (a) the collected effluent was acidified (HCl) to pH 2 in order to dissolve the particles; (b) the solution was neutralized (NaOH) to pH 6.5-7.5; (c) the solution was mixed well to ensure uniform concentration; and (d) the Ca^{++} concentration was measured with the specific-ion electrode.

The total mass of calcium in the effluent was the product of the Ca^{++} concentration and the total volume of effluent. The mass of Ca^{++} pumped into the column was known from the volume and concentration of the CaCl_2 fed. The amount of calcium which precipitated on the limestone surfaces was

determined by difference. To confirm this result, the mass of scale which formed on the limestone was also determined by weighing the dry limestone grains before and after each experiment.

4.2.4 Results--The amount of Ca^{++} which remained on the limestone, as calculated from the mass balance described above, agreed within 12% with the increase in mass of the limestone particles, if we assumed the Ca^{++} precipitated as CaCO_3 . (See Table 4.1) If the precipitate was assumed to be Ca(OH)_2 , the calculated increase in mass of the limestone was generally 25% less than the measured increase. Thus we concluded the scale was CaCO_3 .

Table 4.1
Calcium Remaining in Limestone Bed*

By Mass Balance on Ca^{++}		By Weighing the Limestone
as Ca^{++}	as CaCO_3	
1.51 g	3.8 g	4.3 g

*60-70 mesh chips; residence time: 68 sec.

Regardless of the height of the fluidized bed, the effluent solutions remained clear, as long as the concentrations of Ca^{++} and $\text{CO}_3^{=}$ in the fluid bed were kept sufficiently low that their product was less than 10^{-3} M^2 , i.e.

$$[\text{Ca}^{++}][\text{CO}_3^{=}] < 10^{-3} \text{ mol}^2/\text{l}^2 \quad (4.3)$$

The clarity of the solutions indicated that no CaCO_3 precipitate had formed in the bulk liquid. The effluents were, however, supersaturated. Some had concentration products $[\text{Ca}^{++}][\text{CO}_3^{=}]$ as high as $5 \times 10^{-4} \text{ mol}^2/\text{l}^2$. (The solubility product for CaCO_3 is about $5 \times 10^{-9} \text{ mol}^2/\text{l}^2$).

That the effluent should be supersaturated with CaCO_3 yet remain clear was not entirely unexpected, because metastable supersaturated solutions of

calcium salts are well-known. However, when the product $[Ca^{++}][CO_3^{=}]$ exceeded 10^{-2} M, the effluent was turbid; most of the entering Ca^{++} formed a fine precipitate which was swept from the column. Thus we conclude that, in an oil reservoir where the ion concentrations would presumably be low, the $CaCO_3$ would precipitate as scale rather than as particulates.

4.3 Effect of Concentration on Precipitation Rate

4.3.1 Introduction--The concentration variable in the above discussion and in the discussion which follows is expressed as the product of the ion concentrations, rather than as an individual concentration. This is because one would expect the precipitation rate to depend upon how far the concentrations are above saturation, and saturation is described by the solubility product K_{sp} .

$$K_{sp} = ([Ca^{++}][CO_3^{=}])_{\text{at equilibrium}} \quad (4.4)$$

Mathematically then, the rate depends upon the difference between K_{sp} and the product $[Ca^{++}][CO_3^{=}]$ as given by Eq. 4.5.

$$d[Ca^{++}]/dt = -k\{[Ca^{++}][CO_3^{=}] - K_{sp}\} \quad (4.5)$$

This is a reasonable formulation inasmuch as when the concentrations drop to saturation so that Eq. 4.4 is satisfied, the rate given by Eq. 4.5 is zero.

4.3.2 Results--The effect of concentration changes upon the rate of $CaCO_3$ precipitation is illustrated by the results presented in Table 4.2. They show that the fraction of entering Ca^{++} which remained in the bed (as scale) increased as the product $[Ca^{++}][CO_3^{=}]$ increased. As before, the effluents were clear, suggesting that no Ca^{++} had precipitated in the bulk liquid.

The results in Table 4.2 represent average precipitation rates within the fluidized bed. Because the precipitation rate is a strong function of

Table 4.2

Precipitation on Limestone Increases with
 Concentrations of Ca^{++} and CO_3^-
 (Fluidized beds of 60-70 mesh particles)

Residence time, sec	$[\text{Ca}^{++}][\text{CO}_3^-]^*$ mol ² /l ²	Fraction of Entering Ca^{++} which Precipitated as Scale
41	1.2×10^{-4}	0.17
45	9.0×10^{-4}	0.45

*Based upon concentrations of feed solutions after mixing
 within the fluidized bed.

the product $[\text{Ca}^{++}][\text{CO}_3^-]$, the rate does not vary linearly from the bottom of the bed to the top. That is, the rate also depends upon the residence time in a non-linear fashion. Accordingly, further discussion of precipitation rate and its dependence upon concentration is postponed until residence time is considered (following section).

4.4 Effect of Residence Time On CaCO_3 Precipitation

4.4.1 Introduction--The residence time of the Ca^{++} and CO_3^- ions was varied by changing the amount of limestone in the bed and, hence, the bed height. Changing the flow rate of the solution was impractical, because the height of a fluid bed increases as the fluid velocity increases. Thus the residence time would not be strictly inversely proportional to the fluid velocity.

4.4.2 Results--As expected, the fraction of entering Ca^{++} which precipitated as scale also increased as the residence time of the the mixed CaCl_2 and Na_2CO_3 solutions increased. (See Table 4.3)

Table 4.3

Scale Formation on Limestone Favored
by Increased Residence Time

Residence Time, sec	$[Ca^{++}][CO_3^{=}]^*$ mol ² /l ²	Fraction of Entering Ca ⁺⁺ Precipitating as Scale
45	9×10^{-4}	0.45
133	8×10^{-5}	0.90

*Based upon concentrations of feed solutions after mixing within fluidized bed.

Again, no particles of CaCO₃ were seen in the effluent. These observations imply that, under the conditions found in a reservoir, all precipitation would be as scale.

4.4.3 Importance of Concentration Changes.--The fraction of calcium removed is not linearly proportional to the residence time. Nor should we expect it to be. This is because the precipitation rate is not constant. The concentrations of Ca⁺⁺ and CO₃⁼ decrease as they move up through the bed and the rate of scale formation depends upon those concentrations, as previously stated. In the present experiments, the residence time was varied by changing the bed height, so Ca⁺⁺ concentrations and precipitation rates were much greater in the shorter beds than in the taller ones.

That the concentration of Ca⁺⁺ is a non-linear function of bed height is illustrated by the results presented in Fig. 4.2. Had the precipitation rate been constant throughout the bed (i.e., independent of Ca⁺⁺ and CO₃⁼ concentrations), the reduction of Ca⁺⁺ concentration would have been proportional to bed height and the results depicted in Fig. 4.2 would have formed a straight line.

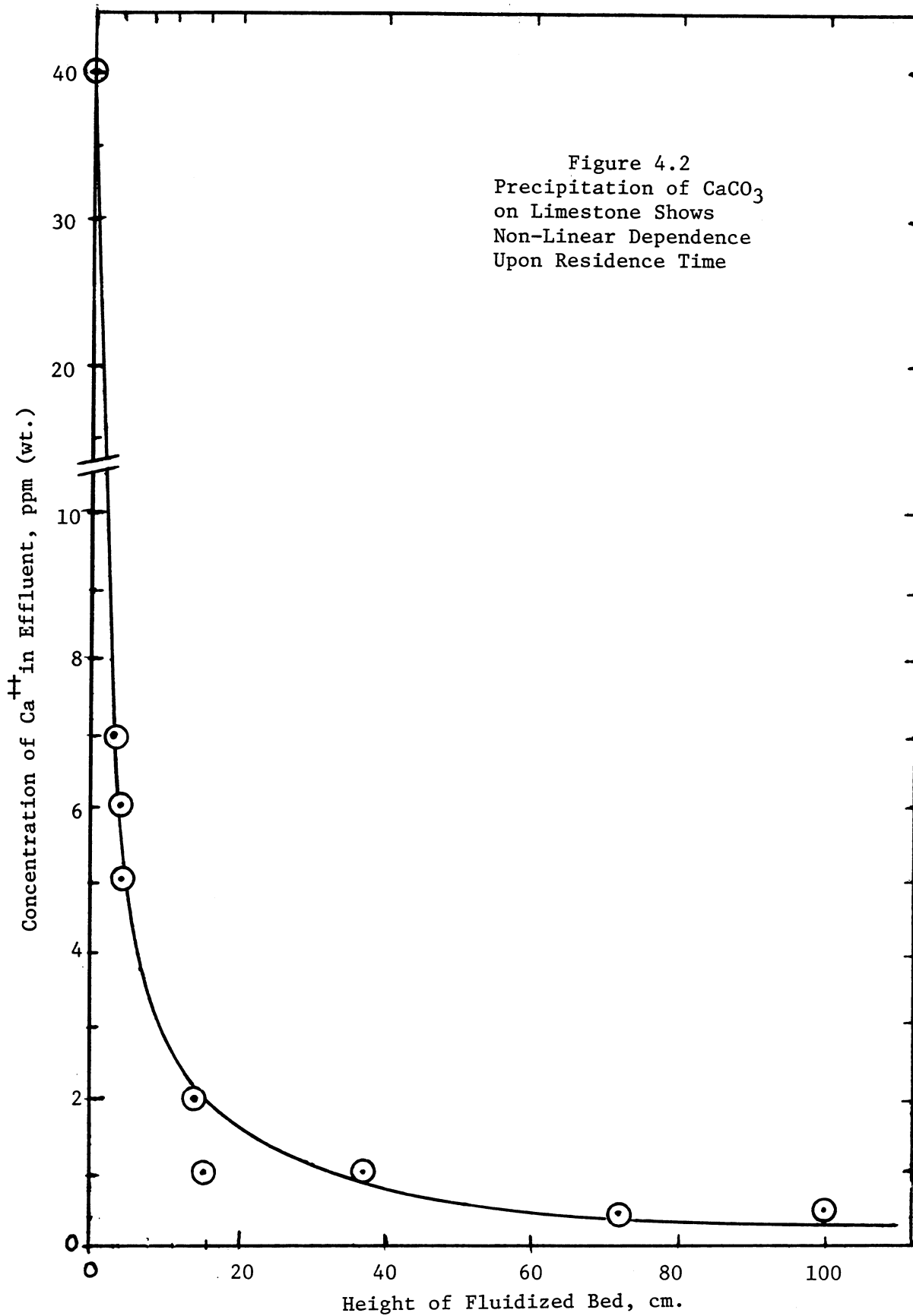


Figure 4.2
 Precipitation of CaCO_3
 on Limestone Shows
 Non-Linear Dependence
 Upon Residence Time

4.4.4 Equation Accounts for Concentration Changes.--A rate expression which satisfactorily fits the results is Eq. 4.6. (Its derivation and a discussion of an alternate model are found in Appendix M).

$$1/[Ca^{++}]_e = k(A/F)(0.025M)h + 1/[Ca^{++}]_o \quad (4.6)$$

where $[Ca^{++}]_e$ is the concentration of Ca^{++} in the effluent,

$[Ca^{++}]_o$ is the concentration of Ca^{++} as it enters the fluid bed,

k is the rate constant for precipitation of $CaCO_3$ on limestone.

Equation 4.6 predicts that if the reciprocal of $[Ca^{++}]$ is plotted against bed height, h, the result will be a straight line. Such a plot (Fig. 4.3) is, indeed, linear within the limits of experimental error, suggesting the model is valid.

Although we established that the rate is second-order with respect to $[Ca^{++}]$, we did not determine how the rate depends on $[CO_3^{=}]$. Thus, the most specific rate expression we can write is Eq. 4.7.

$$d[Ca^{++}]/dh = -K(A/F)[Ca^{++}]^2[CO_3^{=}]^b \quad (4.7)$$

where the exponent b is undetermined. Further experimentation would be required to establish its value.

4.4.5 Applicability to a CO_2 Flood.--Although Eq. 4.7 represents the experimental results satisfactorily, it cannot be used to describe a CO_2 flood for two reasons. First, under the conditions expected to prevail in a reservoir, the concentrations of Ca^{++} and $CO_3^{=}$ might be so low that K_{sp} would not be negligible compared with $[Ca^{++}][CO_3^{=}]$. Hence the more complete form of the rate expression would have to be used, i.e., Eq. 4.8

$$d[Ca^{++}]/dh = -k(A/F)\{[Ca^{++}][CO_3^{=}] - K_{sp}\}^n \quad (4.8)$$

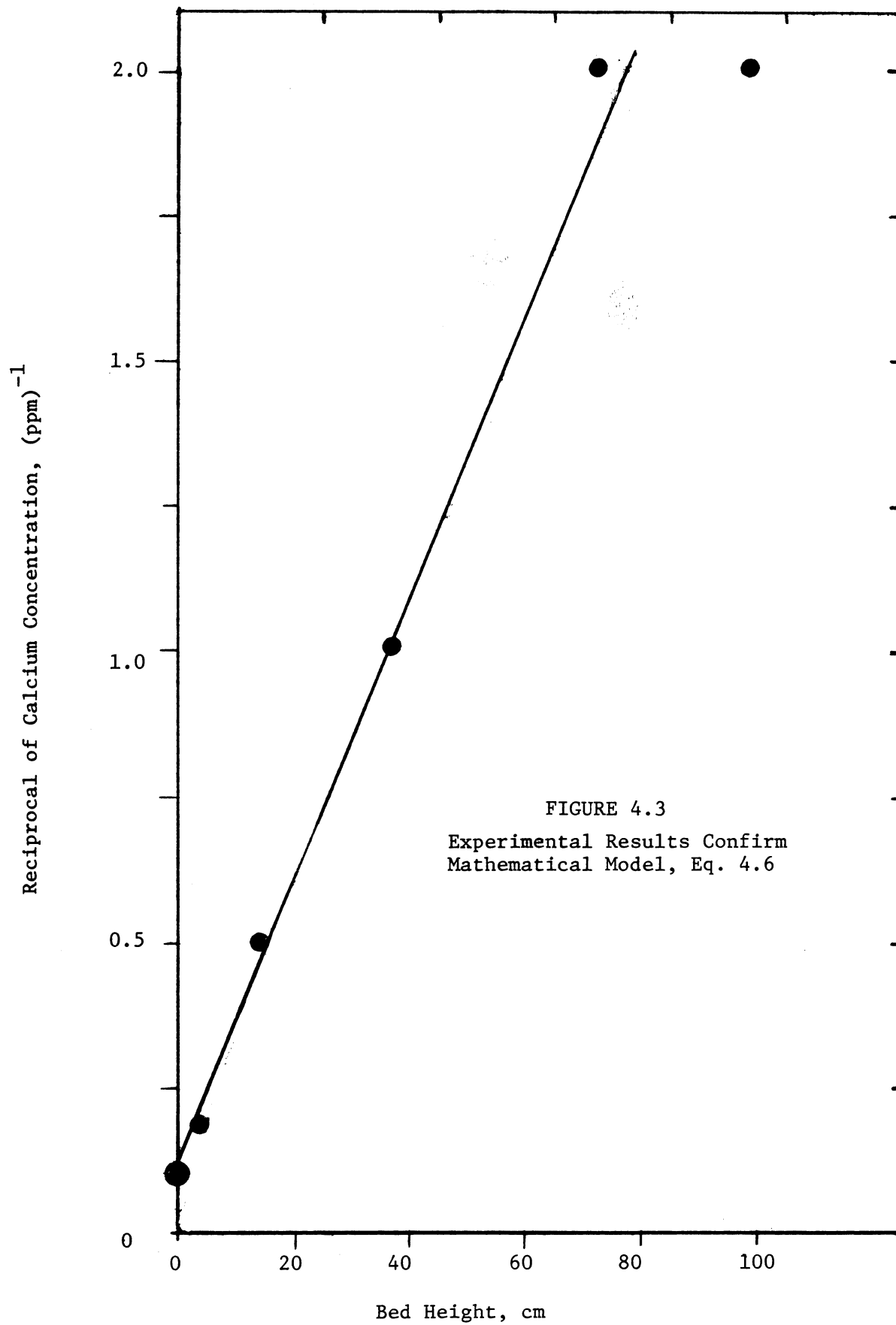


FIGURE 4.3
Experimental Results Confirm
Mathematical Model, Eq. 4.6

Second, the carbonate concentration would not be related to $[Ca^{++}]$ in a simple way. Most of the carbonate would be present as HCO_3^- , not $CO_3^{=}$; and the concentration of $CO_3^{=}$ depends upon the equilibrium depicted by Eq. 4.9



4.4.6 Conclusions.--Despite the limitations of the math model, the experimental results permit two statements to be made about a CO_2 flood. First, the extent of supersaturation of Ca^{++} would not be great, because the precipitation rate would increase much faster than the concentration of Ca^{++} . (Eq. 4.7 shows the rate is second-order in Ca^{++} concentration.) As a result of low supersaturation, the precipitation rate would be low. Consequently, only $CaCO_3$ scale would form in the reservoir; no particles would be formed.

Second, because the extent of precipitation is proportional to residence time, and because residence time would be great during a CO_2 flood, precipitation would proceed until the concentrations of Ca^{++} and $CO_3^{=}$ had essentially reached the solubility product. The concentrations of Ca^{++} and $CO_3^{=}$ at any point in the reservoir could then be calculated if the CO_2 pressure, the temperature, and the appropriate equilibrium constants were known. Finally, if the flow of Ca-saturated brine could be estimated, the amount of $CaCO_3$ which precipitates between any two points in a reservoir (where pressures are known) could be calculated. (Such calculations have been done, and the effect upon reservoir permeability predicted. See section 4.7).

4.5 Dependence upon Nature of Surface

4.5.1 Introduction.--Although most reservoirs are characterized as water-wet, some are believed to be oil-wet. Accordingly, it was of interest to determine

how the precipitation of CaCO_3 would be affected by changing the nature of the surface on which it deposited.

It was not surprising to observe that CaCO_3 precipitates rapidly on limestone, since limestone is a form of CaCO_3 . However, if the surface were chemically different, even hydrophobic, CaCO_3 scale might not form upon it. Thus, if solid CaCO_3 formed, it would have to be as fine particles in the bulk liquid. As mentioned previously, this could have a devastating effect on the reservoir permeability. To study this possibility, we performed experiments that were similar to those which employed crushed limestone.

4.5.2 Procedure.--The same apparatus was used as in the studies with limestone (see section 4.2.2), but the limestone was replaced by tiny beads of glass (typically, 35-45 mesh USA standard) that had been coated with a silicone resin. In later studies we also used uncoated glass beads.* (Additional information about these materials will be found in Appendix N.) As before, the beads were fluidized by the upward-flowing solutions of CaCl_2 and Na_2CO_3 , and any particles of CaCO_3 which formed in the liquid were swept from the bed.

4.5.3 Results.--Within minutes of first being exposed to the supersaturated solution, both the silicone resin-coated beads and the uncoated glass beads became coated with CaCO_3 scale. Since the surfaces were then practically identical, they removed Ca^{++} from the surrounding solution with nearly equal efficiency. As shown in Table 4.4, the fractions of Ca^{++} removed from the entering solutions were comparable to those observed when the fluid bed was limestone. This was true despite the fact that the surface area of silicone-coated beads was only 80% as great as that of the limestone particles. (See Table 4.5.)

*Glass was of interest because it represented, chemically, silicate minerals such as sandstones which are typical of many reservoirs.

Table 4.4
Experimental Results for Precipitation of CaCO₃
on Three Different Surfaces

Particles in Bed	Residence Time, min	Entering Ca ⁺⁺ Collected As Scale, %	[Ca ⁺⁺][CO ₃ ⁼] entering mol ² /l ²
Silicone-	2.6	84	2.0 x 10 ⁻⁵
Coated Glass	2.2	90	8.0 x 10 ⁻⁵
Uncoated	3.1	94	1.5 x 10 ⁻⁵
Glass	2.9	90	1.9 x 10 ⁻⁵
Crushed	3.9	90	5.0 x 10 ⁻⁵
Limestone	2.2	84	2.5 x 10 ⁻⁵

Table 4.5
Surface Areas of the Materials Used
in the Experiments Described in Table 4.4

Particles in Bed	Mesh U.S.A. Std.	Mass g	Surface Area, cm ² per gm	total
Limestone	60-70	158	30*	4740
Glass Beads	70-80	178	12.7	2260
Beads with silicone coating	35-45	672	5.8	3900

*from Ref. 18

The precipitates on both the coated and uncoated glass beads were shown to be CaCO₃ in two ways. First, the mass of the bed increased by the amount predicted from the mass balance on Ca⁺⁺. (See Tables 4.6 and 4.7.) Second, when the beads were rinsed with dilute acid after an experiment, the white

Table 4.6

Calcium Remaining in Fluid Bed
of Silicone-Coated Beads*

By Mass as Ca ⁺⁺	Balance on Ca ⁺⁺ as CaCO ₃	By Weighing the Beads
4.4 g	11.0 g	10.9 g
4.3 g	10.7 g	10.8 g

*35-45 mesh USA std; bed ht. = 112 and 120 cm

Table 4.7

Calcium Remaining on Glass Beads**

By Mass as Ca ⁺⁺	Balance on Ca ⁺⁺ as CaCO ₃	By Weighing the Beads
4.29 g	10.72 g	10.52 g

**Bed ht. = 112 cm; Residence time = 1.2 min.

coating readily dissolved with effervescence, and the percentage of Ca in the coating was that expected for CaCO₃, namely, 40% by wt.

As in the experiments with limestone, no turbidity was seen in the effluent above the fluidized bed, suggesting that the only precipitate which formed was scale on the beads. However, the total concentration of calcium* in the effluent was measurably greater than the concentration of soluble calcium as measured by the specific-ion electrode during the experiment. These results are given in Table 4.8.

*The total calcium concentration was determined by acidifying a sample of effluent to dissolve any CaCO₃ precipitate, then neutralizing the sample with NaOH to pH 6.5-7.5. Experiments had shown that H⁺ ion was not a serious interference when pH was greater than 6.5.

Table 4.8

Comparison of Soluble and Insoluble Calcium
in Effluents from Fluidized Beds

Particles in Bed	Residence Time, min	Ca ⁺⁺ in Effluent, ppm (wt)	
		soluble	insoluble
Glass beads	2.4	3.2	6.8
	2.9	2.3	2.7
	1.0	1.6	2.3
Silicone- coated beads	1.2	2.5	7.5

The differences between the concentrations of soluble and insoluble calcium suggest that some particles of CaCO₃ of sub-micron size were forming in the bulk liquid. The amounts were small, however, and represent, at most, 14% of the Ca⁺⁺ entering the fluidized bed. Thus, for the experiment with silicone-coated beads listed in Table 4.8, 79% of the entering Ca⁺⁺ precipitated as scale, 14% of the Ca⁺⁺ precipitated in the bulk liquid, and 7% remained in solution. Usually, less than 6% of the entering Ca⁺⁺ precipitated in the bulk liquid, while 90% formed scale.

The influence of residence time and ion concentrations upon the extent of precipitation were not studied specifically. However, the results in Table 4.4 suggest that increasing either the concentrations or the residence time also increases the fraction of Ca⁺⁺ which forms scale. (This is true as long as the product of calcium and carbonate concentrations is sufficiently small that particulate-formation is not significant)

4.5.4 Rate of Scale Growth.--As previously mentioned, the surfaces of the glass beads and silicone-coated beads became covered with CaCO₃ within minutes after exposure to a supersaturated solution of Ca⁺⁺ and CO₃⁼. After this happened, any difference between the surfaces was obscured.

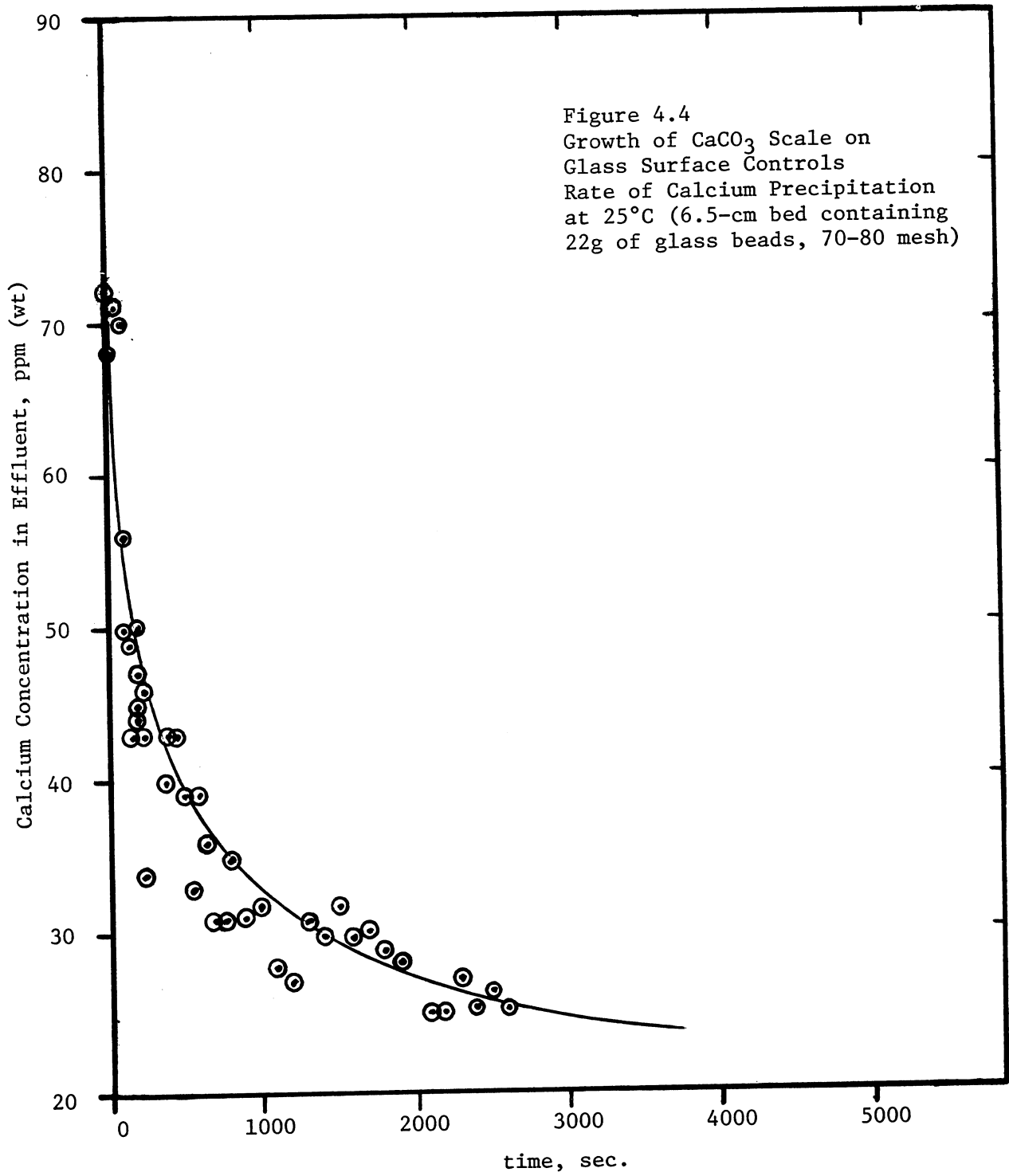
To observe these differences and measure the rates at which the surfaces became covered with scale, we changed the procedure of Section 4.2 in two ways. First, we reduced the height of the fluidized bed and hence the residence time of the calcium solution. Second, we measured the Ca^{++} concentration in the effluent at 20-sec intervals as soon as Ca^{++} and $\text{CO}_3^{=}$ began entering the bed.

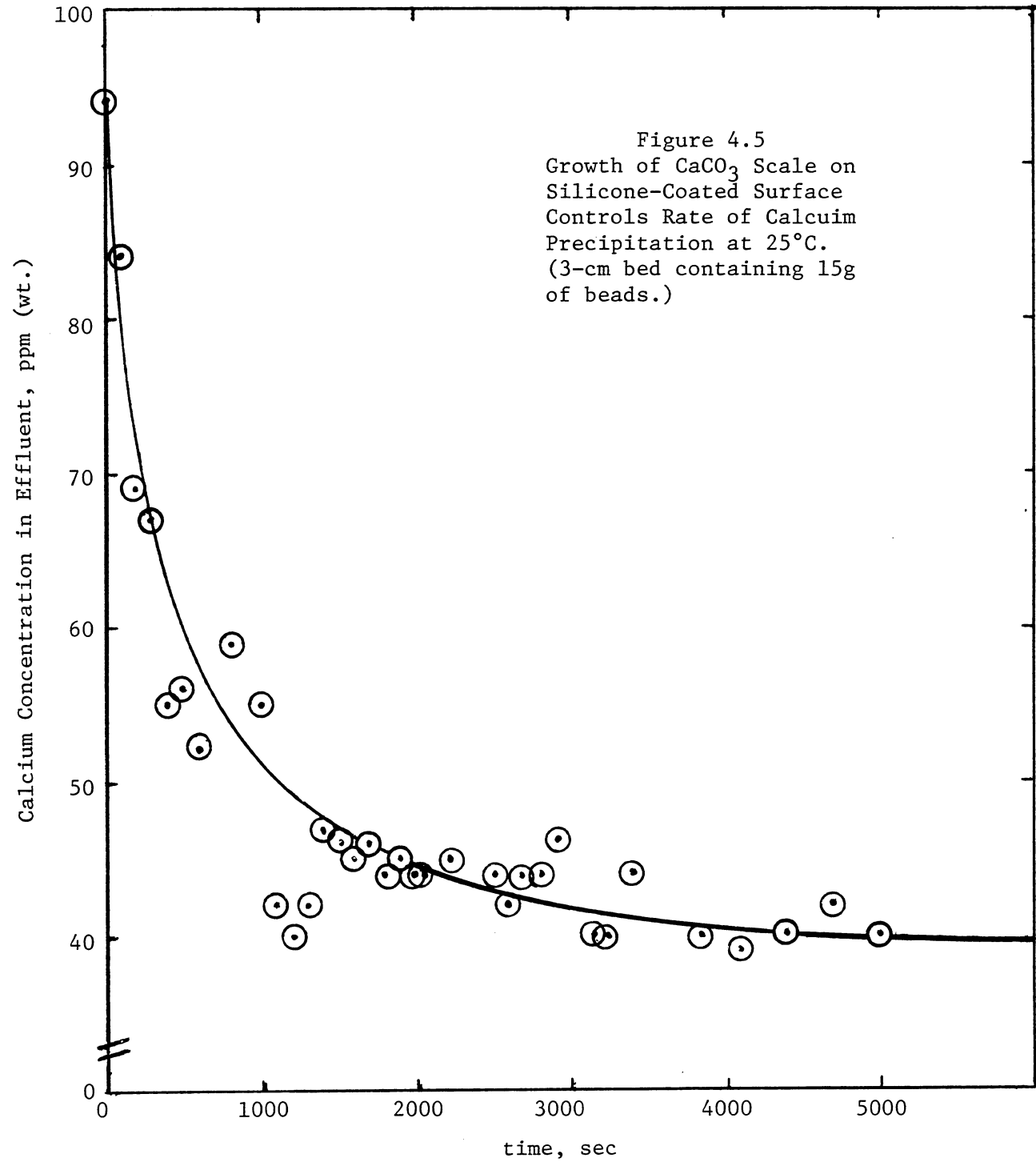
Typical results are depicted in Figs. 4.4 and 4.5 which show that the Ca^{++} concentration in the effluent decreases with time, reaching a limiting value which is considerably above the concentration corresponding to equilibrium (i.e., the solution is still supersaturated with CaCO_3 .) The limiting concentrations and the corresponding concentration products are presented in Table 4.9.

Table 4.9
Limiting Concentrations Observed During
Scale-Formation Experiments

Beads in Bed	Surface Area, cm^2	Limiting Effluent Concentrations		
		$[\text{Ca}^{++}]$, M	$[\text{CO}_3^{=}]$, M	$[\text{Ca}^{++}][\text{CO}_3^{=}]$, M^2
Uncoated glass	280	6.3×10^{-4}	1.17×10^{-3}	7.4×10^{-7}
Silicone-coated	160	1.0×10^{-3}	1.27×10^{-3}	1.3×10^{-6}

The limiting concentrations are reached as the beads become completely covered by a layer of CaCO_3 . The gradual decrease in effluent Ca^{++} concentration is attributed to the gradual growth of the CaCO_3 scale over the glass or silicone surface. The CaCO_3 scale, once it forms, is apparently much more effective in collecting CaCO_3 precipitate than are the scale-free surfaces. This is why the final Ca^{++} concentrations depicted in Figs. 4.4 and 4.5 are much lower than initial Ca^{++} concentrations.





The covering of CaCO_3 scale apparently grows much faster on glass than on the silicone resin. Comparing Figs. 4.4 and 4.5 shows the Ca^{++} concentration dropped from 80 ppm to 40 ppm within 400 sec when the scale grew upon glass surfaces, but it took about 800 sec for the Ca^{++} concentration to drop by a corresponding amount (90 ppm to 50 ppm) when the scale grew upon silicone resin.

The mass of CaCO_3 which precipitated during the period of scale growth corresponded to a layer about 5 μm thick, but this value is misleading, for it is based on the assumption that the scale is a solid coating of uniform thickness. In fact, microscopic examination revealed that the coating is very irregular. (Photomicrographs are presented in Figs. 4.8-4.10 in section 4.5.6 where the nature of the coating is discussed more fully).

4.5.5 Mathematical Model for Precipitation on Various Surfaces--The change in effluent Ca^{++} concentration with time is adequately modelled by Eq. 4.10.*

$$([\text{Ca}^{++}]_f - [\text{Ca}^{++}]_e) / [\text{Ca}^{++}]_e^2 = k_2 (V/F) A_0 [1 - \exp(-kt)] \quad (4.10)$$

where k_2 = rate constant for precipitation of CaCO_3 on scale,

$[\text{Ca}^{++}]_e$ = concentration of Ca^{++} leaving fluidized bed, mol/l

$[\text{Ca}^{++}]_f$ = concentration of Ca^{++} entering fluidized bed with feed, mol/l

A_0 = surface area of beads before scale formation, cm^2

The suitability of Eq. 4.10 can be judged by inspecting Figs. 4.6 and 4.7. There, the experimental results from Figs. 4.4 and 4.5 are plotted in the manner suggested by Eq. 4.10. After taking logarithms of both sides of that equation and rearranging we have:

*The derivation of this equation is presented in Appendix 0.

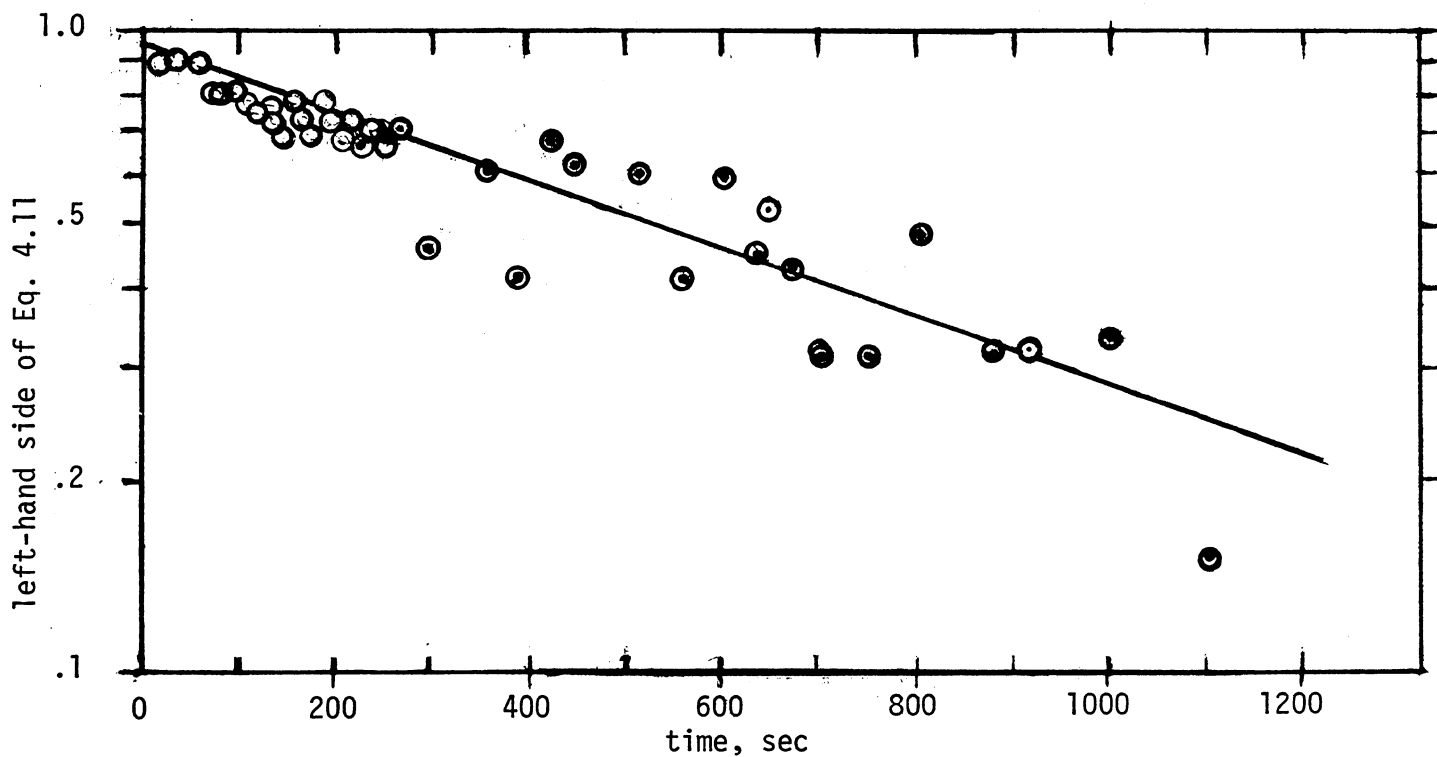


Figure 4.6 Comparison of Math Model (Eq. 4.10) with Experimental Results (glass beads, 70-80 US Std. mesh; 25°C)

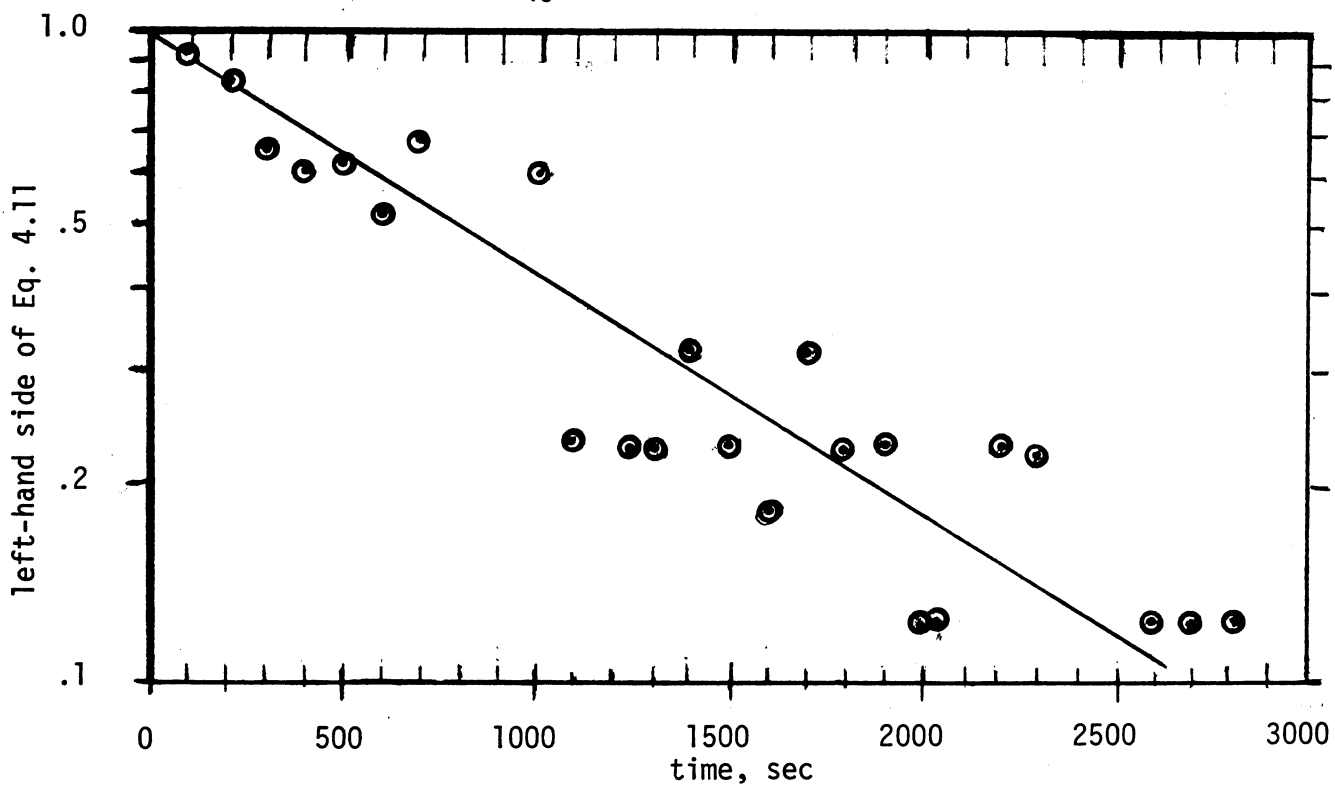


Figure 4.7 Comparison of Math Model (Eq. 4.10) with Experimental Results (Silicone-coated Beads, 35-45 U.S. Std. mesh; 25°C)

$$\log_{10} \left\{ 1 - \frac{[\text{Ca}^{++}]_f - [\text{Ca}^{++}]_e}{k_2(V/F)A_0 \cdot [\text{Ca}^{++}]_e^2} \right\} = -kt/2.303 \quad (4.11)$$

Thus, if Eq. 4.11 is appropriate, a straight line will result when the quantity in braces is plotted against time on semi-log paper as has been done in Figs. 4.6 and 4.7.

In Eqs. 4.10 and 4.11, the rate constant k reflects the rate of scale growth and is given by Eq. 4.12.

$$k = k_3([\text{Ca}^{++}]_e [\text{CO}_3^{=}]_e)_{\text{avg}} \quad (4.12)$$

where $([\text{Ca}^{++}]_e [\text{CO}_3^{=}]_e)_{\text{avg}}$ is the time-average concentration product during the experiment.

Eq. 4.10 reflects the growth of CaCO_3 scale over the surface with time, and it assumes the rate at which $[\text{Ca}^{++}]_e [\text{CO}_3^{=}]_e$ changes is small compared to the rate at which the surface area of glass decreases. Furthermore, it assumes that $[\text{Ca}^{++}]_e = [\text{CO}_3^{=}]_e$ during the entire experiment.

The numerical value of the rate constant k_2 (in Eq. 4.10) can be estimated from the limiting concentrations (as $t \rightarrow \infty$) which are depicted in Figs. 4.4 and 4.5. Those estimates are compared in Table 4.10.

Since the rate constants k_2 represent CaCO_3 precipitation on the same kind of surface (i.e., the CaCO_3 scale), we would expect the values given in Table 4.10 to be equal. That they disagree by a factor of 2 can be attributed entirely to the fact that the concentrations of Ca^{++} and $\text{CO}_3^{=}$ were not equal throughout the experiment involving glass beads, although equality was assumed during the derivation of Eq. 4.10. As Table 4.9 showed, by the end of the experiment involving glass beads, the carbonate concentration was about twice as great as the calcium concentration.

Table 4.10

Rate Constants for CaCO_3 Precipitation
(based on model given by Eq. 4.10)

Beads in Fluid Bed before CaCO_3 Scale Formed	Precipitation Rate Constant, k_2 $\ell/(\text{mol sec cm}^2)$
uncoated glass	5.0
silicone-coated	2.5

Another factor contributing to the disagreement between the values in Table 4.10 is the fact that Eq. 4.10 neglects precipitation on the scale-free surface. More precisely, it presumes that the rate constant, k_1 , for CaCO_3 precipitation on glass or silicone resin is much smaller than that for precipitation on the scale already formed, hence k_1 is ignored.

Precipitation on glass or silicone resin is represented in the model by k_3 (Eq. 4.12). The constant k_3 represents the growth in area of the CaCO_3 coating, and it depends strongly upon nature of the surface as shown in Table 4.11.

Table 4.11

Rate Constants for Growth of CaCO_3 Scale
Over Glass and Silicone-Coated Surfaces

Surface	Rate Constant, k_3 $\ell^2/(\text{mol}^2 \text{ sec})$
Glass	1.0×10^3
Silicone resin	4.6×10^2

4.5.6 Character of CaCO₃ Scale--The beads used in these experiments were smooth spheres, and apparently flawless as indicated by photomicrographs. Fig. 4.8 is typical.

As CaCO₃ precipitated on the beads, a scale (less than 5 μm thick) formed. In Fig. 4.9 some of the scale has been broken from the larger sphere and lies beside it. Careful study of Fig. 4.9 and photomicrographs like it shows the scale has a very irregular surface, but it covers the sphere completely. As this coating grows, the surface area of CaCO₃ scale is increasing rapidly.

Further precipitation seems to occur at specific sites; because, instead of the coating growing uniformly thicker, the irregular nature of the surface becomes even more pronounced. As depicted by Fig. 4.10, dozens of small crystals form, making the edges appear very jagged. In interpreting our results, we assumed that, once crystals began to form, the surface area available for CaCO₃ precipitation changed only slowly.

4.6 Effect of CaCO₃ Deposition on Permeability

4.6.1 Introduction--Because the pore structures of limestones and dolomites are complicated (19,20), there is no way to predict how their structures will change with time if CaCO₃ precipitates within them. Accordingly, the changes in permeability and porosity cannot be predicted, so experiments had to be performed to relate porosity and permeability to CaCO₃ precipitation.

The results are presented as correlations between permeability and porosity, because several such relationships have been developed from theoretical models by others (21,22).

4.6.2 Permeability and Darcy's Law--'Permeability' is the term used for the conductivity of the porous medium with respect to permeation by a Newtonian

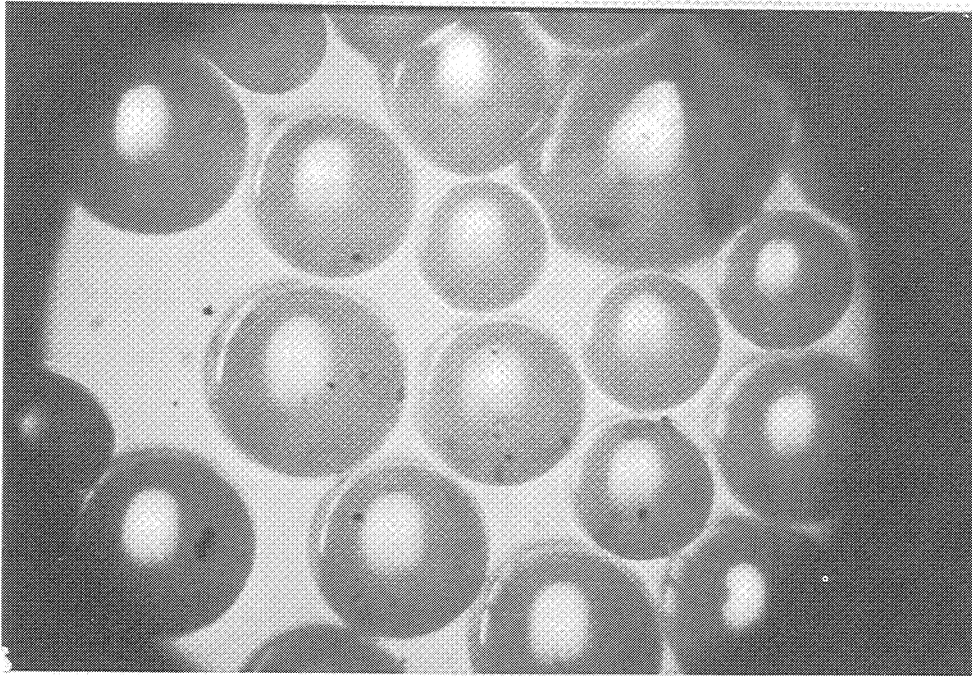


Fig. 4.8 Silicone-Coated Glass Beads 35-45 U.S. Std. Mesh (magnification x 50) (Black spots are dirt on camera lens)

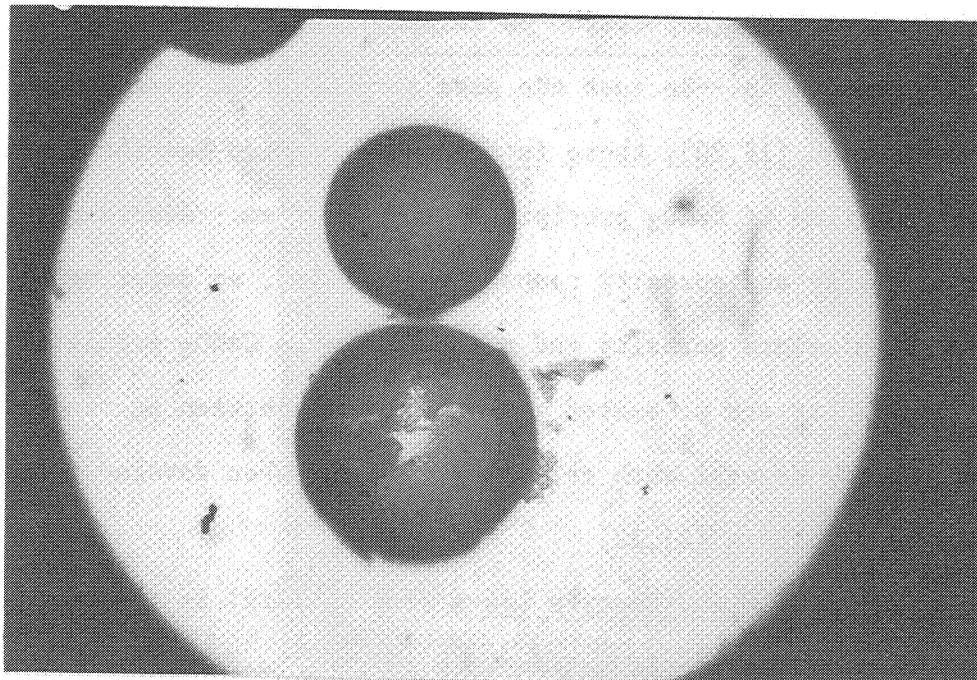


Fig. 4.9 Silicone-Coated Beads after CaCO₃ Scale has Covered Them (magnification: x 50)

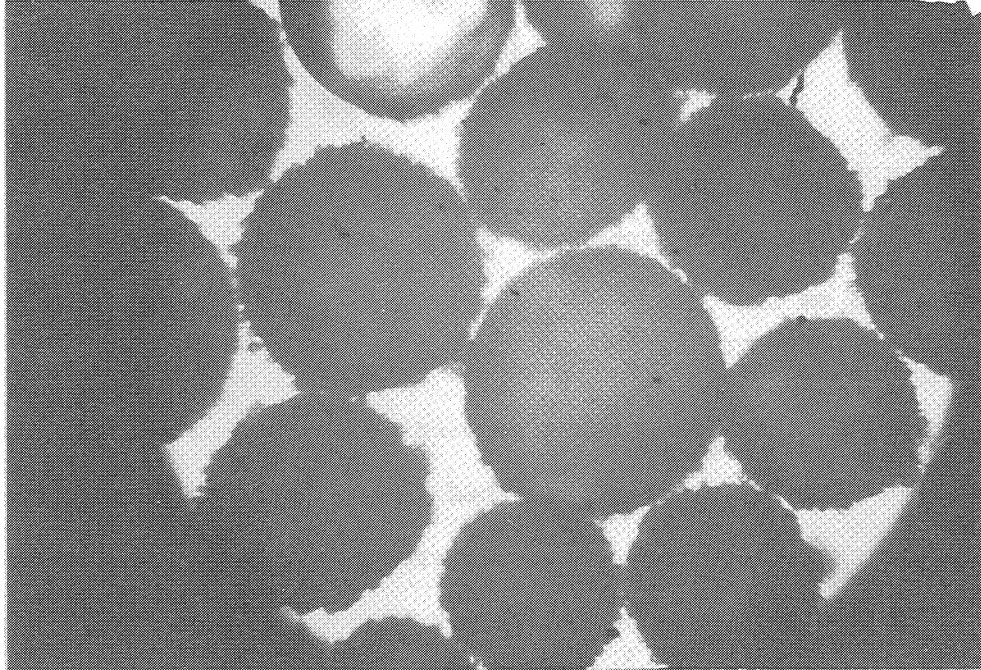


Fig. 4.10 Silicone-Coated Beads Showing Crystal Growth Upon CaCO_3 Scale (magnification: $\times 50$)

fluid (19b). Mathematically, the permeability k is defined by Darcy's Law, Eq. 4.13

$$Q = -(kA/\mu)(\Delta P/L) \quad (4.13)$$

In Eq. 4.13, Q is the volumetric flow rate (or "discharge"), A the cross-sectional area of the porous medium normal to the direction of flow, L the length of the porous medium in the macroscopic flow direction, μ the viscosity of the fluid, and ΔP the pressure change in the fluid flowing through the porous medium. Eq. 4.13 was used to calculate the experimentally determined permeabilities presented in the results section 4.6.5.

The practical unit of permeability is the "darcy." A porous material has a permeability equal to 1 darcy if a pressure difference of 1 atm will produce a flow rate of $1 \text{ cm}^3/\text{sec}$ of a fluid with 1 cP viscosity through a

cube having sides 1 cm in length. Thus,

$$1 \text{ darcy} = \frac{1(\text{cm}^3/\text{sec})}{1(\text{cm}^2)} \frac{1 \text{ (cp)}}{1 \text{ (atm/cm)}} \quad (4.14)$$

4.6.3 Apparatus--Unconsolidated packs of crushed limestone were used to simulate the qualitative aspects of a reservoir. The packs were held vertically in a 3.8 cm i.d. glass pipe constructed from 3 glass tees, each 17.5 cm long. (See Fig. 4.11). The side-arms of the tees served as pressure taps and separated the pack into three sections: upper, middle, and lower. Pipe connectors having Teflon gaskets joined the tees and provided watertight seals.

The unconsolidated packs were prepared as follows: the crushed limestone (25 to 30 US std mesh) was poured slowly into the column after the column had been filled with water. The column was vibrated continuously, and each portion of limestone was stirred immediately after it was added in order to free it of entrained air bubbles.

During operation of the apparatus, aqueous solutions of CaCl_2 and Na_2CO_3 , containing equimolar amounts of Ca^{++} and $\text{CO}_3^{=}$ as well as 3% (wt.) NaCl , were continuously pumped into the top of the column with a positive displacement metering pump (Crane, model 20; not shown). Simultaneously, effluent was recycled from the bottom of the column to the top at a rate ten times that of the entering feed solutions. The recycled solution diluted the feed solutions and promoted good mixing, thereby keeping CaCO_3 from precipitating before the solutions could enter the pack. The recycled effluent also decreased the residence time of the supersaturated solution, making the precipitation rate more uniform throughout the pack.

The recycled solution passed through a small chamber where pH and calcium concentration were measured before the solution re-entered the top of the column.

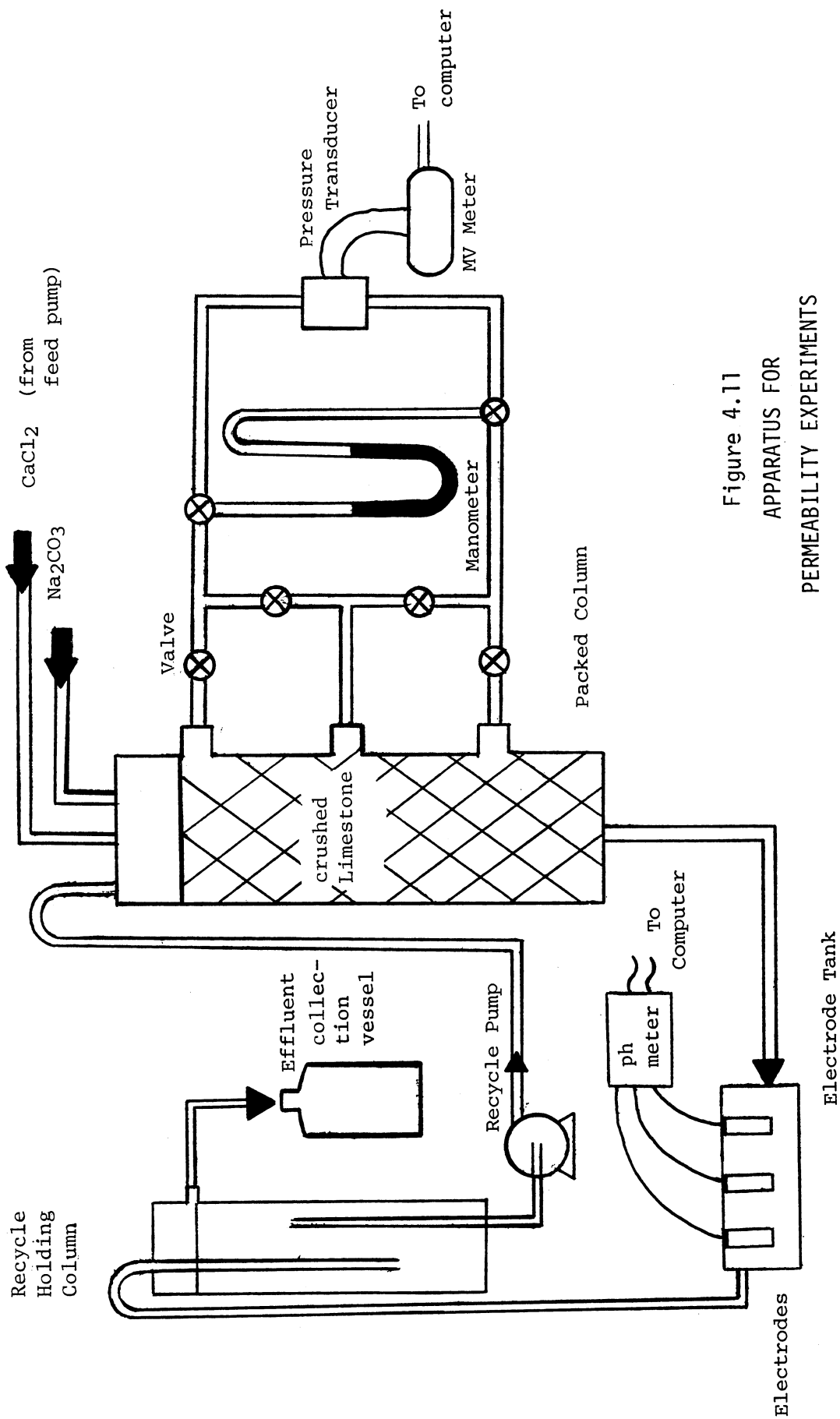


Figure 4.11
 APPARATUS FOR
 PERMEABILITY EXPERIMENTS

The pH was measured with a glass electrode containing an internal reference electrode (Fisher, model E-5A) connected to a pH meter (Sargent-Welch, model IP). Calcium was measured by a specific ion electrode (Orion, model 93-20) in conjunction with a calomel reference electrode (Fisher, model E-6A) connected to a millivolt meter (Fisher, model 620). The meter was interfaced with a digital computer (Hewlett-Packard, model 1000) for data recording and processing. Readings were automatically compensated for temperature changes by a temperature compensation probe (Orion, model 917002) immersed in the solution.

The pressure differences between the pairs of pressure taps were measured with a pressure transducer (Validyne, model DP215-64). Pressure was transmitted from each tap to the transducer through 1/4-in. stainless steel tubes filled with brine. The measured pressure drops were transmitted by electronic signal to the previously-mentioned computer for storage and processing. The readings provided by the pressure transducer were periodically checked by comparing them with those provided by Bourdon gages at each pressure tap.

The recycle pump (Fluid Metering Inc., model RP-D) tended to suck the solution out of the bottom of the packed column faster than the fluid could flow through the packing, thereby creating a vacuum in the lower section. To prevent this, a glass column, 53 cm long, was positioned between the vessel containing the electrodes and the recycle pump (See Figure 4.11). Overflow from this column was collected in a 20-liter jug for later analysis for calcium.

4.6.4 Procedure--At the beginning of each experiment and periodically thereafter, the porosity was measured. To do this, a solution of KMnO_4 containing 10% (wt.) CaCl_2 was slowly passed upward into the packed column (after the flows of feed solutions and recycle were interrupted). The volume of added permanganate was measured periodically as the interface between the purple

solution and the colorless brine moved upward. Thus the porosity in each section of the packing could be calculated.

The permeability was calculated using Darcy's law (see section 4.6.2) which relates permeability to three measured variables: flow rate, pressure drop, and the dimensions of the packed bed.

The amount of CaCO_3 which precipitated in the pack was determined by performing a mass balance on Ca^{++} . To do this, the solution leaving the system was collected and analyzed for calcium*. The total mass of calcium that had left the system was calculated by multiplying the concentration of Ca^{++} by the total volume of effluent. Similarly the mass of calcium that had entered the system was calculated from the volume and concentration of the CaCl_2 fed. The amount of calcium which precipitated on the limestone surfaces was determined by difference.

4.6.5 Results--The permeability of the unconsolidated limestone pack decreased more rapidly near the top, where fresh solutions of Ca^{++} and $\text{CO}_3^{=}$ were entering, than at locations near the bottom, where the degree of supersaturation was less. This is depicted by Fig. 4.12 which shows the permeability profile of a pack of 8-12 mesh (U.S. std.) marble chips after 0.15 pore volume (PV) of CaCO_3 had precipitated within it over a period of one month. (The glass column containing the pack had been specially fabricated and was equipped with seven pressure taps).

*Some of the calcium had precipitated as CaCO_3 before the analysis was begun. It was brought into solution and included in the analysis by first acidifying the solution (to pH 2) with HCl to dissolve the precipitate, then neutralizing the solution (NaOH , to pH 6.5-7.5) and mixing it well to ensure uniform concentration. The Ca^{++} concentration was measured with the specific-ion electrode.

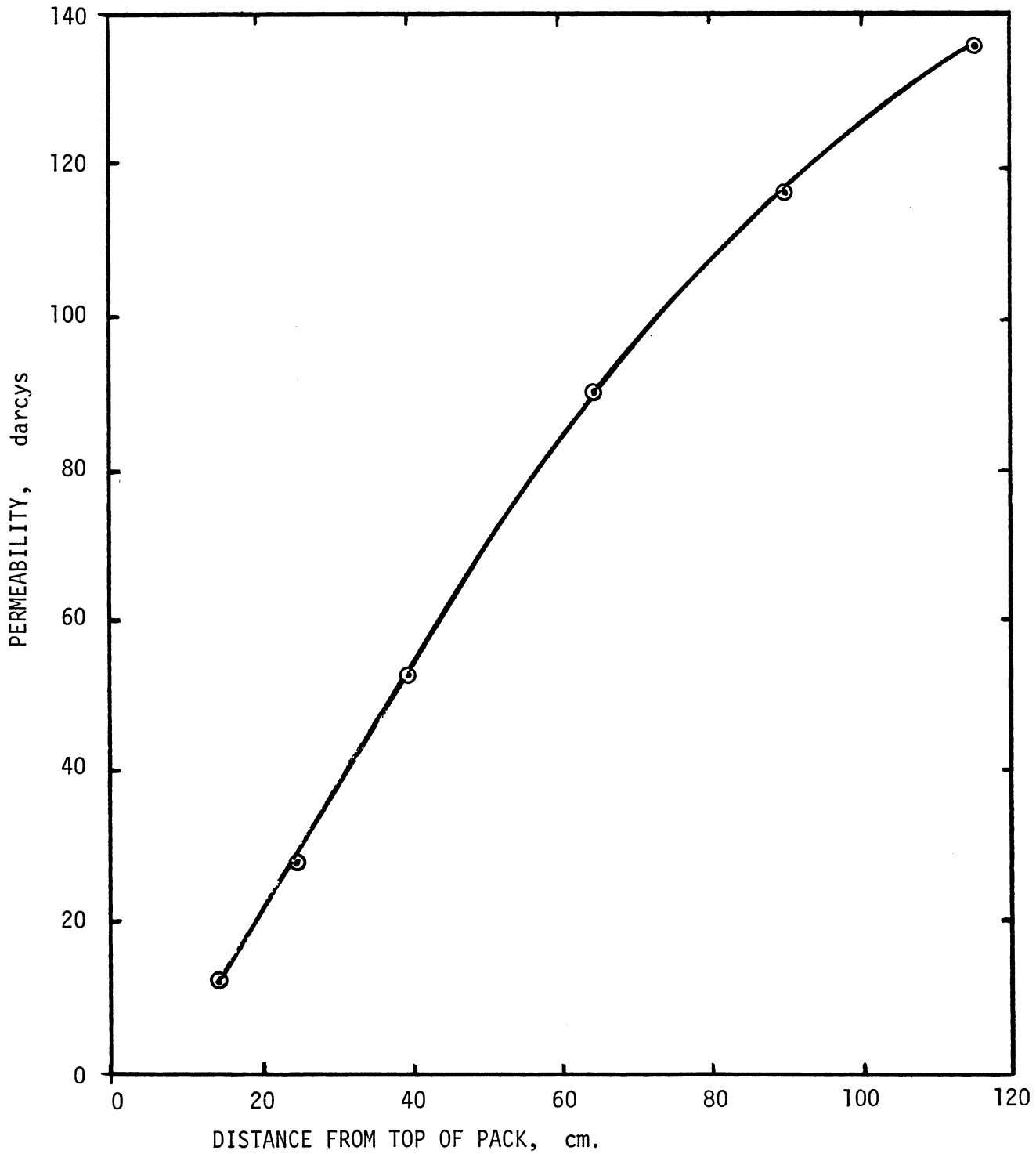


Figure 4.12 Permeability Profile of Unconsolidated Pack of Limestone Chips

At any given position in the pack, the permeability decreased exponentially (See Fig. 4.13*). Thus, there was a rapid decrease in permeability as CaCO₃ began to be deposited, but when the permeability had decreased by about one-half of the initial value, permeability decreased at a much slower rate.

4.6.6 Mathematical Model--To apply these results to oil reservoirs whose permeabilities are measured in millidarcys, a correlation between permeability and the deposition of CaCO₃ is needed, so that our results may be reliably extrapolated. Such theoretical considerations should be based on an analysis of the microscopic properties of flow.

The flow through a porous medium is assumed to occur through channels. One elementary view of such channels is depicted in Fig. 4.14 which shows them as a bundle of capillary tubes. This is the simplest case: a bundle of straight parallel tubes of uniform diameter.

For the bundle of capillary tubes, the following expression** is obtained for permeability:

$$k = D^2\phi/32 \quad (4.15)$$

where D is the pore diameter and ϕ is the porosity of the medium.

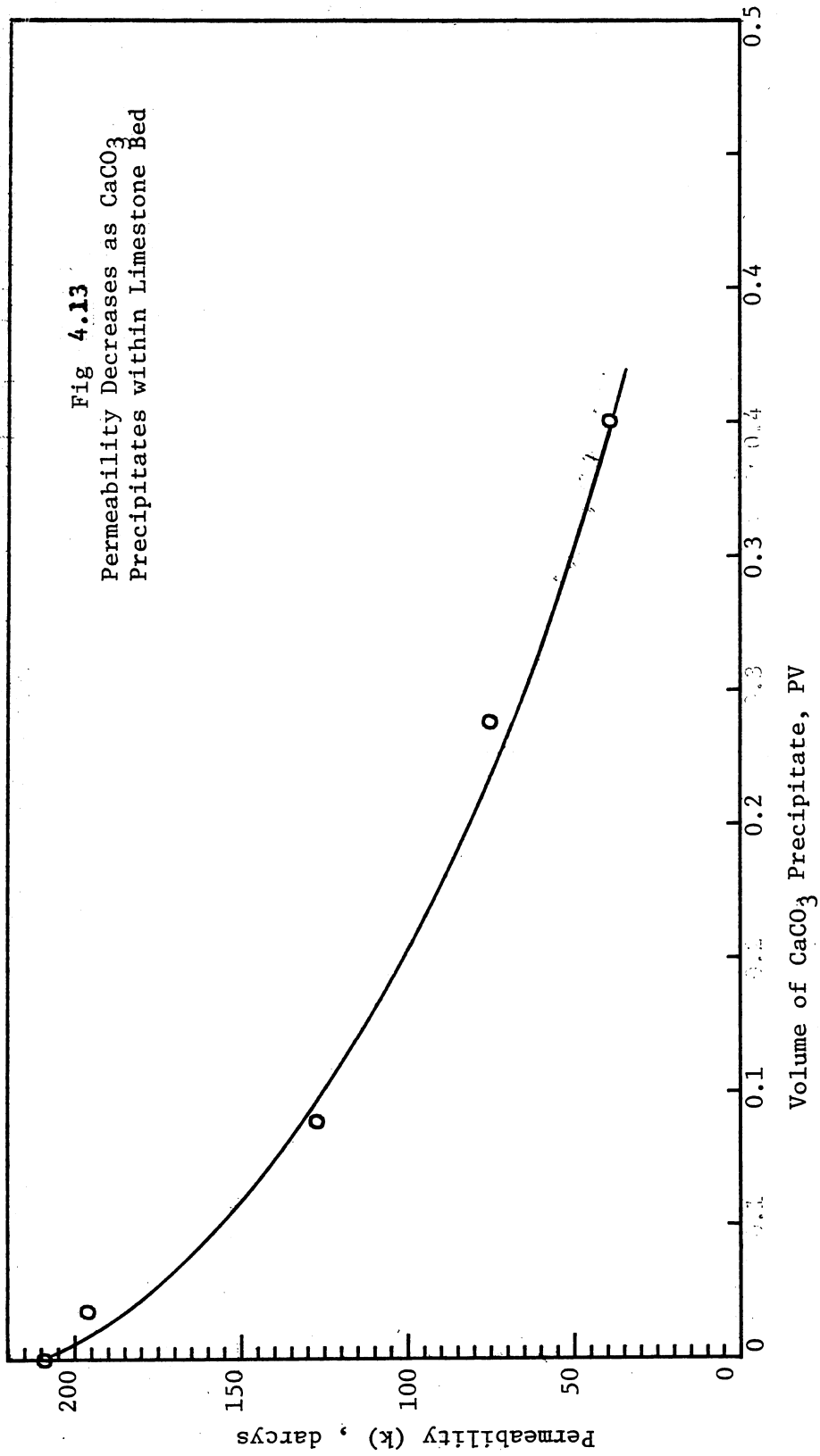
As CaCO₃ scale deposits on the walls of the capillaries, both D and the porosity ϕ decrease. To predict how these changes affect k, we first express D² in terms of the porosity ϕ . According to the model, ϕ is given by Eq. 4.16.

$$\phi = \frac{\text{total volume of capillaries}}{\text{total volume of the medium}} = \frac{n(\pi D^2/4)L}{A L} \quad (4.16)$$

where n is the number of capillaries in the medium. Solving Eq. 4.16 for D²

*Raw data are presented in Appendix L.

**This equation and other "capillaric models" have been reviewed by Scheidegger (21).



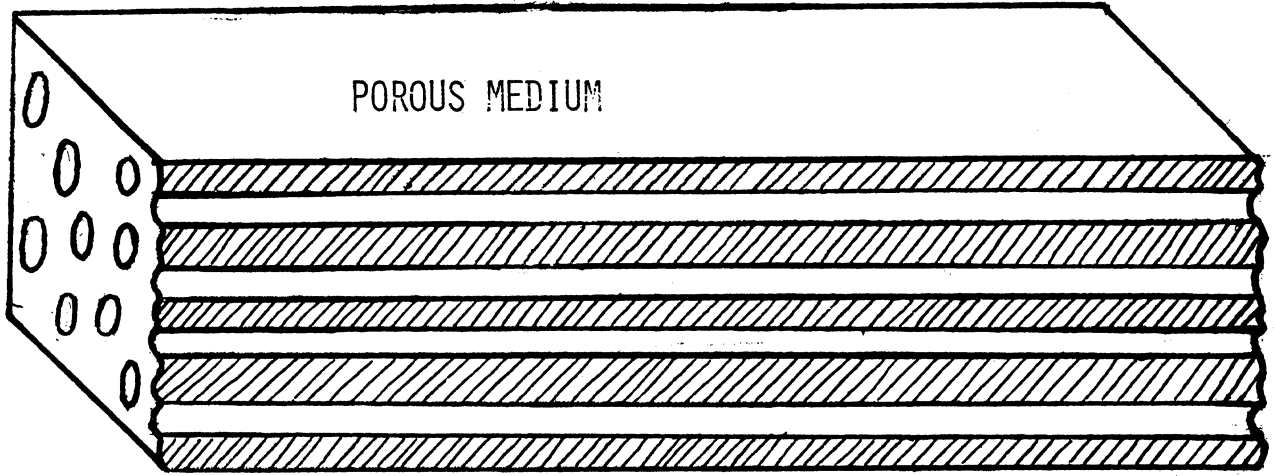


Figure 4.14 Parallel Capillaries Provide Simple Model

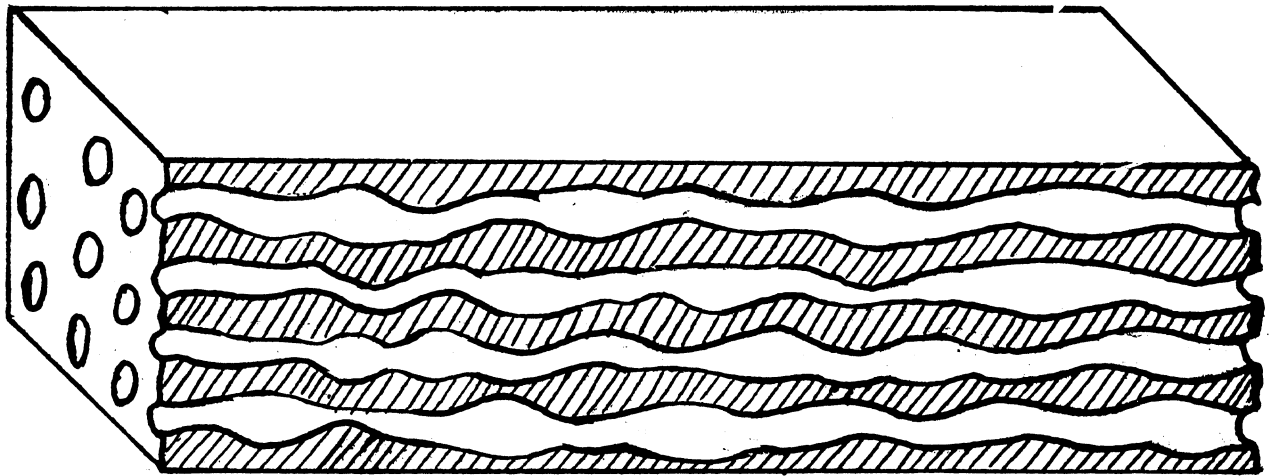


Figure 4.15 A More Realistic Model of a Porous Medium

$$D^2 = \frac{4 A \phi}{\pi n} \quad (4.17)$$

Substituting this result into Eq. 4.9 gives the desired expression relating k to ϕ :

$$k = \phi^2 / 8\pi(n/A) \quad (4.18)$$

Note that n/A is the "pore density" and is a parameter that characterizes the medium.

Eq. 4.18 predicts that, as scale forms in the capillaries, permeability decreases as the square of porosity. To test this model, k was plotted against ϕ^2 (see Fig. 4.16). The result is a straight line, as Eq. 4.18 predicts, but the y-intercept is not zero. In other words, the experimental results predict that the permeability k will become zero before the porosity does. Therefore, an equation which is more consistent with the experimental results, because it includes a second term, is Eq. 4.19.

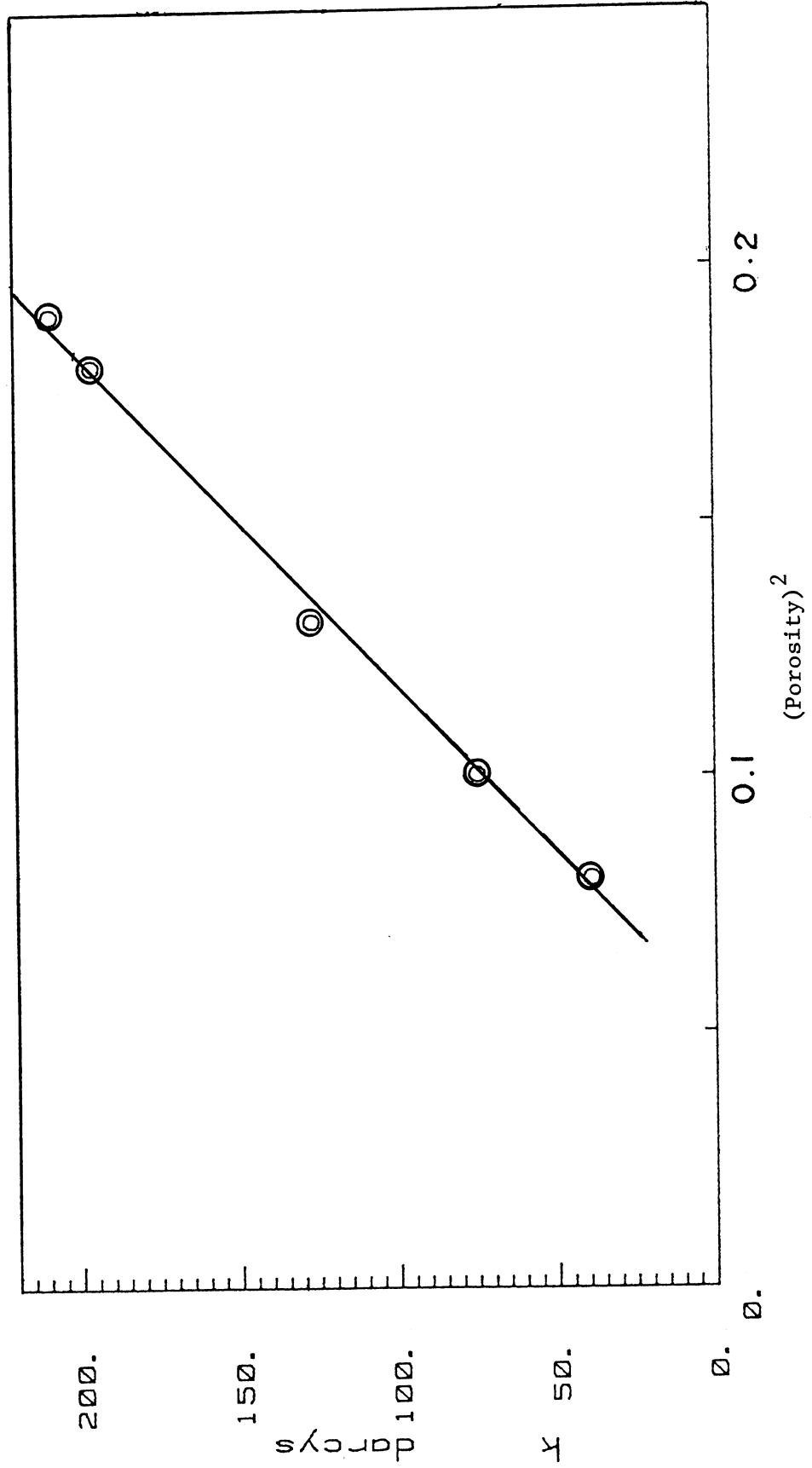
$$k = 1575 \phi^2 - 85 \quad (4.19)$$

The size of the second term (-85) in Eq. 4.19 probably depends strongly upon the original structure of the unconsolidated pack, especially the large size of the interstitial voids involved in our experiments. It seems more reasonable that, in porous media such as oil reservoirs (where porosity is typically 10-times less), the term would be negligible.

Similarly, the coefficient on ϕ^2 (slope of line on Fig. 4.16) probably depends upon the original permeability and cannot be used to predict the rate at which k would decrease in a reservoir; but the ϕ -squared dependence seems real and applicable. Accordingly, a relationship which would probably be useful for predictions is Eq. 4.20.

$$k = (k_o / \phi_o^2) \phi^2 \quad (4.20)$$

Figure 4.16. Experimental Results Plotted to Test Equation 4.18



where the subscript refers to initial properties of the porous medium. This equation was used in the simulation of a CO_2 flood, described in section 4.7.

4.6.7 Physical Explanation--One possible interpretation of the behavior depicted in Fig. 4.16 is that there is some minimum pore diameter, below which no flow will occur. Therefore, an improved model would be one that predicts permeability to be zero after some minimum porosity value, i.e., when all remaining pores become sufficiently closed.

Another improvement in the model would be to recognize that the pores do not have the same diameter. Some channels are large; others have small diameters. Interconnections among the pores have also been ignored, as has the effect of CaCO_3 deposition upon the flow pattern.

In reality, the flow would be far from uniform. Channels with small diameters would not have much fluid flowing through them, since flow follows the path of least resistance. Conversely, fluid would flow rapidly through the large pores. It is in these large pores, where most of the CaCO_3 would be deposited. In time, the CaCO_3 deposits would decrease the average diameter of these large pores so much that the flow through them would be severely reduced. To restore the flow to its original rate, the pressure gradient which drives the fluid would have to be increased. Because the measured permeability is inversely proportional to the pressure gradient, the permeability would decline.

Another phenomenon should also be considered. As deposition proceeds, the pore diameter may decrease more rapidly at one location than another. Very narrow necks may form at some points along the pores, and the channels might appear as shown in Fig. 4.15. These localized blockages would divert

the flow through lateral interconnecting pores* and into adjacent parallel pores. The fluid could flow around the blockage, then return to its original channel. Clearly, this would increase the distance the fluid would have to travel and it would increase the tortuosity of the flow path. Both of these changes would cause an increase in the resistance to flow and further reduce the measured permeability.

4.6.8 Other Mathematical Models--The most apparent shortcoming of the capillary model of Fig. 4.14 is the assumption that all the tubes have a constant diameter along their entire length at all times. A more realistic model would be one of variable diameters as illustrated in Fig. 4.15. One equation that has been derived for this improved model is the Carman-Kozeny (22) equation:

$$k_{ck} = \frac{\beta \phi^3}{S_o^2 (1 - \phi)^2} \quad (4.21)$$

where k_{ck} = permeability (darcys),

β = a constant which reflects the properties of the porous medium,

S_o = surface exposed to the fluid per unit volume of solid material,

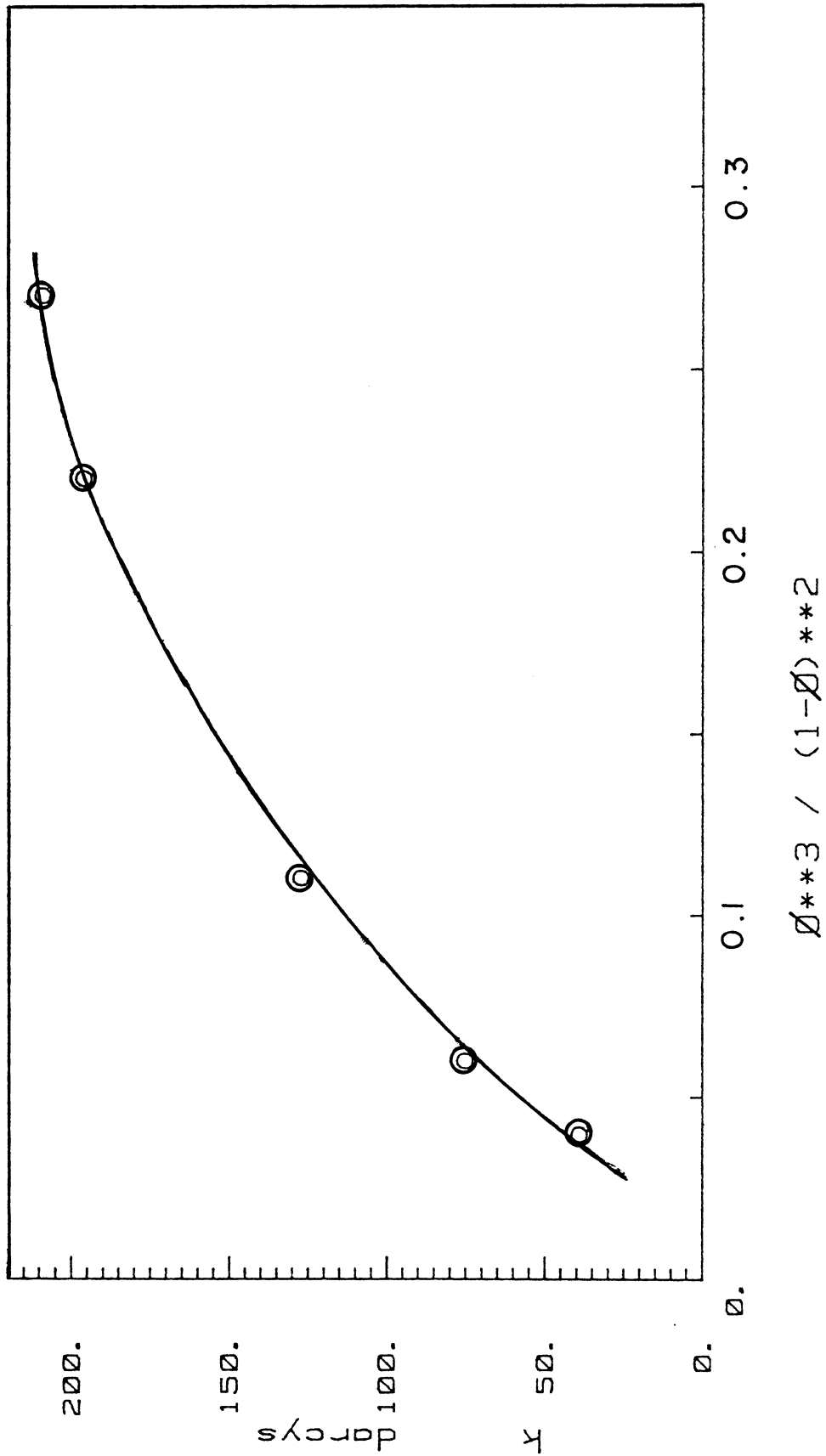
ϕ = porosity.

In this model, the variability of diameter is taken into account by the value chosen for S_o .

A test of Eq. 4.21 is presented in Fig. 4.17 where permeability is plotted against $\phi^3/(1 - \phi)^2$. If Eq. 4.21 is to provide an acceptable correlation for permeability, the data points should lie in a straight line. However, the result is obviously non-linear, and we conclude that the Carman-Kozeny equation is inferior to Eq. 4.19.

*These interconnecting pores are not shown in Figs. 4.14 and 4.15, but are known to exist in most porous media.

Figure 4.17. Experimental Results Plotted to Test Equation 4.21. (Result should be a straight line.)



4.6.9 Porosity Changes--One would expect a linear relationship between the amount of CaCO_3 deposited and the change in porosity in a porous medium. This is because the CaCO_3 which precipitates will occupy space that formerly was void. Although the uncertainty in the porosity measurements was great, our results showed that porosity does decline in a linear manner. Of greater importance, the rate of decline was never greater than that predicted from the mass of CaCO_3 precipitate (calculated from mass balance on Ca^{++}) and the specific gravity of crystalline CaCO_3 . In other words, we found no evidence that the precipitate was porous or had an apparent volume greater than that of the crystalline material. Thus, changes in porosity can, apparently, be calculated directly from the mass of CaCO_3 which precipitates, as was done in the simulation described below.

4.7 Reservoir Damage During a CO_2 Flood

4.7.1 Introduction

A computerized simulation (described in Appendix P) was done to predict the severity of damage during a CO_2 flood during which calcium carbonate precipitation was occurring. Among the major assumptions inherent in the model are these:

- a. Damage is caused only by calcium-saturated water behind the oil front and the precipitation of CaCO_3 from this water as it moves toward the producing well.
- b. The oil bank, the CO_2 , and the mobilized water behind them move in a piston-like manner toward the producing well. The fluids approach the well from all directions, so axial symmetry is maintained about the well.
- c. The calcium concentration in the water at any point in the reservoir can be predicted from the solubility of CaCO_3 . The

solubility can be estimated from relationships which depend on temperature and CO_2 pressure.

- d. The reservoir pressure decreases as the production well is approached, but does not drop to that of the well until the wellbore is reached.

4.7.2 Results

Because of assumption "a", damage does not occur at the producing well until the calcium-saturated water reaches it. (As explained below, damage at even short distances from the well is negligible compared to that at the well.) Thus, the production rate is unaffected for weeks or months, then it begins to decrease abruptly as soon as the water breaks through.

The behavior predicted by our model is depicted in Fig. 4.18 for a reservoir and well having these properties:

1. initial permeability to brine, 1.9 mD
2. initial porosity, 0.039
3. temperature, 130°F
4. wellbore diameter, 1.0 ft.
5. downhole pressure, 300 psig
6. thickness of pay, 30 ft.
7. radius of drainage, 500 ft.
8. pressure at radius of drainage, 4000 psig
9. viscosity of brine, 0.65 cp

The flow drops to zero in a matter of hours after breakthrough, because of CaCO_3 scale in the pores at the rock face. Precipitation of CaCO_3 is not very severe, however, in the surrounding reservoir. As Fig. 4.19 shows, during the first hour after break-through, the porosity decreases 7% in the region that is within 1 inch of the wellbore; but 6 inches from the wellbore, the porosity decreases only 1%. Permeability is affected in a similar manner.

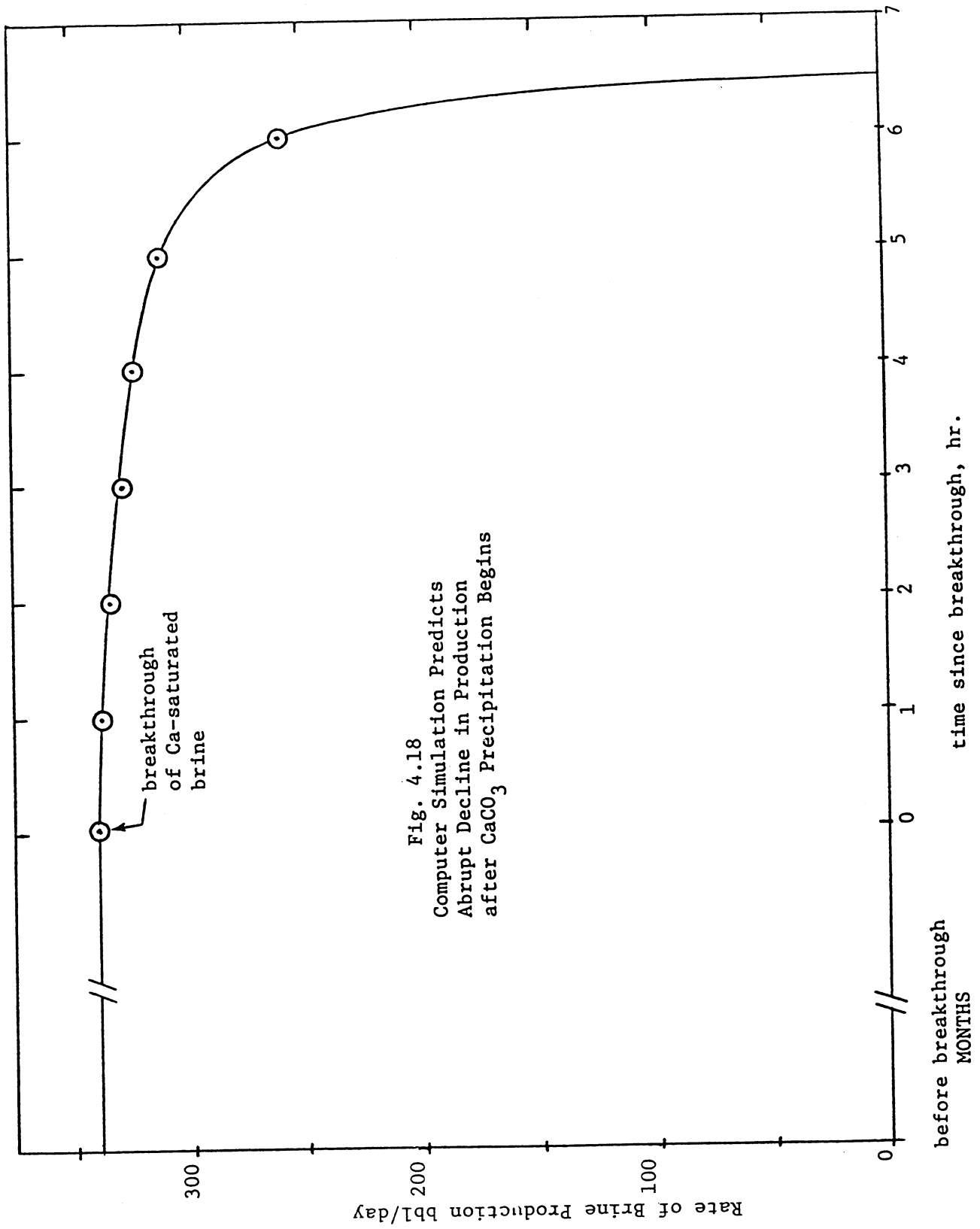


Fig. 4.18
 Computer Simulation Predicts
 Abrupt Decline in Production
 after CaCO₃ Precipitation Begins

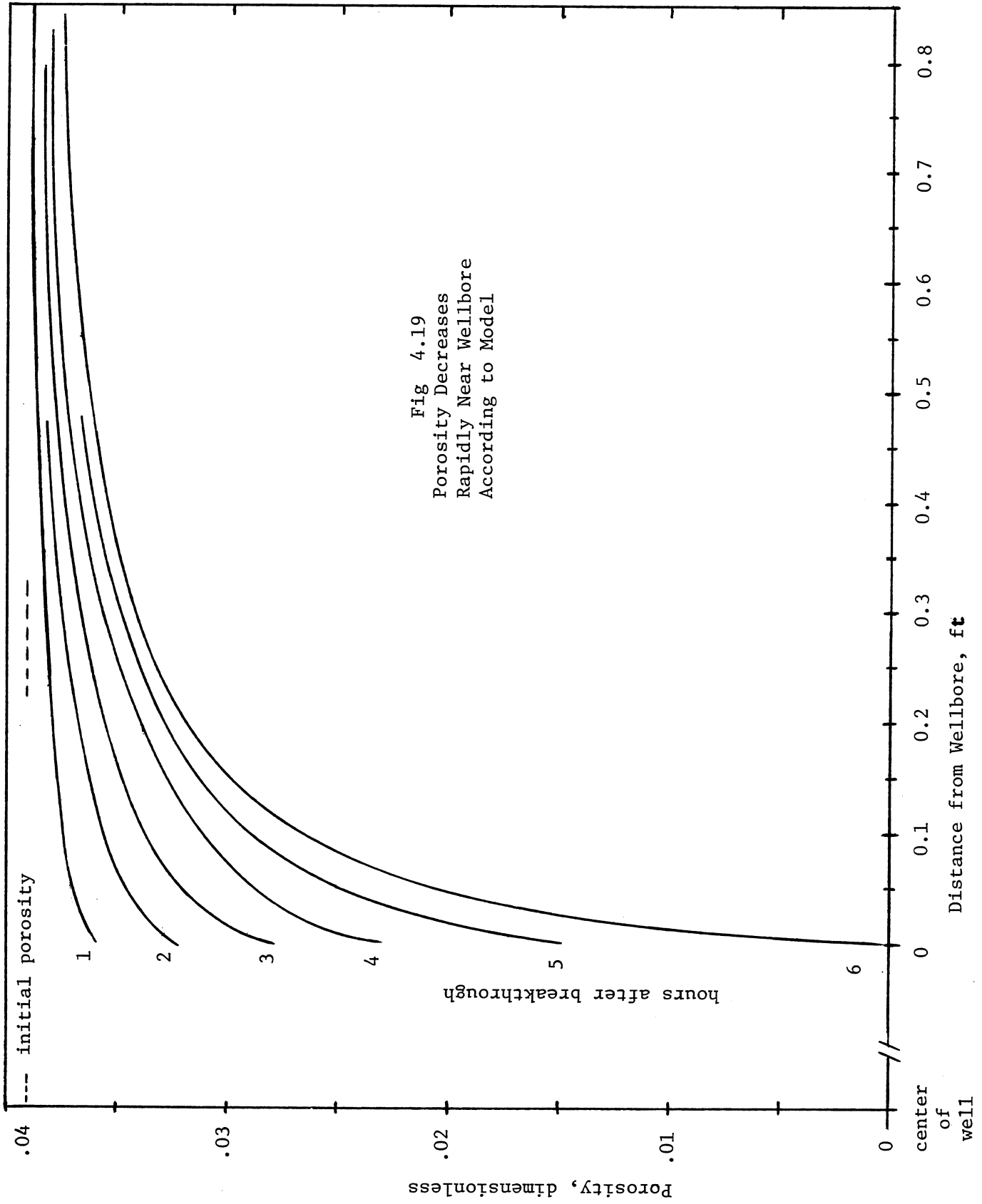


Fig 4.19
 Porosity Decreases
 Rapidly Near Wellbore
 According to Model

Within 1 inch of the wellbore, it drops 14% the first hour; but 6 inches away it drops only 3%. (See Fig. 4.20).

4.7.3 Physical interpretation--The surprising result shown in Fig. 4.18 is due to 3 factors.

1. The pressure gradient is greatest at the wellbore. As a result, the change in Ca^{++} concentration is greatest right at the wellbore, and so is the rate of CaCO_3 deposition.
2. The reservoir volume (per linear inch, measured away from the wellbore) is less at the wellbore than at greater distances. Thus, the pore volume in which the CaCO_3 precipitate may be deposited is less at the wellbore than at any other location. This factor, coupled with the first, ensures that porosity and permeability decrease faster at the wellbore than anywhere else.
3. The region around the wellbore is a bottleneck to the in-flowing brine. It is the place where the area perpendicular to the direction of brine flow is the least. Consequently, it is the most crucial region in the reservoir, and the permeability of this region governs the entire CO_2 flood.

4.7.4 Applicability to a real CO_2 flood--The results suggest that formation damage can be reduced either by increasing the reservoir permeability in the region around the wellbore, or by increasing the diameter of the wellbore. Both of these improvements could be achieved by fracturing and acidizing the well when completing it. Although the physical dimensions of the wellbore would not be appreciably increased, the area of rock face through which fluid could drain into the well would be greatly increased. This would reduce the bottleneck described above.

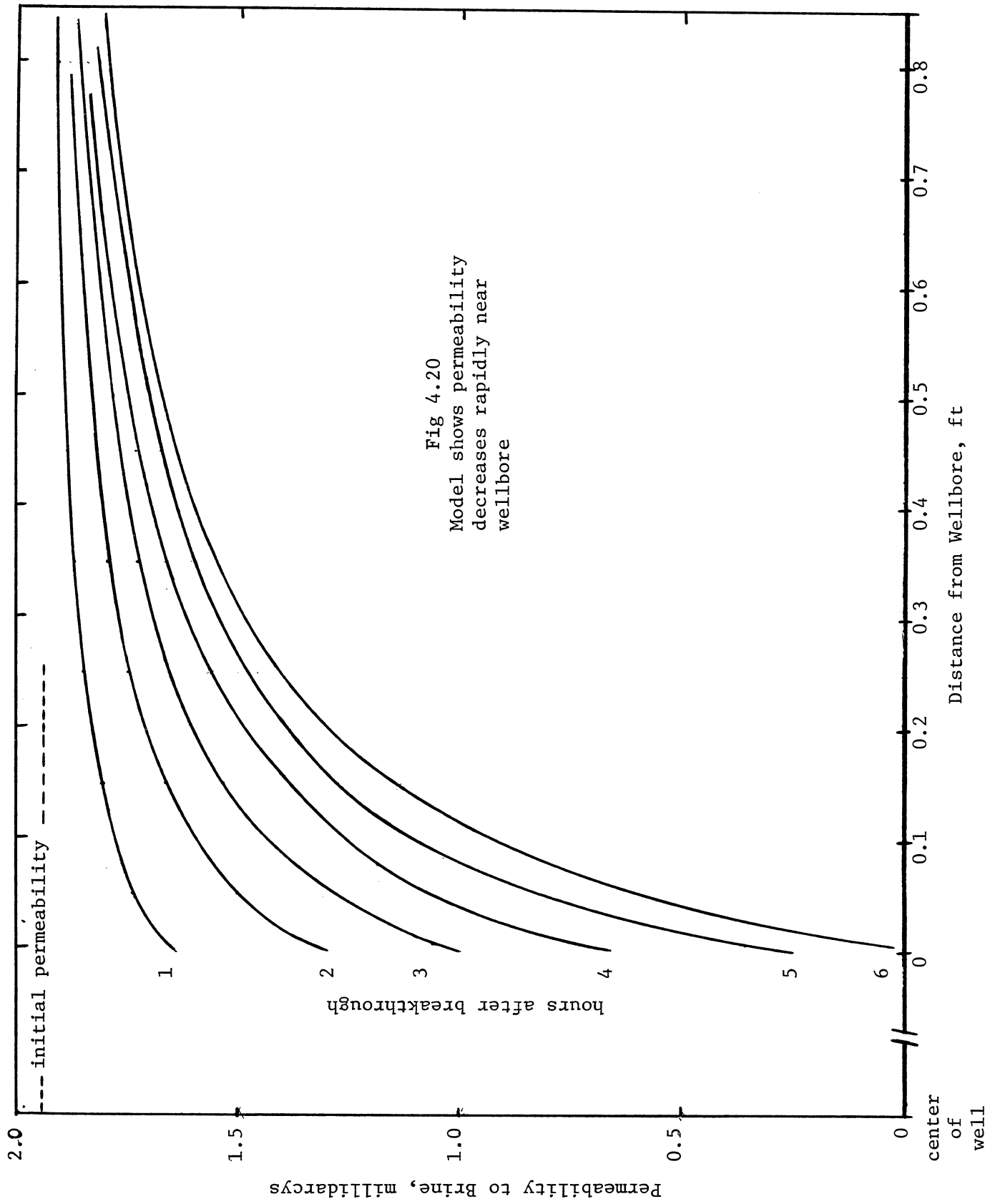


Fig 4.20
 Model shows permeability
 decreases rapidly near
 wellbore

Because of the greater permeability and effective area, the permeability would decrease at a much slower rate than the model predicts. Damage would require months to be evidenced, instead of hours.

SECTION FIVE
DEPOSITION OF FERRIC HYDROXIDE

5.1 Introduction

Pennzoil reported (26) that production rates decreased severely during their experimental CO₂ flood in the Rock Creek field in West Virginia. Although production rates could be restored by acidizing the production well, the cure was only temporary. Because high concentrations of iron were observed in the produced water after the well was stimulated, an iron precipitate was suspected to be the culprit. The source of the precipitate was believed to be the reservoir itself, analogous to the calcium problem described in Section Four.

The mechanism of damage was presumed to involve dissolution of iron-containing minerals by carbonic acid; specifically, the acid was attacking the reservoir rock, bringing ferric ions into solution. As the CO₂ was released in the low pressure region near the producing well, carbonic acid was decomposing in accord with Eq. 5.1.



As this was happening, the pH was rising and the iron was precipitating as ferric hydroxide (Eq. 5.2).



To confirm this hypothesized mechanism, laboratory tests were performed on cores taken from the affected reservoir.

5.2 Apparatus

Core samples were placed in a stainless steel pressure vessel having a glass liner as depicted in Fig. 5.1. A sampling tube (1/4 inch, stainless steel) extended through the upper flange. To the bottom of the tube was

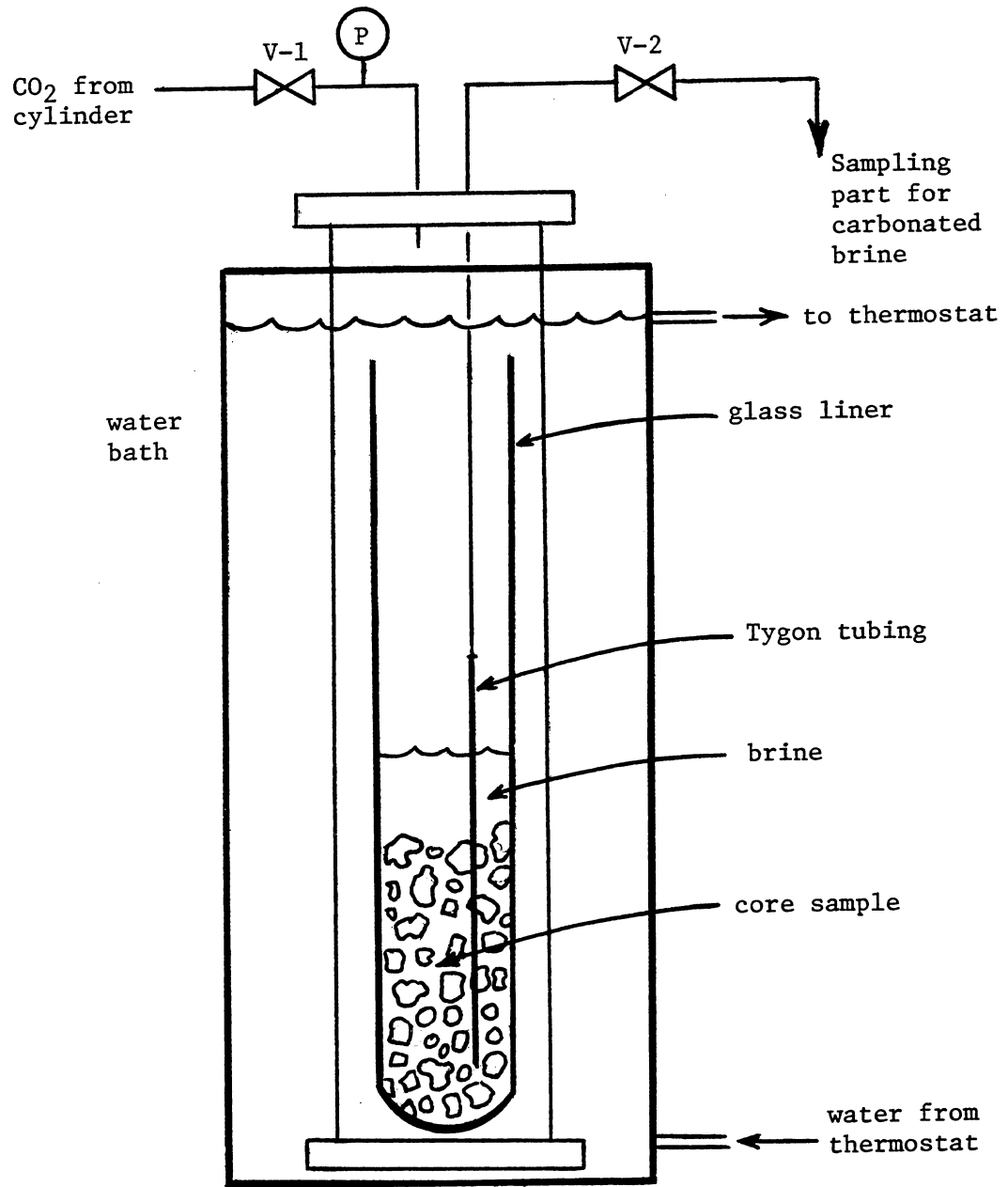


Fig 5.1 Lined Vessel for Carbonated Brine

clamped a length of Tygon tubing. Thus, no metal was in contact with the sample or the solution surrounding it.

A second stainless steel tube connected the pressure vessel to a cylinder of carbon dioxide. To maintain a constant temperature, the vessel was almost entirely submerged in a thermostatted water bath.

Samples taken from the aqueous phase were analyzed for iron using a Bausch and Lomb Spectronic 20 spectrometer.

5.3 Procedure

5.3.1 Dissolution in carbonic acid.--A sample of the core was crushed to pieces less than 1 cm in diameter and dried 4 hours in air at 150°C. After cooling, 58.8 g of this material was placed in the bottom of the glass vessel. To this sample was added 100 ml of 3% (wt) NaCl solution prepared from conductance water. After securing the top flange, the vessel was pressurized to 900 psig with carbon dioxide. The system was sealed by closing valve V-1 and maintained under pressure at 25°C for 3 months.

At the end of that time, a 25-ml aliquot of the carbonated brine was withdrawn by carefully opening valve V-2 and allowing some of the contents to discharge into a 250-ml beaker.

5.3.2. Treatment with strong acids.--In a subsequent experiment, a fresh sample of the core (1.0 g) was powdered and soaked in 25 ml of concentrated nitric acid, to which 2 ml of hydrofluoric acid had been added. After 2 hours of mild heating (70-80°C) the mixture was cooled, diluted with 250 ml of water and filtered. An aliquot of the filtrate was diluted 10:1 with water and analyzed for Fe⁺⁺⁺.

5.3.3. Sodium carbonate fusion.--A third sample (1.0 g) of core was powdered and subjected to a sodium carbonate fusion to bring silicates into solution. (The procedure is detailed in many texts on analytical chemistry; e.g. Ref. 27.) The soluble extract was analyzed for Fe⁺⁺⁺, too.

5.3.4. Analyses.--The iron content of each solution was determined by first acidifying it with a few drops of HCl (if it was not already acidic), then oxidizing any Fe^{++} to Fe^{+++} with 3 drops of hydrogen peroxide and adding excess solid NaSCN to form the deep red FeSCN^{++} complex. The concentration of this complex was determined by measuring the absorbance of the solution at 560 millimicrons and comparing the result with the absorbancies of FeSCN^{++} solutions of known concentration.

5.4 Experimental Results

5.4.1 Iron extracted with carbonated brine.--Within minutes after being withdrawn from the high-pressure vessel, the pale yellow brine yielded a gelatinous orange precipitate as CO_2 bubbled out of solution. The precipitate was soluble in dilute acid (HCl), and the acidified solution turned dark red upon addition of NaSCN.

Spectrometric analysis of this solution (after dilution) showed that about 21 mg of iron had been extracted from the core. This corresponds to 0.04% (wt) of the core.

5.4.2 Acid-soluble iron.-- The sample that had been treated with hot nitric-hydrofluoric acid yielded no detectable amount of iron. The sample showed no decrease in weight (± 0.5 mg) nor did the filtrate turn red when NaSCN was added after the filtrate had been partially neutralized (pH 5) with NaOH. The filtrate was not even pink to the eye, suggesting that less than 0.1 mg of Fe had been leached from the core.

5.4.3 Sodium carbonate fusion.--After the fusion, only 11% of the core sample remained insoluble. The filtrate contained 0.03 g Fe, suggesting that at least 3% (wt) of the core was iron.

5.5 Conclusions

5.5.1 Extraction of iron.--It was not surprising that the core was insoluble in acid, for mineralogical assays (Appendix Q) had shown it to be a silicate. Long-term leaching by carbonic acid, however, succeeded in bringing over 1% of the available iron into solution.

5.5.2 Applicability to CO₂ flood.--The iron content of our carbonated brine corresponded to 0.42 g Fe³⁺/liter or 0.028 lb ferric hydroxide (Fe(OH)₃) per bbl of reservoir brine. However, ferric hydroxide is far more damaging to permeability than the above figures would suggest, because the precipitate is very gelatinous and contains a large proportion of occluded water. Thus its volume and effective mass may be 10-100 times greater than the formula Fe(OH)₃ indicates. The result is that it readily plugs porous media, as most chemistry students who have tried to filter it can attest.

5.5.3 Remedy for damage.--The abrupt rise in pH caused by the decrease in pressure as the brine entered the producing well was, apparently, the underlying cause of the damage observed by Pennzoil. Accordingly, we suggested they maintain a higher downhole pressure and allow most of the pressure drop to occur at the surface. This operating change had a significant mitigating effect. Pennzoil reported (28) that production rate decline has been greatly minimized, resulting in much longer-lived acid stimulation jobs.

SECTION SIX

ACCEPTABLE LEVELS OF FORMATION DAMAGE

6.1 Introduction

The problem of quantifying the degree of damage that can be tolerated without impairing the commercial viability of a carbon dioxide flood remains only partially resolved. Each individual reservoir, with its unique operating problems and carbon dioxide supply costs, has a different tolerable damage level. Obviously, if all production or injection wells were to become plugged or nearly so due to the injection of carbon dioxide, the flood would end in failure. Fortunately, this has never been observed and is not likely to be experienced in normal field operations. It is, therefore, not totally surprising that allowable damage was found to be difficult if not impossible to quantify.

6.2 Miscible Floods

Miscible floods are expected to be more seriously affected by the reservoir damage process than immiscible floods. As reservoir damage occurs it is manifested in higher pressure gradients during the course of the flooding operation. High pressure gradients, when imposed in the region surrounding the injection well, minimize the fraction of the reservoir volume which can be maintained above the minimum miscibility pressure, unless one holds an unreasonably high back-pressure on the formation. It is well recognized that the region surrounding the producing well will be below the pressure required to achieve miscible displacement in a carbon dioxide flood. The advent of formation damage moves the boundary, at which the minimum miscibility pressure is not obtained, further out in the reservoir. This eliminates an ever-increasing volume of the reservoir unaffected by miscible displacement and, thus, decreases the overall efficiency of the displacement process.

This phenomenon would most likely result from the precipitation of particulates, as carbon dioxide dissolves in the reservoir oil. Fortuitously, the types of oil most amenable to miscible displacement are also least likely to generate particulates when contacted by carbon dioxide.

The mechanism of carbonate deposition in the region surrounding the producing well would, in effect, impose an artificial back-pressure on the reservoir. Although producing rate would be curtailed, this would increase the fraction of the reservoir maintained above the minimum miscibility pressure.

6.3 Immiscible Floods

For floods employing the immiscible carbon dioxide flooding process, the probability of formation damage reducing the commercial prospect must be viewed in a different perspective. As was the case for the miscible flood, both formation of organic particulates as well as precipitation of insoluble deposits around the producing well are of concern. The experimental data obtained in this study suggests that a permeability reduction greater than 25 percent would be unlikely to occur due to the deposition of organic particulates. This phenomenon would be largely confined to the major portion of reservoir, well removed from the vicinity of either injection or producing well. In this region, a 25 percent reduction in permeability would have only a minor effect on fluid flow rates which control the expected rate-of-return for the venture.

Inorganic precipitation, (for example, calcium carbonate) in the area around the producing wellbore represents more of a problem for the immiscible process than it did in the miscible case. This is because the immiscible process depends on the propagation of the CO₂-mobilized oil by water injection. It is this injected water which, when it becomes supersaturated with respect to calcium carbonate, can cause formation damage in the vicinity of the producing well. Although this form of damage can usually be corrected

by acidization, fracturing or other stimulation treatments, the economics of the process would be adversely affected. Unfortunately, this phenomenon is not limited to any given percentage of damage around a producing wellbore. Damage can easily exceed 90 percent if the process is allowed to continue. Obviously corrective measures will be taken long before damage reaches a maximum value and, hence, the allowable damage is more a function of rate rather than an absolute value.

6.4 Frequency of Stimulation

It would be very undesirable, if not economically disabling, to have to stimulate a producing well more often than three to four times each year. In fact, there are many locations where acid treatments more frequent than even twice a year might be costly enough to make the operation unprofitable. Although this rate effect can not be accurately quantified, it might be fair to assume that tight formations will be the most likely candidates for crippling wellbore formation damage. Formations having permeabilities in the 5 to 50 millidarcy range will be probable candidates for having their economics adversely affected. Formations having permeabilities above 500 millidarcy can probably be expected to experience only minor difficulties and the impact of formation damage on the overall economics of CO₂ flooding in these reservoirs should be minimal.

SECTION SEVEN
SUMMARY AND CONCLUSIONS

Laboratory experiments have identified four general type mechanisms that potentially could cause formation damage during the injection of carbon dioxide into an oil reservoir. These four general mechanisms involve interactions that occur when CO₂ dissolves in oil and formation water or is trapped in the reservoir pores. They can be further subdivided into the seven mechanism classifications shown below:

1. Dissolution of carbonate rock by carbonic acid in the vicinity of the injection well followed by precipitation of carbonates (calcium, iron or magnesium) in the region around the producing wells where the CO₂ pressure and, hence, carbonate solubility is less.
2. Attack by carbonic acid on carbonate rock in such a way that "fingering" is aggravated.
3. Dissolution of calcium sulfate or barium sulfate in the high-pressure region near the injection well followed by precipitation of these compounds in lower-pressure regions; thereby, causing plugging of pores.
4. Attack by carbonic acid on feldspars present in the reservoir rock; thereby, forming clay minerals that could plug pores.
5. Attack by carbonic acid on feldspar or carbonate minerals which cement sandstones together, thereby releasing tiny sand grains that could plug pores.
6. Formation of insoluble organic particulates when CO₂ dissolves in crude oil. Such particulates might be swept along by the CO₂ flood until they became lodged in pore constrictions.

7. The formation of an immobile gas phase that greatly reduces the effective permeability to oil and, especially, to water.

The extensive search of the published literature uncovered no documented cases of carbon dioxide damage occurring during field tests of either miscible or immiscible enhancement of tertiary oil production by carbon dioxide. However, current work on DOE's sponsored field experiment conducted in the Rock Creek field confirms the validity of mechanism 1.

The results of laboratory experiments indicate that mechanisms 2, 3 and 6 are unlikely to cause any problems in the field. Mechanism 1, the precipitation of reservoir minerals in the low pressure region surrounding the producing wells is a real problem, but it should exist only in those reservoirs where sufficient water is injected to displace the carbonic acid from the center of the reservoir to the producing well. This situation will occur mainly in immiscible CO₂ flooding.

The only solution to scaling up of producing wells appears to be frequent acidization of the wells to restore lost permeability. The problem can be mitigated; however, by operating the producing well at a minimum draw down (high back pressure) in order to keep as much carbon dioxide dissolved in the water phase as possible. In field experiments involving the immiscible displacement process, pressures as high as 250 psig have been successfully employed with no detrimental effect on oil production rate.

Mechanisms 4 and 5 pose real problems for CO₂ recovery processes conducted in consolidated sandstone. Although the number of CO₂ candidate sandstone reservoirs is very few relative to carbonates, some damage would be expected. In those instances it appears that conventional well stimulation such as fracturing and acidizing could be an acceptable solution to the damage problem. It is unlikely that fines would significantly plug the reservoir

at a distance more than 20 feet from the well bore. Also, it is possible that any damage occurring away from the injection well would improve productivity by enhancing conformance.

Mechanism 7 is a real problem which will be experienced in almost every carbon dioxide flood, especially those utilizing the WAG process. It is not unique to carbon dioxide and should be in evidence during the injection of any gas which is largely insoluble in both crude oil and water. In the case of carbon dioxide the damage should be self-healing, as its measureable solubility in water will allow the residual CO₂ phase to be gradually removed during subsequent water injection.

In conclusion, several possible damage mechanisms have been identified, although none seem severe to the point of destroying the profitability of the recovery process. If laboratory experiments suggest that a given reservoir is a commercial candidate for carbon dioxide flooding, a decision can be made to proceed with the process while staying alert to the possible need to remedy some future reservoir damage.

One technique that has been used to increase the injectivity of carbon dioxide is to employ liquid rather than gaseous phase injection. In most instances this can be accomplished by simply cooling the gas stream at the well head to below 88°F. An injection temperature of about 70°F would appear to be optimal with respect to energy conservation.

REFERENCES

1. Shelton, J. L. and Yarborough, L., "Multiple Phase Behavior in Porous Media During CO₂ or Rich Gas Flooding," J. Pet. Tech., 1977, 19(9), pp. 1171-1178.
2. Simmon, R., Rosman, A. and Zana, E., "Phase Behavior Properties of CO₂ Reservoir Oil Systems," Soc. Pet. Eng. J., 1978, 18(2), pp. 20-26.
3. Richardson, C. I., The Modern Asphalt Pavement, J. Wiley & Sons, New York (1905).
4. Orr, F. M., New Mexico Institute of Mining and Technology, Petroleum Recovery Research Center, Socorro, NM, private communication.
5. Champlin letter dated November 13, 1978, J. R. Carter, Jr. to J. C. Scherer, cc to Dr. John T. Patton, Inspection Analysis of Wilmington Crude Oil.
6. Watts, R. J., et al., "A Single CO₂ Injection Well Minitest in a Low Permeability Eastern Carbonate Reservoir," A Preliminary Report, SPE 9430.
7. Bland, W. F. and Davidson, R. L., Petroleum Processing Hand Book, McGraw-Hill Book Company, Hightstown, New Jersey, 1967, pp. 21-22.
8. McKinney, C. M. and Garton, E. L., "Analysis of Crude Oils from 470 Important Oil Fields in the United States," Bureau of Mines Rept. Invest. 5376, 1957, p. 276.
9. State of California, "Department of Natural Resources," Bulletin 170, Map 33, Geology of Wilmington Oil Field.
10. Deckert, L., CONOCO Production Co., Hobbs, New Mexico, private communication.
11. Foster, R., New Mexico Institute of Mining and Technology, Petroleum Recovery Research Center, Socorro, New Mexico, private communication.
12. Lien, C., New Mexico Institute of Mining and Technology, Petroleum Recovery Research Center, Socorro, New Mexico, private communication.
13. New Mexico Petroleum Recovery Research Center letter dated February 18, 1981, C. L. Lien to G. Smith (NMSU), Physical Properties and G. C. Analysis of Maljamar Crude.
14. Orr, F. M., Letter of transmittal dated March 7, 1980 to Drs. A. W. Pappano and T. G. Monger, Department of Chemical Engineering, West Virginia University, Morgantown, West Virginia.

References (continued)

15. Oddo, J. E. and M. B. Tomson, "Simplified Calculation of CaCO_3 Saturation at High Temperatures and Pressures in Brine Solutions," J. Pet. Tech., July 1982, pp. 1583-1590.
16. Robinson, R. A. and R. H. Stokes, "Electrolyte Solutions," Butterworths, London (1959).
17. Perry, R. H. and C. H. Chilton, "Chemical Engineers Handbook," 5th Ed., McGraw-Hill, New York (1973).
18. Gross, John, "Crushing and Grinding," U.S. Bur. Mines Bull. 402 (1938), in Foust, et al., "Principles of Unit Operations," Wiley, New York (1960), p. 536.
19. Dullien, F. A. L., "Porous Media; Fluid Transport and Pore Structure," Academic Press, New York (1979), (a) pp. 88-89, 140; (b) p. 78.
20. Davis, S. N., "Flow Through Porous Media" (R. J. M. de Wiest, ed.), Academic Press, New York (1969), pp. 54-90.
21. Scheidegger, A. E., "The Physics of Flow Through Porous Media, 3rd. ed." Univ. of Toronto Press, Toronto (1974).
22. Carman, P. C., Trans. Inst. Chem. Eng. London 15, 1937, p. 150, in reference 19.
23. Kane, A. V., "Performance Review of a Large Scale CO_2 -WAG Project SACROC Unit - Kelly Snyder Field," (Transaction), J. Pet. Techn., Feb. 1979, pp. 217-231.
24. Holm, W., Union Oil Co. of California, Brea, CA, private communication.
25. Stiff, H. A. and L. E. Davis, "A Method for Predicting the Tendency of Oil Field Waters to Deposit Calcium Carbonate, Pet. Trans., Vol. 195, (1952), pp. 213-216.
26. King, P., Pennzoil Corp., Parkersburg, W. Va., private communication, December 1981.
27. Hillebrand, W.F., et al., "Applied Inorganic Analysis," John Wiley, New York (1953).
28. King, P., Pennzoil Corp., private communication, October 1982.

APPENDIX A

Literature Relating to Plausible Mechanisms of CO₂-Caused Reservoir Damage

References are listed, with abstracts, in serial order on the following pages. Both a subject index and an alphabetical index by author are also provided.

Classification by Subject

Table A.1 lists the references by major subject area. The numbers listed there are serial numbers.

Table A.1

References by Subject

<u>Subject</u>	<u>Serial Number of Reference</u>
Field Trials	7,8,13,17,24,26,32,36,54,56-59,63-65,68,74,75,88,92,97,98
Lab Studies	8,9,11,12,14-16,18,19,21-24,27-29,31,32,34-37,39-44,47-53,55-57,59,63,67,69,70,72,77-85,87,89-96,99,101-105,107-110
Theoretical	10,11,18,20,23,25,27,33,38,44-47,62,73,76,81,86,91,104
CO ₂ -Crude Equilibria	16-18,20,21,32,33,70,80,90-96,98,102
Carbonate Solubility	11-14,19,34,36,37,40,45,47,51,54,56,59,64,73-76,78,79,84-86,88,99
Sulfate Solubility	8-11,15,22-24,35-38,40-46,48-50,52,53,56,59,62,64,75,77,82,83,86,87,89,101
Scale Inhibitors	13,24,35,37,40,52,54-59,63-66,68,69,72,75
Feldspar Decomposition, Geochemistry	25-29,31,39,67,81,97,100,103-110

REFERENCES BY AUTHOR

13. Beasley, A. E. and I. McKinney, 'Prevention of Calcium Carbonate Scale Deposition in Mill Water Systems,' Society of Mining Engineers, March 1973. pp. 32-37.
67. Bernard, G. G., 'Effect of Clays, Limestone, and Gypsum on Soluble Oil Flooding,' Journal of Petroleum Technology, Feb. 1975, pp. 179-180.
34. Bernard, G. G., 'Effect of Calcium Carbonate Supersaturation of Flood Water of Rock Permeability,' Producers Monthly, July 1957, pp. 32-36.
36. Bernard, G. G., 'A Survey of the Use of Incompatible Flood Waters,' Producers Monthly, February 1957, pp. 34-37.
25. Berner, R. A., 'Rate Control of Mineral Dissolution Under Earth Surface Conditions,' American Journal of Science. Vol. 278, No. 9 (1978), pp. 1235-1252.
26. Berner, R. A. and G. R. Holdren, Jr., 'Mechanism of Feldspar Weathering-II. Observations of Feldspar from Soils,' Geochim. Cosmochim. Acta, Vol. 43, No. 8 (1979). pp. 1173-1186.
54. Bezemer, C. And K. A. Bauer, 'Prevention of Carbonate Scale Deposition: A Well-Packing Technique with Controlled Solubility Phosphates,' Journal of Petroleum Technology, April 1969, pp. 505-514.
50. Blount. C. W. and F. W. Dickson, 'Gypsum-Anhydrite Equilibria in Systems $\text{CaSO}_4\text{-H}_2\text{O}$ and $\text{CaCO}_3(\text{sic})\text{-NaCl-H}_2\text{O}$,' American Mineralogist, Vol. 58, 1973. pp. 323-331.
89. Bock, E., 'On the Solubility of Anhydrous Calcium Sulphate and of Gypsum in Concentrated Solutions of Sodium Chloride at 25°C, 30°C, 40°C, and 50°C,' Can. J. Chem., Vol. 39 (1961), pp. 1746-1751.
55. Bsharah, L., 'Test Unit Evaluates Scale Inhibitors,' Oil and Gas Journal, April 7, 1969, pp. 166-170.
35. Burcik, E. J., 'The Inhibition of Gypsum Precipitation by Sodium Phosphates,' Producers Monthly, Nov 1954, pp. 42-44.
110. Busenburg, E., 'The Products of the Interaction of Feldspars with Aqueous Solutions at 25°C.' Geochim. Cosmochim. Acta, Vol. 42 (1978), pp. 1679-1686.
31. Busenberg, E. and C. V. Clemency, 'The Dissolution Kinetics of Feldspars at 25 Degrees C and at 1 Atm CO_2 Partial Pressure,' Geochim. Cosmochim. Acta, Vol. 40, No. 1 (1976), pp. 41-49.
68. Canapary, R. C., 'How to Control Refinery Fouling,' Oil and Gas Journal, Oct. 9, 1961, pp. 114-118.

106. Chafetz, H. S., 'Surface Diagenesis of Limestone,' J. of Sed. Pet., Vol. 42 (1972), pp. 325-329.
71. Chorley, R. J., 'The Role of Water in Rock Disintegration,' in: Introduction to Fluvial Processes, Methuen, London (1969), pp. 53-74.
61. Correns, C. W., 'Experiments on the Decomposition of Silicates and Discussion of Chemical Weathering,' Tenth Annual Conference on Clays and Clay Minerals, pp. 443-459.
75. Cowan, J. C. and D. J. Weintritt, 'Water-Formed Scale Deposits,' Gulf Pub. Co., Houston (1976), pp. 343-376.
37. Crawford, P. B., 'Sequestration and Chelation,' Producers Monthly, July 1957, p. 17.
9. Davis, J. W. and A. G. Collins, 'Solubility of Barium and Strontium Sulfates in Strong Electrolyte Solutions,' Environmental Science and Technology, Vol. 5, No. 10 (Oct. 1971), pp. 1039-1043.
60. DeBiesse, Y., G. de Lomballerie and F. Leandri, 'Etude Experimentale du Drainage d'une Huile Legere par Gaz Carbonique ou Eau Carbonatee,' Revue de L'Institut Francais du Petrole, Vol. 23, No. 4 (April 1968), pp. 486-507.
87. Dickson, F. W., C. W. Blount and G. Tunell, 'Use of Hydrothermal Solution Equipment to Determine the Solubility of Anhydrite in Water from 100°C to 275°C and from 1 Bar to 1000 Bars Pressure,' Am. J. of Science, Vol. 261 (1963), pp. 61-78.
7. Dixon, B. P. and L. E. Newton, Jr., 'Reinjection of Large Volumes of Produced Water in Secondary Operations,' Journal of Petroleum Technology, July 1965, pp. 781-788.
42. Doremus, R. H., 'Crystallization of Slightly Soluble Salts From Solution,' Journal of Physical Chemistry, Vol. 74, No. 7 (April 2, 1970), pp. 1405-1408.
44. Doremus, R. H., 'Precipitation Kinetics of Ionic Salts From Solution,' Journal of Physical Chemistry, Vol. 62 (1958), pp. 1068-1075.
65. Earllougher, R. C. and W. W. Love, 'Sequestering Agents for Prevention of Scale Deposition in Oil Wells,' Journal of Petroleum Technology, April 1957, pp. 17-20.
76. Edmond, J. M. and J. M. T. M. Gieskes, 'On the Calculation of the Degree of Saturation of Sea Water with Respect To Calcium Carbonate Under In Situ Conditions,' Geochim. Cosmochim. Acta, Vol. 34 (1970), pp. 1261-1291.
78. Ellis, A. J., 'The Solubility of Calcite in Carbon Dioxide Solutions,' Amer. J. Sci., Vol. 257 (May 1959), pp. 354-365.

3. Ellis, A. J. and I. M. McFadden, 'Partial Molal Volumes of Ions in Hydrothermal Solutions,' Geochim. Cosmochim. Acta, Vol. 36 (1972), pp. 413-426.
14. Englander, H. E., 'Conductometric Measurement of Carbonate Scale Inhibitors Effectiveness,' Journal of Petroleum Technology, July 1975, pp. 827-834.
64. Featherston, A. B., R. G. Mihram, and A. B. Waters, 'Minimization of Scale Deposits in Oil Wells by Placement of Phosphates in Producing Zones,' Journal of Petroleum Technology, March 1959, pp. 29-32.
69. Frazier, A. W., J. G. Huddle, and W. R. Power, 'New, Fast Approach To Reduced Preheat-Exchanger Fouling,' Oil and Gas Journal, May 3, 1956, pp. 117-122.
53. Fulford, R. S., 'Effects of Brine Concentration and Pressure Drop on Gypsum Scaling in Oil Wells,' Journal of Petroleum Technology, Vol. 20, June 1968, pp. 559-564.
15. Gainey, R. J., C. A. Thorp and E. A. Cadwallader, 'Calcium Sulfate Seeding Prevents Calcium Sulfate Scale,' Ind. and Eng. Chem., Vol. 55, No. 3 (March, 1963).
18. Gardner, J. W., F. M. Orr, and P. D. Patel, 'The Effect of Phase Behavior on CO₂ Flood Displacement Efficiency,' SPE 8367, presented at SPE 54th Annual Fall Meeting; Las Vegas, Nev. (Sept. 23-26, 1979).
86. Garrels, R. M. and M. E. Thompson, 'A Chemical Model for Sea Water at 25°C and One Atmosphere Total Pressure,' Amer. J. Science, Vol. 260 (1962), pp. 57-66.
85. Garrels, R. M., M. E. Thompson and R. Siever, 'Control of Carbonate Solubility by Carbonate Complexes,' Amer. J. Science, Vol. 259 (1961), pp. 24-25.
22. Glater, J., L. Ssutv and J. W. McCutchan, 'Laboratory Method For Predicting Calcium Sulfate Scaling Thresholds,' Env. Sci. and Tech., Vol. 1, No. 1 (Jan. 1967), pp. 41-45.
32. Government, Department of Energy (Formerly Energy Research and Development Administration), 'Enhanced Oil and Gas Recovery and Improved Drilling Methods,' DOE Quarterly Publications (1975, 1976, 1977, 1978, 1979).
41. Gunn, D. J. and M. S. Murthy, 'Kinetics and Mechanisms of Precipitations,' Chemical Engineering Society, Vol. 27 (1972), pp. 1293-1313.
51. Hawley, J. and Z. M. Pytkowicz, 'Solubility of Calcium Carbonate in Seawater at High Pressures,' Geochim. Cosmochim. Acta, Vol. 33 (1969), pp. 1557-1561.
33. Herbeck, E. F., R. C. Heinty and J. R. Hastings, 'Fundamentals of Tertiary Oil Recovery, Part 5 - Carbon Dioxide Miscible Process,' Petroleum Engineering, May 1976, pp. 114-120.

28. Holdren, G. R., Jr., and R. A. Berner, 'Mechanism of Feldspar Weathering-I, Experimental Studies,' Geochim. Cosmochim. Acta, Vol. 43, No. 8 (1979), pp. 1161-1172.
80. Holm, L. W., 'Oil Recovery Process,' U. S. Patent 3,065,790, Official Gazette, Vol. 784, No. 4 (Nov. 27, 1962), p. 1240.
98. Holm, L. W., 'Carbon Dioxide Solvent Flooding for Increased Oil Recovery,' Petroleum Transactions, Vol. 216 (1959), pp. 225-231.
16. Huang, E. T. S. and J. H. Tracht 'The Displacement of Residual Oil by Carbon Dioxide,' SPE 4735, presented at the SPE 3rd Symposium on Improved Oil Recovery; Tulsa, Okla. (April 1974).
29. Huang, W. H., 'Experimental Studies of Kinetics and Mechanisms of Simulated Organo-Chemical Weathering of Silicate Minerals,' Ph.D. Dissertation, Univ. of Missouri, Columbia, Missouri (1970).
105. Huang, W. H. and W. C. Kiang, 'Laboratory Dissolution of Plagioclase Feldspars in Water and Organic Acids at Room Temperature,' American Minerologist, Vol. 57 (1972), pp. 1849-1859.
20. Hutchinson C. A., Jr., and P. H. Braun, 'Phase Relations of Miscible Displacement in Oil Recovery', A.I.Ch.E. Journal, March 1961, pp. 66-72.
45. Kaschier, D., 'Nucleation at Time-Dependent Supersaturation,' Surface Science, Vol. 22 (1970), pp. 319-324.
40. Kleber, J. P., 'The Use of Calgon in Primary Production and Water Flooding,' Producers Monthly, January 1951, pp. 18-24.
5. Kolthoff, I. M. and V. A. Stenger, 'Error in Quantitative Neutralizations,' in: Volumetric Analysis, Vol. 1, 2nd ed., Interscience, New York (1954).
6. Kolthoff, I. M. and V. A. Stenger, 'Neutralization and Ionic Combination Reactions,' in: Volumetric Analysis, Vol. 1, 2nd ed., Interscience, New York (1954).
4. Kolthoff, I. M. and H. A. Laitinen, 'Acids and Bases; the pH of Aqueous Solutions,' in: pH and Electrotitration, 2nd ed., John Wiley, New York (1947).
27. Kramer, K. F., 'Oxygen Compound Acidity and Oxygen Polarization as a Control in Silicate Weathering,' Ph.D. Dissertation, Florida State University, Gainesville, Florida (1968).
39. Krynine, P. D., 'Mineralogy Of Water Flooding,' Producers Monthly, December 1938, pp. 10-13.
81. Lagache, M., 'New Data on the Kinetics of the Dissolution of Alkali Feldspars at 200 Degrees C in CO₂ Charged Water,' Geochim. Cosmochim. Acta, Vol. 40, No. 2 (1976), pp. 157-161.

56. Lasater, R. M., T. R. Gardner, and T. M. Glasscock, 'Scale Deposits Are Controlled,' Oil and Gas Journal, Jan. 15, 1968, pp. 83-93.
100. Legand, H. E. and V. T. Stringfield, 'Differential Erosion of Carbonate-Rock Terranes,' Southwest Geology, Vol. 13, No. 1 (1971), pp. 1-17.
19. Lowe, L. C., M. C. McPhillips and A. C. Riddiford, 'On the Wetting of Carbonate Surfaces by Oil and Water,' Journal of Canadian Petroleum Technology, April-June 1973, pp. 33-40.
49. Madgin, W. M. and D. A. Swales, 'Solubilities in the System CaSO_4 - $\text{NaCl-H}_2\text{O}$ at 25° and 35°,' J. Appl. Chem., Nov. 1956, pp. 482-487.
77. Marshall, W. L., R. Slusher and E. V. Jones, 'Solubility and Thermodynamic Relationships for CaSO_4 in $\text{NaCl-H}_2\text{O}$ Solutions from 40° to 200°C., 0 to 4 Molal NaCl ,' J. of Chem. and Eng. Data, Vol. 9 (1964) pp. 187-191.
48. Metler, A. V. and A. G. Ostroff, 'The Proximate Calculation of the Solubility of Gypsum in Natural Brines from 28° to 70°C.,' Environ. Science and Tech., Vol. 1 (1967), pp. 815-819.
57. Miles, L., 'New Well Treatment Inhibits Scale,' Oil and Gas Journal, June 8, 1970, pp. 96-99.
12. Miller, J. P., 'A Portion of the System Calcium Carbonate-Carbon Dioxide-Water, with Geological Implications,' American Journal of Science, Vol. 250, March 1952, pp. 161-203.
88. Nakayama, F. S., 'Calcium Activity, Complex and Ion-Pair in Saturated CaCO_3 Solutions,' Soil Science, Vol. 106 (1968), pp. 429-434.
111. Nancollas, G. H. and K. Sawada, 'The Formation of Scales of Calcium Carbonate Polymorphs. The influence of Magnesium Ion and Inhibitors,' SPE 9992, SPE Fifth International Symposium on Oilfield and Geothermal Chemistry, Stanford, California, pp. 167-177.
2. Nancollas, G. H. and M. M. Reddy, 'The Kinetics of Crystallization of Scale-Forming Minerals,' Society of Petroleum Engineers Journal, April 1974, pp. 117-126.
52. Nancollas, G. H., A. E. Eralp and J. S. Gill, 'Calcium Sulfate Scale Formation: A Kinetic Approach,' Society of Petroleum Engineers Journal, April 1978, pp. 133-138.
82. Nancollas, G. H., and S. T. Liu, 'Crystal Growth and Dissolution of Barium Sulfate,' Soc. of Pet. Eng. of AIME, 1975, pp. 69-79.
99. Nathan, C., 'Vaterite in Lake Water,' Nature Physical Science, Vol. 231, No. 24 (June 14, 1971), p. 158.
102. Nathan, C., 'Solubility Studies on High Molecular Weight Paraffin Hydrocarbons Obtained from Petroleum Rod Waxes', Petroleum Transactions, AIME, Vol.204 (1955), pp. 151-155.

103. Nixon, R. A., 'Differences in Incongruent Weathering of Plagioclase and Microcline-Cation Leaching Versus Precipitates,' Geology, Vol. 7 (1979), pp. 221-224.
107. Nooner, D. W., J. Oro, J. M. Gilbert, L. V. Ray and J. E. Mann, 'Ubiquity of Hydrocarbons in Nature: Aliphatic Hydrocarbons in Weathered Limestone,' Geochim. Cosmochim. Acta, Vol. 36 (1972), pp. 953-959.
91. Orr, F. M., Jr., A. D. Yu, and C. L. Lien, 'Phase Behavior of CO₂ and Crude Oil in Low Temperature Reservoirs,' First Joint SPE/DOE Symposium on Enhanced Oil Recovery, Tulsa, Oklahoma, April 20-23, 1980, pp. 17-32.
72. Ostroff, A. G. and A. V. Metler, 'Apparatus for Testing Scale and Corrosion Inhibitors,' Producers Monthly, May 1965, pp. 8-12.
73. Ostroff, A. G., 'Compatibility of Waters for Secondary Recovery,' Producers Monthly, March 1963, pp. 2-9.
1. Owen, B. B. and S. R. Brinkley, 'Calculations of the Effect of Pressure Upon Ionic Equilibria in Pure Water and in Salt Solutions,' Chemistry Reviews, Vol. 29 (1941), pp. 461-471.
108. Perkins, A. T., 'Decomposition of Silicate Minerals by Acid Extractions Chemical Composition and Exchange Capacity,' Transactions Kansas Academy of Sci., Vol. 67, (1964), pp. 486-495.
17. Perry, G. E., A. J. Guillory, J. D. Baron and M. B. Moranville, 'Weeks Island 'S' Sand Reservoir B Gravity Stable Miscible CO₂ Displacement, Iberia Parish, Louisiana,' Fourth Annual DOE Symposium on Enhanced Oil and Gas Recovery, Tulsa, Oklahoma, Aug. 29-31, 1978.
21. Peterson, A. V., 'Optimal Recovery Experiments with Nitrogen and Carbon Dioxide,' Pet. Eng. Int., Nov. 1978, pp. 40-50.
109. Petrovic, R., R. A. Berner and M. B. Goldhaber, 'Rate Control in Dissolution of Alkali Feldspars - I. Study of Residual Feldspar Grains by X-ray Photoelectron Spectroscopy,' Geochim. Cosmochim. Acta, Vol. 40 (1976), pp. 537-548.
93. Pilat, S. and M. Godlewicz, 'Method of Treating Mineral Oils,' U. S. Patent No. 2,315,131 (Jan. 30, 1934).
94. Pilat, S. and M. Godlewicz, 'Method of Separating High Molecular Mixtures,' U. S. Patent No. 2,188,013 (April 27, 1936).
30. Pytkowicz, R. M., 'Rates of Inorganic Calcium Carbonate Nucleation,' Geological Notes, 1964, pp. 196-199.
59. Ralston, P. H., 'Scale Control with Aminomethylene phosphonates,' Journal of Petroleum Technology, August 1969, pp. 1029-1036.

97. Reed, M. G., 'Formation Permeability Damage by Mica Alteration and Carbonate Disolution,' Journal of Petroleum Technology, Vol. 29 (September 1977). pp. 1056-1060.
104. Rodgers, G. P. and H. D. Holland, 'Weathering Products Within Microcracks in Feldspars,' Geology, Vol. 7 (1979), pp. 278-280.
90. Rutherford, W. M., 'Miscibility Relationships in the Displacement of Oil by Light Hydrocarbons,' Society of Petroleum Engineers Journal, Vol. 2, (December 1962), pp. 340-346.
70. Shelton, J. L. and F. N. Schneider, 'The Effects of Water Injection on Miscible Flooding Methods Using Hydrocarbons and Carbon Dioxide,' Society of Petroleum Engineers Journal, June 1975, pp. 217-226.
96. Shelton, J. L. and L. Yarbrough, 'Multiple Phase Behavior in Porous Media During CO₂ or Rich-Gas Flooding,' Journal of Petroleum Technology, September 1977, pp. 1171-1178.
95. Simon, R., A. Rosman, and E. Zana, 'Phase-Behavior Properties of CO₂-Reservoir Oil Systems,' Society of Petroleum Engineers Journal, February 1978. pp. 20-26.
74. Slaton, L., R. Laster, and J. Knox, 'Scale Deposition and Removal,' Producers Monthly, September 1965, pp. 8-10.
63. Sloat, B. 'Controlled Solubility Phosphates--A Versatile Solution to Oilfield Scale Problems,' Journal of Petroleum Technology, November 1960, pp. 30-36.
24. Smith, C. F., T. J. Nolan and P. L. Czenshaw, 'Removal and Inhibition of Calcium Sulfate Scale in Waterflood Projects,' J. Petroleum Technology, Nov. 1968. pp. 1249-1256.
58. Spriggs, D. M. and G. W. Hover, 'Field Performance of a Liquid Scale Inhibitor Squeeze Program,' Journal of Petroleum Technology, July 1972, pp. 812-816.
92. Stalkup, F. I., 'Carbon Dioxide Miscible Flooding: Past, Present, and Outlook for the Future,' Fifth Symposium on Improved Methods for Oil Recovery, Soc. Pet. Engrs. of AIME; Tulsa, Oklahoma (April 16-19, 1978), pp. 39-50.
47. Stiff, H. A. and L. E. Davis, 'A Method for Predicting the Tendency of Oil Field Waters to Deposit Calcium Carbonate,' Pet. Trans., Vol. 195 (1952). pp. 213-216.
46. Stiff, H. A. and L. E. Davis, 'A Method for Predicting the Tendency of Oil Field Waters to Deposit Calcium Sulfate,' Pet. Trans., Vol. 195 (1952), pp. 25-28.
79. Stumper, R., 'Physicochemical Investigations of the Precipitation of Calcium Carbonate from Water,' Agnew. Chem., Vol. 48, No. 7 (1935). pp. 117-124.

101. Tate, J. F., R. L. Venable and C. C. Nathan, 'The Solubility of Gypsum in Oil Field Brines,' ACS National Meeting (1964).
43. Templeton, C. C., 'Solubility of Barium Sulfate in Sodium Chloride Solutions from 25 to 95 Degrees Centigrade,' Journal of Chemical and Engineering Data, Vol. 5, No. 4 (Oct. 1960), pp. 514-516.
23. Templeton, C. C. and J. C. Rodgers, 'Prediction of Anhydrite Precipitation in Field Water-Heating Systems,' J. Pet. Tech., April 1968, pp. 423-432.
83. Uchameyshvili, N. Y., S. D. Malinin and N. I. Khitarov, 'Solubility of Barite in Concentrated Chloride Solutions of Some Metals at Elevated Temperatures in Relation to Problems of the Genesis of Barite Deposits,' Geokhimiya, Vol. 3 (1966), pp. 951-961.
10. Vetter, O. J., 'How Barium Sulfate is Formed: An Interpretation,' Journal of Petroleum Technology, December 1975, pp. 1515-1524.
66. Vetter, O. J., 'The Chemical Squeeze Process--Some New Information On Some Old Misconceptions,' Journal of Petroleum Technology, March 1973, pp. 339-352.
62. Vetter, O. J. and R. C. Phillips, 'Prediction of Deposition of Calcium Sulfate Scale Under Downhole Conditions,' Soc. of Pet. Eng., SPE 2620, 44th Annual Fall Meeting, Denver, Colo. (Sept. 28 - Oct. 1, 1969).
112. Vetter, O. J. and V. Kandarpa, 'Prediction of CaCO₃ Scale Under Downhole Conditions,' SPE 8991, SPE Fifth International Symposium on Oilfield and Geothermal Chemistry, Stanford, California, pp. 155-165.
11. Walton, A. G., 'The Nucleation of Sparingly Soluble Salts from Solution,' Analytica Chemica Acta, Vol. 29 (1963), pp. 434-441.
8. Weintritt, D. J. and J. C. Cowan, 'Unique Characteristics of Barium Sulfate Scale Deposition,' Journal of Petroleum Technology, October 1967, pp. 1381-1394.
84. Weyl, P. K., 'The Solution Kinetics of Calcite,' J. of Geology, Vol. 66 (1958), pp. 163-175.
38. Yuster, S. T., 'The Gypsum Problem in Water Flooding,' Producers Monthly, April 1939, pp. 27-35.

1. Owen, B. B., and Brinkley, S. R.: "Calculations of the Effect of Pressure Upon Ionic Equilibria in Pure Water and in Salt Solutions", Chem. Reviews (1941) vol. 29, pp. 461-471.

Abstract

Tables of standard partial molal and ionic volumes, and their pressure coefficients, are given for aqueous solutions at 25° C. These are used to estimate the effect of pressure upon the ionization constants of water and weak acids, and the solubility constants of several minerals.

2. Nancollas, G. H. and Reddy, M. M.: "The Kinetics of Crystallization of Scale Forming Minerals", Soc. of Pet. Eng. J. (April, 1974) pp. 117-126.

Abstract

This article examines the kinetics of the crystallization of sparingly soluble minerals such as calcium carbonate, calcium sulfate, and barium sulfate, which frequently cause scaling problems in oil fields. For all three electrolytes, the crystal growth is surface controlled and follows a second order rate law with an activation energy for the growth process of 10 to 20 kcal/mol. The growth of calcium sulfate seeded crystal above 100°C. demonstrates the importance of characterizing polymorphic transformation processes. Phosphonate scale inhibitors show differing modes of inhibition in systems precipitating CaCO_3 and CaSO_4 .

3. Ellis, A. J. and McFadden, I. M.: "Partial Molal Volumes of Ions in Hydrothermal Solutions", Geochimica et Cosmochimica Acta, vol. 36 (1972) pp. 413-426.

Abstract

Partial molal volume data are reported for NaHCO_3 and NaHS up to 200°C ., derived from solution density measurements. A summary is given of molal volumes of ions of principle interest in natural hydrothermal equilibria. Examples are given of the use of these data to calculate the effect of pressure on equilibria involving ions (H_2S - H_2CO_3 ionization; CaCO_3 , CaSO_4 solubility). In the latter case the agreement between the calculated and experimental solubility is very good to at least 250°C and 1000. bars.

4. Kolthoff, I. M., and Laitinen, H. A.: "Acids and Bases; The pH of Aqueous Solutions", pH and Electrotitration, 2nd ed. (1947) pub. John Wiley, pp. 8-11.

Abstract

A method for calculating the hydrogen ion concentration of a dibasic acid is shown on pages 8 to 11 of this book. This method can also be used with bases. A table of ionization constants and pK values is presented for some acids and bases at room temperature.

5. Kolthoff, I. M., and Stenger, V. A.: "Error in Quantitative Neutralizations", Volumetric Analysis, vol. 1, 2nd ed. (1954) pub. Interscience, N.Y., pp. 151-152.

Abstract

A method for calculating the error encountered when titrating a dibasic acid is presented on pages 151 to 152 of this book.

6. Kolthoff, I. M., and Stenger, V. A., "Neutralization and Ionic Combination Reactions" Volumetric Analysis, 2nd ed. (1954) pub. Interscience, N.Y., pp. 26-29.

Abstract

A method for calculating the hydrogen ion concentration (pH) of a solution containing two weak acids is presented on pages 26 to 29 of this book. Two sets of sample calculations are included.

7. Dixon, B. P., and Newton, L. E., Jr.: "Reinjection of Large Volumes of Produced Water in Secondary Operations", Journal of Pet. Tech. (July, 1965) pp. 781-788.

Abstract

A study was made of the operating performance histories of a pressure-maintenance and four waterflood projects in the Permian Basin area, where large volumes of produced water have been reinjected into the producing formations. The projects reviewed include a wide range of characteristics: (1) open and closed water systems, (2) volumes of reinjected water from 2,200 to 12,500 B/D, (3) sand and limestone formations, (4) depths of 1,300 to 6,750 ft. (5) average permeabilities from 17 to 275 md, (6) bare and protected facilities, and (7) 10- to 50-year project life.

Each project exhibited performance data which indicated that reinjection of large volumes of produced water provides a good source of injection fluid, results in practical and prudent salt water disposal and, in many cases, results in conservation of fresh water for future domestic needs.

8. Weintritt, D. J., and Cowan, J. C.: "Unique Characteristics of Barium Sulfate Scale Deposition": Jour. of Pet. Tech., (Oct., 1967) pp. 1381-1394.

Abstract

Methods of studying oilfield mineral scale deposition in the laboratory do not work for barium sulfate because only small nonadhering crystals are formed. On the other hand, barium sulfate scale found in down-hole or surface equipment is strongly adhering and may contain very large crystals. Results suggest that most of the difference derives from the extremely low solubility of barium sulfate. Firm adherence of scale and the consistent development of oriented crystals 100 microns and larger suggest a relationship between scale adherence and crystal growth.

Data from this study indicate some reasons for barium sulfate's occurring as a deposit in oilfield waters. The unique characteristics as well as the associative properties of barium sulfate scale as related to calcium carbonate and calcium sulfate are shown.

9. Davis, J. W., and Collins, A. G.: "Solubility of Barium and Strontium Sulfates in Strong Electrolyte Solutions", Environ. Science and Tech., vol. 5, No. 10, (Oct., 1971) pp. 1039-1043.

Abstract

Knowledge of the solubilities of BaSO_4 and SrSO_4 in solutions containing NaCl , CaCl_2 , MgCl_2 , and NaHCO_3 is needed to solve geologic and petroleum production problems. Samples of the sulfates were tagged with ^{35}S and prepared by precipitation. The solubility was measured in various concentrations of the major solutes by use of a liquid scintillation technique to detect the SO_2 in solution. The observed solubilities plotted against ionic strength of the solution are similar for strong electrolytes. They reach a maximum at concentration levels beginning at ionic strength of near 1. The sulfate solubility in synthetic brines (principally NaCl) confirms the ionic strength-sulfate solubility relationships.

10. Vetter, O. J. G.: "How Barium Sulfate is Formed: An Interpretation", Jour. of Pet. Tech., (Dec., 1975) pp. 1515-1524.

Abstract

Basic thermodynamic relations are used to predict the locations and rates of BaSO_4 scale formation under field conditions. When kinetics are considered, the prediction method is much improved. However, the inclusion of hydrodynamic factors in the predictive model makes it possible to explain the full range of BaSO_4 scale formation in the oil field.

11. Walton, A. G.: "The Nucleation of Sparingly Soluble Salts from Solution", Anal Chim. ACTA (1963) Vol. 29, pp. 434-441.

Abstract

An examination of some of the latest ideas in the nucleation of salts from solution shows that many of the older precipitation data may be interpreted in a similar manner. Former difficulties which resulted from the interplay of heterogeneous and homogeneous nucleation processes have been resolved and the implications in the optimization of grain size in precipitates examined. Some of the possible future developments relating the interfacial tension to the environment of the nucleus are outlined and calculated values for some of the required parameters obtained both from previously published and unpublished data are presented.

12. Miller, J. P.: "A Portion of the System Calcium Carbonate - Carbon Dioxide - Water, With Geological Implications", Am. Jour. of Sci., vol. 250 (March, 1952) pp. 161-203.

Abstract

The solubility of CaCO_3 in water depends on the presence of CO_2 , the concentration of which is a function of temperature and pressure of CO_2 in equilibrium with the water. As CO_2 -pressure increases at constant temperature the solubility of CaCO_3 increases, and at constant CO_2 pressure the solubility of CaCO_3 increases with decreasing temperature.

In the investigation conducted in this article, 259 determinations of solubility were made at temperatures ranging from 0° to 105°C and at CO_2 - pressures ranging from 1 to 100 bars. Three types of CaCO_3 - optical grade calcite, solenhofen limestone, and Venus mercenaria shells - were used for the experiments. Solvents were distilled water, 0.5 M NaCl solution, and standard sea water.

13. Beasley, A. E. and McKinney, I.: "Prevention of Calcium Carbonate Scale Deposition in Mill Water Systems", Society of Mining Engineers (March, 1973) pp. 32-37.

Abstract

This article examines various aspects of the scale deposition problem in mill water systems. Topics discussed include 1) the causes of scale deposition and 2) the methods used to combat the scale problem.

14. Englander, H. E.: "Conductometric Measurement of Carbonate Scale Inhibitors Effectiveness", Journ. of Pet. Tech. (July, 1975) pp. 827-834.

Abstract

This paper discusses the use of electrolytic conductometry for determining quantitatively an oil field brine's capacity to precipitate calcium carbonate under given conditions, and for determining the optimum dosage of scale inhibitor for specific brines.

Electrolytic conductometry involves the measurement of a solution's conductance. A change in a sample's dissolved calcium carbonate concentration causes a small, reproducible change in the solution's conductance. The amount of calcium carbonate precipitated can be determined from the change in conductance using a precalibrated graph. Correlations between laboratory tests and field data have shown that electrolytic conductometry is a useful tool for predicting scaling quantitatively.

15. Gainey, R. J., Thorp, C. A. and Cadwallader, E. A.: "Calcium Sulfate Seeding Prevents Calcium Sulfate Scale", Ind. and Eng. Chem., Vol. 55, No. 3 (March, 1963) pp. 39-43.

Abstract

Laboratory and pilot plant tests were conducted to determine the feasibility of preventing calcium sulfate scale formation in an evaporator by maintaining a sludge of calcium sulfate particles in the evaporator. This technique is based on the theory that the precipitating calcium sulfate will have a natural affinity to collect on the surface of the calcium sulfate particles introduced into the evaporator rather than on the evaporator surface. The results of these laboratory and pilot plant tests show that this technique effectively eliminates calcium sulfate scale formation in an evaporator.

16. Huang, E. T. S. and Tracht, J. H., "The Displacement of Residual Oil by Carbon Dioxide", SPE 4735, presented at the SPE 3rd Symposium on Improved Oil Recovery; Tulsa, Okla. (April, 1974).

Abstract

Displacement of a 36° API West Texas oil from watered-out cores with carbon dioxide was investigated at reservoir conditions of 90°F and 1250 psig. Phase behavior of the CO₂-West Texas oil system was also investigated. The objectives of the study were (1) to determine the oil recovery efficiency, and (2) to improve understanding of the oil recovery mechanisms, especially in relation to the phase behavior.

The phase behavior studies indicate that CO₂ efficiently swells the oil and forms two equilibrium liquid phases with the oil. Significant amounts of light and intermediate hydrocarbons are shown to be extracted into the CO₂ rich liquid phase from the oil phase. The CO₂ displacement studies conducted on watered-out cores indicate that a continuous CO₂ drive can achieve a maximum recovery of 69 percent of residual oil from a 6-ft Berea core and 65 percent from a 20 ft. sand-packed core. The minimum CO₂ slug size required in a water-propelled CO₂ drive for maximum recovery is 0.42 pore volume for the Berea core and 0.27 pore volume for the sand-packed core. In both cases, the required slug sizes are slightly greater than residual oil saturations.

An analysis of the results of the phase behavior and displacement studies indicates that CO₂ swelling and CO₂ extraction of oil are the dominant mechanisms responsible for recovering residual oil.

17. Perry, G. E., Guillory, A. J., Baron, J. D. and Moranville, M. B.: "Weeks Island 'S' Sand Reservoir B Gravity Stable Miscible CO₂ Displacement, Iberia Parish, Louisiana", presented at the 4th Annual DOE Symposium on Enhanced Oil and Gas Recovery; Tulsa, Okla., (Aug. 29-31, 1978).

Abstract

Shell Oil Company in conjunction with the Department of Energy is conducting a gravity stable field test of the miscible CO₂ process. The test is being conducted in a 12,800-foot deep Gulf Coast reservoir. The future producing well was drilled in December of 1977. The residual hydrocarbon saturation has been investigated using logging devices and cores.

Shell has investigated the miscibility and phase behavior of the CO₂ and reservoir crude. Injection facilities have been constructed and CO₂ injection has been targeted for the Second Quarter of 1978.

18. Gardner, J. W., Orr, F. M. and Patel, P. D.: "The Effect of Phase Behavior on CO₂ Flood Displacement Efficiency", SPE 8367, presented at SPE 54th Annual Fall Meeting; Las Vegas, Nev. (Sept. 23-26, 1979).

Abstract

The relationship between phase behavior and displacement efficiency regards the displacement of Wasson crude oil by CO₂ is examined at two different pressures - the lower one at which three co-existing hydrocarbon phases are encountered. At both pressures experimental phase behavior data, consisting primarily of phase volume fractions observed in both single contact and multiple contact experiments, are presented. Pseudo-ternary representations of the phase behavior are incorporated into a simple, one dimensional, finite difference simulator to relate the phase behavior to displacement efficiency. At the appropriate dispersion level, displacement efficiencies computed with the model are consistent with high oil recovery efficiencies obtained experimentally in slim tube displacements, and indicate the displacement efficiency of the process should be high in certain consolidated media as well.

19. Lowe, L. C., Phillips, M. C., and Riddiford, A. C.: "On the Wetting of Carbonate Surfaces By Oil and Water", Journal of Canadian Pet. Tech. (April, 1973) pp. 33-40.

Abstract

The relaxation of initially advancing and receding contact angles has been studied for two basic systems, water/saturated air/marble, and aqueous solution/oil/marble, and static advancing contact angles have been studied in the water/air/marble system. All experiments were conducted at room temperature, but other experimental conditions have been varied so as to permit comparison between these laboratory results and certain aspects of the recovery of oil from limestone fields. A preliminary study also has been made to elucidate which components of crude oil affect the wettability of calcium carbonate, and assess the stability of the adsorbed layers to solvent attack and to oxidation.

20. Hutchinson, C. A., Jr., and Braum, P. H. "Phase Relations of Miscible Displacement in Oil Recovery", A.I.Ch.E. Journal (March, 1961) pp 66-72.

Abstract

Miscible displacement as an oil recovery process has received wide interest in the literature recently. Essentially three basic processes have been proposed for attaining miscible displacement in our oil reservoirs: high pressure gas, enriched gas, and miscible slug processes.

The present paper relates and compares the phase relations and mass transfer mechanisms of these various basic miscible displacement processes. It also discusses the effects of the various operating variables, such as pressure, temperature, injected gas composition, etc., on the applicability of the process and considers the pertinent conditions that restrict the application of each process. It is to be recognized that at times a miscible displacement may be attempted but not attained, or unforeseen conditions may destroy miscibility once it has been attained. The authors discuss the results of such conditions. The mechanisms of the miscible displacement processes are explained in a conceptual analysis based on the triangular phase diagram. Although the multicomponent reservoir fluid system cannot be represented rigorously from a thermodynamics standpoint by these diagrams, they are useful for conceptual analysis. Their limitations are presented by the authors along with data supporting the concepts developed.

21. Peterson, A. V.: "Optimal Recovery Experiments With Nitrogen and Carbon Dioxide", Pet. Eng. Int. (Nov., 1978) pp. 40-50.

Abstract

Oil recovery experiments were conducted to determine the relative effectiveness of nitrogen and carbon dioxide as enhanced oil recovery agents. Data presented in this article include pressure-consumption diagrams for the following systems: crude oil-carbon dioxide, crude oil-nitrogen, condensate (volatile portion of the crude oil) - carbon dioxide, and condensate-nitrogen. The data indicates that carbon dioxide is a more effective oil recovery agent than nitrogen, but the author points out that nitrogen has economic advantages over carbon dioxide that may make its use more practical.

22. Glater, J., Ssutv, L., and McCutchan, J. W.: "Laboratory Method For Predicting Calcium Sulfate Scaling Thresholds", Env. Sci. and Tech., Vol. 1, No. 1, (Jan., 1967) pp. 41-45.

Abstract

An experimental method for measuring calcium sulfate scaling thresholds of natural saline water samples at 100°C. is based on visual observation of freshly formed hemihydrate needles from evaporating brine solution. A novel all-glass laboratory evaporator has been developed. The crystal phase was identified as pure calcium sulfate hemihydrate by x-ray diffraction. Critical concentration factors measured for sea water, Roswell brackish water, and Salton Sea water were 3.2, 2.6, and 1.1 respectively. The influence of ionic strength on calcium sulfate solubility is clearly indicated. A graphical method relates scaling threshold to calcium and sulfate ion concentration for a given saline water. This technique should be useful in estimating the calcium sulfate scaling potential of any natural water in a distillation process.

23. Templeton, C. C. and Rodgers, J. C.: "Prediction of Anhydrite Precipitation in Field Water-Heating Systems", J. Pet. Tech. (April, 1968) pp. 423-432.

Abstract

A key step in feed water treatment for generating wet steam for thermal oil recovery is the removal of calcium and magnesium hardness by cation-exchange series softening. Knowing the solubility of any scale-forming salts in brines at elevated temperatures is necessary for fixing the level to which the feed water must be softened. Such calcium sulfate solubility data, previously not available above 392F, were determined by the authors in a flow equilibrium apparatus and will be reported elsewhere. These data were used to develop a method for predicting the solubility of anhydrite in hot water or steam droplets for saturated steam pressures as high as 2,000 psig (637F). (The calcium sulfate solubility product is represented by a combination of two factors, one reflecting the effects of ionic strength and the other accounting for the effects of complex ion formation in either calcium-magnesium-rich or sulfate-rich brines.)

The method is applied to a calcium-magnesium-rich brine of moderately high salinity from a pilot hot-water flood, and to several sulfate-rich, low-salinity feed waters and blowdown (cooled steam droplets) samples from steam soak operations. The predicted calcium hardness levels corresponding to the calcium sulfate solubilities agreed reasonably well with the results of laboratory solubility determinations run on the field samples. Further testing of the method is needed for brines of other composition classes. Existing field cation exchange softeners in the cases tested are performing adequately since all the samples were found to be unsaturated with respect to calcium sulfate at their operating temperatures.

24. Smith, C. F., Nolan, T. J., and Czenshaw, P. L.: "Removal and Inhibition of Calcium Sulfate Scale in Waterflood Projects", J. Pet. Tech. (Nov., 1968) pp. 1249-1256.

Abstract

The problem of preventing calcium sulfate scale deposition has become increasingly important in the last few years due to the increasing use of waterflood as a means of secondary recovery. Many methods have been proposed for removing or preventing scale deposition. A few chemicals and treatment methods have been effective, but there are many ineffective scale-removal agents and inhibitors still on the market today. This paper describes the results of a laboratory testing program that evaluated 98 potential-scale inhibitors and 20 scale-removal agents. The paper also describes a field testing program in which various removal methods and inhibitor placement techniques were evaluated in 19 wells, and it compares field and laboratory results.

25. Berner, R. A.: "Rate Control of Mineral Dissolution Under Earth Surface Conditions", Am. Journ. of Sci., vol. 278, no. 9 (1978) pp. 1235-1252.

Abstract

Dissolution of minerals by water is an important Earth surface geochemical process. Actual dissolution rates generally cannot be accurately predicted from laboratory experiments, because experiments ordinarily fail to reproduce the composition and structure of natural mineral surfaces, especially with regard to adsorbed trace inhibitor species, and poorly understood biological factors are usually ignored. Laboratory experiments can be helpful, however, in distinguishing rate-limiting mechanisms, or in other words, whether dissolution is primarily controlled by surface reactions or by transport of ions away from the surface.

Although much work has been done in predicting, from thermodynamic calculations, whether or not dissolution can occur, little attempt has been made to describe how dissolution occurs under natural conditions. The purpose of this paper is to point out some of the factors that control the rate of dissolution and to yield a better understanding of the applicability of chemical kinetics to the solution of geochemical problems.

26. Berner, Robert A. and Holdren, George R. Jr. "Mechanism of Feldspars From Soils", *Geochem Cosmochem Acta* (III) (GCACAK), Vol. 43, No. 8, 00167037 pp. 1173-1186, 1979 illus.

Abstract

Examination of the surface morphology (via scanning electron microscopy) and surface composition (via X-ray photoelectron spectroscopy) of sodic plagioclase and potash feldspar grains taken from four different soils, provides little or no evidence for the existence of a tightly adhering protective surface layer of altered composition on the feldspar surface. Grains, from which all adhering clay has been removed by ultrasonic cleaning, exhibit the same chemical composition in the outermost few tens of angstroms as the underlying feldspar. Aluminum-rich 'clay' coatings which continue to adhere to the grains after ultrasonic treatment are patchy, highly hydrous, and unlikely to act as major diffusion-limiting, and thus protective, barriers. Attack by dissolution of the feldspar surface is non-uniform and follows a definite etching sequence characterized by the development and growth of distinctive etch pits. This dissolution sequence can be reproduced by treating fresh feldspars in the laboratory with strong $\text{HF-H}_2\text{SO}_4$ solutions and, thus, the sequence is unaffected by the composition of the attacking solution. All of our results suggest that the dissolution of feldspar during weathering is controlled by selective chemical reaction at the feldspar-solution interface and not by uniform diffusion through a protective surface layer.

27. Kramer, K. F.: "Oxygen Compound Acidity and Oxygen Polarization as a Control in Silicate Weathering", Ph.D. Dissertation, Florida State University, Gainesville, Florida. (1968).

Abstract

This article discusses the solution chemistry involved in silicate alteration. It is discussed using an acid-base model based on anion polarization. The model was developed for oxygen compounds.

28. Holdren, George R. Jr., and Berner, Robert A.: "Mechanism of Feldspar Weathering - I, Experimental Studies Geochem Cosmochem Acta (III) (GCACAK), Vol. 43, No. 8, 00167037 pp. 1161-1172, 1979 illus.

Abstract

It has been widely accepted that a chemically altered, protective surface layer regulates the dissolution, and hence the weathering, of plagioclase feldspars under Earth's surface conditions. In this study, we examine this hypothesis in detail with the aid of scanning electron microscopy (SEM) and X-ray photoelectron spectroscopy (XPS). Using these techniques, we have been unable to find any direct evidence suggesting the presence of a chemically altered coating on feldspar surfaces which have been weathered in the lab. Instead, our results suggest that the mechanism controlling feldspar weathering is a surface controlled reaction.

Based on SEM observations and measurements of rate of release of silica, we postulate that the process of feldspar dissolution proceeds in two stages in the lab. Initially, one observes the dissolution of ultrafine ($1\mu\text{m}$ diameter) particles which are produced during grinding of the sample, and which adhere tenaciously to the surfaces of larger grains. This is the stage which results in the non-linear rates of dissolution which are commonly observed in the lab (parabolic kinetics). Secondly, the dissolution occurs at sites of excess surface energy such as at dislocations or similar crystal defects. This process yields linear rates of dissolution, and it dominates the weathering of feldspars in the field.

29. Huang, Wen Hsing. "Experimental Studies of Kinetics and Mechanisms of Simulated Organo-Chemical Weathering of Silicate Minerals", Ph.D. Dissertation, Univ. of Missouri; Columbia, Missouri (1970).

μ = mu = micron

Abstract

Freshly fractured olivine, augite, muscovite, labradarite, and microcline in particle sizes 297μ - 149μ in diameter, after washing, were shaken at room temperature in deionized water, CO_2 charged water, .01M acetic acid and .01M aspartic acid of weakly complexing organic acids, .01M salicylic acid and .01M tartaric at strongly complexing organic acids, in closed systems. Samples of solute were drawn at 0.36, 1.2, 5.1 and 21.2 days and analyzed for Si, Al, Fe, Mg, Ca, Na, K, ph and conductivity.

30. Kovalenko, E. N.: "Growth Kinetics of Calcite Decomposition Nuclei", Ph.D. Dissertation, Univ. of Utah, Salt Lake City, Utah (1964).

Abstract

The article shows the thermal decomposition of calcite single crystals was found to occur at surface point defects at which decomposition pits or nuclei eventually developed. An initial heat treatment in CO_2 overpressure would anneal out many surface defects; however, longer annealing drastically increased the defect concentration. The thermal decomposition kinetics in terms of the movement of the CaCO_3 -CaO interface were measured during nucleation over wide ranges of temperature and CO_2 overpressure.

31. Busenberg, E. and Clemency, C. V.: "The Dissolution Kinetics of Feldspars at 25°C. and 1 atm. CO_2 Partial Pressure", Geochem. Cosmochim. Acta., vol. 40, no. 1 (1976) pp. 41-49.

Abstract

The dissolution kinetics of 5% by weight suspensions of two potassium feldspars and six plagioclases were studied for 400-1200 hr at 1 atm P_{CO_2} . The less than 37 μm particles had surface areas ranging from 0-83 to 1-84 m^2/g . At frequent intervals, the pH of the stirred suspensions were measured in the reaction cell as the solutions were sampled. The filtered aqueous samples were acidified and then were analyzed for Si, Al, K, Na, Ca, Mg, and Fe.

The following sequence of events were recognized in the artificial weathering of all the feldspars: (1) an initial ion exchange stage lasting approximately 1 min during which the surface cations were replaced by hydrogen ions from the bulk solution, (2) an up to 4 day non-parabolic stage characterized by the very rapid release of cations and silicic acid into the bulk solution, (3) a diffusion-controlled parabolic stage lasting approximately 19 days, and (4) a steady-state stage characterized by the very slow release of cations and silicic acid. All the rate constants for all the feldspars were evaluated at the pH of about 5. The calculated parabolic rate constants range from 3.4×10^{-14} to 9.3×10^{-13} $\text{mole}/\text{cm}^2/\text{sec}$, $^{1/2}$ the linear rate constants range from 3.2×10^{-17} to 2.5×10^{-15} $\text{mole}/\text{cm}^2/\text{sec}$, and the apparent diffusion coefficients range from 1×10^{-22} to 5×10^{-21} cm^2/sec .

32. Department of Energy (Formerly Energy Research and Development Administration): "Enhanced Oil and Gas Recovery and Improved Drilling Methods", D.O.E. quarterly publication. (1975, 1976, 1977, 1978, 1979).

Abstract

These reports, which are issued quarterly by the U.S. Department of Energy, contain useful information on the objectives, background, and Technical Progress of DOE sponsored field projects and supporting research. A number of topics are covered, including chemical flooding, carbon dioxide injection, thermal/heavy oil projects, western gas studies, eastern gas studies, improved drilling methods, residual oil studies, environmental studies, and petroleum technology.

The CO₂ field projects include Granny's Creek Field, West VA., Griffithsville Field, West Va., Rock Creek Field, West VA., and Weeks Island Reservoir, LA. Supporting research is being performed on corrosion problems, oil recovery, and displacement of residual oil.

33. Herbeck, E. F., Heintz, R. C. and Hastings, J. R.: Fundamentals of Tertiary Oil Recovery, Part 5 - Carbon Dioxide Miscible Process", Pet. Eng. (May, 1976) pp. 114-120.

Abstract

Miscibility in a CO₂ - Flood Process is achieved only after several contacts between the injected CO₂ and the reservoir fluid. The minimum miscibility pressure in the case of CO₂ is less than 1,500 PSI for many reservoirs. CO₂ can also extract heavier components of hydrocarbons in the range of C6 to C30 and achieve miscibility even with crude oils that have little intermediate (C2 to C6) components. This makes the process more versatile. It is particularly suited for reservoirs containing crude oils with 25 API and above. A practical upper limit of operating pressure in a CO₂ injection process is 6000 PSI; the lower limit is 1500 PSI. The density of CO₂ is close to that of crude oil and approaches that of water under some reservoir conditions. As a result, effects of gravity override are minimized in this process. The process also gives better sweep efficiency than hydrocarbon miscible processes because CO₂ viscosity is two to four times higher than hydrocarbon solvents, over usual ranges of pressure. However, alternate CO₂ and water injection is often necessary to achieve a reasonable miscibility ratio. CO₂ with water forms carbonic acid which is highly corrosive. Special metal alloys and coatings may be required for facilities. Dual injection systems for water and CO₂ are usually used. Availability and cost of CO₂ are important economic factors that should be considered in this process.

34. Bernard, G. C.: "Effect of Calcium Carbonate Supersaturation of Flood Water on Rock Permeability", Producers Monthly (July, 1957) pp. 32-36.

Abstract

A laboratory investigation was carried out to determine the maximum amount of CaCO_3 supersaturation that can be carried in a flood-water without plugging injection wells. It appears that up to 60 ppm. of CaCO_3 supersaturation can be tolerated in a floodwater entering the reservoir in the temperature range of 80 to 130°F. Thus, it is likely that the closed system will be satisfactory for many floodwaters that were formerly thought to require calcium carbonate stabilization. Since the closed system is considerably more economical to build and to maintain than the open system, application of this information may result in reduced floodwater treating costs.

35. Burick, E. J.: "The Inhibition of Gypsum Precipitation by Sodium Polyphosphates", Prods. Monthly (Nov., 1954) pp. 42-44.

Abstract

Experiments were conducted to determine the effectiveness of several dehydrated sodium polyphosphates at inhibiting gypsum precipitation in an aqueous solution. Results show that the sodium polyphosphates are effective as inhibitors in concentrations far below the concentration actually needed to form complexes with all of the calcium ions. The polyphosphates apparently work by adsorbing on the surface of the gypsum crystals to prevent further growth, rather than by tying up all of the calcium ions.

The experiments were conducted with inhibitor concentrations of 50, 25, and 12.5 p.p.m. and time periods of 1 hr., 10 hr., and 11.5 days. Several of the polyphosphates inhibited precipitate formation past the 10 hr. period, but all the solutions had precipitated after 11.5 days.

36. Bernard, G. S.: "A Survey on the Use of Incompatible Flood Waters", Producers Monthly (Feb., 1957) pp. 34-37.

Abstract

Experimental data indicate that incompatible waters do not react in, nor decrease the permeability of, a reservoir. Apparently, during the displacement process the main body of injection water does not mix with the main body of interstitial water.

A questionnaire was prepared requesting information concerning field experience with injection waters that were incompatible with interstitial waters, during water flooding of oil reservoirs. This was sent to fifty persons who had had considerable experience with all phases of water flooding. In the questionnaires that were returned, five water floods were reported in which incompatible waters had been used without any injurious effects. Thus far, no case has been reported in which the use of incompatible waters had a deleterious effect.

It is concluded that there is little danger of plugging a reservoir rock by injecting into it a water which is incompatible with the reservoir interstitial water.

37. Crawford, P. B.: "Sequestration and Chelation", Producers Monthly (July, 1957) p. 17.

Abstract

This article briefly discusses how the polyphosphates prevent calcium and barium ions from precipitating in flood waters. Equilibrium data for several of the reactions involving the polyphosphates and calcium ions is presented and explained. Diagrams showing the structures of several of the polyphosphates are shown.

38. Yuster, S. T.: "The Gypsum Problem in Water Flooding", The Producers Monthly (April, 1939) pp. 27-35.

Abstract

The factors involved in the precipitation of calcium sulfate (gypsum) from aqueous solutions are examined to determine which factors are responsible for calcium sulfate scaling in water flood projects. The three factors discussed are temperature change, evaporation of solvent, and chemical precipitation.

Calculations are presented to show the relative contributions of each of these factors to the total scaling problem. Results show that temperature change and evaporation of solvent are of minor importance. Chemical precipitation due to the mixing of incompatible waters is probably the major contributor to calcium sulfate scaling in water flood projects.

39. Krynine, P. D.: "Mineralogy of Water Flooding", The Producers Monthly (Dec., 1938) pp. 10-13.

Abstract

In order to predict the behavior of a reservoir during a water flood, it is important to know not only the porosity and permeability of the reservoir, but to understand the structural factors within the reservoir which determine these values. The structural factors involved fall into the three general categories of the structure and texture of the sand; the physical properties of the surface of the walls of the voids, which includes wettability and adsorption; and the chemical properties of the reservoir, which includes the solubilities of the various constituents found in the reservoir. Methods for determining and evaluating these structural factors are presented in this article.

40. Kleber, J. P.: "The Use of Calgon in Primary Production and Water Flooding", Producers Monthly (January, 1951) pp. 18-24.

Abstract

Calgon is a molecularly dehydrated phosphate which has proved to be effective in overcoming many scaling and corrosion problems encountered in the petroleum industry. The most important of these problems may be listed as follows:

1. The deposition of relatively insoluble salts such as calcium carbonate, barium sulfate, and strontium sulfate resulting from the mixing of various waters and brines.
2. The deposition of calcium carbonate scale resulting from the loss of carbon dioxide due to pressure reduction or temperature changes.
3. The deposition of calcium carbonate scale resulting from the addition of alkali in treating the brine or fresh water prior to injection.
4. The deposition of soluble iron or manganese resulting from the exposure of the water to the air or to oxidizing disinfecting agents such as chlorine.
5. The deposition of iron oxide and the decreased life of lines and equipment due to the corrosive action of oxygen or carbon dioxide.

41. Gunn, D. J. and Murthy, M. S.: "Kinetics and Mechanisms of Precipitations", Chem. Eng. Sci., vol. 27 (1972) pp. 1293-1313.

Abstract

The kinetics of crystal growth of a number of sparingly soluble salts have been studied. The crystallization of barium sulphate was studied in detail; the concentration of the crystallizing solution and the surface area of the precipitate were measured as the crystallization proceeded, and the particle size distribution was measured at the termination of the growth period.

The induction period was measured for three sparingly soluble salts at a number of different concentrations. The rate of growth of barium sulphate was found to show a third order dependence on concentration when the crystals were small. For larger crystals at low supersaturations the dependence was found to be first order.

The measurements of concentration, surface area and particle size distribution were used to calculate the rates of primary and secondary nucleation of barium sulphate. Other evidence concerning secondary nucleation is presented and found to be consistent with the kinetic measurements.

The development of crystal shape is related to diffusion in the solution and the surface reaction. It is shown that the induction period may be simply related to the rate of growth of small crystals.

42. Doremus, R. H.: "Crystallization of Slightly Soluble Salts from Solution", Journ. of Phys. Chem., vol. 74, No. 7 (April 2, 1970) pp. 1405-1408.

Abstract

The rate of crystallization of barium sulfate from aqueous solution was studied simultaneously with two methods, electrical conductivity of the solution and light scattering from the particles. From these measurements the particle size was estimated and the interface growth coefficient was calculated. The results indicated that the particles coagulated in the later stages of precipitation. Results of several authors on crystallization of salts from solution are compared. The order of the crystallization process depends upon the stoichiometry of the salt and its supersaturation. The effect of supersaturation may result from different growth processes on different crystal faces. The interface growth coefficients for different salts, orders of crystallization, and supersaturation are compared. These coefficients are usually not a function of order or supersaturation, but do depend upon the type of salt crystallizing.

43. Templeton, C. C.: "Solubility of Barium Sulfate in Sodium Chloride Solutions from 25° to 95°C." Journ. of Chem. and Eng. Data, vol. 5, no. 4 (Oct., 1960) pp. 514-516.

Abstract

The deposition of barium sulfate as scale from highly concentrated brines produced from oil wells is a fairly common occurrence. As part of a study of this scale formation problem, the concentration solubility product of barium sulfate in the $\text{BaSO}_4 - \text{NaCl} - \text{H}_2\text{O}$ system has been determined at several temperatures between 25°C and 95°C for sodium chloride molalities between about .1 and 5.0.

44. Doremus, R. H.: "Precipitation Kinetics of Ionic Salts from Solution", Journ. of Phys. Chem., vol. 62 (1958) pp. 1068-1075.

Abstract

Mechanisms for ionic crystal growth from solution are discussed and compared to experimental measurements of salt precipitation rates. In the systems considered the crystal growth rate is shown to be controlled by an interface process, rather than by bulk diffusion of solute. An adsorbed surface layer on the growing salt particles is proposed as the first stage in crystal growth from solution, and this proposal is shown to be consistent with the experimental results. It is concluded that in the systems considered nucleation occurs rapidly and the number of salt particles is constant during the measured growth period, and that factors as well as solute supersaturation influence the nucleation process.

45. Kaschier, D.: "Nucleation at Time-Dependent Supersaturation", Surface Science, Vol. 22 (1977) pp. 319-324.

Abstract

Homogeneous nucleation taking place at time-dependent supersaturation is considered. Expressions are derived for the nucleation rate and for the total number of nuclei formed in the system. After simple modification these expressions may also be used in the case of heterogeneous nucleation. Finally, a linear supersaturation change during the process is considered as an example.

46. Stiff, H. A. and Davis, L. E.: "A Method For Predicting the Tendency of Oil Field Waters to Deposit Calcium Sulfate", Pet. Trans., Vol: 195 (1952) pp. 25-28.

Abstract

A graphic method was developed which can be used to predict the tendency of oil field waters to precipitate calcium sulfate under a variety of conditions. Application of this method is made to the prediction of sulfate scale formation in heater treaters, boilers, oil wells, cooling systems and water injection wells.

47. Stiff, H. A. and Davis, L. E.: "A Method for Predicting the Tendency of Oil Field Waters to Deposit Calcium Carbonate", Pet. Trans. vol. 195 (1952) pp. 213-216.

Abstract

The authors previously presented a method for predicting the tendency of oil field waters to deposit calcium sulfate. The present paper gives a similar method for calcium carbonate.

Methods for predicting calcium carbonate scaling tendencies in fresh waters have been available for some time, but these could not be used for brines. By experimentally deriving the value of the K term in the Langelier equation, a method has been developed which applies to waters of high salt content. A statistical study is included which shows that the experimentally derived values of K are in good agreement with actual conditions. Several applications of the final equation to production practice are given.

48. Metler, A. V., and Ostroff, A. G.: "The Proximate Calculation of the Solubility of Gypsum in Natural Brines from 28° to 70° C.", Environ. Science and Tech. (1967) vol. 1, pp. 815-819.

Abstract

Formulas are derived for calculation of the solubility of calcium sulfate in various concentrations of sodium, magnesium, calcium, chloride, and sulfate ions in solution at 28°, 38°, 50°, and 70° C. Corrections are included to account for the effect of a wide concentration range of excess common ion (Ca^{+2} or SO_4^-). Results are compared with a large number of solubility determinations in solutions of widely varying salt content. Examples demonstrating the use of these formulas are given.

49. Madgin, W. M. and Swales, D. A.: "Solubilities in the System $\text{CaSO}_4 - \text{NaCl} - \text{H}_2\text{O}$ at 25° and 35°", J. Appl. Chem. (Nov., 1956) pp. 482-487.

Abstract

Solubilities of both gypsum and anhydrite in solution with sodium chloride, varied in concentration up to saturation, have been determined at 25° and for gypsum only at 35°. Sodium chloride lowers the temperature (42°) at which both forms of calcium sulphate have the same solubility and the salt concentration to cause this at 25° has been determined. The influence of small amounts of sodium sulphate, in addition to sodium chloride, has also been investigated.

It has been found that calcium sulphate, never present as much as 1% by weight, has very little if any influence on the solubility of sodium chloride.

50. Blount, C. W., and Dickson, F. W.,: "Gypsum - Anhydrite Equilibria in Systems $\text{CaSO}_4 - \text{H}_2\text{O}$ and $\text{CaCO}_3 - \text{NaCl} - \text{H}_2\text{O}$ " Am. Mineralogist, vol. 58 (1973) pp. 323-331.

Abstract

The equilibria of gypsum and anhydrite with solution and vapor were studied by the use of solubilities, which were in part gained from downward extrapolation of solubilities measured at high temperatures to avoid kinetic difficulties encountered below 70°C. The 4-phase invariant equilibrium of gypsum, anhydrite, simple H_2O solution, and vapor is set at $56^\circ\text{C} \pm 3^\circ\text{C}$ and 124 ± 9 torr. The pressure change required to increase the univariant equilibrium temperature of gypsum, anhydrite and H_2O solution 1°C is about 78 bars, which agrees well with values calculated from thermochemistry. The 3-phase univariant equilibrium of gypsum, anhydrite, and vapor ranges from 124 torr at 56°C to 13.6 torr at 20°C . The effect of NaCl concentration on the 4-phase univariant equilibrium of gypsum, anhydrite, NaCl- H_2O solution, and vapor, is to lower the equilibrium temperature from that of the invariant point, 56°C for zero NaCl concentration, to: 48°C , 2 molal NaCl; 36°C , 4 molal NaCl; and 20°C , molal NaCl. The uncertainty in the temperatures in NaCl solutions is $\pm 4^\circ\text{C}$.

51. Hawley, J. and Pytkowicz, Z. M.: "Solubility of Calcium Carbonate in Seawater at High Pressures", Geo. Cos. ACTA, Vol 33 (1969) pp. 1557-1561.

Abstract

The solubility product of calcium carbonate in seawater at high pressure was determined at 2°C. Results were used to study the degree of calcium carbonate saturation in the Pacific Ocean, and to determine the change in molal volume upon solution of calcium carbonate.

52. Nancollas, G. H., Erlap, A. E., and Gill, J. S.: "Calcium Sulfate Scale Formation: A Kinetic Approach", Soc. of Pet. Eng. Jour. (April, 1978) pp. 133-138.

Abstract

The growth and phase transformation of calcium sulfate dihydrate and hemihydrate crystals were studied at temperatures from 70° to 130°C. At 70°C the second-order rate constant for dihydrate crystal growth did not change by more than 20 percent over a pH range of 3.2 to 9.2. It was also independent of ionic strength up to 2.0 M. Growth in stable supersaturated calcium sulfate solution was completely inhibited by $7. \times 10^{-7}$ M phytic acid for about 24 hours at 70°C. The seeded crystallization of calcium sulfate hemihydrate at temperatures from 90 to 140°C and the phase changes from alpha to beta hemihydrate were investigated by X-ray diffraction, specific surface area analysis, and scanning electron microscopy. Organic phosphonates were found to be effective inhibitors of crystal growth of all the phases at high temperatures.

53. Fulford, R. S.,: "Effects of Brine Concentration and Pressure Drop on Gypsum Scaling in Oil Wells", J. of Pet. Tech., vol. 20 (June, 1968) pp. 559-564.

Abstract

This article studies the effects of brine concentration and pressure drop on gypsum scaling in oil wells. The study reveals that the amounts of scale formed at a given pressure drop and temperature depend on the amount of sodium chloride and other salts dissolved in the brine. The quantity of gypsum deposited increases with salt concentration to a maximum, then decreases until, with strong brines, no scale is formed.

54. Bezemer, C. and Bauer, K. A.,: "Prevention of Carbonate Scale Deposition: A Well-Packing Technique With Controlled Solubility Phosphates", J. of Pet. Tech. (April, 1969) pp. 505-514.

Abstract

This article looks at the prevention of carbonate scale deposition using polyphosphate well packs. Equations and graphs are presented for selecting the kind and amount of polyphosphate to be used for scale prevention. Results of field tests conducted on wells in the south Sumatran fields (Indonesia) are presented. Results show that the method has been successful in preventing scale in these wells.

55. Bsharah, L.,: "Test Unit Evaluates Scale Inhibitors", The Oil and Gas Journ. (April 7, 1969) pp. 166-170.

Abstract

This article presents a method for testing the effectiveness of scale inhibitors. A diagram of the testing apparatus is shown and procedures for its use are presented. Results of tests conducted to evaluate the effectiveness of numerous scale inhibitors are shown.

56. Lasater, R. M., Gardner, T. R., and Glasscock, F.M., : "Scale Deposits are Controlled", The Oil and Gas Journ. (Jan. 15, 1968) pp. 88-93.

Abstract

The usual techniques for applying scale inhibitors to wells usually uses the scale inhibitor in its solid form. There are instances however, where the scale inhibitor could be more effectively applied as a liquid.

This article looks at the effectiveness of liquid scale inhibitors in preventing scale deposits in wells. Results of laboratory tests using several liquid scale inhibitors with CaSO_4 and CaCO_3 are shown. The results of field tests conducted on several producing wells are reported.

57. Miles, L.: "New Well Treatment Inhibits Scale", The Oil and Gas Journ. (June 8, 1970) pp. 96-99.

Abstract

Scale formation in producing and injection wells is a problem frequently encountered in the petroleum industry. This article discusses the effectiveness of one scale inhibitor, ArcoHib S-232, at combatting this problem. Results of laboratory and field tests are presented.

58. Spriggs, D. M. and Hover, G. W.: "Field Performance of a Liquid Scale Inhibitor Squeeze Program", J. of Pet. Tech. (July, 1972) pp. 812-816.

Abstract

This article presents the field test results of a liquid scale-inhibitor squeeze program. The results were collected from 100 liquid squeezes performed in 60 wells. The production performance of these wells indicates that the inhibitor squeeze program has been effective in preventing scale buildup.

59. Ralston, P.H.: "Scale Control with Aminomethylenephosphonates", J. of Pet. Tech. (Aug., 1969) pp. 1029-1036.

Abstract

This article discusses the use of aminomethylenephosphonates (AMP) in controlling scale in producing wells. Topics include information on the properties of AMP, the mode of action of AMP as a scale inhibitor, and laboratory and field test results.

Laboratory results show the effectiveness of AMP in controlling water-formed deposits. Calcium sulfate, barium sulfate, and calcium carbonate can be controlled with .2 to 20 mg/l of AMP based products.

Field results confirm that AMP -type compositions (1) inhibit scale from produced, injection, and heater-treater waters, (2) possess desirable solution stability for surface and down-hole applications and (3) improve profitability in oil recovery by reducing maintenance and work over costs.

60. Poetker, R. H. and Stone, J. D.: "Squeezing Inhibitor into Formation", The Pet. Eng. (May, 1956) pp. B29-B34.

Abstract

This article presents a method for inhibiting corrosion in gas-lift wells by squeezing inhibitors back into the formation. This method has been used to treat corrosion problems in eleven wells. The case histories of several of these wells are presented.

61. Kerver, J.K., and Hanson, H.R.: "Corrosion Inhibitor Squeeze Technique - Field Evaluation of Engineered Squeezes", Journal of Pet. Tech. (January, 1965) pp. 50-58.

Abstract

Successful corrosion control in well tubing by the inhibitor squeeze technique depends on the adsorption of inhibitor on reservoir rock and then slow desorption into the produced fluids. Lack of fundamental data has, heretofore, handicapped the treating procedures. Methods are presented for the laboratory measurement of adsorption and desorption characteristics of reservoir core samples. The amount of corrosion inhibitor adsorbed by formation cores and the amount reversibly desorbed varied widely. Laboratory-determined adsorption and desorption characteristics of reservoir cores samples were used in the design of field squeeze treatments. Important variables determined were the required quantity of inhibitor, concentration in the carrier fluid, volume of formation to contact, amount of overflush needed, and necessary shut-in time. Engineered field tests are compared and correlated to laboratory core data. Results of repeated squeezes on the same well illustrate the reversible physical adsorption and irreversible chemisorption of sand and clay.

62. Vetter, O. J. and Phillips, R. C.: "Prediction of Deposition of Calcium Sulfate Scale Under Downhole Conditions", Soc. of Pet. Eng., SPE 2620, 44th Annual Fall Meeting, Denver, Colo. (Sept. 28 - Oct. 1, 1969) 15 p.

Abstract

The purpose of this paper is to describe the use of fundamental thermodynamic relations to determine where and how much CaSO_4 scale is deposited under bottomhole conditions. The simplifications used in our calculations are explained and a method for proving the validity of published solubility data is submitted. Experimental solubility data, published by different authors, are used for the presented calculations. Some fundamental relationships concerning the behavior of CaSO_4 under downhole conditions are given. These relationships have proved to be valuable in fighting scale.

63. Sloat, B., "Controlled Solubility Phosphates - A Versatile Solution to Oilfield Scale Problems", Journal of Pet. Tech., (November, 1960) pp. 30-36.

Abstract

Water flooding has focused attention on the problem of scale in producing wells. Four reasons why scale forms are discussed. A new theory which will help explain the severe scale build-up that occurs in any producing wells at the time of water breakthrough is presented.

A recently developed family of scale preventives - the controlled solubility phosphates - are described chemically and physically. Factors which influence the performance of these unique phosphates in oilfield brines are evaluated in terms of laboratory test data. Case histories of producing wells treated with controlled solubility phosphates are summarized. The importance of bottom-hole temperature, the role of produced-fluid mineral characteristics and the value of knowing down-hole flow conditions are pointed out. Economic considerations well known to engineers and production men are used to compare the cost of conventional treatment and the cost of the new controlled solubility phosphate scale-prevention approach.

64. Featherston, A. B., Mihram, R. G., Waters, A. B.: "Minimization of Scale Deposits in Oil Wells by Placement of Phosphates in Producing Zones", Journal of Pet Tech., (March, 1959) pp. 29-32.

Abstract

Deposition of compounds such as calcium carbonate, calcium sulfate and barium sulfate in formation flow channels, on tubing, casing and producing equipment has continuously plagued the oil industry. Although polyphosphates have a long history in scale inhibition, only relatively recently have the extremely slow solubility di-metallic polyphosphates been injected into producing zones in conjunction with fracturing.

As a result of such treatments, scale deposition in the formation in addition to the wellbore and producing equipment has been checked in some cases for over a year. Characteristics to be considered when selecting a phosphate for this type treatment have been outlined with the effect each has on scale prevention and on length of time they will be effective.

65. Earlougher, R. C. and Love, W. W.: "Sequestering Agents for Prevention of Scale Deposition in Oil Wells", J. of Pet. Tech., (April, 1957) pp. 17-20.

Astract

This article discusses the field performance of phosphate sequestering agents in the prevention of scale deposition in oil wells. Soluble phosphates are mixed with the sand injected into the producing formation during fracturing treatments. More than 30 wells have been treated by this special phosphate fracturing method, and production data indicate that the problem of formation plugging by mineral deposition is being effectively overcome.

66. Vetter, O. J.: "The Chemical Squeeze Process - Some New Information on Some Old Misconceptions", J. of Pet. Tech. (March, 1973) pp. 339-552.

Abstract

This article discusses new information learned about the chemical squeeze process. Among the things learned through a series of tests was that adsorption isotherms, contrary to common theory, are not very important to the process. And some factors that have been largely ignored - flow velocity, for example - are very important.

67. Bernard, G. C.: "Effects of Clays, Limestone, and Gypsum on Soluble Oil Flooding", J. of Pet. Tech. (Feb., 1975) pp. 179-180.

Abstract

This study is concerned with the effect of rock minerals (clays, limestone, and gypsum) on soluble oil flooding. Flooding experiments were conducted in sandpicks containing from 0 to 2 percent of either gypsum, montmorillonite clay, or calcium carbonate. The oil recovery efficiency is calculated at various bed compositions and the results compared graphically.

68. Canapary, R. C.: "How to Control Refinery Fouling", The Oil and Gas Journ. (Oct. 9, 1961) pp. 114-118.

Abstract

This article discusses the techniques used to control fouling of refinery equipment. Topics presented include a review of the causes of fouling and a discussion of the chemicals that can be used and the operational changes that can be made to help solve the problem.

69. Frazier, A. W., Huddle, J. G. and Power, W. R.: "New, Fast Approach To Reduced Preheat-Exchanger Fouling", The Oil and Gas Journ. (May 3, 1965) pp. 117-122.

Abstract

This paper presents a laboratory test procedure for determining the fouling tendency of refinery process streams. The information obtained from the laboratory test can be used to predict where fouling problems will occur in plant equipment and to predict the effectiveness of anti-fouling chemicals. Results of the laboratory test compare favorably with plant operating data.

70. Shelton, J. L. and Schneider, F. N.: "The Effects of Water Injection on Miscible Flooding Methods Using Hydro Carbons and Carbon Dioxide", Am. Inst. of Min., Met., and Pet. Eng. Inc., (June, 1975) pp. 217-226.

Abstract

The effects of mobile water saturations on oil recovery and solvent requirements were studied in miscible displacement tests on sandstone cores. It was found that (1) oil, if trapped by mobile water, cannot be easily contacted by solvent, and the amount of oil is directly related to measureable relative-permeability characteristics; (2) miscible displacement performances for secondary and tertiary conditions are equivalent; (3) long-core tests describe the movement of fluid banks that would occur in field floods; and (4) flooding response for solvent developed from multiple contact of crude oil with carbon dioxide or rich gas in long cores is the same as that for liquid solvents with first-contact miscibility.

71. Schneider, F. N.: "Relative Permeability Studies of Gas-Water Flow Following Solvent Injection in Carbonate Rocks", Soc. of Pet. Eng. Journ (Feb., 1976) pp. 23-30.

Abstract

Flow studies were conducted of 19 preserved cores from four oil-wet carbonate reservoirs to provide data for evaluating the water-rich, gas-injection improved recovery process. Results indicate that these cores were water repellent following displacement of oil by a solvent similar to the reservoir solvent. Tests of some of the same cores following cleaning by a polar solvent yielded water-wet flow behavior. These results indicate that tests of preserved (water repellent) cores are required if water-gas flow data applicable to oil-wet reservoirs are to be obtained.

Water-gas relative permeability data also were obtained from preserved cores following both complete and incomplete displacement of oil by solvent. The presence of a small "bypassed" oil saturation significantly increased the trapped gas saturation and reduced water permeability. Use of these data in a mathematical model of the reservoir process gave water injectivities similar to those experienced in the field.

72. Ostroff, A. G. and Metler, A. V.: "Apparatus for Testing Scale and Corrosion Inhibitors", Producers Monthly (May, 1965) pp. 8-12.

Abstract

An apparatus is described for the simultaneous testing of scale and corrosion inhibitors. The apparatus assembly provides for evaluation of inhibitory efficiency under flowing conditions over a range comparable to actual oil field conditions of temperature, pressure, pH, flow rate, and composition of corrodant. Any type of steel or other alloy can be tested. Results of tests with several specific chemicals and with several proprietary materials are presented.

73. Orstroff, A. G.: "Compatibility of Waters for Secondary Recovery", The Producers Monthly (March, 1963) pp. 2-9.

Abstract

The water used for water floods in oil recovery projects may come from many different sources. It is important that mixed waters be chemically compatible or else problems will be encountered with deposits precipitated from incompatible waters. This article contains information on the calcium carbonate and iron scale problems. Procedures for testing for incompatibility are reviewed and methods for predicting incompatibility are discussed.

74. Slaton, L., Lasater, R. and Knox, J.: "Scale Deposition and Removal" Producers Monthly, (Sept., 1965) pp. 8-10

Abstract

Scale deposition in injection wells and producing wells presents itself primarily as a result of: pressure drop, temperature changes, incompatible waters, microbial reactions, improper well treatments. Scale removal becomes a consideration of type of scale, connate waters, and previous treatment.

Several examples of scale problems encountered in industry and their solutions are discussed.

75. Cowan, J. C. and Weintritt, D. J.: "Water-Formed Scale Deposits", Gulf Pub. Co., Houston, TX. (1976) pp. 343-376.

Abstract

The scale problem in the petrochemical industry is discussed on pages 343-376 of this book. Topics include a discussion of the various types of scale encountered in the petrochemical industry and the use of scale inhibitors to combat the problem.

76. Edmond, J. M. and Gieskes, J. M. T. M.: "On the Calculation of the Degree of Saturation of Sea Water with Respect To Calcium Carbonate Under In Situ Conditions", Geo. Cos. ACTA, vol. 34 (1970) pp. 1261-1291.

Abstract

A discussion is presented of the computation of the in situ degree of saturation of sea water with respect to calcite or aragonite, Ω , using apparent thermodynamic constants. It is found that when the various reported values of the constants are recomputed so as to be strictly comparable the resulting concordance is generally good. A systematic error in Ω of not more than 10 per cent is estimated to result from the uncertainties in the constants. This is equivalent to an error of 1 per cent in the measured values of A_t or ΣCO_2 . A profile of A_t and ΣCO_2 from the Brazil Basin in the equatorial South Atlantic is used as an example of the computation procedure.

77. Marshall, W. L., Slusher, R., and Jones, E. V.: "Solubility and Thermodynamic Relationships for CaSO_4 in $\text{NaCl-H}_2\text{O}$ Solutions from 40° to 200° C., 0 to 4 Molal NaCl ", J. of Chem. and Eng. Data (1964) vol. 9, pp. 187-191.

Abstract

The solubility of metastable $\text{CaSO}_4 \cdot 2\text{H}_2\text{O}$ has been determined at 40° and 60°C., of metastable $\text{CaSO}_4 \cdot \frac{1}{2}\text{H}_2\text{O}$ at 125 °C, and CaSO_4 (anhydrite) at 125°, 150°, 175°, and 200°C in $\text{NaCl-H}_2\text{O}$ solutions varying from 0 to 4 molal NaCl . These data, combined with additional literature values, agreed with Debye-Huckel theory at all temperatures and over the range of concentration (except at the highest concentrations at temperatures below 100°C.) when a function of the ionic strength, I , is $I^{1/2}/(1 + AI^{1/2})$, where $A = 1.5$, was used. This agreement lends confidence to the application of Debye-Huckel theory to this system at varying temperatures using a constant value for A . The solubility product, K° , for the reaction, $\text{CaSO}_4(\text{solid}) \rightleftharpoons \text{Ca}^{+2} + \text{SO}_4^{-2}$, decreased from 63.0×10^{-6} at 25° C. to 0.114×10^{-6} at 200°C., giving values of ΔF° varying from +5.75 to +15.0 kcal./mole, respectively. Values of ΔH° and ΔS° changed from -1.9 to -18 kcal./mole and from -26 to -70 cal. mole⁻¹ deg.⁻¹, respectively, over the same range of temperature. For $\text{CaSO}_4 \cdot 2\text{H}_2\text{O}$ at 60° C., $K^\circ = 35.7 \times 10^{-6}$ was obtained and for $\text{CaSO}_4 \cdot \frac{1}{2}\text{H}_2\text{O}$ at 125° C., $K^\circ = 9.49 \times 10^{-6}$.

78. Ellis, A. J.: "The Solubility of Calcite in Carbon Dioxide Solutions", Amer. J. Sci., vol. 257 (May, 1959) pp. 354-365.

Abstract

The solubility of calcite in water is reported for temperatures between 100 and 300°, at partial pressures of carbon dioxide ranging from 1-40 atmospheres. Values for the solubility product and the free energy of solution of calcite are derived.

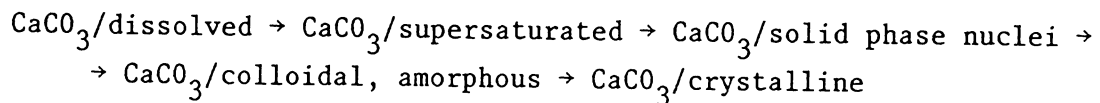
From a study of the kinetics of solution of a single calcite crystal at these temperatures the Arrhenius energy of activation was found to be very low. The rate determining step is suggested to be a diffusion or desorption process.

79. Stumper, R.: "Physicochemical Investigations of the Precipitation of Calcium Carbonate From Water", Angew. Chem., 48, No. 7 (1935) pp. 117-124.

Abstract

In order for CaCO_3 to precipitate the following conditions must be met. 1) The free CO_2 content must fall below the equilibrium value for "pertinent carbonic acid" or the partial pressure of CO_2 in the gas phase must fall below the CO_2 partial pressure corresponding to this value. 2) The ion product, $[\text{Ca}^{++}] \cdot [\text{CO}_3^{--}]$ must exceed the solubility product, $[\text{Ca}^{++}] \cdot [\text{CO}_3^{--}] = k$. 3). The supersaturation of the solution in CaCO_3 must be eliminated.

The chief factors regulating the precipitation of CaCO_3 from pure $\text{Ca}(\text{HCO}_3)_2$ solutions are, in general, the partial pressure of CO_2 and the rate of formation of the solid phase:



The precipitation of CaCO_3 from supersaturated solutions begins only after an induction period has passed. Between this period (I) and the initial concentration (C) there is a simple relationship: $C \cdot I = \text{const.}$ The induction period is very sensitive to the presence of foreign substances.

80. Holm, L. W.: "Oil Recovery Process", U. S. Patent 3,065,790 (Nov. 27, 1962).

Abstract

This patent describes a process for producing a petroleum oil from an oil-bearing, limestone rock reservoir, by injecting carbon dioxide into the well. The process involves injecting 500 to 3500 s.c.f. of carbon dioxide per barrel of oil in place, to provide an elevated pressure of not less than 700 p.s.i. in the reservoir. An aqueous drive fluid is then injected into the reservoir until breakthrough of the fluid occurs at the producing well. Oil can then be produced from the reservoir until the pressure is depleted.

81. Lagache, M.: "New Data on the Kinetics of the Dissolution of Alkali Feldspars at 200°C. in CO₂ Charged Water", Geochim. Cosmochim. Acta., vol. 40, no. 2 (1976) pp. 157-161.

Abstract

The kinetics of the dissolution of several feldspars were studied experimentally at 200°C as a function of the surface area and time. The molalities of Na⁺ and K⁺ have been plotted against the product of the surface area and time. For two feldspars (albite and adularia) the rates of dissolution of Na⁺ and K⁺ are smooth, continuous functions of surface area-time, which implies that they are controlled by the composition of the fluid.

The comparison between the dissolution of pure sodium or potassium feldspars and that of an intermediate feldspar (sanidine) shows that the intermediate feldspar dissolves as if it were composed of sodium and potassium feldspar grains in the proportions corresponding to its composition.

A mechanism proposed by others to describe the method of dissolution is reviewed. This mechanism proposes that the dissolution could be described by a process of diffusional mass transfer through a surface layer of reaction products.

The present experiments do not agree with such an interpretation of the mechanism of dissolution.

82. Nancollas, G. H., and Liu, S. T.: "Crystal Growth and Dissolution of Barium Sulfate", Soc. of Pet. Eng. of AIME (1975) pp. 69-79.

Abstract

The kinetics of crystallization and dissolution of barium sulfate seed crystals have been investigated conductimetrically. Growth is characterized by an initial surge, due to secondary nucleation, followed by a rate which is proportional to the square of the supersaturation. Studies have been made using seed material of differing morphology and in all cases the crystallization is surface controlled. A surface reaction also appears to be rate determining for the corresponding dissolution process but the overall rate constant is considerably greater than that for growth. Crystallization and dissolution have been studied in the presence of potential phosphonate and polyphosphate scaling inhibitors and in some cases, both processes are markedly inhibited. The incorporation of the anti-scalant into the developing crystals may pose problems in their down-hole application.

83. Uchameyshvili, N. Y., Malinin, S. D., and Khitarov, N. I.: "Solubility of Barite in Concentrated Chloride Solutions of Some Metals at Elevated Temperatures in Relation to Problems of the Genesis of Barite Deposits", Geokhimiya (1966) Vol. 3, pp. 951-961.

Abstract

The solubility of barite in chloride solutions depends both on the concentration and on the type of chloride. For pure water and 0.25 N solutions of KCl and NaCl, the solubility of barite passes a maximum in the temperature interval 100-300° C. However, in solutions of CaCl₂, MgCl₂ and 2 N NaCl, barite solubility increases continuously with temperature, and in a 1 N NaCl solution the solubility curve has an inflection. The authors propose that the dissolution of barite in CaCl₂, MgCl₂ (>1N) may be accompanied by the formation of new phases (CaSO₄, MgSO₄, and Na₂SO₄); only CaSO₄ was observed directly. On the basis of experimental solubility data and data from fluid inclusion study, it is suggested that anhydrite paragenetically preceded barite, in a barite deposit in the Caucasus.

84. Weyl, P. K., "The Solution Kinetics of Calcite", J. of Geology (1958) Vol. 66, pp. 163-175.

Abstract

The solution alteration of a limestone depends on the rate at which water entering the rock becomes saturated. This rate is governed by the rate of transport of solute away from the solid-liquid interface, where the solution is always saturated. For laminar flow in a straight circular capillary of radius a , the solution will be 90 per cent saturated after penetrating a distance $0.572\gamma a^2/D$, where γ is the average flow velocity of the fluid and D is the diffusion constant of the solute in the solution. Under normal conditions below the water table, γ and a are sufficiently small that the water in a limestone is always saturated with respect to calcium carbonate. Solution alteration can therefore take place only where the water first enters the rock or where the solubility changes.

85. Garrels, R. M., Thompson, M. E., and Siever, R.: "Control of Carbonate Solubility by Carbonate Complexes", Am. J. of. Science (1961) Vol. 259, pp. 24-25.

Abstract

Activity coefficients of HCO_3^- and CO_3^{--} were determined in aqueous solutions of NaCl, MgCl_2 , and of NaCl- MgCl_2 mixture of approximately the same mol ratio as sea water. The values obtained in "synthetic sea water" correspond to those observed in actual sea water.

The data for CO_3^{--} are interpreted in terms of two complexes:

Calculations show that of the total CO_3^{--} in sea water, as determined by titration and not including HCO_3^- , about 75 percent is MgCO_3^0 , 15 percent NaCO_3^- , and 10 percent free CO_3^{--} .

The data for HCO_3^- also indicate the presence of complexes of Na^+ and Mg^{++} , but these are less strongly associated, and are not fully characterized.

It is shown that the concentration of Ca^{++} , in equilibrium with calcite, is greater in "synthetic sea water" than in Mg-free NaCl solutions. The observed apparent supersaturation of sea water in calcite is not fully explained here. Although the total concentration of CO_3^{--} in sea water can be predicted from these data, that of Ca^{++} cannot.

86. Garrels, R. M. and Thompson, M. E.: "A Chemical Model for Sea Water at 25°C and One Atmosphere Total Pressure", Am. J. of Science (1962) Vol. 260, pp. 57-66.

Abstract

Dissociation constants involving Ca^{++} , Mg^{++} , Na^+ , K^+ , SO_4 , HCO_3^- and CO_3^{--} ions, and individual ion activity coefficients have been used to calculate the distribution of dissolved species in sea water at 25° C and one atmosphere total pressure. The distribution obtained for sea water of chlorinity 19% and pH 8.1 are:

Ion	Molality (Total)	% Free Ion	% Me- SO_4 pair	% Me- HCO_3 pair	% Me- CO_3 pair
Ca^{++}	0.0104	91	8	1	0.2
Mg^{++}	0.0540	87	11	1	0.3
Na^+	0.4752	99	1.2	0.01	-
K^+	0.0100	99	1	-	-

Ion	Molality (total)	% Free Ion	% Ca-anion pair	% Mg-anion pair	% Na-anion pair	% K-anion pair
SO_4^{--}	0.0284	54	3	21.5	21	0.5
HCO_3^-	0.00238	69	4	19	8	-
CO_3^{--}	0.000269	9	7	67	17	-

The activities calculated for free ions are $a_{\text{Ca}^{++}} = 0.00264$, $a_{\text{Mg}^{++}} = 0.0169$, $a_{\text{Na}^+} = 0.356$, $a_{\text{K}^+} = 0.0063$, $a_{\text{CO}_3^{--}} = 4.7(10^{-6})$, $a_{\text{HCO}_3^-} = 9.75(10^{-4})$, $a_{\text{SO}_4} = 1.79(10^{-3})$.

87. Dickson, F. W., Blount, C. W., and Tunell, G.: "Use of Hydrothermal Solution Equipment to Determine the Solubility of Anhydrite in Water from 100°C to 275°C and from 1 Bar to 1000 Bars Pressure", Am. J. of Science (1963). Vol. 261, pp. 61-78.

Abstract

Specially designed "hydrothermal solution" equipment was used to determine the solubility of anhydrite in H₂O from 100°C to 275°C and from 1 bar to 1000 bars. The solubility of anhydrite decreases with increasing temperature and increases with increasing pressure.

The hydrothermal solution equipment consists of a deformable teflon sample cell held in a stainless steel pressure vessel and sealed in such a way as to prevent interchange of material between the sample cell and the steel bomb. Separate pressure lines leading to the sample cell and to the steel bomb allow liquid to be pumped into or taken out of each container independently. Liquid and solid phases may be allowed to come to equilibrium in the teflon cell at constant temperature and pressure. The experimental mixtures are stirred by means of a teflon-coated bar magnet turned by an externally applied pulsating magnetic field. An internally filtered liquid sample can be withdrawn without significant disturbance of the equilibrium temperature and pressure, by pumping liquid into the steel vessel at the same rate that saturated solution is removed from the teflon cell.

From the solubility data obtained the following geologic conclusions can be drawn. Initially saturated solutions of anhydrite in water, migrating toward the Earth's surface, would become undersaturated. The increase in solubility caused by decreased temperature more than compensates for the decrease in solubility caused by decreased pressure. Anhydrite would precipitate from saturated solutions in sediments as burial takes place and the temperature rises, or from ground waters moving downward to regions of higher temperature. Anhydrite would precipitate from saturated solutions moving from a region of high pressure to a region of low pressure, as would be the case in rocks near openings toward which a fluid pressure gradient exists.

88. Nakayama, F. S.: "Calcium Activity, Complex and Ion-Pair in Saturated CaCO_3 Solutions", Soil Science (1968) Vol. 106, pp. 429-434.

Abstract

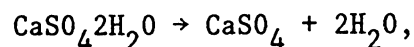
The chemical behavior of all soil-related Ca compounds is of vital interest to soil scientists. This is evidenced in part by the work on determining and explaining the differences in solubility of calcite and aragonite CaCO_3 (1, 14) and on ascertaining the presence and values of stability constants of soil organic Ca complexes (13, 17). Clark (2), in studying the pH of calcareous soils, noted Ca complexes besides those of sulfate were present, but did not specify their actual forms. In order to describe the correct Ca equilibrium relation of the soil-gypsum and soil-phosphate systems, investigators have used the dissociation constant together with the solubility product constant of CaSO_4 (3,15,20). This procedure is necessary because all of the Ca in solution is not in the ionic form. Workers thus far have not taken into account the possibilities of Ca ion-pairs and Ca complexes in the soil- CaCO_3 system, probably because of the unavailability of appropriate dissociation constants for the different Ca forms in solution. Furthermore, controversy still exists regarding the presence or absence of Ca complex in bicarbonate-carbonate solutions (6,7).

This paper reports on the different forms of Ca that may be present in equilibrium with CaCO_3 together with their appropriate dissociation or association constants. A theory is formulated for determining the various Ca species when the necessary H- and Ca-ion activity measurements are available.

89. Bock, E.: "On the Solubility of Anhydrous Calcium Sulphate and of Gypsum in Concentrated Solutions of Sodium Chloride at 25°C, 30°C, 40°C, and 50°C", Can. J. Chem. (1961) Vol. 39, pp. 1746-1751.

Abstract

The solubilities of anhydrous CaSO_4 and $\text{CaSO}_4 \cdot 2\text{H}_2\text{O}$ in concentrated aqueous solutions of NaCl at a series of temperatures (25°C, 30°C, 40°C, and 50°C) have been determined. It was found that the transition temperature for the reaction



which in pure water has a value of 42°C, is shifted progressively to lower temperatures with increasing NaCl concentration. It was also found that the variation of the transition temperature with NaCl concentration could be adequately represented by the equation

$$\Delta G = \Delta H - T\Delta S + 2RT \ln P/P_0,$$

where ΔG , ΔH , and ΔS are the Gibbs free energy, enthalpy, and entropy of the reaction and P_0 and P are the vapor pressures of pure water and the solution respectively at the absolute temperature T .

90. Rutherford, W. M.: "Miscibility Relationships in the Displacement of Oil by Light Hydrocarbons", Soc. of Pet. Eng. Journ., vol. 2 (Dec., 1962) pp. 340-346.

Abstract

A knowledge of the limits of miscibility between reservoir oil and possible injection fluids is required for selection of the optimum miscible-injection fluid. Limits of miscibility can be estimated from the results of equilibrium phase-behavior experiments. They can also be determined by means of displacement experiments conducted in a high pressure sandpack. This paper describes the equipment and procedure which have been developed for determining miscibility conditions by stable displacement.

A systematic series of displacements of a West Texas reservoir oil was carried out. The results indicate that, at constant pressure, miscibility is a function only of the pseudocritical temperature of the injection gas. This fact, together with improved experimental methods, makes the displacement technique a rapid, reliable means for determining miscibility conditions. In conjunction with the displacement experiments, phase diagrams were constructed for the oil with dry gas and propane and with dry gas and ethane. Phase behavior of the methane-ethane-propane system was determined at 110°F.

The experimental work demonstrates the feasibility of using ethane-rich gases to reduce cost and pressure requirements for miscible displacement.

91. Orr, F. M., Jr., Yu, A. D. and Lien, C. L.: "Phase Behavior of CO₂ and Crude Oil in Low Temperature Reservoirs", Soc. of Pet. Eng., Symp. on Enhanced Oil Recovery (April 20-23, 1980) pp. 17-32.

Abstract

Phase behavior of carbon dioxide-crude oil mixtures which exhibit liquid-liquid and liquid-liquid-vapor equilibria is examined. Results of single contact phase behavior experiments for CO₂ separator oil mixtures are reported. Experimental results are interpreted using pseudo-ternary phase diagrams based on a review of phase behavior data for binary and ternary mixtures of CO₂ with alkanes. Implications for the displacement process of liquid-liquid-vapor phase behavior are examined using a one-dimensional finite difference simulator. Results of the analysis suggest that liquid-liquid and liquid-liquid-vapor equilibria will occur for CO₂-crude oil mixtures at temperatures below about 50°C (122°F), and that development of miscibility occurs by extraction of hydrocarbons from the oil into a CO₂ rich liquid phase in such systems.

92. Stalkup, F. L.: "Carbon Dioxide Miscible Flooding: Past, Present, and Outlook for the Future", Soc. of Pet. Eng. of A.I.M.E., Symp. on Improved Methods of Oil Recovery (April 16-19, 1978)

Abstract

This paper gives an overview of the carbon dioxide miscible-flooding process. It contains a review of current technology, a discussion of past and current field testing, and an assessment of the state-of-the-art. The discussion in one section identifies and evaluates carbon dioxide sources. This is followed by projections of potential oil recovery and producing rate along with an opinion of the near-future outlook. Several areas are identified where improvements in technology and additional laboratory research and field testing are needed.

93. Pilat, S. and Godlewicz, M.: "Method of Treating Mineral Oils", U.S. Patent 2,315,131 (Jan. 30, 1934).

Abstract

This patent describes a method for separating mineral oils into fractions of different physical and chemical properties, and is particularly concerned with the treatment of relatively viscous mineral oils, petroleum residues, and other hydrocarbon mixtures, using gases under pressure. Auxiliary solvents and deasphaltizing agents may be used.

Briefly, the invention consists of introducing into a mineral oil a gas under pressure until a concentration is reached at which the oil separates into two phases. Relative quantities and compositions of the oil portions in the phases are regulated by maintaining suitable temperatures and pressures, as well as by selection of the gaseous treating agent. The gaseous treating agent may be methane, ethane, carbon dioxide, hydrogen or any other substance or mixture of substances, which is gaseous at the temperature and pressure employed and which is capable, on being introduced in the gaseous state under pressure, of making the oil separate into phases. The two phases can then be easily separated.

94. Pilat, S. and Godlewicz, M.: "Method of Separating High Molecular Mixtures", U.S. Patent 2,188,013 (April 27, 1936).

Abstract

This patent describes a method for separating mixtures of high molecular weight substances into two or more fractions by injecting carbon dioxide under high pressure into the mixture. This patent is a continuation-in-part of patent no. 2,315,131 (see reference 93).

Briefly, the invention consists of introducing carbon dioxide under pressure (but below its condensation pressure) into a high molecular weight oil until a concentration is reached at which the oil separates into two phases. Relative quantities and compositions of the oil portions in the phases are regulated by maintaining suitable temperatures and pressures, as well as by using appropriate solvents and deasphaltizing agents. A separation of higher molecular weight components from lower molecular weight components can be accomplished by physically separating the different phases.

95. Simon, R., Rasman, A. and Zana, E.: "Phase-Behavior Properties of CO₂ - Reservoir Oil Systems", Soc. of Pet. Eng. J. (Feb., 1978) pp. 20-26.

Abstract

This paper presents experimental phase behavior data on two CO₂ reservoir oil systems at reservoir pressures and temperatures.

The data include (1) pressure-composition diagrams with bubble points, dew points and critical points; (2) vapor-liquid equilibrium compositions and related K values; (3) vapor and liquid densities compared with values calculated by the Redlich-Kwong equation of state; (4) vapor and liquid viscosities compared with predictions by the Lohrenz-Bray-Clark correlation; and (5) interfacial tensions for six vapor-liquid mixtures compared with values calculated by the Weinaug-Katz parachor equation.

These and other published data contribute to development of the generalized correlations needed by reservoir and production engineers for evaluating, designing, and efficiently operating CO₂ -injection projects.

96. Shelton, J. L. and Yarborough, L.: "Multiple Phase Behavior in Porous Media During CO₂ or Rich Gas Flooding", J. of Pet. Tech. (Sept., 1977) pp. 1171-1178.

Abstract

Mixing oil with high-ethane-content hydrocarbon gases or CO₂ can produce multiple liquid phases and an asphaltic precipitate in low-temperature reservoirs. The residual saturation that occurs in a reservoir displacement is not significant from a recovery standpoint, but may produce three phase relative permeability effects that reduce injectivity and, thus, oil recovery rate during alternate gas-water injection.

97. Reed, M.G.: "Formation Permeability Damage by Mica Alteration and Carbonate Dissolution", Journal of Petroleum Technology (Sept, 1977), pp. 1056-1060.

Abstract

This article proposes two mechanisms to account for at least some of the permeability damage observed in some friable micaceous sands. The two mechanisms are supported by present laboratory and field data which are shown in the report.

98. Holm, L. W.: "Carbon Dioxide Solvent Flooding for Increased Oil Recovery", Pet. Trans., vol. 216 (1959) pp. 225-231.

Abstract

Laboratory flooding experiments on linear flow systems indicated that high oil displacement, approaching that obtained from completely miscible solvents, can be attained by injecting a small slug of carbon dioxide into a reservoir and driving it with plain or carbonated water. Data are presented in this paper which show the results of laboratory work designed to evaluate this oil recovery process, particularly at reservoir temperatures above 100°F and in the pressure range of 600 to 2,600 psi.

100. Le Grand, H. E. and Stringfield, V. T.: "Differential Erosion of Carbonate - Rock Terranes", Southeast Geol., (SOG EAY), vol. 13, no. 1 (1971) pp. 1-17.

Abstract

The topography of carbonate-rock terranes takes on many different forms. These forms can be explained in terms of "differential erosion" of the terrane. The factors involved in "differential erosion" include amount of cover over the carbonate-rock formation, purity of the carbonate rock, topographic relief, and precipitation. This article looks at some of the categories of topography found in carbonate-rock terranes and discusses the conditions involved in their formation.

103. Nixon, R. A.: "Differences in Incongruent Weathering of Plagioclase and Microcline-Cation Leaching Versus Precipitates", Geology (1979) Vol. 7, pp. 221-224.

Abstract

Comparisons of plagioclase and microcline taken from different weathering environments show that the mechanisms of feldspar dissolution are independent of the weathering environment. However, microcline and plagioclase do not weather by identical mechanisms. Calcium and sodium can be removed from the plagioclase lattice to depths greater than one or two unit cells, which implies that the "leached layer" may form on weathering plagioclase grains. The larger potassium ions cannot be removed from the microcline lattice deeper than one or two unit cells unless the anionic lattice is distorted or disrupted. Macroscopic solution features on plagioclase parallel the arrangement of calcium and sodium ions within the crystal. Solution features that develop on microcline may begin at dislocations on the crystal surface, or they may be located at inclusions of plagioclase. Scanning electron microscopy of microcline indicates that a precipitate as thick as 1 μm may form at the surface of the mineral. The rate of dissolution of microcline may be related to the cation exchange capacity of this layer and by reactions within the layer.

104. Rodgers, G. P., and Holland, H. D.: "Weathering Products Within Microcracks in Feldspars", Geology (1979) Vol. 7, pp. 278-280.

Abstract

Tonalite cobbles from moraines in the Tobacco Root Mountains, Montana, have weathering rinds in which the feldspars are altered to clays along microcracks. Energy-dispersive X-ray and X-ray diffraction analyses have shown that microcracks in orthoclase contain only kaolinite but that microcracks in oligoclase contain a central zone of kaolinite surrounded by a zone of smectite. These observations are in accord with predictions based on activity diagrams for the appropriate chemical systems. Feldspar dissolution was probably the rate-determining step in the development of the microcracks and their clay fillings.

105. Huang, W. H., and Kiang, W. C.: "Laboratory Dissolution of Plagioclase Feldspars in Water and Organic Acids at Room Temperature", American Mineralogist (1972) Vol. 57, pp. 1849-1859

Abstract

Freshly fractured albite, oligoclase, labradorite, bytownite, anorthite, and a high-K variety of plagioclase in particle sizes between 44 μm and 150 μm were dissolved at room temperature in deionized water, 0.01 M acetic and aspartic acids (weakly complexing), and salicylic and citric acids (strongly complexing). Solutes of centrifuged solution were analyzed for pH, and for Si, Al, Fe, Mg, Ca, Na, and K.

Ca-rich plagioclases dissolved in organic acids more readily than did Na-rich plagioclases, whereas Na-rich plagioclases were the more soluble in deionized water. Al was preferentially dissolved over Si in particular from Ca-rich plagioclase in complexing acids. Ca was relatively more soluble than was Na in both organic acids and water.

The organic solvents, in order of increasing effect of dissolution, were acetic, aspartic, salicylic, and citric acids, which is the order of complexing capacities. Citric acid was more effective than other acids in extracting Al and Ca, particularly from Ca-rich plagioclases, presumably because of the formation of Al- and Ca- complexes.

106. Chafetz, H. S.: "Surface Diagenesis of Limestone", J. of Sed. Pet. (1972) Vol. 42, pp. 325-329.

Abstract

Surface diagenesis of the Morgan Creek Limestone has resulted in dedolomitization, silicification, and aggradational recrystallization. Horizons displaying similar diagenetic properties in subsurface carbonate data are indicative of superjacent unconformities.

107. Nooner, D. W., Oro, J., Gilbert, J. M., Ray, V. L., and Mann, J. E.,: "Ubiquity of Hydrocarbons in Nature: Aliphatic Hydrocarbons in Weathered Limestone", Geochim et Cosmochim ACTA (1972) Vol. 36, pp. 953-959.

Abstract

The aliphatic hydrocarbons in two specimens of limestone (one from Texas and the other from Italy) which were weathered in place as parts of building structures have been investigated using gas chromatography and gas chromatography-mass spectrometry. The hydrocarbons in (i) the limestone from Texas and (ii) algae cultured from this limestone have similar distributions, i.e. the predominating hydrocarbon in both cases is n-C₁₇, thus indicating that most of the aliphatic hydrocarbons in the limestone may be derived from recent algal growth. The hydrocarbons in the limestone from Italy, in which n-C₁₇, is a maximum but which also include relatively large amounts of pristane, phytane and other aliphatic hydrocarbons, appear to be a mixture of in situ biogenically derived hydrocarbons and extraneously fossil hydrocarbons.

108. Perkins, A. T.: "Decomposition of Silicate Minerals by Acid Extractions Chemical Composition and Exchange Capacity", Transactions of the Kans. Academy of Sci. (1964) Vol. 67, pp. 486-495.

Abstract

A 100-day citric-phosphoric extraction of California bentonite (Filtrol) and vermiculite, minerals with high cation exchange capacities, dissolves, respectively, about 37% and 49% of the minerals by weight, removes about 75% of the R₂O₃ group of each mineral and only 10% and 13% of the SiO₂. The loss of exchange capacity parallels the loss of the R₂O₃ group.

A similar extraction of muscovite and kaolinite, minerals with low exchange capacities, dissolves little if any of the minerals and does not change their chemical composition.

109. Petrovic, R., Berner, R. A., and Goldhaber, M. B.: "Rate Control in Dissolution of Alkali Feldspars - I. Study of Residual Feldspar Grains by X-ray Photoelectron Spectroscopy", Geochim Cosmochim ACTA (1976) Vol. 40, pp. 537-548.

Abstract

Sanidine grains (100-600) μm in diameter) were subjected to dissolution at 82°C in aqueous electrolyte solutions of pH ranging from 4 to 8 for 293 or 377 hr. Dissolution equivalent to the removal of silica from the outer 300-900 Å of these grains was accomplished. The shallow subsurfaces of feldspar grains were then analyzed for K, Al, and Si by X-ray photoelectron spectroscopy. The results rule out any continuous precipitate layer; if an alkali-depleted subsurface zone (leached layer) was present in the feldspar, the thickness of such a zone approximated by linear increase of alkali concentration with depth was not more than about 17Å.

It is concluded that in the absence of a compact precipitate layer, dissolution of feldspars in the temperature range corresponding to deep diagenesis is controlled by the processes at the feldspar-solution interface and a leached layer more than one feldspar unit cell thick does not form. Whether the same applies at the temperatures of shallow diagenesis and weathering cannot be judged with certainty, but parallels with leached layers on alkali silicate glasses suggest that it does.

110. Busenburg, E.: "The Products of the Interaction of Feldspars with Aqueous Solutions at 25°C", Geochim. Cosmochim. ACTA (1978) Vol. 42, pp. 1679-1686.

Abstract

Chemical analyses of 300 solutions produced by the artificial weathering of eight different feldspars in fourteen experiments of up to 1200 hr duration were used to study the evolution of water during weathering. The range of pH was between 4 and 5.5. Within 4 hr of dissolution, the activity of Al was controlled by the pH and the solubility of microcrystalline gibbsite. After 100 hr of dissolution, the pH and microcrystalline halloysite controlled the activities of Al and silicic acid in all of the solutions.

Microcrystalline halloysite was the only phase identified in the weathering of plagioclases in distilled water and 1 atm CO₂ partial pressure. Montmorillonites, halloysite and other clay minerals were produced from oligoclase in aqueous solutions containing high initial concentrations of Ca, Mg, K and SiO₂.

The experimentally determined log solubility product of microcrystalline gibbsite was -32.78 ± 0.04 and log K for the hydrolysis of microcrystalline halloysite was 11.58 ± 0.05 . The results suggest that very poorly crystalline metastable phases may control the initial compositions of some waters in contact with rocks containing feldspar minerals.

APPENDIX B.

Computerized Data Bases

Data Bases Searched

The electronic data search system called ORBIT, provided by System Development Corporation, was employed. The six data bases which were searched are described below.

Manual searches were performed using the following indices, 1970-1979, inclusive:

1. Engineering Index
2. Comprehensive Index of American Association of Petroleum Geologists
3. International Petroleum Abstracts, and
4. J. Petroleum Technology annual indices.

Computerized data bases were:

1. CAS77 and CAS7276

Provides worldwide coverage of the chemical sciences literature from over 12,000 journals, patents from 26 countries, new books, conference proceedings, and government research reports. Coverage corresponds to the printed Chemical Abstracts Condensates, including 80 main subject sections such as biochemistry, organic chemistry, macromolecular chemistry, applied chemistry and chemical engineering, and physical and analytical chemistry. Includes special searching features from Chemical Abstracts Subject Index Alert (e.g., registry numbers, molecular formula fragment).

PREPARED BY: Chemical Abstracts Service

FILE SIZE: CAS77: Approximately 390,000 citations/yr since 1976

CAS7276: Approximately 2,500,000 citations

COVERAGE: CAS77: January 1977 to present

CAS7276: January 1972 to December 1976

UPDATING: CAS77: Bi-weekly, approximately 12,000 citations

2. CDI

Comprehensive Dissertation Index, containing all dissertations accepted for academic doctoral degrees granted by U.S. educational institutions and over 122 foreign universities. Contents correspond to two printed products: Dissertation Abstracts International and American Doctoral Dissertations.

Subject coverage is multi-disciplinary, and includes the humanities, social sciences, science, and engineering.

PREPARED BY: University Microfilms International (UMI)

FILE SIZE: Approxiamtely 46,000 citations per year

COVERAGE: 1861 to present

UPDATING: Monthly, approximately 3,000 citations

3. CHEM 7071

Provides the same literature coverage as CAS77 and CAS7276 without the merger of Chemical Abstracts Subject Index Alert.

PREPARED BY: Chemical Abstracts Service

FILE SIZE: Approximately 600,000 citations

COVERAGE: January 1970 to December 1971

4. COMPENDEX

Corresponds to Engineering Index Monthly. Covers civil-environmental-geological engineering; mining-metals-petroleum-fuel engineering; mechanical-automotive-nuclear-aerospace engineering; electrical-electronics-control engineering; chemical-agricultural-food engineering; and industrial engineering, management, mathematics, physics, and instruments, including approximately 1,500 serials and over 900 monographic publications.

PREPARED BY: Engineering Index, Inc.
FILE SIZE: Approximately 84,000 citations per year
COVERAGE: January 1970 to present
UPDATED: Monthly, approximately 6,000 citations

5. GeoRef

Geological Reference file, covering geosciences literature from 3,000 journals, plus conferences and major symposia and monographs, in such areas as geology, economic geology, engineering-environment geology, geochemistry, geochronology, geomorphology, igneous and metamorphic petrology, solid earth geophysics, and stratigraphy; a total of some 29 different geoscience areas. Includes citations from Bibliography and Index of Geology and more.

PREPARED BY: The American Geological Institute
FILE SIZE: Approximately 36,000 citations per year
COVERAGE: January 1967 to present
UPDATING: Monthly, approximately 4,000 citations

6. Tulsa

Covers worldwide literature and patents related to oil and natural gas exploration, development, and production in such areas as petroleum geology, exploration geophysics and geochemistry; well drilling; well logging, well completion and servicing; oil and gas production; reservoir studies and recovery methods; pollution; alternative fuels and storage. Corresponds in coverage to Petroleum Abstracts.

PREPARED BY: University of Tulsa, Information Service Department
FILE SIZE: Approximately 18,000 citations per year
COVERAGE: 1965 to present
UPDATING: Monthly, approximately 1,500 citations

APPENDIX C.

Descriptors for Computerized Literature Search

A. Plugging of Reservoirs

1. OIL AND (ALL RESERVOIR:/IT OR ALL FIELD:/IT OR ALL FORMATION:/IT OR ALL WELL:/IT OR CRUDE)
2. STIMULATION OR INJECTION
3. ALL FLOOD
4. DAMAGE OR PLUGGING OR ATTACK OR ALL SCAL:/IT OR ALL PRECIPITAT:/IT
5. PERMEABILITY AND (LOSS OR DECREASE)
6. INJECTIVITY AND (LOSS OR DECREASE)
7. PRESSURE AND (DROP OR DECREASE)
8. 4 OR 5 OR 6 OR 7
9. 1 AND 8
10. 1 AND (2 OR 3) AND 8
11. (CARBON DIOXIDE) OR CO2 OR (CARBONIC ACID) OR (CARBONATED WATER) OR ORCO
12. 1 AND 8 AND 11
13. TUBING OR PIPES OR LINES
14. 1 AND 8 AND 13

B. Attack by Acids on Rocks

15. FELDSPAR OR DOLOMITE OR LIMESTONE OR SILICATE OR CARBONATE OR SULFATE
16. ATTACK OR ALL DECOMPOS:/IT OR DECAY OR ALL DISSOLV:/IT OR ALL WEATHER:/IT
17. 15 AND 16
18. 11 AND 17

19. 1 AND 11 AND 17

20. 1 AND 17

C. Asphaltene Precipitation

21. ASPHALTENE OR ALL PRECIPITAT:/IT OR ALL SOLID:/IT

22. PRECIPITAT:/IT OR DEPOSITS OR SOLUBILITY OR SCALE

23. 11 AND 21

24. 1 AND 11 AND 21

25. 17 AND 22 AND NOT (CONCRETE OR CORROSION)

APPENDIX D

Persons Attending First Conference on CO₂ Formation Damage
at New Mexico State University

<u>Name</u>	<u>Affiliation</u>	<u>Location</u>
Dave Locke	U.S. Department of Energy	Morgantown, WV
Loyd Jones	Amoco Production Research	Tulsa, OK
Gary Charlson	ARCO Production Research	Plano, TX
Lynn Orr	Petroleum Recovery Research Center	Socorro, NM
John Heller	Petroleum Recovery Reseach Center	Socorro, NM
Stan Walker	Chevron, USA, Inc.	Snyder, TX
Royal Watts	U.S. Department of Energy	Morgantown, WV
Chap Cronquist	Gulf Universities Research Consortium	Houston, TX
Kenneth S. Lee	Shell Development Corp.	Houston, TX
John T. Patton	New Mexico State University	Las Cruces, NM
Patrick Phelan	New Mexico State University	Las Cruces, NM
Stan Holbrook	New Mexico State University	Las Cruces, NM

APPENDIX E

Properties of Crude Oils

Introduction--It has been industry practice to separate crude oils into three broad classifications or bases. The three bases, "paraffin," "intermediate" and "naphthene" are useful as general classifications but lead to ambiguity in many cases. The reason is that a crude may exhibit one set of characteristics for its light materials and another set for the heavy-lube fractions. To avoid this problem, the U.S. Bureau of Mines has developed the following, more useful method of classifying oils.

Two fractions are obtained in the standard Hempel distillation procedure which are called key fractions. Key Fraction 1 is the material which boils between 527 and 572°F at 40 mm absolute pressure. Key Fraction 2 is the remainder. Both fractions are tested for API gravity, and Key Fraction 2 is tested for cloud point. In naming the type of oil, the base of light material, (Key Fraction 1), is named first, and the base of the heavy material, (Key Fraction 2), is named second. If the cloud point of Key Fraction 2 is above 5°F, the term "wax-bearing" is added. If the pour point is below 5°F, it is termed "wax-free."

Thus "paraffin intermediate wax-free" would designate a crude whose gasoline portion is paraffinic and whose lube portion is intermediate yet has very little wax.

Summary of Properties--Table E.1 compares the general characteristics of the crudes used in this study.

Wilmington Crude--This oil is an aromatic-based oil with gravity ranging from 13 to 32° API (5). Below 17° API the crude contains from 1.7 to 2.5 percent sulfur. The sulfur content decreases with an increase in gravity

TABLE E.1
COMPARISON OF CRUDE OILS USED IN THIS STUDY
(Ref: 5-7)

Property	Crude Oil		
	Maljamar	Wilmington	Hilly Upland
Crude Gravity, °API	38.6	22.3	42.0
Salt as NaCl, lb/M Bbl		3.3	
Sulfur Content, wt.%	0.70	1.33	0.06
Nitrogen Content, wt.%		0.61	
Viscosity SUS at 100°F, sec	37	210	39
Carbon Residue of Residuum, wt.%	8.8	6.3	1.4
Heptane Insolubles, wt.%		3.66	
Gasoline & Naptha:			
Percent	37.5	16.7	28.9
°API	57.7	52.5	63.6
Kerosine:			
Percent	4.7	-	16.0
°API	42.8	-	46.7
Gas Oil:			
Percent	19.7	19.4	13.7
°API	35.6	33.0	40.2
Lubricating:			
Percent	17.3	20.7	14.4
°API	30.8-24.2	27.1-17.1	38.0-31.8
Residuum:			
Percent	19.0	42.1	25.9
°API	15.7	8.7	28.2

and ranges from 0.6 to 0.9 percent for oil of 29° API. Gasoline content ranges from 8 percent for the 16° API to 31 percent for 29° API (9).

The Hempel and Batch Distillation and inspection analyses were performed on Universal Oil Products Sample No. 28-513 using the Bureau of Mines Routine Method. The results are presented in Tables E.2 and E.3.

The analyses were provided by the Champlin Petroleum Company at Wilmington, California and were those of a blend (40% LAX 3, 60% LAX 6).

Maljamar Crude--This oil is intermediate between a paraffinic and an aromatic crude. Its distillation characteristics are presented in Table E.4. The analysis presented there was performed by the Bureau of Mines, Bartlesville, OK, Laboratory. Their sample number: 41464.

The oil used in our studies was provided by Conoco and was a 37.2° API crude. It was a stock tank composite from two producing pay zones.

Hilly Upland Crude--The distillation analysis, whose results are presented in Table E.5, was performed on a sample obtained December 11, 1979 from well A-389. The oil is a paraffin-based, Pennsylvania grade oil. A bottom hole sample taken in February 1976 showed the minimum miscibility pressure for CO₂ was 1000 psi.

Effect of CO₂ Upon Viscosity--The results presented in Table E.6 show that the viscosity of the CO₂-saturated liquid phase reservoir fluid is inversely proportional to pressure (6) from the bubble point (1115 psia) down to atmospheric pressure. Above the bubble point, the viscosity in the liquid phase is directly proportional to CO₂ pressure.

Corresponding data for the Maljamar crude and the Wilmington Crude are not available.

Other data--The reservoirs from which the crudes came are described in Appendix H. The compositions of the crudes, as determined by gas chromatography, are presented in Appendix I.

TABLE E.2
 HEMPEL AND VACUUM DISTILLATION ANALYSIS OF
 WILMINGTON CRUDE (BLEND: 40% LAX 3, 6% LAX 6)
 (Source: Ref. 5)

Fraction:	Crude Oil	...Gasoline...		Depentanized Naptha 375° F EP	Diesel 450-650°FGas Oils....			Residuum 1000°F+	
		IBP 375°F EP	D 86			D 86	U 1	650-750°F		750-1000°F
Distillation Type: D 1160										
I.B.P., °F	D 1160	D 86	D 86	D 86	D 86	U 1	D 1160	D 1160	D 1160	D 1160
5%	137	106	190	370	460	640	739	739	950	950
10	235	148	205	377	472	644	776	776	978	978
20	320	175	214	380	481	647	792	792	1002	1002
30	450	207	226	384	495	652	805	805	1045	1045
40	558	227	238	387	504	656	819	819	1063	1063
50	660	243	252	390	515	662	835	835		
60	760	259	266	394	528	668	850	850		
70	850	275	282	398	543	674	865	865		
80	940	293	298	403	559	681	885	885		
90	1020	311	315	410	573	691	910	910		
95		332	335	422	601	707	947	947		
E.P., °F		350	350	432	618	722	972	972		
% Recovered	79.0	380	382	450	651	750	1008	1008	25.0	25.0
% Bottoms	21.0	98.5	99.0	99.0	99.0	98.5	99.0	99.0	85.0	85.0
% Loss		1.0	1.0	1.0	1.0	1.5	1.0	1.0		
		0.5								

TABLE E.3
 PROPERTIES OF DISTILLATE FRACTIONS FROM WILMINGTON CRUDE
 (Reference 5)

Fraction	Depentanizer Overhead		IBP 375°F		EP 375°F		Depentanized Naptha 375-450°F		Diesel 450-650°F		Gas Oils			Residuum 1000°F+
	1.4	0.0-1.4	14.1	0.0-14.1	12.7	1.4-14.1	3.9	14.1-18.0	21.2	18.0-39.2	9.3	21.9	750-1000°F	
Yield Volume l of Crude														
Position in Crude Oil, L.V.I.														
Analyses of Fractions														
Gravity, API at 60°F			55.8		52.2		38.8		29.4		21.9		16.6	5.8
Specific Gravity of 60°F			0.7555		0.7703		0.8309		0.8794		0.0224		0.9534	1.0306
Total Sulfur, Wt.%					0.059		0.237		0.92		1.51		1.60	2.45
Mercaptan Sulfur Wt.%							0.0012							
Hydrogen Sulfide, Wt.%							0.0020							
Bromine Number							0.0020							
F.I.A Analysis, L.V.%														
Paraffins + Naphthanas					92.3		81.2				8.1		10.2	
Aromatics					7.7		18.8							
Nitrogen Content, Total ppm					1.4		38.2							
Aniline Point °F							122.7		129.7				4960.	
Calculated Cetane Index(C.P.R.)									40.4					
Heptane Insolubles, Wt.%														10.3
Smoke Point														
Pour Point °F									-30		30		80	140
Freezing Point														
Conradson Carbon Residue, Wt%											0.01		0.26	18.9
Molecular Weight											307		411	
Viscosities														
Kinematic at 100°F., cSt							1.404		3.873		23.64			
Kinematic at 122°F., cSt													172.9	
Kinematic at 210°F., cSt									1.359		3.741		16.40	
Universal at 100°F., sec							29.6		38.8		113.5		802	
Universal at 122°F., sec									29.3		38.6		83.3	
Universal at 210°F., sec														

TABLE E.4
 DISTILLATION CHARACTERISTICS OF MALJAMAR CRUDE
 (Ref. 8, p. 145)

Stage 1--Distillation at 742 mm Hg

Fraction No.	Cut °C	Temp. °F	Percent	Sum, Percent	Sp. gr., 60/60°F	A.P.I. 60°F	C.I.	S.U. Visc. 100°F	Cloud Test °F
1.....	50	122	2.9	2.9	0.636	91.0	-		
2.....	75	167	3.5	6.4	0.675	78.1	9.8		
3.....	100	212	6.5	12.9	0.727	63.1	25		
4.....	125	257	7.7	20.6	0.756	55.7	29		
5.....	150	302	6.2	26.8	0.776	50.9	31		
6.....	175	347	5.7	32.5	0.789	47.8	31		
7.....	200	392	5.0	37.5	0.800	45.4	30		
8.....	225	437	4.7	42.2	0.812	42.8	30		
9.....	250	482	5.0	47.2	0.826	39.8	31		
10.....	275	527	6.3	53.5	0.841	36.8	33		

Stage 2--Distillation Continued at 40 mm Hg

11.....	200	392	2.9	56.4	0.857	33.6	37	40	10
12.....	225	437	6.4	62.8	0.866	31.9	37	45	30
13.....	250	482	4.9	67.7	0.881	29.1	41	58	50
14.....	275	527	5.1	72.8	0.892	27.1	43	89	70
15.....	300	572	6.4	79.2	0.903	25.2	46	180	90
Residum	-	-	19.0	98.2	0.961	15.7	-	-	-

TABLE E.5
DISTILLATION CHARACTERISTICS OF HILLY UPLAND CRUDE

Stage 1--Distillation at 743 mm Hg										
Fraction No.	Cut Temp. °F	Percent	Sum percent	Sp. gr., 60/60°F	°API. 60°F	C.I.	Refractive Index n _D at 20°C	Specific Dispersion	S.U. visc. 100°F	Cloud test °F
1.....	122	2.8	2.8	0.631	92.7			128.6		
2.....	167	2.7	5.5	.673	78.8	8.9	1.37867	133.4		
3.....	212	4.4	9.9	.708	68.4	16	1.39568	133.4		
4.....	257	5.8	15.7	.731	62.1	18	1.40761	138.4		
5.....	302	5.0	20.7	.748	57.7	18	1.41710	140.1		
6.....	347	6.1	26.8	.763	54.0	18	1.42532	138.7		
7.....	392	2.1	28.9	.776	50.8	18	1.43193	138.4		
8.....	437	4.9	33.8	.782	49.4	15	1.43514	137.3		
9.....	482	5.4	39.2	.793	46.9	15	1.44067	137.7		
10.....	527	5.7	44.9	.805	44.3	16	1.44698			
Stage 2 - Distillation Continued at 40 mm. Hg										
11.....	392	5.6	50.5	0.817	41.7	18	1.45277	138.3	37	12
12.....	437	6.0	56.5	.826	39.8	19	1.45805	137.3	42	34
13.....	482	5.4	61.9	.836	37.8	20	1.46299	138.9	51	50
14.....	527	4.9	66.8	.847	35.6	22			63	70
15.....	572	6.2	73.0	.859	33.2	25			88	92
Residuum	-	25.9	98.9	.886	28.2					

TABLE E.6
 VISCOSITY OF HILLY UPLAND CRUDE SATURATED
 WITH CARBON DIOXIDE AT 78°F
 (Ref. 6)

Pressure psia	Viscosity Centipoise
2015	0.56
1815	0.55
1615	0.54
1415	0.53
1215	0.52
1115	(bubble point)
1050	0.51
1015	0.53
915	0.61
715	0.91
515	1.30
315	1.78
215	2.04
115	2.22
15	4.81

APPENDIX F
Apparatus for Filtration Experiments

A. Sight Glass

Mfr: Jerguson Gage & Valve Co
15 Adams St.
Burlington, Mass. 01803

Model: series 19T20

Test pressure: 2660 psig (5 min)

Max. operating pressure: 2000 psig.

B. Filter (described more fully on next page)

Mfr: Millipore Corp.
Bedford, Mass. 01730

Housing: 25-mm diam.

Model: PN 4502500

Filter medium: 2 micron pores

Type: MF

C. Positive - Displacement Pump

Mfr: Ruska Instrument Corp.
3601 Dunvale
Houston, TX 77063

Model: 2245-803

D. Pressure Transducer

Mfr: Bourns, Inc.
Instrument Div.
6135 Magnolia Blvd.
Riverside, CA 92506

Model: 5020

FILTER AND FILTERING MEDIUM

All mixtures of CO₂ and crude oil were filtered using a 25-mm high pressure stainless steel filter housing (Millipore PN-XX4502500), containing an 8 μm 25-mm filter membrane Millipore type MF. The 8-micron pores in the element were believed to be representative of many reservoirs.

The MF type filter membrane, composed of mixed cellulose acetate and nitrate esters, was chosen for the filtration medium since this type of filter is not attacked by dilute acids or alkalies, aliphatic or aromatic hydrocarbons, or water. The MF filter has the highest flow rate of all the Millipore filters, including the Miltex filter (Teflon). Millipore recommended the MF type filter for all analytical experiments below 75°C.

The MF type filter membrane has a mean pore size of 8.0 μm, a typical porosity of 84% and a mean bubble point of 4 psid±10% (0.28 kg/cm²). The free flow rate of water through the MF filter under a differential pressure of 10 psi (52 cm Hg) is 630 ml/min/cm². For the filter element we used, this is 3093 ml/min. By contrast, the Teflon type filter element (porosity 68%) would permit only 618 ml/min.

APPENDIX G

FILTRATION TESTS USING VARIOUS CRUDE OILS

TABLE G.1
 RESULTS OF FILTRATION TESTS USING WILMINGTON CRUDE
 SATURATED WITH CO₂ at 50.5±2°C

CO₂ Pressure

500 psig		1000 psig		1500 psig	
Time (Sec)	Volume (ml)	Time (Sec)	Volume (ml)	Time (Sec)	Volume (ml)
0	27.78	0	30.28	0	34.32
15	27.20	15	29.13	15	32.97
30	24.70	30	28.93	30	32.59
45	24.32	45	27.78	45	32.40
60	23.92	60	27.20	60	32.20
90	23.74	100	25.66	90	31.82
120	23.55	125	24.70	120	31.63
150	22.97	150	23.93	150	31.24
200	22.00	175	23.16	200	30.47
250	21.62	200	22.39	250	29.70
300	21.24	250	21.05	300	28.93
450	20.47	300	20.47	400	27.00
500	19.51	350	20.08	500	25.28
600	18.93	400	19.51	750	21.62
700	18.35	600	17.58	1000	18.74
900	17.78	750	17.01	1206	17.00
1200	17.20	1000	16.05	1600	13.82
1600	16.05	1800	12.00	1800	12.32
1800	15.47			2000	10.85

TABLE G.2
RESULTS OF FILTRATION TESTS USING MALJAMAR CRUDE
SATURATED WITH CO₂ at 27±2°C

CO₂ Pressure

1000 psig		1500 psig		1800 psig	
Time (Sec)	Volume (ml)	Time (Sec)	Volume (ml)	Time (Sec)	Volume (ml)
0	30.04	0	25.86	0	22.54
15	26.97	15	23.90	15	21.19
30	25.81	30	23.32	45	19.27
45	24.85	45	22.94	60	18.11
60	24.08	60	22.36	80	17.34
100	22.73	120	21.78	100	16.19
125	21.96	180	20.82	120	15.80
150	21.38	250	20.05	150	15.42
175	20.81	350	19.66	180	15.03
200	20.04	400	19.66	200	14.84
225	19.65	500	19.47	220	14.65
250	19.07	750	19.47	250	14.26
300	17.73	1000	19.47	275	14.07
350	16.38	2000	19.47	300	13.88
400	15.42			325	13.88
450	14.07			360	13.69
505	12.72			400	13.69
600	10.61			425	13.49
				450	13.11
				475	12.92
				500	12.72
				550	12.72
				600	12.34
				650	12.34
				700	12.34
				750	12.34
				1000	12.34

TABLE G.3
 RESULTS OF FILTRATION TESTS USING
 MALJAMAR CRUDE SATURATED WITH CO₂ AT 37±1°C

CO₂ Pressure

1000 psig		1500 psig		1800 psig	
Time (Sec)	Volume (ml)	Time (Sec)	Volume (ml)	Time (Sec)	Volume (ml)
0	28.50	0	25.81	0	20.81
15	26.82	15	25.08	15	20.04
30	26.00	30	25.04	30	19.84
45	25.43	45	24.85	45	19.75
60	25.02	60	24.83	60	19.70
100	24.62	100	24.66	100	19.65
125	24.23	150	24.66	130	19.58
150	23.86	200	24.66	250	19.46
175	23.65			400	19.07
200	23.37			500	19.07
250	22.80			700	19.07
300	22.25			1000	19.07
400	21.18				
500	20.30				
600	19.50				
775	18.18				
1000	16.81				
1400	15.44				
1700	14.50				
2000	13.63				

TABLE G.4
RESULTS OF FILTRATION TESTS USING MALJAMAR CRUDE
SATURATED WITH CO₂ AT 50.5±1°C

CO₂ Pressure

1000 psig		1500 psig		1800 psig	
Time (Sec)	Volume (ml)	Time (Sec)	Volume (ml)	Time (Sec)	Volume (ml)
0	30.28	0	32.01	0	19.84
15	27.24	15	30.47	15	19.65
30	26.86	30	29.96	30	19.57
45	26.34	45	29.51	45	19.46
60	25.96	60	29.32	60	19.38
100	25.09	100	28.74	100	19.31
125	24.12	125	28.36	125	19.27
150	23.74	150	28.16	150	19.23
175	23.16	180	27.59	175	19.19
215	22.20	200	27.39	200	19.18
250	21.43	250	26.82	250	19.15
300	20.08	300	26.05	300	19.11
350	18.93	350	25.37	500	19.07
400	17.58	400	24.52	750	18.30
500	15.28	500	22.97	1000	17.92
600	12.97	600	21.24	1700	17.65
700	10.41	750	19.32	1900	17.53
		1000	16.24	2000	17.42
		1250	13.74		
		1900	9.70		

TABLE G.5
RESULTS OF FILTRATION TESTS USING HILLY UPLAND CRUDE
SATURATED WITH CO₂ AT 28±0.5°C

CO₂ Pressure

300 psig		500 psig		800 psig		800 psig		950 psig	
Time (Sec)	Volume (ml)								
0	31.77	0	31.77	0	41.21	0	37.01	0	40.44
15	30.43	15	30.42	15	39.48	15	35.47	15	37.94
30	29.08	30	29.08	30	38.90	30	34.70	30	37.17
45	27.93	45	27.92	45	38.32	45	34.32	45	36.78
60	26.77	60	26.58	60	37.55	60	33.74	60	36.20
75	25.62	75	25.42	75	36.97	75	32.97	90	35.43
100	23.69	100	23.69	100	35.82	100	32.01	120	34.66
125	21.58	125	21.77	125	34.66	125	31.05	150	34.09
150	19.46	150	20.04	150	33.70	150	30.28	200	32.93
175	17.34	175	18.11	175	32.74	175	29.32	250	31.58
200	15.03	200	15.99	200	31.58	200	28.36	300	30.43
211	14.26	250	14.07	225	30.81	225	27.01	365	28.70
225	13.11	300	9.64	250	29.85	250	26.05	400	27.73
236	12.34			275	28.70	275	25.09	450	26.39
250	11.18			300	27.54	300	23.93	500	24.66
				340	25.81	325	22.97	750	18.11
				375	23.89	350	22.01	830	16.00
				410	22.35	400	19.70	1000	11.18
				450	20.42	450	17.39		
				500	18.30	500	14.70		
				550	16.19	525	13.54		
				600	14.07	550	12.39		
				650	11.57	575	11.23		
						640	8.54		

APPENDIX H

Reservoirs From Which the Crude Oils of This Study Were Obtained

Wilimington Reservoir--This reservoir is situated in Los Angeles County, California and contains numerous pay zones between 2400-4700 feet. The age of this reservoir is Miocene. Additional data are presented in Table H.1.

Maljamar Reservoir--This reservoir is situated in Lea County, New Mexico. The oil we studied was a composite from two pay zones: an upper zone, located at 3700 ft in the Grayburg sands (zone number 9, MCA unit well 36) and a lower zone, located at 4000 ft in the San Andres sands (MCA unit well 271). The age of both production zones in the Maljamar reservoir is Permian (10).

Additional data for the Maljamar reservoir are presented in Table H.2.

Hilly Upland Reservoir--This reservoir was discovered in 1963. Field exploration and development were essentially complete by 1970 (6). The reservoir lies in the base of the Greenbrier Limestone Formation of middle Mississippian age. The pay zones of the Hilly Upland oil field occurring between 2102-2116 feet are designated in many parts of West Virginia as the "Big Injun" pay by drillers. This term includes pay zones in the lower Greenbrier and Upper Pocono formations.

The porosity of the Basal Greenbrier Limestone Formation averages 14% and shows the result of local dolomitization. Permeability averages between 2 and 3 md. Oil saturation at the start of the CO₂ flood was approximately 65% (6). Additional data about this reservoir are presented in Table H.3.

TABLE H.1

TAR ZONE RESERVOIR DATA
 WILMINGTON OIL FIELD
 (Ref. 5)

Discovery, Development	1936-Present
Formation	Tar I
Area, acres	13,329
Depth, ft	2,500
Reservoir Temperature, °F	123
Reservoir Pressure, Original, psig	1,110
Reservoir Pressure, Lowest, psig	300
Net Sand, ft	400
Porosity, %	33.7 Avg.
Formation Vol. Factor at 1100 psi	1.062
Water Saturation, Avg., %	21
Oil Saturation, Residual, %	25
Oil in place, Bbl/Acre Ft.	1,944
Mobility Ratio	15.75

TABLE H.2

RESERVOIR DATA
MALJAMAR OIL FIELD
(Ref. 10, 11)

Formation	Grayburg/San Andres
Area, acres	*
Depth, ft	3600-4100
Reservoir Temperature, °F	92-100
Reservoir Pressure, Original	*
Reservoir Pressure, Present, psig	1540-1770
Net Sand, ft	12-20
Porosity, Average, %	20
Permeability, md	3-9
Number of Wells	400
Formation Volume Factor @ 60°F	*
Specific Gravity @ 60°F	0.8388
API Gravity @ 60°F	37.2
Viscosity, Centipose	*
Water Saturation	*
Oil Saturation	*
Gas Saturation	*
Oil in Place, Bbl/acre ft	*

*Information not available.

TABLE H.3

RESERVOIR DATA FOR THE HILLY UPLAND
OILFIELD AND PILOT AREA
(Ref. 6)

Discovery, Development	1968-69
Formation	Greenbrier Big Injun
Area, acres	200
Depth, ft	1800 - 2100
Reservoir Temperature, °F	77 - 80
Reservoir Pressure, Original, psig	>700
Reservoir Pressure, Present, psig	300 - 500
Net Sand, ft	9 - 18 (Avg. 12.5)
Porosity, %	9 - 20.5 (Avg. 14)
Permeability, mD	0.1-6 (Avg. 2 - 4)
Formation Volume Factor	1.145 at 445 psi
Specific Gravity at 78° F	0.7363
API Gravity at 60°F	42
Viscosity, Centipoise	1.75
Water Saturation, %	20 - 30
Oil Saturation, %	70 - 80
Gas Saturation, %	10 - 70
Oil in Place in Pilot Area, bbl/acre	>8000

APPENDIX I

Gas Chromatographic Analyses of Crudes

Wilmington Crude.--The composition of the dead crude (see Table I.1) shows it is practically devoid of light hydrocarbons. Only 30% of it has carbon number less than 36. Its (calculated) average molecular weight is 287, assuming the average carbon number of the C₃₆+ fraction is 40.

Maljamar Crude.--The analysis (Table I.2) shows 70% (wt.) of the crude has carbon number less than 36. Its average molecular weight was calculated to be 184(4). The average molecular weight determined from freezing-point depression is 181 (4,12).

Hilly Upland Crude.--The average molecular weight of this crude (dead) was calculated by Orr (14) to be 258 from the gas chromatographic analysis (Table I.3). The fraction with carbon number 36+ was assumed to be C₄₀.

TABLE I.1
ANALYSIS OF WILMINGTON CRUDE OIL
(Ref. 12)

<u>Carbon Number</u>	<u>Weight %</u>	<u>Carbon Number</u>	<u>Weight %</u>
5	0.060	21	0.813
6	0.055	22	1.176
7	0.118	23	1.195
8	0.222	24	1.190
9	0.271	25	0.798
10	0.448	26	1.226
11	0.772	27	0.852
12	0.947	28	1.424
13	1.371	29	1.036
14	1.169	30	1.036
15	1.320	31	1.050
16	1.707	32	1.035
17	1.116	33	0.967
18	1.161	34	0.935
19	1.174	35	0.906
20	1.570	36+	71.332

TABLE I.2
ANALYSIS OF MALJAMAR CRUDE OIL
(Ref. 13)

<u>Carbon Number</u>	<u>Weight%</u>	<u>Carbon Number</u>	<u>Weight%</u>
5	1.56	21	1.78
6	2.37	22	1.78
7	3.69	23	1.74
8	7.01	24	1.62
9	4.94	25	1.08
10	3.80	26	1.63
11	3.72	27	1.63
12	3.00	28	1.64
13	3.05	29	1.14
14	1.75	30	1.22
15	2.97	31	1.17
16	2.49	32	1.18
17	1.99	33	1.20
18	1.91	34	1.29
19	1.78	35	1.27
20	1.74	36+	30.86

TABLE I.3
ANALYSIS OF HILLY UPLAND CRUDE OIL
(Ref. 6, 12)

<u>Carbon Number</u>	<u>Weight%</u>	<u>Carbon Number</u>	<u>Weight%</u>
5	0.12	21	2.00
6	1.15	22	1.95
7	1.74	23	1.94
8	5.63	24	1.88
9	3.81	25	1.86
10	4.81	26	1.83
11	3.74	27	1.80
12	3.78	28	1.78
13	3.18	29	1.76
14	3.78	30	1.65
15	3.15	31	0.81
16	2.98	32	0.78
17	3.29	33	0.79
18	2.19	34	0.77
19	2.94	35	1.46
20	2.04	36+	28.60

APPENDIX J

Apparatus for Flow Tests Using Unconsolidated Sand Pack

Formation Model (Sand Pack)

Bulk Volume = 759 cm³

Pore Volume = 316 cm³

Porosity = 41%

Absolute Permeability = 274 md at $S_w = 1.00$

Oil Transfer Cylinder

Transfer Volume = 795 cm³ (2.5 pore volumes)

Water Transfer Cylinder

Transfer Volume = 1250 cm³ (4.0 pore volumes)

CO₂ Transfer Cylinder

Transfer Volume = 895 cm³ (2.8 pore volumes)

APPENDIX K
 EXPERIMENTAL RESULTS FROM OIL DISPLACEMENT TESTS
 USING AN UNCONSOLIDATED SAND PACK

Table K.1
 Injection of Maljamar Crude During Preparation of Sand Pack

WATER PRODUCED Cumulative, cc	OIL INJECTED, Cumulative, cc	FLOW RATE OF OIL cc/sec
203.0	203.0	.107
210.7	211.5	.074
211.0	212.5	.033
212.1	216.6	.074
213.2	221.3	.094
214.0	227.3	.120
214.8	233.3	.120
215.8	240.8	.150
216.8	248.4	.152
216.8	253.9	.110

Table K.2
 Conventional Waterflood with Brine
 No CO₂ Present

(These data are plotted in Fig. 3.9 in the text)

Oil Produced, Cumulative		Brine Injected, Cumulative		Brine Flow
cc	PV	cc	PV	cc/sec
147.5	.465	147.5	.465	.049
150.8	.476	152.2	.480	.047
152.8	.482	156.1	.492	.078
154.2	.486	160.0	.505	.078
155.4	.490	163.1	.515	.062
156.2	.493	166.2	.524	.062
157.0	.495	169.3	.534	.062
157.6	.497	172.1	.543	.056
158.6	.500	175.1	.552	.060
159.3	.503	177.8	.561	.054
159.8	.504	180.7	.570	.058
160.3	.506	183.3	.578	.052
170.1	.537	255.1	.805	.060
177.1	.559	397.1	1.255	.079
178.6	.563	465.6	1.469	.076
181.6	.573	550.6	1.737	.085
181.7	.573	635.6	2.005	.085
183.7	.580	729.6	2.302	.088
183.8	.580	799.6	2.522	.089
183.8	.580	845.6	2.667	.090

Table K.3
 Resaturation with Maljamar Crude
 before the CO₂-Enhanced Secondary Waterflood

Water Produced, Cumulative cc	Oil Injected, Cumulative cc	Flow Rate of Oil cc/sec
147.6	147.6	.090
150.3	150.8	.178
153.0	153.7	.058
154.0	159.1	.108
155.4	165.3	.124
156.6	169.3	.080
157.1	178.5	.092
158.5	185.4	.138
159.7	194.8	.094
167.7	245.3	.084
173.2	297.3	.087
177.2	348.3	.085
179.2	397.3	.082
181.2	447.3	.083
183.2	496.3	.082
183.2	516.3	.080

Table K.4
Secondary CO₂-Enhanced Waterflood

(These data are plotted in Fig. 3.9 in the text.)

Oil Produced, Cumulative		Brine Injected, Cumulative		Brine Flow
cc	PV	cc	PV	cc/sec
167.3	.528	147.0	.464	.049
168.3	.531	149.9	.473	.104
170.7	.539	159.5	.503	.110
171.9	.542	166.7	.526	.114
173.0	.546	171.8	.542	.102
173.4	.547	178.6	.563	.136
174.3	.550	183.2	.578	.092
175.7	.554	192.9	.609	.097
176.7	.557	199.7	.630	.136
181.0	.571	255.7	.807	.093
183.9	.580	303.7	.958	.080
185.3	.585	356.7	1.125	.088
187.5	.591	410.2	1.294	.089
188.6	.595	464.2	1.464	.090

APPENDIX L

Experimental Results from
CaCO₃ Precipitation Tests
Using Static Bed of Limestone

Table L.1
Porosity Changes and Amounts of CaCO₃ Deposited

Mass of CaCO ₃ Deposited in Entire Bed, g	Measured Porosity		Estimated Mass CaCO ₃		
	Upper Part of Bed	Middle of Bed	Upper Part, g	Middle Part, g	Lower Part, g
0.0	0.44	0.44	0.0	0.0	0.0
19.4	0.42	0.41	4.6	6.83	8.13
64.1	0.36	0.34	21.9	27.1	15.1
138.0	0.31	0.30	58.8	64.0	15.2
187.0	0.28	0.28	86.3	82.3	18.4

Table L.2
Permeability Changes and Porosity

Upper Part of Bed		Middle Part of Bed	
Porosity	Permeability, Darcys	Porosity	Permeability, Darcys
0.44	209	0.44	247
0.42	196	0.41	154
0.36	127	0.34	138
0.31	75	0.30	176
0.28	39	0.28	138

Table L.3
Calculated Volumes of CaCO₃ Precipitate

Total Amount of CaCO ₃ Deposited		Volume of CaCO ₃ , cm ³		
g	cm ³	Upper Part	Middle Part	Lower Part
0.0	0.0	0.0	0.0	0.0
19.4	6.2	1.7	2.5	2.0
64.1	20.7	8.1	10.0	2.6
138.0	48.0	21.7	23.6	2.7
187.0	66.1	31.9	30.4	3.8

APPENDIX M

Derivation of the Equations Presented in Section 4.4

Introduction--The goal of the following is to develop an equation relating Ca^{++} concentration to residence time, while recognizing that the precipitation rate is a function of both the Ca^{++} and $\text{CO}_3^{=}$ concentrations.

First Model--Suppose the precipitation rate is taken to be proportional to the concentrations of Ca^{++} and $\text{CO}_3^{=}$ in the manner given by Eq. M.1. The difference between the product of the concentrations and the solubility product, K_{sp} , is a measure of the supersaturation and, hence, of the driving force for precipitation.

$$d[\text{Ca}^{++}]/dt = -k\{[\text{Ca}^{++}][\text{CO}_3^{=}] - K_{sp}\} \quad (\text{M.1})$$

For a particular flow rate, F , of solution and height, h , of the fluidized bed, Eq. M.2 gives the residence time, t .

$$t = hA/F \quad (\text{M.2})$$

where A is the cross-sectional area of the bed. Upon differentiating,

$$dt = (A/F)dh \quad (\text{M.3})$$

By substituting Eq. M.3 for dt in Eq. M.1, we have, after rearranging,

$$d[\text{Ca}^{++}]/dh = -k(A/F)\{[\text{Ca}^{++}][\text{CO}_3^{=}] - K_{sp}\} \quad (\text{M.4})$$

Pseudo-First Order Conditions--To integrate Eq. M.4 we must know how $[\text{CO}_3^{=}]$ varies with $[\text{Ca}^{++}]$. In the experiment whose results were presented in Fig. 4.1, the $\text{CO}_3^{=}$ concentration was 25 times that of Ca^{++} . Thus, $[\text{CO}_3^{=}]$ may be assumed constant at 0.025 M with less than 4% error over the period of the experiment. Eq. M.4 can be further simplified by noting that the product, $[\text{Ca}^{++}][\text{CO}_3^{=}]$ was never less than $3 \times 10^{-7} \text{ M}^2$ during the experiment, so K_{sp} ($5 \times 10^9 \text{ M}^2$) is negligible by comparison. With these changes Eq. M.4 becomes

$$d[\text{Ca}^{++}]/dh = -k(A/F)(0.025\text{M})[\text{Ca}^{++}] \quad (\text{M.5})$$

Integration of Eq. M.5 yields:

$$\ln[\text{Ca}^{++}] = -k(A/F)(0.025M)h + \ln[\text{Ca}^{++}]_0 \quad (\text{M.6})$$

where $[\text{Ca}^{++}]_0$ is the concentration of calcium entering the fluidized bed after dilution by the carbonate solution.

Test of Eq. M.6--The equation predicts that a plot of $[\text{Ca}^{++}]$ against bed height will be linear on semi-log paper. Such a plot is presented in Fig. M.1, but it is obviously non-linear. This suggests the rate expression, Eq. M.4, is incorrect; the precipitation rate is more strongly dependent upon $[\text{Ca}^{++}]$ than was assumed.

Kinetics are Second-Order in Ca^{++} Concentration--An improved rate expression would be

$$d[\text{Ca}^{++}]/dh = -k(A/F)(0.025M)[\text{Ca}^{++}]^2 \quad (\text{M.7})$$

The integrated form (Eq. M.8) predicts that if the reciprocal of $[\text{Ca}^{++}]$ is plotted against bed height, the result will be a straight line.

$$1/[\text{Ca}^{++}] = k(A/F)(0.025M)h + 1/[\text{Ca}^{++}]_0 \quad (\text{M.8})$$

Such a plot is, indeed linear, as Fig. 4.3 shows. Thus, Eqs. M.7 and M.8 are suitable models for our experiments.

Limitation of Model--Note that we have established that the rate is second-order with respect to $[\text{Ca}^{++}]$, but we have not determined how the rate depends on $[\text{CO}_3^-]$. Thus, the most specific rate expression we can write is Eq. M.9,

$$d[\text{Ca}^{++}]/dh = -K(A/F)[\text{Ca}^{++}]^2[\text{CO}_3^-]^b \quad (\text{M.9})$$

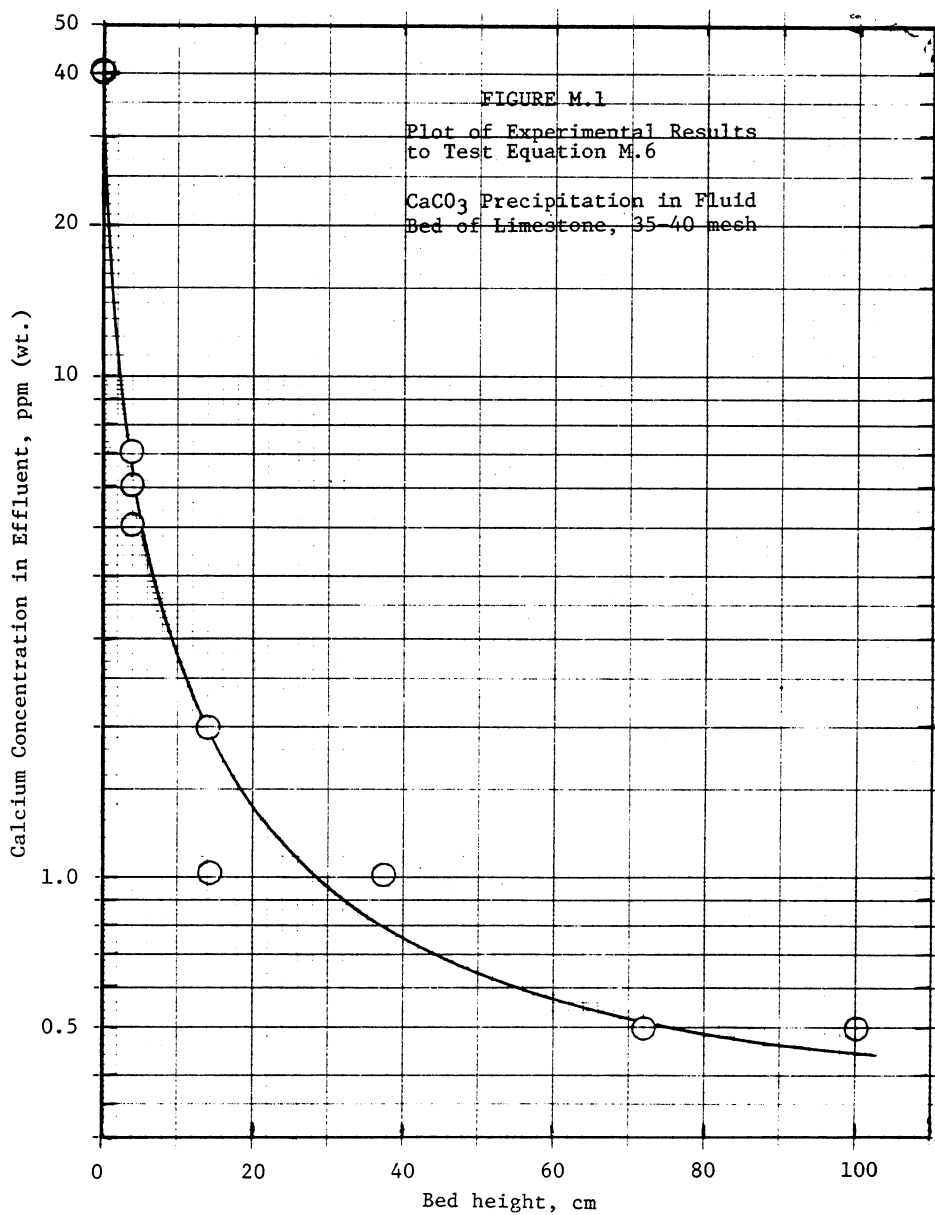
where the exponent b and rate constant K are undetermined. Further experimentation would be required to establish their values.

Applicability to a CO_2 Flood--Although Eq. M.8 represents the experimental results satisfactorily, it cannot be used to describe a CO_2 flood. Under the conditions expected to prevail in a reservoir, the concentrations of Ca^{++} and CO_3^- might be sufficiently low that K_{sp} is not negligible compared

with $[Ca^{++}][CO_3^{=}]$. Hence the more complete form of the rate expression would have to be used, i.e.,

$$d[Ca^{++}]/dh = -k(A/F)\{[Ca^{++}][CO_3^{=}] - K_{sp}\}^n \quad (M.10)$$

Besides that, the carbonate concentration is not constant. It depends upon the CO_2 pressure, which governs the amount of $CaCO_3$ which dissolves. Most of the carbonate would be present as HCO_3^- , not $CO_3^{=}$; and the concentration of $CO_3^{=}$ depends upon the equilibrium depicted by Eq. M.11



APPENDIX N

Materials Used in Fluid Bed Experiments

A. Limestone

Origin: northern Mexico
Supplier: M & M Rock Co.
110 Inglewood
El Paso, Texas 79917
Purity: 99.5 percent CaCO_3

B. Glass Beads

Type: soda lime glass (P-008)
Specific gravity: 2.46 - 2.49
Softening point: 730°C
Size range: 70-80 U.S. std. sieves
Manufacturer: Potters Industries, Inc.
Hasbrouck Heights, NJ 07604

C. Silicone-Coated Glass Beads

Glass: soda lime glass
(properties as above)
Size range: 35-45 U.S. std. sieves
Coating: silicone resin
Manufacturer: Potters Industries, Inc.
Hasbrouck Heights, NJ 07604

APPENDIX O

Derivation of Math Model for Scale Growth on Glass or Resin-Coated Surfaces

Physical Model--If a bed of glass particles is fluidized with a super-saturated solution of Ca^{++} and $\text{CO}_3^{=}$, a scale of CaCO_3 will grow over the surfaces until they are completely covered. Because the CaCO_3 surface provides better sites for CaCO_3 precipitation than the glass, the rate of precipitation increases with time as glass surface is replaced by CaCO_3 scale. The rate becomes constant once the glass particle is completely covered.

The fluidizing solutions (Ca^{++} and $\text{CO}_3^{=}$) are of constant composition and enter at a constant rate. However, the concentrations of Ca^{++} and $\text{CO}_3^{=}$ in the effluent are less than those in the entering solutions, because CaCO_3 is removed by the particles in the bed. And because the surface area is changing, the effluent concentrations change with time.

Goal--Because the Ca^{++} concentration in the effluent is the physical variable we can most easily measure as function of time, the purpose of the following is to develop a mathematical expression relating calcium concentration, $[\text{Ca}^{++}]$, to time, t .

Rate Equation--The fluidized bed is short enough that back-mixing is rapid compared to the rate of change of Ca^{++} concentration, so the bed can be considered a stirred tank in the sense of a CSTR. Accordingly, the concentration of Ca^{++} leaving the bed equals the Ca^{++} concentration within the bed,

$$[\text{Ca}^{++}] = [\text{Ca}^{++}]_e \quad (0.1)$$

where, $[Ca^{++}]_e$ = concentration of Ca^{++} in the effluent, mol/l

and $[Ca^{++}]_f$ = concentration of Ca^{++} in the bed, mol/l

Over a short time interval, we may assume pseudo-steady-state conditions, so the following mass-balance applies (Eq. 0.2)

$$F\{[Ca^{++}]_f - [Ca^{++}]_e\} = \text{rate of } Ca^{++} \text{ precipitation with bed, mol/sec} \quad (0.2)$$

where F = volumetric flow rate of Ca^{++} solution, cm^3/s

and $[Ca^{++}]_f$ = concentration of Ca^{++} entering the fluidized bed with the feed, mol/l

The rate of Ca^{++} precipitation depends upon the volume of the bed, V , and the extent of supersaturation. The latter is expressed by the difference, $[Ca^{++}]_e [CO_3^{=}]_e - K_{sp}$.

If the extent of supersaturation is low enough that particles of precipitate do not form in the bulk liquid (as is the case in the present experiments), then precipitation occurs only on the glass surfaces or on the $CaCO_3$ scale that has already formed. Consequently, the rate expression includes only two rate constants, as shown in Eq. 0.3.

$$\text{rate of } Ca^{++} \text{ precipitation} = V[k_1 A_g + k_2 A_s] \{ [Ca^{++}]_e [CO_3^{=}]_e - K_{sp} \} \quad (0.3)$$

where V = volume of fluid bed, cm^3

A_g = surface area of the glass that is free of scale, cm^2

A_s = surface area that is covered by scale, cm^2

k_1 = precipitation rate constant for glass surface, $1/mol/sec \text{ } cm^2$

k_2 = precipitation rate constant for $CaCO_3$ scale, $1/mol/sec \text{ } cm^2$

Equating Eqns. 0.2 and 0.3 gives

$$F\{[Ca^{++}]_f - [Ca^{++}]_e\} = V(k_1 A_g + k_2 A_s) \{ [Ca^{++}]_e [CO_3^{=}]_e - K_{sp} \} \quad (0.4)$$

The first simplification of Eq. 0.4 is achieved by noting that the areas of scale and uncoated glass are related by Eq. 0.5, if we assume the CaCO_3 scale is a thin coat of uniform thickness¹

$$A_s = A_{g,o} - A_g \quad (0.5)$$

where $A_{g,o}$ is the surface area of the glass particles in the bed before the experiment begins. Substituting Eq. 0.5 for A_s in Eq. 0.4 gives an expression in terms of A_g alone.

$$F\{[\text{Ca}^{++}]_f - [\text{Ca}^{++}]_e\} = V[(k_1 - k_2)A_g - k_2A_{g,o}]\{[\text{Ca}^{++}]_e[\text{CO}_3^{=}]_e - K_{sp}\} \quad (0.6)$$

Equation 0.6 can be simplified three more ways. First, in the present experiments, the product $[\text{Ca}^{++}]_e[\text{CO}_3^{=}]_e$ is always 10^3 times greater than K_{sp} , so K_{sp} is negligible by comparison. Second, because the concentration of $\text{CO}_3^{=}$ is approximately equal to the concentration of Ca^{++} , we can replace $[\text{CO}_3^{=}]_e$ by $[\text{Ca}^{++}]_e$. Finally, because the CaCO_3 scale provides more or better sites for precipitation than does the glass surface, the specific rate of precipitation² on the glass is much less than that on the scale, so k_1 is negligible compared to k_2 . Under the conditions just described, Eq. 0.6 becomes

$$F([\text{Ca}^{++}]_f - [\text{Ca}^{++}]_e) = k_2V(A_{g,o} - A_g)[\text{Ca}^{++}]_e^2 \quad (0.7)$$

The area of glass surface is assumed to decrease at a rate proportional both to the area of glass that remains, and to the concentration product

¹In fact, the CaCO_3 precipitate is not a uniform covering but is highly porous or has protruding crystallites distributed at random. Accordingly, its surface area is much greater than that given by Eq. 0.5. However, the area A_s may be considered to be proportional to $(A_{g,o} - A_g)$ with the proportionality factor included in the constant k_2 . Thus the formulation which follows is unaffected.

²Here, specific rate means rate per unit area of surface, gm $\text{CaCO}_3/\text{cm}^2 \text{ sec}$

$[Ca^{++}]_e [CO_3^{=}]_e$, as depicted by Eq. 0.8. However, in the experiments

$$dA_g/dt = -k_3 A_g [Ca^{++}]_e [CO_3^{=}]_e \quad (0.8)$$

reported here, $[Ca^{++}]_e [CO_3^{=}]_e$ varies but slowly and by only a factor of five while A_g varies over two orders of magnitude. Consequently, the percentage change in $[Ca^{++}]_e [CO_3^{=}]_e$ is much less rapid than that of A_g , and, as a first approximation, Eq. 0.8 may be written as

$$dA_g/dt = -k_3 \{ [Ca^{++}]_e [CO_3^{=}]_e \}_{avg} A_g \quad (0.9)$$

where $\{ [Ca^{++}]_e [CO_3^{=}]_e \}_{avg}$ = the average value of the concentration product during the experiment. Eq. 0.9 may be integrated to give

$$\ln(A_g/A_{g,o}) = -k_3 \{ [Ca^{++}]_e [CO_3^{=}]_e \}_{avg} t \quad (0.10)$$

or

$$A_g = A_{g,o} \exp(-k_3 \{ [Ca^{++}]_e [CO_3^{=}]_e \}_{avg} t) \quad (0.11)$$

Using Eq. 0.11 in Eq. 0.7 yields

$$F([Ca^{++}]_f - [Ca^{++}]_e) = k_2 V A_{g,o} [Ca^{++}]_e^2 (1 - \exp\{-k_3 [Ca^{++}]_e [CO_3^{=}]_e \}_{avg} t\}) \quad (0.12)$$

Upon rearranging Eq. 0.12,

$$\frac{[Ca^{++}]_f - [Ca^{++}]_e}{[Ca^{++}]_e^2} = k_2 (V/F) A_{g,o} (1 - \exp(-Kt)) \quad (0.13)$$

where

$$K = k_3 ([Ca^{++}]_e [CO_3^{=}]_e)_{avg} \quad (0.14)$$

The value of k_2 can be determined experimentally by considering the asymptotic limit which $[Ca^{++}]_e$ approaches as t approaches infinity. Let that limit be designated $[Ca^{++}]_{e,\infty}$. Then as $t > \infty$, Eq. 0.13 becomes

$$\frac{[Ca^{++}]_f - [Ca^{++}]_{e,\infty}}{[Ca^{++}]_{e,\infty}^2} \rightarrow k_2 (V/F) A_{g,o} \quad (0.15)$$

Once a value for k_2 is known, Eq. 0.13 can be tested by rearranging it into the form of Eq. 0.16

$$\frac{1}{k_2(V/F)A_{g,o}} \left(\frac{[Ca^{++}]_f - [Ca^{++}]_e}{[Ca^{++}]_e^2} \right) = 1 - \exp(-Kt) \quad (0.16)$$

Alternately, Eq. 0.16 may be written,

$$\ln \left\{ 1 - \frac{1}{k_2(V/F)A_{g,o}} \left(\frac{[Ca^{++}]_f - [Ca^{++}]_e}{[Ca^{++}]_e^2} \right) \right\} = -Kt \quad (0.17)$$

Thus, if the model fits the experimental data, the data will yield a straight line when plotted in the form given by Eq. 0.17. And the rate constant k_3 can be determined by the slope of that line using Eq. 0.14.

APPENDIX P

Computer Simulation for Predicting the Production History of an Oil Well During a CO₂ Flood Accompanied by Formation Damage

PART ONE. MATHEMATICAL MODEL

Introduction--The following describes the parameters and calculation procedure employed in the computer simulation of an oil field undergoing a CO₂ flood. It is presumed that, during the flood, the reservoir permeability is decreasing because of CaCO₃ deposition near the producing well. Because CaCO₃ deposition at a given point does not begin until the carbonated brine reaches that point, and because the most crucial region is at the producing well, it is reasonable to assume that significant damage does not begin to occur until the carbonated brine breaks through.

The following presents a sample calculation, in detail. A listing of the FORTRAN program is presented as Fig. P.2

I. Given: (References: 23,24)

Producing well centered at location, $r = 0$

Radius of wellbore, $r_w = 0.5$ ft

Pressure in wellbore, $p_w = 300$ psig

Reservoir thickness, $H = 20$ ft

Initial permeability to brine, $k_o = 1.94$ mD*

Initial porosity, $\phi_o = 0.0393$

Radius of drainage, $r_d = 500$ ft

Pressure at r_d , $p_d = 4000$ psig

Reservoir temperature, $T = 130^\circ\text{F}$ (54°C)

*Assumed to be one-tenth the absolute permeability of reservoir rock.

Viscosity of brine, $\mu = 0.65$ cP

Salinity = 7.9% (wt) NaCl (1.35 mol/liter)

- II. Wanted: a. Initial flow rate, Q_0
b. Initial concentration profile of Ca^{++}
c. Deposition of CaCO_3 , during first hour, as function of distance.
d. Change in permeability with position r .
e. Flow rate Q at end of first hour.
- III. Basis: Reservoir thickness $h = 1$ ft (30.48 cm); one-hour time increments, during which pseudo-steady-state conditions are assumed to apply.

IV. Assumptions:

- a. Breakthrough of Ca^{++} -saturated water has occurred at producing well. This event occurs at time $t=0$ in this model.
- b. Water behind oil front is saturated with respect to CaCO_3 at reservoir temperature and local pressure, i.e., $[\text{Ca}^{++}] = f(P,T)$.
- c. Reservoir temperature is constant with respect to time and position.
- d. Enough injection wells are located about 1000 ft from the producing well that reservoir pressure and water (brine) flow are cylindrically symmetric about the producing well. Thus, the only independent variables of concern are radial distance r and time t .
- e. Total flow of water Q into any circle surrounding the well at distance r varies with time, but is independent of r ; thus,

$$Q = 2\pi rhq \quad (1)$$

where $q =$ water flux, ft^3/ft^2 day

- f. Pressure at radius of drainage remains constant with time.
g. Pressure at wellbore remains constant with time.

- h. Time intervals are short enough that pressure profile, porosity and permeability may be assumed constant during the interval.
- i. The gas phase contains 10 mol % hydrocarbon vapor on dry basis; so

$$P = P_{CO_2} + P_{HC} + P_{H_2O} \quad (2a)$$

$$= P_{CO_2} + (1/9) P_{CO_2} + P_{H_2O} \quad (2b)$$

where P_{CO_2} , P_{HC} and P_{H_2O} are the partial pressures of CO_2 , hydrocarbons and H_2O , respectively, and P is the total pressure.

V. Solution:

A. Initial Flow of Brine

$$Q = (2\pi k_o h / \mu) (p_d - p_w) / \ln(r_d / r_w) \quad (3a)$$

$$Q = \frac{2\pi(0.00194) \text{ (cm}^3\text{/sec)(cP)} \cdot 30.48\text{cm}}{0.65 \text{ cP (cm}^2\text{) (atm/cm) ln(1000)}} (251.7 \text{ atm}) = \frac{20.8 \text{ cm}^3}{\text{sec}} \quad (3b)$$

In alternate units

$$Q = 2.65 \text{ ft}^3\text{/hr} \quad \text{or} \quad 11.3 \text{ bbl/day} \quad (4)$$

B. Pressure Profile Before Damage Begins

The differential form of Eq. 3 is

$$Q = [k_o (2\pi r h) / \mu] dP / dr \quad (5)$$

Integration of Eq. 5 over the limits (0.5, 300) to (r, P) while recognizing k_o is a constant at $t = 0$, gives (after rearrangement)

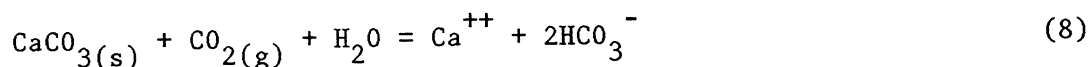
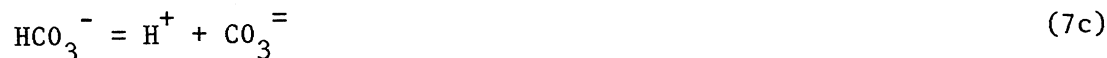
$$P = Q\mu \ln(r/r_w) / (2\pi k_o h) + p_w \quad (6)$$

C. Concentration Profile

C.1 Approach to Problem

Clearly, the concentration of Ca^{++} in solution is expected to be

pressure-dependent, because of the equilibria depicted by Eq. 7 and 8:



The solubility of CO_2 is assumed to obey Henry's law. In the present derivation (see footnote)

$$\alpha(\text{H}_2\text{CO}_3^*) = H p_{\text{CO}_2} \quad (9)$$

where H is Henry's constant,

p_{CO_2} is the partial pressure of CO_2 , psi,

$\alpha(\text{H}_2\text{CO}_3^*)$ is the sum of the activities of aqueous CO_2 and the true carbonic acid, H_2CO_3 .

The solutions are far from ideal, because the brine has 7.9% NaCl. Consequently the equilibrium constants associated with Eq. 7-9 (K_1 , K_2 , K_{sp} , H) must be corrected for ionic strength. Similarly, because of the high pressures and elevated temperature, the equilibrium constants must be considered functions of T and P as well.

The derivation of an expression for Ca^{++} concentration begins with the definition of the solubility product K_{sp} . The result is an equation in terms of the partial pressure of CO_2 , the mean activity coefficient for Ca^{++} , and 4 equilibrium constants. The latter are expressed as polynomials having ionic strength, temperature and total pressure as independent variables.

The more conventional symbol for the activity is $\alpha_{\text{H}_2\text{CO}_3^}$

C.2 Derivation of Concentration Expression

The solubility product K_{sp} for CaCO_3 is defined as

$$K_{sp} = \alpha(\text{Ca}^{++})\alpha(\text{CO}_3^{=}) \quad (10)$$

where $\alpha(\text{Ca}^{++})$ and $\alpha(\text{CO}_3^{=})$ are the activities of the calcium and carbonate ions, respectively, at equilibrium.

An expression for $\alpha(\text{CO}_3^{=})$ is developed as follows:

The second equilibrium constant for carbonic acid (see Eq. 7c) is

$$K_2 = \alpha(\text{CO}_3^{=})\alpha(\text{H}^+)/\alpha(\text{HCO}_3^{-}) \quad (11)$$

Thus,

$$\alpha(\text{CO}_3^{=}) = K_2\alpha(\text{HCO}_3^{-})/\alpha(\text{H}^+) \quad (12)$$

An expression for $\alpha(\text{H}^+)$ can be obtained from the first apparent equilibrium constant for carbonic acid (see Eq. 7b):

$$K_1 = \alpha(\text{H}^+)\alpha(\text{HCO}_3^{-})/\alpha(\text{H}_2\text{CO}_3^*) \quad (13)$$

From Eq. 13

$$\alpha(\text{H}^+) = K_1\alpha(\text{H}_2\text{CO}_3^*)/\alpha(\text{HCO}_3^{-}) \quad (14)$$

Substituting the above result for $\alpha(\text{H}^+)$ into Eq. 12 gives

$$\alpha(\text{CO}_3^{=}) = K_2\{\alpha(\text{HCO}_3^{-})\}^2/[K_1\alpha(\text{H}_2\text{CO}_3^*)] \quad (15)$$

The activity of carbonic acid, $\alpha(\text{H}_2\text{CO}_3^*)$, can be eliminated by substituting Eq. 9 into Eq. 15, giving the desired intermediate result:

$$\alpha(\text{CO}_3^{=}) = K_2\{\alpha(\text{HCO}_3^{-})\}^2/(K_1\text{Hp}_{\text{CO}_2}) \quad (16)$$

Returning to Eq. 10, and using the result of Eq. 16, the expression for K_{sp} becomes

$$K_{sp} = \alpha(\text{Ca}^{++})K_2\{\alpha(\text{HCO}_3^-)\}^2/(K_1\text{H}_p\text{CO}_2) \quad (17)$$

Finally, to get an expression in terms of calcium concentration $[\text{Ca}^{++}]$, we replace activity by the product of concentration and activity coefficient:

$$\alpha(\text{HCO}_3^-) = \gamma_{\pm}[\text{HCO}_3^-] \quad (18)$$

$$\alpha(\text{Ca}^{++}) = \gamma_{\pm}[\text{Ca}^{++}] \quad (19)$$

where γ_{\pm} is the mean activity coefficient for $\text{Ca}(\text{HCO}_3)_2$ and the brackets denote molar concentration.

Substituting Eqs. 18 and 19 into Eq. 17 gives

$$K_{sp} = \gamma_{\pm}[\text{Ca}^{++}](\gamma_{\pm}[\text{HCO}_3^-])^2K_2/(K_1\text{H}_p\text{CO}_2) \quad (20)$$

Because the equilibria depicted by Eqs. 7a and 7b lie so far to the right, and because the solubility product of CaCO_3 is so small compared to that of $\text{Ca}(\text{HCO}_3)_2$, the vast majority of carbonate species are bicarbonate HCO_3^- . Concentrations of $\text{CO}_2(\text{aq})$, H_2CO_3 and $\text{CO}_3^{=}$ are negligible by comparison.

For the final step of this derivation, we note that each ion of Ca^{++} which derives from CaCO_3 requires 2 moles of HCO_3^- be formed (in accord with the stoichiometry depicted by Eq. 8). Thus we may relate bicarbonate concentration to that of calcium by Eq. 21.

$$[\text{HCO}_3^-] = 2[\text{Ca}^{++}] \quad (21)$$

Substituting Eq. 21 into Eq. 20 and solving for $[\text{Ca}^{++}]$ gives the desired final result.

$$K_{sp} = \gamma_{\pm}^3 4[\text{Ca}^{++}]^3K_2/p_{\text{CO}_2}K_1\text{H} \quad (22)$$

or

$$[\text{Ca}^{++}] = \{p_{\text{CO}_2}K_1\text{H}K_{sp}/4K_2\}^{1/3}/\gamma_{\pm} \quad (23)$$

C.3 Partial Pressure of CO₂

Because CaCO₃ does not begin to precipitate until the pressure is reduced and HCO₃ decomposes to CO₂ and H₂O, we assume gaseous CO₂ is present, and in accord with Eq. 2

$$p_{\text{CO}_2} = 0.9(P - p_{\text{H}_2\text{O}}) \quad (24)$$

Using this result in Eq. 23 gives

$$[\text{Ca}^{++}] = [0.9(P - p_{\text{H}_2\text{O}})K_1H K_{\text{sp}}/(4K_2)]^{1/3}/\gamma_{\pm} \quad (25)$$

The partial pressure of water can be estimated by comparing the 8% brine solution to a Na₂CO₃ solution for which vapor pressure data are available. A 8% brine solution is equivalent (on a molar ionic basis) to a 10% Na₂CO₃ solution:

$$\frac{8 \text{ g NaCl}}{100 \text{ g soln}} \times \frac{2 \text{ moles ions}}{58.5 \text{ g NaCl}} \times \frac{106 \text{ g Na}_2\text{CO}_3}{3 \text{ moles ions}} = \frac{10 \text{ g Na}_2\text{CO}_3}{100 \text{ g soln}}$$

Reference 17 gives the following for Na₂CO₃ solutions at 130°F (54°C), (after interpolation on temperature):

Table P.1 Vapor Pressure of Water Above Solutions of NaCl and Na₂CO₃ at 54°C (Ref. 17)

Concentration, wt. %		Vapor Pressure	
Na ₂ CO ₃	NaCl	mm Hg	psi
5	4.2	115	2.22
10	8.4	112.5	2.17
15	12.6	110	2.13

Thus, for a 7.9% NaCl solution,

$$P_{H_2O} = 2.2 \text{ psi} \quad (26)$$

and Eq. 25 becomes

$$[Ca^{++}] = [0.9(P - 2.2)K_1 H K_{sp} / (4K_2)]^{1/3} / \gamma_{\pm} \quad (27)$$

C.4 Expressions for Equilibrium Constants

Oddo and Tomson (15) developed polynomials relating the equilibrium constants to temperature (T), pressure (P) and ionic strength (I):

$$\begin{aligned} -\log K_1 = & 6.41 - 1.594 \times 10^{-3}T + 3.52 \times 10^{-6}T^2 \\ & - 3.07 \times 10^{-5}P - 0.4772 \sqrt{I} + 0.1180 I \end{aligned} \quad (28)$$

$$\begin{aligned} -\log K_2 = & 10.61 - 4.97 \times 10^{-3}T + 1.331 \times 10^{-5}T^2 \\ & - 2.624 \times 10^{-5}P - 1.166 \sqrt{I} + 0.3466 I \end{aligned} \quad (29)$$

$$\begin{aligned} -\log K_{sp} = & 7.82 + 6.46 \times 10^{-3}T + 8.59 \times 10^{-6}T^2 \\ & - 7.00 \times 10^{-5}P - 3.21\sqrt{I} + 1.073 I \end{aligned} \quad (30)$$

$$-\log H = 2.27 + 5.65 \times 10^{-3}T - 8.06 \times 10^{-6}T^2 + 0.075 I \quad (31)$$

Note: T is in °F, P is in psi, and I is in molar units.

Equations 28-31 may be combined by addition or subtraction to give

$$\begin{aligned} -\log (K_1 K_{sp} H / K_2) = & 5.89 + 1.5486 \times 10^{-2}T \\ & - 9.26 \times 10^{-6}T^2 - 7.446 \times 10^{-5}P \\ & - 2.5212\sqrt{I} + 0.9194 I \end{aligned} \quad (32a)$$

For a temperature of 130°F, this equation simplifies further to

$$\begin{aligned} -\log(K_1 K_{sp} H / K_2) = & 7.74669 - 7.446 \times 10^{-5}P \\ & - 2.5212\sqrt{I} + 0.9194 I \end{aligned} \quad (32b)$$

When Eq. 32 is used in conjunction with Eq. 27, only the activity coefficient γ_{\pm} remains unknown.

C.5 Estimation of Mean Activity Coefficient, γ_{\pm}

Stokes and Robinson (16) have developed an expression which considers the effect of ionic strength up to 2.0 molar and accounts for hydration of the ions. For an aqueous solution at 25°C,

$$\log \gamma_{\pm} = - \frac{0.5115 |z_1 z_2| \sqrt{I}}{1 + 0.3291 \sqrt{I} \left\{ \left[\frac{3}{4\pi} (30h + V_1) \right]^{1/3} + r_2 - \Delta \right\}} - \frac{h}{v} \log a_w - \log[1 - 0.018(h - v)m] \quad (33)$$

$Z_1 = +2$ charge on cation

$Z_2 = -1$ charge on anion

$\Delta = 1.3 \text{ \AA}$ penetration distance for 2:1 salts

$v = 3$ number of moles of ions formed from 1 mole of electrolyte

$m =$ moles solute per kg of solvent

$a_w =$ activity of water

$r_2 =$ crystal radius of anion, \AA

$h =$ hydration number

$V_1 =$ apparent molal volume of the cation (Ca^{++}) in \AA^3

The crystal radius r_2 of the anion, HCO_3^- , was taken to be 2.2\AA .

This is consistent with the atomic radius of oxygen (0.66\AA) and the carbon-oxygen bond distances (C-O is 1.4\AA , C=O is 1.2\AA).

The ionic radius for Ca^{++} is typically 1.0\AA . Accordingly 0.52\AA^3 was used as an approximation of V_1 .

For calcium halides, the hydration number, h , varies between 12 and 17 (16). Using the average (14.5) gives

$$30h + V_1 = 435$$

The activity of water, a_w , in 1.4 molal NaCl is 0.953 at 25°C (16). The activity is not sensitive to changes in temperature over small ranges. The effect can be estimated using Equation 34 and assuming $\Delta\bar{G}^{\text{ex}}$ is constant

$$\gamma_{\text{water}} = \exp[\Delta\bar{G}^{\text{ex}}/RT] \quad (34)$$

where $\Delta\bar{G}$ is the molar excess Gibbs free energy

R is the ideal gas law constant

T is the temperature (absolute scale)

At 130°F (327 K), the activity is estimated by Eq. 34 to be 0.957. The mean value (0.955) was used for a_w in all subsequent calculations.

Using the above results for r_2 , V_1 , h and a_w in Eq. 33 gives

$$\log \gamma_{\pm} = - \frac{0.5115 |2(-1)| \sqrt{I}}{1 + 0.3291 \sqrt{I} \{ [103.8A^3]^{1/3} + 2.2\text{\AA} - 1.3\text{\AA} \}} - 4.833(0.0200) - \log [1-0.018(11.5 \cdot m)] \quad (35)$$

$$\log \gamma_{\pm} = - \frac{1.023 \sqrt{I}}{1 + 1.843 \sqrt{I}} + 0.0967 - \log [1-0.207 \cdot m] \quad (36)$$

If one assumes that NaCl and $\text{Ca}(\text{HCO}_3)_2$ are the only solutes present in significant amount, the ionic strength is given by Eq. 37a.

$$I = 1/2([\text{Na}^+](+1)^2 + [\text{Cl}^-](-1)^2 + [\text{Ca}^{++}](+2)^2 + [\text{HCO}_3^-](-1)^2) \quad (37a)$$

The concentration of Na^+ is assumed to equal that of Cl^- . Furthermore, if Eq. 21 may be used to relate $[\text{HCO}_3^-]$ to $[\text{Ca}^{++}]$, Equation 37 may be further simplified to

$$I = [\text{Na}^+] + 3[\text{Ca}^{++}] \quad (37b)$$

C.6 Iterative Calculation of $[Ca^{++}]$

Because ionic strength I and molality m depend on the Ca^{++} concentration $[Ca^{++}]$ which is initially unknown, the activity γ_{\pm} must first be estimated. Then γ_{\pm} must be corrected after $[Ca^{++}]$ is computed. The procedure is

- (1) Assume a value for $[Ca^{++}]$.
- (2) Calculate m and I .
- (3) Compute γ_{\pm} using Eq. 36.
- (4) Compute $[Ca^{++}]$ using Eqs. 32 and 27.
- (5) Return to Step (2) and use this improved estimate of $[Ca^{++}]$ to calculate m and I .
- (6) Repeat procedure thru step 5 until $[Ca^{++}]$ and γ_{\pm} do not change.

In practice, this is a tedious process only for the initial position r_w and its corresponding pressure. For subsequent positions (r) and increments (Δr), the first trial value for $[Ca^{++}]$ is the value of $[Ca^{++}]$ calculated for the preceding position increment. A sample calculation follows.

C.7 Calculation of Calcium Concentration

Objective: Calculate $[Ca^{++}]$ at $r_w = 0.5$ ft

$P = 300$ psig and $T = 130^{\circ}F$

The initial guess for $[Ca^{++}]$ will be 0.1 M. Ionic strength

(by Eq. 37), is

$$I = 1.35 + 3(0.1) = 1.65 \text{ M}$$

The concentration of 0.1 M $Ca(HCO_3)_2$ may be expressed in molal units (mol/kg H_2O) by assuming the density of these solution varies with concentration (wt%) in the same manner as $CaCl_2$ solutions do. Data for $CaCl_2$ solutions are available (17). This predicted dependence is shown in Fig.

P.1. Thus, 0.10 mol/l corresponds to approximately 0.10 molal.

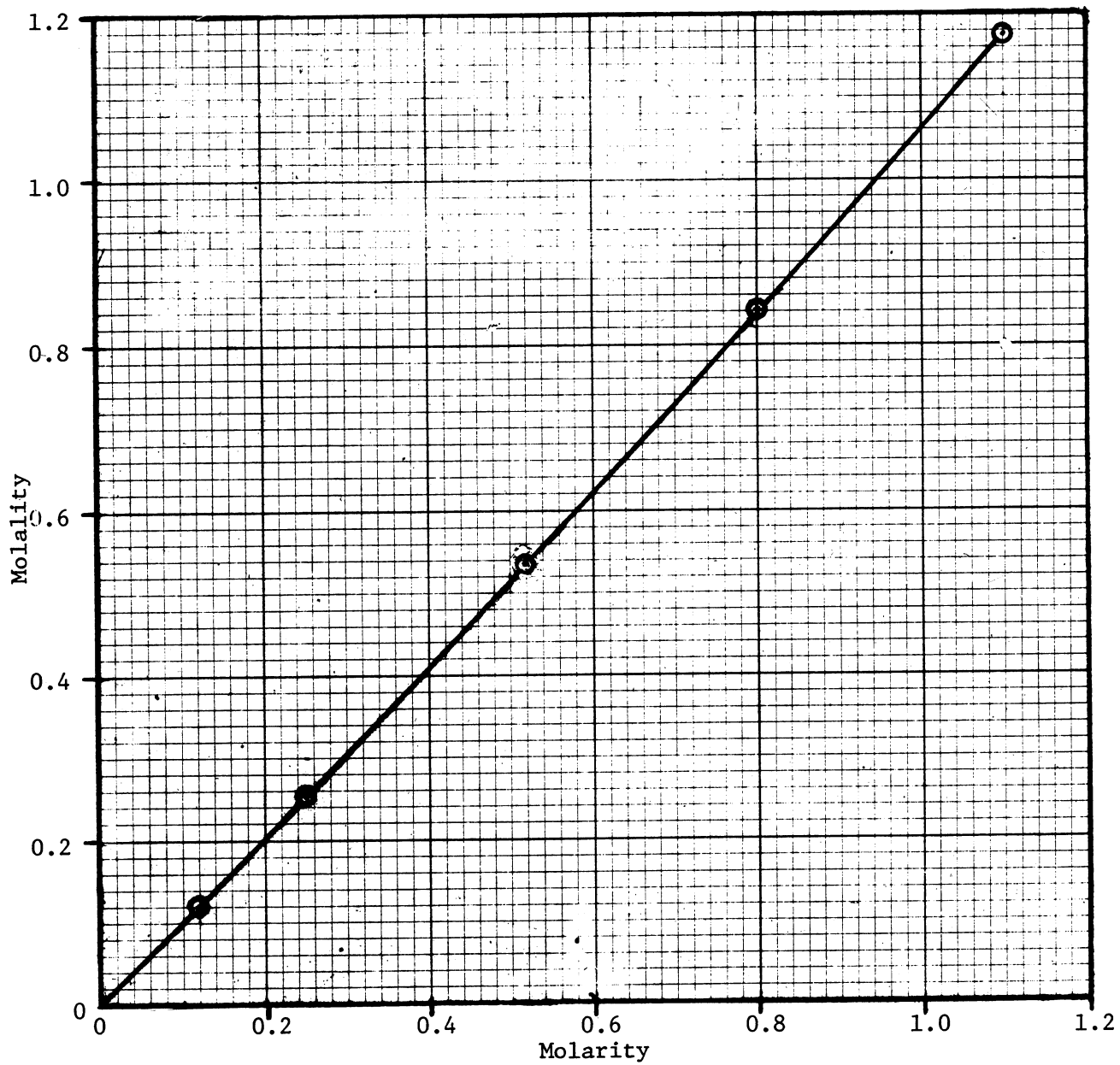


Figure P.1. Conversion of Molarity (mol/l) to Molality (mol/1000g H_2O) for $\text{Ca}(\text{HCO}_3)_2$ Solutions at 60°C

Using Eq. 36 to calculate the activity coefficient,

$$\log \gamma_{\pm} = \frac{-1.023 \sqrt{1.65}}{1 + 1.843 \sqrt{1.65}} + 0.0967 - \log[1 - 0.207(0.10)] \quad (38a)$$

$$\log \gamma_{\pm} = -0.3902 + 0.0967 + 0.0091 = -0.2844 \quad (38b)$$

$$\gamma_{\pm} = 0.5195 \quad (39)$$

Using Eq. 32,

$$-\log \left(\frac{K_1 K_{sp} H}{K_2} \right) = 7.446 \times 10^{-5} \cdot (314.7)$$

$$-2.5212 \sqrt{1.65} + 0.9194(1.65) \quad (40)$$

$$K_1 K_{sp} H / K_2 = 9.963 \times 10^{-7} \quad (41)$$

Using the results of Eqs. 39 and 41 in Eq. 27:

$$[Ca^{++}] = [(0.9/4)(314.7 - 2.2)(9.954 \times 10^{-7})]^{1/3} / 0.5195 = 0.0794 \text{ M} \quad (42)$$

For the second guess, use $[Ca^{++}] = 0.080 \text{ M}$ and $m = 0.080$.

Proceeding as above,

$$I = 1.590 \quad (43a)$$

$$\gamma_{\pm} = 0.5198 \quad (43b)$$

$$K_1 K_{sp} H / K_2 = 9.86 \times 10^{-7} \quad (43c)$$

$$\text{and } [Ca^{++}] = 0.07903 \text{ M} \quad (44)$$

After two more iterations, the result is reliable to 5 figures.

$$[Ca^{++}] = 0.079015 \text{ M} \quad (45)$$

C.7 Calcium Concentration at Positions within Reservoir

At $r = 1.0 \text{ ft}$

Because of the repetitive nature of this calculation, only that for the first position increment ($r = 1.0 \text{ ft}$) will be shown here. From Eq. 6, using $Q = 20.83 \text{ cm}^3/\text{sec}$

$$P(1.0 \text{ ft}) = \frac{20.83 \text{ cm}^3(0.65 \text{ cP})\ln(1 \text{ ft}/0.5 \text{ ft})}{\sec(2\pi)(.00194 \text{ D})(30.48 \text{ cm})} + 21.41 \text{ atm} \quad (46)$$

The units associated with 1 Darcy are consistent with those in the above expression when pressures are in atmospheres. Thus

$$\begin{aligned} P(1.0 \text{ ft}) &= 25.26 \text{ atm} + 21.41 \text{ atm} \\ &= 46.67 \text{ atm} (686.0 \text{ psia}) \end{aligned} \quad (47)$$

Using the above value for P, and taking 0.079 M as the first estimate of $[\text{Ca}^{++}]$, we find (after four iterations):

$$[\text{Ca}^{++}] = 0.1053 \quad (48)$$

At other locations

Using Eq. 6 to estimate pressures and proceeding as shown above, the Ca^{++} concentrations at other locations were found to be as listed in Table P.2.

Table P.2 Calcium Concentration Profile
Before CaCO_3 Deposition Begins

Distance from Center of Producing Well, ft	Pressure psia	$[\text{Ca}^{++}]$ mol/l
0.5	314.7	0.0790
1.0	685.	0.1053
4.0	1369.	0.1410
16.0	2171.	0.1693
64.0	2914.	0.1948
128.	3285.	0.2070
256.	3656.	0.2189
500.	4015.	0.2300

C.8 Deposition of CaCO_3 During First Hour

If we denote the decrease in Ca^{++} concentration over increment i by $\Delta[\text{Ca}^{++}]_i$, the volume of precipitate which forms in that increment is

$$V = \Delta[\text{Ca}^{++}]_i \times Q \times 100 \times 1 \text{ day} / \rho_{\text{CaCO}_3} \quad (49)$$

where Q is the volumetric flow rate of brine, cm³/sec

100 is the molecular weight of CaCO₃

ρ is the density of CaCO₃, 2.71 g/cm³

Δ[Ca⁺⁺]_i is the concentration change, mol/l

Using numerical values for the first increment

$$V(\text{precipitate}) = (0.1053 - 0.0790) \text{ mol/liter} \times$$

$$\frac{100 \text{ g}}{\text{mol}} \frac{\text{cm}^3}{2.71 \text{ g}} \frac{3.532 \times 10^{-5} \text{ ft}^3}{\text{cm}^3} \frac{20.8 \text{ cm}^3}{\text{sec}} \frac{3600 \text{ sec}}{\text{hr}} \frac{\text{liter}}{10^3 \text{ cm}^3}$$

$$V(\text{precipitate}) = 0.00257 \text{ ft}^3 \quad (50)$$

The volume of reservoir within the ith increment

$$V(\text{reservoir}) = \pi(R_i^2 - R_{i-1}^2)h \quad (51)$$

Using numerical values for the first increment

$$V(\text{reservoir}) = \pi(1.0^2 - 0.5^2)\text{ft}^2 \times (1.0 \text{ ft}) = 2.356 \text{ ft}^3 \quad (52)$$

D. Change in Porosity and Permeability

D.1 Introduction

Because the change in calcium concentration is greatest at the wellbore, precipitation and, hence, damage is greatest there. Using the previously-obtained value for the volume of precipitate (Eq. 50), the change in porosity and then the change in permeability can be calculated.

D.2 Porosity at Wellbore

Between $r = 0.5 \text{ ft}$ and $r = 1.0 \text{ ft}$,

$$\text{Porosity decrease, } \Delta\phi_1 = \frac{V(\text{precipitate})}{V(\text{reservoir})} = \frac{2.57 \times 10^{-3} \text{ ft}^3}{2.356 \text{ ft}^3}$$

$$\Delta\phi_1 = 1.09 \times 10^{-3} \quad (53)$$

Porosity 1 hour after breakthrough, in first increment,

$$\phi_1 = \phi_0 - \Delta\phi_1 = 0.0393 - 0.00109 = 0.0382 \quad (54)$$

D.3 Permeability, k

Experimental results showed that k varies with the square of porosity.

We assumed

$$k = (k_o/\phi_o^2)\phi^2 \quad (55)$$

so the permeability 1 hour after breakthrough

$$k_1 = (1.94 \text{ mD}/0.0393^2) \times 0.0382^2 = 1.83 \text{ mD} \quad (56)$$

D.4 Porosity and Permeability at Other Locations

In an analogous fashion ϕ , and k_1 are computed for all positions in the reservoir, using Eq. 53-56.

E. Brine Flow

The flow Q is obtained by integrating Eq. 5, but now it must be done numerically because permeability is not constant with position, i.e.

$$k_1 = f(r) \quad (57)$$

Rearranging Eq. 5 and indicating the required integration

$$Q_1 \int_{r_w}^{r_d} \frac{dr}{rk_1} = \frac{2\pi h}{\mu} \int_{P_w}^{P_d} dp = (2\pi h/\mu) (P_d - P_w) \quad (58)$$

where the subscript 1 indicates conditions after 1 hour. Solving Eq. 58 for Q_1 gives

$$Q_1 = \frac{2\pi h}{\mu} (P_d - P_w) / \int_{r_w}^{r_d} \frac{dr}{rk_1} \quad (59)$$

The integral is evaluated using a computer. (See Fig. P.2 for a listing of the program.)

F. Subsequent Calculations

Once Q_1 has been calculated, the pressure profile can be obtained from Eq. 60, which can be derived from Eq. 58, when the integrals are written as indefinite integrals:

$$Q_1 \int_{r_w}^r \frac{dr}{rk_1} = \frac{2\pi h}{\mu} \int_{P_w}^P dp = (2\pi h/\mu) (P - P_w) \quad (60a)$$

After rearranging Eq. 60a,

$$P = \frac{Q_1}{2\pi h/\mu} \int_{r_w}^r \frac{dr}{rk_1} - P_w \quad (60b)$$

As before, the integral is evaluated numerically using the computer program.

With the pressure profile established, the concentration of Ca^{++} can be calculated at each location, as can the volume of $CaCO_3$ precipitate deposited during the second hour. The reduction in porosity and permeability are calculated as before, and, by repetition, the flow Q is calculated for subsequent hours.

PART TWO. STRUCTURE OF COMPUTER PROGRAM

The computational sequence is outlined below. The program, in FORTRAN code, is listed in Fig. P.2.

FIRST, CALCULATE INITIAL CONDITIONS (t = 0 hr)

Input: C_{NaCl} , T, r_{well} , r_{drainage} , k_o , ϕ_o , $P(r_{\text{drain}})$, $P(r_{\text{well}})$

A. Boundary Conditions $R_o = r_{\text{well}}$

1. Total flow Q_1 during first hour (from Darcy's eq.)
2. Pressure, $P_{R_o} = P(r_{\text{well}})$
3. Calcium concentration at R_o

(Use subroutine. Take 0.1M as first guess.)

B. Distances at Which the Reservoir Properties Will Be Evaluated

1. Increments are very small (ca. 0.1 ft) near the well ($r=0$), becoming large as distance increases.
2. Calculate reservoir volume associated with each increment.

$$V(\text{reservoir})_i = \pi(R_i^2 - R_{i-1}^2)h$$

C. Calculate Pressure Profile

$$P(R_i) = Q\mu \ln(R_i/R_o)/(2\pi k_o h) + P(R_o)$$

SECOND, CALCULATE CHANGES IN RESERVOIR, HOUR-BY-HOUR, $j=1, 2, \dots$

A. Calculate Profile of Ca^{++} Concentration

Use subroutine. Take $[\text{Ca}^{++}]$ at R_0 as first guess.

B. Calculate Volume of CaCO_3 Precipitate in Increment i .

$$V_{R_i} = Q_0(1 \text{ hr})\{[\text{Ca}^{++}]_{R_i} - [\text{Ca}^{++}]_{R_{i-1}}\}(\text{m.w. of CaCO}_3)/\rho_{\text{CaCO}_3}$$

C. Calculate Porosity at End of Hour j

$$\phi_{R_i, \text{day } j} = \phi_{r_{i,j}} - V_{R_i, \text{day } j} / \phi_0 V(\text{reservoir})$$

(ϕ_0 represents original porosity of reservoir;)

D. Calculate Permeability at R_{ij} at End of Hour j

$$k(R_{i,j}) = (k_0/\phi_0^2)\phi^2$$

E. Calculate Flow Q_j Using Numerical Integration Over Increments

1. Calculate $\Delta r_i / (r_i k(R_i))$ where $k(R_i)$ is permeability at R_i

2. Add this result to growing sum

3. Record this sum in SUM(I) for each i

4. Return to step 1 and repeat for all increments i

5. $Q_j = (P_{R_d} - P_{R_0})(2\pi h/\mu)/\text{SUM}(N)$

F. Calculate Pressure Profile at End of Hour j

$$P_{R_i} = P_{R_d} - P_{R_0} \cdot \frac{\text{SUM}(I)}{\text{SUM}(N)} + P_{R_0}$$

G. Increment the Hour Count (j) by One and Return to Step A in This Section.

(Repeat calculations for as many hours as desired.)

Figure P.2
 FORTRAN COMPUTER PROGRAM
 Prepared by P. F. Phelan

```

0001 FTN7,L
0002 C
0003 C ***** DEFINITION OF FUNCTIONS *****
0004 C
0005 C
0006 C     FUNCTION P(Q, R, PERM, H)
0007 C     RWELL = 0.5
0008 C     P = Q * 0.65 * ALOG(R/RWELL) / (6.2831853 * PERM * H) + 21.4
0009 C     RETURN
0010 C     END
0011 C
0012 C
0013 C
0014 C ***** DEFINITIONS OF SUBROUTINES *****
0015 C
0016 C     BLOCK DATA
0017 C     REAL KINIT, MU, NACL
0018 C     COMMON/ WELL /RWELL, RDRAIN, PDRAIN, KINIT, MU, PHI0
0019 C     COMMON/CONST2/ NACL, MAX, T, PWELL
0020 C

0021 C
0022 C     DATA RWELL, RDRAIN, PWELL, PDRAIN/ .5, 500., 314.7, 4014.7/
0023 C     DATA KINIT, MU, NACL, PHI0/ 1.94E-03, 0.65, 1.35, 0.0393/
0024 C     DATA MAX/ 28 /
0025 C     DATA T / 130./
0026 C     END
0027 C
0028 C
0029 C
0030 C     SUBROUTINE CALCUM(J)
0031 C
0032 C     REAL NACL, IDNIC(30), LOGRAT
0033 C     DIMENSION CA(30,40), PSI(30,40), GAMM(30), R(30)
0034 C     COMMON/CONST1/ CAO, H
0035 C     COMMON/CONST2/ NACL, MAX, T, PWELL
0036 C     COMMON/BLOCK1/ CA, / BLOCK2/ PSI, /BLOCK3/ R
0037 C
0038 C     DO 500 I = 1, MAX
0039 C
0040 C
0041 C
0042 C     GET INITIAL ESTIMATE OF CALCIUM CONC'N AT POSITION I
0043 C     TAKE CA CONC'N IN PRECEDING INCREMENT AS APPROX TO CA(I)
0044 C     BUT ADJUST FOR CHANGE IN PRESSURE
0045 C     IF (I .GT. 1) GO TO 303
0046 C     CA(1,J) = CAO * (PSI(1,J)/PWELL) ** 0.3333333
0047 C     GO TO 305
0048 C
0049 C     303 CA(I,J) = CA(I-1,J) * (PSI(I,J)/PSI(I-1,J)) ** .3333333
0050 C     305 CONTINUE
0051 C
0052 C     WRITE(6,106) I, CA(I,J)
0053 C

```

```

0054 C
0055 C ENTER ITERATIVE CALCULATION OF CA(I) HERE, BUT FIRST,
0056 C
0057 C
0058 350 DO 400 M = 1, 3
0059 C
0060 C     CALC. IONIC STRENGTH
0061 C     IONIC(I) = NACL + 3.* CA(I,J)
0062 C     ROOTI = SQRT(IONIC(I))
0063 C
0064 C     CALC. THE MEAN ACTIVITY COEFFICIENT
0065 C     ARATIO = 1.023 * ROOTI / (1. + 1.843*ROOTI)
0066 C
0067 C     GAMA = 0.0967 - ARATIO - ALOG10(1.-0.207*CA(I,J))
0068 C     GAMM(I) = 10.0 ** GAMA
0069 C     WRITE(6,108) IONIC(I), GAMM(I)
0070 C
0071 C
0072 C     CALC. THE RATIO OF EQUILIBRIUM CONSTANTS K1**H**KSP/K2
0073 C     LUGRAT=-5.89-0.015486*T+9.26E-06*T**2+7.446E-05*PSI(I,J)
0074 C     1 + 2.5212*RUOTI - 0.9194*IONIC(I)
0075 C     RATIO = 10. ** LUGRAT
0076 C     WRITE(6,110) RATIO, LUGRAT
0077 C
0078 C
0079 C     CALC. IMPROVED ESTIMATE OF CALCIUM CONCENTRATION
0080 C     CA(I,J)= ( (0.9*(PSI(I,J)-2.2)*RATIO/4. )**0.3333333)/GAMM(I)
0081 C
0082 C
0083 C     NOW REFINE THIS ESTIMATE, RETURN TO STATEMENT 350.
0084 C
0085 C
0086 400 CONTINUE
0087 C
0088 C
0089 C     PRINT BEST ESTIMATE OF CALCIUM CONC N AT POSITION I.
0090 C     WRITE(6,105)
0091 C     WRITE(6,112) I, CA(I,J), PSI(I,J)
0092 C
0093 500 CONTINUE
0094 C
0095 C     WRITE(6,111)
0096 C     DO 550 N = 1, MAX
0097 C     WRITE(6,113) N, R(N), PSI(N,J), CA(N,J)
0098 C 550 CONTINUE
0099 C
0100 C
0101 C
0102 C     RETURN
0103 C
0104 C     ***** FORMATS FOR ABOVE SUBROUTINE *****

0105 C
0106 C
0107 105 FORMAT(///20X,'***** ESTIMATE OF CALCIUM CONC *****')
0108 C
0109 106 FORMAT( 9X,'FIRST ESTIMATE OF CA CONC AT POSITION',I3,' IS',
0110 1 F10.6, ' M')
0111 C
0112 108 FORMAT(12X,' IONIC STRENGTH =',F10.7,' GAMMA =',F10.7)
0113 C
0114 C
0115 110 FORMAT( 4X,'RATIO OF EQUILIB. CONSTANTS AND ITS COMMON LOG',
0116 1 2E15.7)
0117 C
0118 111 FORMAT( 7X,'LOCN DISTANCE PSIA CALCIUM CONC')
0119 C
0120 112 FORMAT(19X,'AT POSITION', I3,' IS',F10.6,' MOL/LITER',
0121 1 ' & PSIA', F6.0)
0122 C
0123 113 FORMAT( 8X,I2, F9.2, F16.1, F11.5)
0124 C
0125 C
0126 C     END

```

```

0127 C
0128 C *****
0129 C
0130 C ***** MAIN PROGRAM STARTS HERE *****
0131 C
0132 C *****
0133 C
0134 C
0135 C PROGRAM PHELAN
0136 C
0137 C
0138 C REAL KINIT, K(30,40), R(30), CA(30,40), NA(1), PHI(30,40),
0139 C 1 LOGR(30), RESVOL(30), VOLUME(30,40), MU, Q(40),
0140 C 2 PSI(30,40), SUM(30), LOGRAT(30)
0141 C
0142 C COMMON/CONST1/ CA0, H
0143 C COMMON/WELL/RWELL, RDRAIN, PDRAIN, KINIT, MU, PHI0
0144 C COMMON/CONST2/ NA(1), MAX, T, PWELL
0145 C COMMON/BLOCK1/ CA, / BLOCK2 / PSI, / BLOCK3 / R
0146 C
0147 C
0148 C DEFINITIONS OF VARIABLE NAMES
0149 C
0150 C KINIT = INITIAL PERMEABILITY, DARCYS
0151 C K = PERMEABILITY, DARCYS
0152 C RWELL = WELLBORE RADIUS, FT
0153 C PWELL = PRESSURE IN WELL, PSIA
0154 C DELTAP = PRESSURE DIFFERENCE OVER RADIUS OF DRAINAGE, ATM
0155 C MU = VISCOSITY OF BRINE, CENTIPOISE
0156 C PI=3.14159
0157 C R = DISTANCE FROM PRODUCING WELL, FT
0158 C CA(I,J) = CALCIUM CONC'N AT POSITION I, HOUR J; MOL/LITER
0159 C CA0 = CA CONC AT WELL, MOL/LITER
0160 C I = INCREMENT IN DISTANCE FROM WELL
0161 C PRESS = PRESSURE, ATM
0162 C PSI = PRESSURE, PSIA
0163 C J = HOURS SINCE BREAKTHRU OF CALCIUM-SATURATED WATER
0164 C PHI0 = INITIAL POROSITY OF RESERVOIR, DIMENSIONLESS
0165 C RESVOL = VOLUME OF RESERVOIR BETWEEN R(I) AND R(I-1), CU. FT.
0166 C VOLUME = VOLUME OF CA PRECIPITATE IN RESVOL, CU. FT.
0167 C NA(1) = SALT CONC'N IN WATER, EXCLUDING CALCIUM, MOL/LITER.
0168 C Q(1) = INITIAL FLOW OF BRINE, CC/SEC.
0169 C MAX = NO. OF INCREMENTS INTO WHICH RADIAL DISTANCE IS DIVIDED.
0170 C
0171 C
0172 C
0173 C PART ONE
0174 C
0175 C
0176 C *** CALC INITIAL VALUES OF SOME VARIABLES. ***
0177 C (MOST ARE PROVIDED IN BLOCK DATA.)
0178 C
0179 C WRITE(6,96) RWELL, KINIT
0180 C
0181 C WRITE(6,98) NA(1), T, PHI0, RDRAIN, PDRAIN
0182 C
0183 C H = 30.48
0184 C DELTAP = (PDRAIN - PWELL)/14.7
0185 C Q(1) = 2.*3.14159265*KINIT*H * DELTAP / (MU*ALOG(RDRAIN/
0186 C 1 RWELL))
0187 C
0188 C CA0 = 0.079015

0189 C WRITE(6,100) CA0, Q(1), H
0190 C PI=3.14159
0191 C

```

```

0192 C
0193 C *** DETERMINE DISTANCES AT WHICH RESERVOIR PROPERTIES WILL BE CALC'D ***
0194 C
0195         R(1) = RWELL + 0.01
0196         DO 150 I = 2, 8
0197             R(I) = RWELL + 0.1 * FLOAT(I-1)
0198     150     CONTINUE
0199 C
0200         DO 155 I = 9, 14
0201             R(I) = R(I-1) + 0.2
0202     155     CONTINUE
0203 C
0204         DO 160 I = 15, 21
0205             R(I) = R(I-1) + 0.2 * FLOAT(I-14)
0206     160     CONTINUE
0207 C
0208         DO 165 I = 22, 24
0209             R(I) = R(I-1) + 2.0*FLOAT(I-21)
0210     165     CONTINUE
0211 C
0212         DO 170 I = 25, 28
0213             R(I) = R(I-1) + 2.***(I-20)
0214     170     CONTINUE
0215 C
0216 C         WRITE(6,9) (I, R(I), I = 1, MAX)
0217     9         FORMAT(9X, I2, ' DISTANCE FROM WELL = ', F8.2)
0218 C
0219 C
0220 C *** CALC RESERVOIR VOLUMES IN EACH DONUT BETWEEN I AND I-1 *****
0221 C         (VOLUMES ARE IN CU. FT.)
0222 C
0223         RESVOL(1) = PI * 1.0 * (R(1)**2 - RWELL**2)
0224 C
0225         DO 300 I = 2, MAX
0226             RESVOL(I) = PI * 1.0 * (R(I)**2 - R(I-1)**2)
0227     300     CONTINUE
0228 C         WRITE(6, 10) (R(I), RESVOL(I), I = 1, MAX)
0229     10         FORMAT(9X, 'DISTANCE AND RESERVOIR VOLUME', 2E12.5)
0230 C
0231 C
0232 C ***** PRESSURE PROFILE DURING HOUR ONE *****
0233 C         CALC. PRESSURE IN ATM., THEN IN PSIA.
0234 C
0235         DO 311 I = 1, MAX
0236             PRESS = P(Q(1), R(I), KINIF, H)
0237             PSI(I,1) = 14.7 * PRESS
0238     311     WRITE(6,101) I, R(I), PRESS, PSI(I,1)
0239             CONTINUE
0240 C
0241 C ***** COMPUTE LOG(R(I)/R(I-1)) FOR LATER USE *****
0242 C
0243         DO 400 L = 10, 21
0244             LOGR(L) = ALOG(R(L)/R(L-1))
0245     400     CONTINUE
0246             LOGR(22) = ALOG(RDRAIN/R(21))
0247 C
0248         DO 401 L=10,MAX
0249             LOGRAT(L)= ALOG(RDRAIN/R(L))
0250     401     CONTINUE
0251 C
0252 C
0253 C

```

PART TWO

```

0256 C
0257 C
0258 C ***** CHANGES IN RESERVOIR, HOUR-BY-HOUR *****
0259 C (FIRST, CALCULATE PROFILE OF CALCIUM CONCENTRATION
0260 C AND DEPOSITION OF CaCO3 DURING HOUR J.)
0261 C
0262 C
0263 C DO 900 J = 1, 10
0264 C CALL CALCUM(J)
0265 C
0266 C
0267 C *** VOLUME OF CALCIUM CARBONATE DEPOSITED DURING HOUR J ***
0268 C
0269 C
0270 C DO 690 I = 1, MAX
0271 C IF(I .GT. 1) GO TO 601
0272 C DELCAL = CA(1,J) - CA0

0273 C GO TO 602
0274 C
0275 C 601 DELCAL = CA(1,J) - CA(I-1,J)
0276 C
0277 C 602 VOLUME(I,J) = DELCAL * Q(J) * 7.80973E-5 * 60.
0278 C (60. REPRESENTS 60 MIN)
0279 C WRITE(6,114) I, RESVOL(I), VOLUME(I,J)
0280 C
0281 C 690 CONTINUE
0282 C
0283 C
0284 C
0285 C ***** CALC. POROSITY AT END HR J BY SUBTR'G DECREASE DURING J *****
0286 C DUE TO PRECIPITATE
0287 C
0288 C IF (J .GT. 1) GO TO 715
0289 C DO 710 I = 1, MAX
0290 C PHI(I,1) = PHI0 - VOLUME(I,1) / RESVOL(I)
0291 C 710 CONTINUE
0292 C GO TO 730
0293 C
0294 C 715 DO 720 I = 1, MAX
0295 C PHI(I,J) = PHI(I,J-1) - VOLUME(I,J) / RESVOL(I)
0296 C 720 CONTINUE
0297 C
0298 C 730 CONTINUE
0299 C WRITE(6,116) (PHI0, I, PHI(I,J), I = 1, MAX)
0300 C
0301 C
0302 C ***** IIB. PERMEABILITY AT END OF HOUR J *****
0303 C
0304 C DO 800 I = 1, MAX
0305 C K(I,J) = KINIT * PHI(I,J)**2 / PHI0**2
0306 C 800 CONTINUE
0307 C
0308 C WRITE(6,118) (I, K(I,J), I = 1, MAX)
0309 C
0310 C
0311 C ***** FLOW AT END OF HOUR J, BY NUMERICAL INTEGRATION *****
0312 C
0313 C
0314 C SUM(1) = (R(1)-RWELL)/K(1,J)/0.505
0315 C SUM(2) = SUM(1) + (R(2)-R(1))/K(2,J)/0.555
0316 C DO 840 I = 3, 8
0317 C SUM(I) = SUM(I-1) + 0.10/K(I,J)/(R(I)-0.05)
0318 C 840 CONTINUE
0319 C
0320 C DO 845 I = 9,14
0321 C SUM(I) = SUM(I-1) + 0.20/K(I,J)/(R(I)-0.10)
0322 C 845 CONTINUE
0323 C DO 850 I = 15, 21
0324 C SUM(I) = SUM(I-1) + LUGR(I)/K(I,J)
0325 C 850 CONTINUE
0326 C SUMM = SUM(21) + LUGR(22) / (K(MAX,J) + K(21,J))*2.0
0327 C SUM(22) = SUMM
0328 C

```

```

0329          WRITE(6,107)
0330          WRITE(6,109)(N,R(N),PSI(N,J),CA(N,J),PHI(N,J),K(N,J),
0331 1          N=1,MAX)
0332 C
0333 C
0334          JPLUS1 = J + 1
0335          Q(J+1) = DELTAP * (2.*PI*H/MU)/SUMM
0336          WRITE(6,122) JPLUS1, Q(J+1)
0337 C
0338 C
0339 C ***** PRESSURE PROFILE DURING NEXT HOUR, I.E., HOUR J+1 *****
0340 C
0341          DO 880 I = 1, 21
0342          PSI(I,J+1) = PWELL + (PDRAIN - PWELL)*SUM(I)/SUMM
0343 880      CONTINUE
0344 C
0345 C          (PRESSURES AT POSITIONS BETWEEN 8 & 100 FT. CAN
0346 C          CALCULATED USING AVG. PERMEABILITY OVER EACH
0347 C          DISTANCE INCREMENT.)
0348 C
0349          DO 890 I = 22, MAX
0350          PSI(I,J+1)=PDRAIN-14.7*Q(J+1)*MU*LOGRAT(I)/(2.*PI*H*K(I,J))
0351 890      CONTINUE
0352 C
0353 C
0354 900      CONTINUE
0355 C
0356 C

0357 C
0358          STOP
0359 C
0360 C ***** FORMAT STATEMENTS FOR ABOVE PROGRAM. *****
0361 C
0362 C
0363 C
0364 96  FORMAT(///// 9X,'RADIUS OF WELL =',F4.2,' FT.  INITIAL PERM =',
0365 1 F10.6,' DARCYS')
0366 C
0367 98  FORMAT( 9X,'BRINE CONC =', F8.3, ' M    TEMP =', F6.1,' FAHR'/
0368 1 9X,'INITIAL POROSITY =',F5.4,5X / 9X,'PRESSURE AT RADIUS OF',
0369 2 ' DRAINAGE (', F5.0, ' FT) IS ', F6.1, ' PSIA')
0370 C
0371 100 FORMAT( 9X,'INITIAL CA CONC IS',F7.5,' M.  BRINE FLOW =',F7.5,
0372 1 ' CC/SEC'/9X,'RESEVOIR THICKNESS, CM.', F11.3)
0373 C
0374 101 FORMAT( 5X,'AT POSITION', 14,'  DISTANCE IS', F10.2,' FT.',
0375 1 ' AND PRESSURE IS', F6.1,' ATM', F8.1,' PSIA')
0376 C
0377 104 FORMAT(29X, 'PRESSURE, PISA', F12.2)
0378 C
0379 C
0380 107 FORMAT(5X,'LOCN  DISTANCE      PSIA      CAL CON      POROSITY',
0381 1 ' PERMEABILITY')
0382 C
0383 109 FORMAT(6X,I2,F9.2,F14.1,F11.5,F10.5,E14.5)
0384 C
0385 114 FORMAT( 9X,'INCREMENTAL RESERVOIR VOLUME AT POSITION',I3,
0386 1 F12.3,' CU. FT.' /10X,'VOLUME OF PRECIPITATE =', F12.5 /)
0387 C
0388 116 FORMAT( 9X,'INITIAL POROSITY =', F6.4,'  NEW POROSITY AT LOCAT',
0389 1 I3, ' IS', F8.4)
0390 C
0391 118 FORMAT(9X,'AT POSITION ',I3,' PERMEABILITY =', E14.5,' DARCYS')
0392 C
0393 122 FORMAT(/9X,'FLOW DURING HOUR',I3,' WILL BE', E14.5,' CC/SEC'/)
0394 C
0395 C
0396 C
0397      END

```

APPENDIX Q

Mineralogical Assays of Core Samples
from Pennzoil's CO₂ Pilot Test
in the Rock Creek-Big Injun Reservoir

Table Q.1

X-Ray Diffraction Results

Mineral	Sample Depth, ft	
	2008.5	2021.5
quartz	74	84
feldspar	2	3
calcite	trace	-
siderite	1	-
halite	2	1
clay	21	12
wt.% < 5μ	26.6	31.2
kaolinite	trace	52
illite	14	17
chlorite	92	31

Table Q.2

Thin Section Point Count Data

Characteristics		Sample Depth, ft	
		2008.5	2021.5
WHOLE ROCK 100%	GRAINS MATRIX CEMENT CLAY PORES	75 1 4 4 16	71 1 3 3 22
GRAINS 100%	QUARTZ K-FELDSPAR PLAGIOCLASE DOLOMITE LITHICS ALTERED MUSCOVITE ORGANIC MATL	94 2 trace - 2 trace 1 1	95 trace 1 - 2 1 trace 1
CEMENT TYPES 100%	SILICA CALCITE DOLOMITE CLAY	5 3 1 91	5 1 - 94
CLAY MORPHOLOGY 100%	MATRIX PORE-FILLING GRAIN COATING GRAIN REPLACEMENT	1 15 84 trace	1 8 90 1
POROSITY TYPES 100%	INTERGRANULAR INTRAGRANULAR MICROPOROSITY FRACTURE	70 15 15 -	75 10 15 -
ROUNDNESS	ROUNDED SUB-ROUNDED SUB-ANGULAR ANGULAR	X X X X	X X X X

